The Dissertation Committee for Robert Edison Tsai Certifies that this is the approved version of the following dissertation:

Mass Transfer Area of Structured Packing

Committee:

Gary T. Rochelle, Supervisor

R. Bruce Eldridge, Co-Supervisor

Roger T. Bonnecaze

Gerald G. McGlamery

A. Frank Seibert

Thomas M. Truskett

Mass Transfer Area of Structured Packing

by

Robert Edison Tsai, B.S.

Dissertation

Presented to the Faculty of the Graduate School of

The University of Texas at Austin

in Partial Fulfillment

of the Requirements

for the Degree of

Doctor of Philosophy

The University of Texas at Austin

May 2010

Dedication

To my family and friends.

Acknowledgments

I would first like to acknowledge my advisors, Dr. Bruce Eldridge and Dr. Gary Rochelle. Dr. Eldridge has been both a friend and teacher. Whenever I have come to him with questions or concerns, he has offered sound advice – usually infused with a touch of his humor. He is an excellent mentor and has always fought hard for me, all the way through my search for post-graduate employment. Dr. Rochelle is one of the smartest, most good natured individuals that I have ever known. His enthusiasm for teaching was apparent from the first day that we met, and even if I were to remain his student forever, I do not think that I would ever stop learning from him. He has continually promoted my growth by encouraging me to think creatively and independently. Dr. Rochelle has somehow always managed to make time for not only me but every one of his students, even with the significant expansion of the research group over the past few years, and I am extremely thankful for his dedication.

I would like to additionally thank Dr. Frank Seibert. Dr. Seibert basically served as a third advisor to me and was extremely considerate and flexible with my access to the resources (both equipment and personnel) of the Separations Research Program (SRP).

Mass Transfer Area of Structured Packing

Publication No._____

Robert Edison Tsai, Ph.D.

The University of Texas at Austin, 2010

Supervisors: Gary T. Rochelle and R. Bruce Eldridge

The mass transfer area of nine structured packings was measured as a function of liquid load, surface tension, liquid viscosity, and gas rate in a 0.427 m (16.8 in) ID column via absorption of CO_2 from air into 0.1 mol/L NaOH. Surface tension was decreased from 72 to 30 mN/m via the addition of a surfactant (TERGITOL[TM] NP-7). Viscosity was varied from 1 to 15 mPa·s using poly(ethylene oxide) (POLYOX[TM] WSR N750). A wetted-wall column was used to verify the kinetics of these systems. Literature model predictions matched the wetted-wall column data within 10%. These models were applied in the interpretation of the packing results.

The packing mass transfer area was most strongly dictated by geometric area (125 to 500 m^2/m^3) and liquid load (2.5 to 75 m^3/m^2·h or 1 to 30 gpm/ft^2). A reduction in surface tension enhanced the effective area. The difference was more pronounced for the finer (higher surface area) packings (15 to 20%) than for the coarser ones (10%). Gas velocity (0.6 to 2.3 m/s), liquid viscosity, and channel configuration (45° vs. 60° or

smoothed element interfaces) had no appreciable impact on the area. Surface texture (embossing) increased the area by 10% at most. The ratio of effective area to specific area (a_e/a_p) was correlated within limits of $\pm 13\%$ for the experimental database:

$$\frac{a_e}{a_p} = 1.34 \left[\left(\frac{\rho_L}{\sigma} \right) g^{1/3} \left(\frac{Q}{L_p} \right)^{4/3} \right]^{0.116}$$

This area model is believed to offer better predictive accuracy than the alternatives in the literature, particularly under aqueous conditions.

Supplementary hydraulic measurements were obtained. The channel configuration significantly impacted the pressure drop. For a 45°-to-60° inclination change, pressure drop decreased by more than a factor of two and capacity expanded by 20%. Upwards of a two-fold increase in hold-up was observed from 1 to 15 mPa·s. Liquid load strongly affected both pressure drop and hold-up, increasing them by several-fold over the operational range.

An economic analysis of an absorber in a CO_2 capture process was performed. Mellapak^{TM} 250X yielded the most favorable economics of the investigated packings. The minimum cost for a 7 m MEA system was around \$5-7/tonne CO_2 removed for capacities in the 100 to 800 MW range.

Table of Contents

List of Tables

List of Figures

xxii

xxiv

Glossary

A = cross-sectional area of packed column, m^2

a = mass transfer area, m^2

a_e = effective area of packing, m^2/m^3

a_f = fractional area of packing (a_e/a_p)

a_p = specific (geometric) area of packing, m^2/m^3

a_w = wetted area of packing, m^2/m^3

a_{WWC} = contact area of wetted-wall column; 38.52 cm^2

B = packing channel base, m

Bo_L = Bond number for liquid (defined in equation 6.7)

C_1, C_2, C_3, etc. = constants in various equations

C_E = surface renewal factor in Rocha et al. model (equation 3.9)

C_s = C-factor in GPDC model (defined in equation 3.62), ft/s

Ca_L = Capillary number for liquid (defined in equation 6.4)

CP = capacity parameter in GPDC model (defined in equation 3.61)

c = exponent in Stichlmair et al. model (defined in equation 3.29)

D = diffusion coefficient, m^2/s

D_{eff} = effective diffusion coefficient, m^2/s

d_c = diameter of packed column, m

d_e = equivalent diameter of packing in Brunazzi et al. model (defined in equation 3.15),

    m

d_h = hydraulic diameter of packing in Billet and Schultes model (defined in equation 3.15), m

d_{hG} = hydraulic diameter of gas flow channel in Delft model (defined in equation 3.46), m

d_p = equivalent diameter of packing in various models (defined in equation 3.24), m

d_{PE} = diameter of (random) packing element in Shi and Mersmann model (equation 3.2), m

d_{WWC} = hydraulic diameter of wetted-wall column reaction chamber; 0.44 cm

E = enhancement factor (defined in equation 2.21)

E_∞ = enhancement factor for instantaneous, irreversible reaction (defined in equation 2.25)

e_d = eddy contribution to diffusion coefficient in eddy diffusivity theory, s^{-1}

F_G = gas flow factor (= $u_G(\rho_G)^{0.5}$), (m/s)(kg/m^3)$^{0.5}$ or (Pa)$^{0.5}$

$F_{G,lp}$ = gas flow factor at the loading point in Delft model (defined in equation 3.59), (Pa)$^{0.5}$

F_{load} = loading point enhancement factor in Delft model (defined in equation 3.58)

F_{lv} = flow parameter in GPDC model (defined in equation 3.60)

F_p = packing factor in GPDC model (equation 3.61), ft^{-1}

F_{SE} = surface enhancement factor in Rocha et al. model (equation 3.6)

F_t = hold-up factor in Rocha et al. model (defined in equation 3.6)

f_0 = friction factor in Stichlmair et al. model (defined in equation 3.26)

Fr_L = Froude number for liquid (defined in equation 6.6)

G = gas volumetric flow rate, m^3/s

G_m = gas mass flow rate, kg/s

g = gravitational constant; 9.81 m/s^2

g_{eff} = effective gravity in Rocha et al. model (defined in equation 3.35)

Ga_p = Galileo number for liquid (defined in equation 7.8)

GD = geometric dimension (d_c/S)

H = Henry's constant, m$^3 \cdot$Pa/kmol

Ha = Hatta number (defined in equation 2.22)

$HETP$ = height equivalent to a theoretical plate, m

h = packing crimp height, m

h_0 = pre-loading fractional liquid hold-up in Stichlmair et al. model (defined in equation 3.30), m^3/m^3

h_L = fractional liquid hold-up, m^3/m^3

h_{WWC} = exposed length of wetted-wall column; 9.1 cm

h_{pe} = height of a packing element, m

h_{Na+}, h_{OH-}, h_{CO32-}, h_{CO2} = Barrett contributions in Henry's constant calculation (equation 4.6b), L/mol

I = ionic strength, mol/L

K_G = overall mass transfer coefficient, kmol/m$^2 \cdot$Pa$\cdot$s

K_s = constant associated with Sechenov equation (equation 5.1), L/mol

k_1 = pseudo-first-order reaction rate constant, s^{-1}

k_G = gas-film mass transfer coefficient, kmol/m$^2 \cdot$Pa$\cdot$s (or m/s)

$k_g{'}$ = liquid-film mass transfer coefficient, kmol/m^2·Pa·s

$k_L{^0}$ = (physical) liquid-film mass transfer coefficient, m/s

k_{OH-} = second-order reaction rate constant, m^3/kmol·s

$k_{OH-}{^\infty}$ = second-order reaction rate constant at infinite dilution, m^3/kmol·s

L = liquid load, m^3/m^2·h

L_m = liquid mass flow rate, kg/s

L_p = wetted perimeter in cross-sectional slice of packing, m

l_τ = characteristic flow path length in Billet and Schultes model (defined in equation 3.15), m

M = molecular weight, g/mol

N = molar flux, kmol/m^2·s

N_{Fr} = Froude number in Stichlmair et al. model (defined in equation 3.31)

N_{Ga} = Galileo number in Shetty and Cerro model (defined in equation 7.7)

N_L = number of liquid-phase transfer units

N_{Re} = Reynolds number in Shetty and Cerro model (defined in equation 7.6)

n_+, n_- = ion valencies

n_{pe} = number of packing elements

P = pressure, Pa

p = solid surface period in Shetty and Cerro model (equation 7.7), m

Pe_G = Péclet number for gas (defined in equation 4.8)

Q = liquid volumetric flow rate, m^3/s

q = flow rate per unit width in Shetty and Cerro model (equation 7.6), m^3/m·s

R = ideal gas constant, 8314.5 m^3·Pa/kmol·K

r = chemical reaction rate, kmol/m^3·s

Re_G = Reynolds number for gas in Stichlmair et al. model (defined in equation 3.27)

Re_{Ge} = Reynolds number for gas based on effective gas velocity in Delft model (defined in equation 3.41)

Re_{Grv} = Reynolds number for gas based on relative phase velocities in Delft model (defined in equation 3.42)

Re_L = Reynolds number for liquid (defined differently in various models)

S = packing channel side, m

s = fraction of liquid surface renewed per time in surface renewal theory, s^{-1}

T = temperature, K

T_{corr} = "corrected" (averaged) packed column temperature, K

t = time, s

t_{sheet} = structured packing sheet thickness, m

u = velocity, m/s

u_{film} = average liquid film velocity, m/s

u_{Ge} = effective gas velocity in Rocha et al. (equation 3.10) and Delft (equation 3.38) models, m/s

u_{Le} = effective liquid velocity in Rocha et al. (equation 3.11) and Delft (equation 3.39) models, m/s

V = volume, m^3

w = mass fraction

We_L = Weber number for liquid (defined in equation 6.5)

x = location in theoretical gas-liquid film system, m

y = mole fraction in vapor phase

$y_{CO2,in/out}$ = mole fraction of CO_2 at inlet/outlet

Z = packed height, m

z = location in packed bed, m

GREEK LETTERS

α = corrugation angle (with respect to the horizontal), deg

α_L = effective liquid flow angle (with respect to the horizontal) in Delft model (defined in

   equation 3.40), deg

β = sheet-metal efficiency factor in Fair and Bravo model (defined in equation 3.5)

γ = contact angle, deg

ΔP = pressure drop, Pa

δ = characteristic length (film thickness), m

$\delta_{Nusselt}$ = Nusselt film thickness (defined in equation 3.3), m

ε = packing void fraction, m^3/m^3

ζ = interaction coefficient in Delft model

η = efficiency

κ^{-1} = capillary length (defined in equation 6.12), m

μ = (dynamic) viscosity, kg/m·s or Pa·s

v = kinematic viscosity (μ/ρ), m^2/s

ξ = friction factor in Delft model

ρ = density, kg/m^3

σ = surface tension, N/m

σ_c = critical surface tension in Onda et al. model (equation 3.19), N/m

σ_{SG} = interfacial tension between solid and gas phases, N/m

σ_{SL} = interfacial tension between solid and liquid phases, N/m

φ = fraction of gas flow channel occupied by liquid film in Delft model (defined in equation 3.45)

Ω = fraction of packing surface occupied by perforations in Delft model (equation 3.17)

SUBSCRIPTS

G = gas

L = liquid

LM = log-mean

S = solid

w = (pure) water

SUPERSCRIPTS

* = equilibrium

b = bulk

i = interface

Chapter 1: Introduction

The features of tower internals (trays and packing) used in gas-liquid separation processes are first covered in this chapter. The concern over CO_2-induced global warming is briefly discussed, together with a capture method (aqueous amine absorption) that has been proposed to deal with the CO_2 emission problem. The importance of mass transfer models, and in particular, the need for an accurate area model for structured packing in the context of CO_2-amine systems, is explained. Several past modeling efforts, along with some of their shortcomings, are referenced. Finally, the project objectives are summarized.

1.1 GAS-LIQUID SEPARATIONS

Processes such as distillation, absorption, and stripping rely on efficient gas-liquid contacting. Trays or packing are typically placed inside the columns used for these unit operations.

1.1.1 Trays

Tray towers contain a series of vertically-spaced stages, on top of which liquid is allowed to accumulate. The liquid is upheld by the countercurrent flow of vapor and pressure drop in the downcomers, and mass transfer is facilitated by the bubbling of the vapor through the liquid. The use of trays instead of packing can be advantageous in situations where large fluctuations in vapor or liquid rates are anticipated or when fouling with solid deposits is a problem. Tray towers, however, are also often characterized by

higher pressure drop, lower capacity, and poorer cost efficiency (Peters and Timmerhaus, 1991).

1.1.2 Random Packing

Packing is classified as random or structured. Random packing (also referred to as dumped packing) consists of uniquely shaped objects (Figure 1.1) with nominal sizes ranging from 3 to 75 mm (Geankoplis, 2003). The packing is dumped into a column with minimal regard for arrangement. This jumbled layout, together with the geometry of the packing pieces, promotes liquid surface renewal and mass transfer. A significant portion of mass transfer actually occurs through the break-up of liquid into satellite droplets – that is, independent of the packing surface (Fair and Bravo, 1987).

Figure 1.1. Examples of random packings. From left: CMR #2, IMTP 40, and 2" metal pall ring. Images taken from Wilson (2004).

1.1.3 Structured Packing

Structured packing, which has been the focus of this work, consists of corrugated sheets and is manufactured in modular form to permit stacking in an ordered array (Figure 1.2). The opposing corrugations form a systematic, grid-like arrangement that

allows for the flow of liquid and gas along fairly well defined paths. Stacked elements are typically rotated 90° with respect to each other in order to facilitate the redistribution and mixing of liquid and gas (Olujic et al., 1999). The packing sheets are often perforated for this purpose as well. The majority of gas-liquid contact area is dictated by the packing surface, in contrast with random packings (Weimer and Schaber, 1997). Structured packings are generally more expensive per unit of volume than their random counterparts, but they also offer low pressure drops and more efficient mass transfer (Fair and Bravo, 1987).

Figure 1.2. Example of structured packing: Sulzer Mellapak^{TM} 250X (side and top views).

Structured packing is utilized in many processes, including the chemical (e.g., ethylbenzene/styrene or air separation) and oil industries, as well as in exhaust air cleaning and wastewater treatment. It is a clear favorite in scenarios like vacuum distillation, where stringent pressure drop limitations exist, but its application is certainly not restricted to this niche. Compared with the alternatives, it can be cost-competitive even for higher pressure operations (Fair and Bravo, 1990), although its performance in

3

distillation processes tends to rapidly deteriorate as the system critical pressure is approached. Structured packing is worth considering in practically any tower revamping project, due to the capacity and/or efficiency-related benefits it can offer (Geankoplis, 2003).

1.2 CLIMATE CHANGE AND CO_2 CAPTURE

The Intergovernmental Panel on Climate Change (IPCC) has reported that the average global surface temperature has increased by $0.74°C \pm 0.18°C$ over the past century (Solomon et al., eds., 2007). Many sources, the IPCC included, have suggested this warming to very likely be attributable to increases in anthropogenic greenhouse gas levels – specifically, CO_2. Consequently, the removal of CO_2 from the atmosphere has become an increasingly relevant topic in recent years. The flue gas from coal-fired power plants has been identified as a major CO_2 point source, accounting for about 30% of total U.S. CO_2 emissions (Rochelle, 2009). Approximately 50% of the power generated in the U.S. is attributable to coal, meaning that coal-based power is unlikely to be curtailed any time in the near future. Thus, coal plants should be at the forefront of any endeavors seeking to bring about a significant reduction in CO_2 emissions. Such efforts must consider not only the incorporation of capture technology into new facilities but also, perhaps more importantly, the retrofitting of existing plants.

Various capture strategies have been proposed. Chemical absorption, adsorption, cryogenics, membranes, and microbial/algal systems are among the frontrunners in this discussion (Rao and Rubin, 2002). Of these, absorption with a chemical solvent – in

particular, an aqueous amine such as monoethanolamine (MEA) – is arguably the most mature and readily employable concept, as it has already been in practice for many years in related operations like coal gasification or natural gas treating (Aroonwilas and Tontiwachwuthikul, 1997). Figure 1.3 is a generic representation of such a system.

Treated Gas Lean Solvent CO_2

(1 mol % CO_2) (for Compression/ Sequestration)

Heat Exchanger

Absorber Stripper

Flue Gas Reboiler

(10 mol % CO_2) Rich Solvent (Steam Stripping)
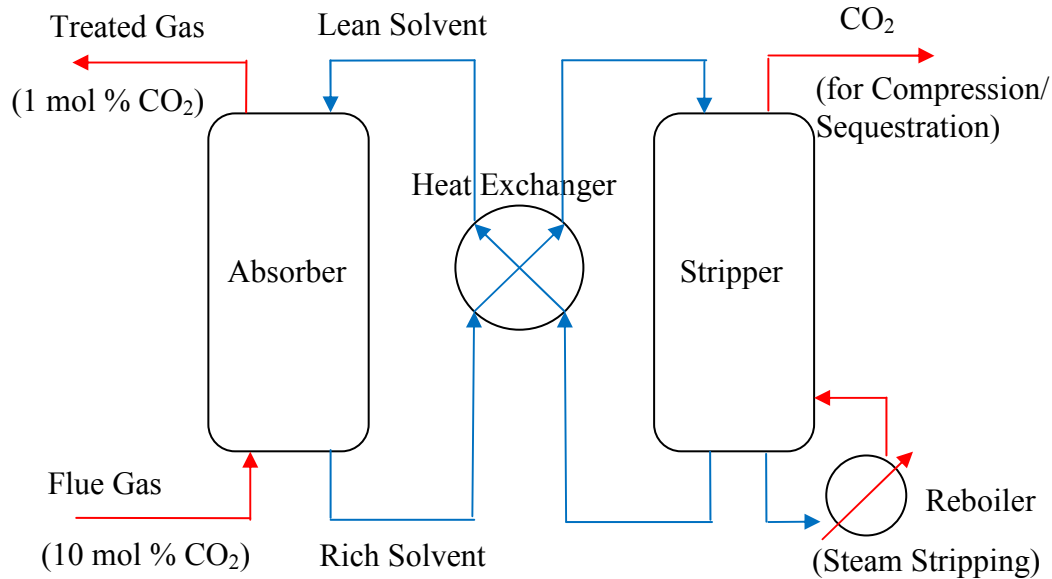
Figure 1.3. Process flow diagram for a CO_2 absorption/stripping process.

The basic concept is to countercurrently contact the flue gas from the plant with lean amine solvent (referred to as lean because it has the lowest CO_2 content in the process), which results in CO_2 being absorbed into the solution. The rich solution is then sent to a stripping column for steam-based regeneration and is finally recycled back to the absorber in lean form. The captured CO_2 is sent to a compression train before being sequestered, with deep saline reservoirs, depleted oil and gas wells, or unmineable coal seams among the possible storage sites (Rao and Rubin, 2002).

Tower internals are obviously an integral part of this process. Structured packing, in particular, has been cited as a highly favorable option in the absorber, due to the need to minimize the required contactor height and associated capital cost (Aroonwilas et al., 2001). The superior pressure drop performance of structured packing may be of great benefit too. Despite the system being operated at moderate-to-high pressure, the massive throughput of gas involved – on the order of 3 x 10^6 ACFM (actual ft^3/min) in a large power plant of 1000 MW – is certain to translate to pressure drop costs that are not trivial.

1.3 GAS-LIQUID MASS TRANSFER PARAMETERS

Reliable mass transfer models are critical for the analysis and design of columns containing structured packing. Towers may be as large as 15 m in diameter for certain refinery vacuum-separation processes (Pilling, 2009), and even greater diameters could be necessary for CO_2 capture. One can imagine that capital costs can become quite daunting and that a poor design effort can have significant financial ramifications.

Mass transfer performance can be characterized in terms of two parameters: the mass transfer coefficient (k_G or k_L^0) and the gas-liquid mass transfer area, also referred to as the effective area (a_e). The focal point of the present research is on the effective area. While the accurate prediction of both mass transfer parameters is, in general, necessary for adequate representation of a process, a good area model is first and foremost desired for the main application of interest: CO_2 capture by aqueous amine absorption. Under most conditions, the CO_2-amine reaction is fast enough that the CO_2 reacts within a short

6

distance of the gas-liquid interface. Consequently, the only packing-related mass transfer parameter that the CO_2 flux depends on is the effective area – *not k_G or k_L^0*. Henriques de Brito et al. (1994) affirm this statement in the context of a CO_2-NaOH system, which is mechanistically analogous to the CO_2-amine system.

1.4 PREVIOUS WORK

Numerous area models for structured packing have been proposed in the literature. Wang et al. (2005) performed an extensive review of these correlations and concluded that the matter has not been satisfactorily solved. Distinguishing features of the various models are discussed in detail in Chapter 3, but several general issues are immediately apparent. Many rely on packing-specific constants, which limit their adaptability and also imply a degree of discontinuity between the seemingly relatable packings. Different and sometimes even contrasting effects of physical properties like liquid viscosity and surface tension are predicted as well, which is clearly a problem when considering the vast ranges of properties exhibited by amines and other chemicals of commercial interest. The internal fluid flow behavior is not well understood, and improvements certainly can be made with respect to current predictive capabilities.

The mass transfer correlations of Rocha et al. (1996) and Billet and Schultes (1993) are two of the most widely used models for structured packing. Both drew upon extensive experimental databases involving a variety of fluid systems and therefore, in theory, captured a range of physical properties and their associated effects. Databases of lumped or overall mass transfer measurements (e.g., *HETP*) were utilized in the

development and corresponding validation of these models, and the individual parameters were basically forced to fit these results. In other words, none of the mass transfer parameters (k_G, k_L^0, a_e) were independently validated. This disconnect makes it difficult to apply the correlations with much confidence, since they have, in all likelihood, been confounded by interacting effects. For instance, a viscosity impact on mass transfer may have been correlated with the effective area, when it really should have been associated with the mass transfer coefficient. The two literature models will be demonstrated later (Section 6.9.1) to be especially poor in their handling of aqueous systems, so the previous issue notwithstanding, the use of either correlation for the modeling of amine systems is not advisable.

In many applications involving packed columns, an understanding of the overall mass transfer is sufficient from a design perspective. While the need to decouple mass transfer coefficients and effective areas has been somewhat limited, experimental methods such as those outlined in Hoffman et al. (2007) or Rejl et al. (2009) that allow for the separation of these parameters via appropriate test system selections and thereby facilitate a cleaner interpretation of the mass transfer performance have long-been established in the literature. Only a handful of works, however, have been published that have utilized this approach and reported mass transfer area data for structured packing (Henriques de Brito et al., 1994; Weimer and Schaber, 1997; Dragan et al., 2000; Wilson, 2004). All of these studies were conducted at water-like conditions ($\rho_L \sim 1000$ kg/m^3, $\mu_L \sim 1$ mPa·s, and $\sigma \sim 72$ mN/m), and none even speculated on the impact of liquid viscosity

and surface tension, which one could foresee impacting the mechanics of liquid flow (i.e., spreading or turbulence) within the packing.

1.5 RESEARCH OBJECTIVES AND SCOPE

The primary goal of the current project is the development of an improved model for the mass transfer area of structured packing. This model is to be based on a comprehensive set of area measurements made in a pilot-scale column (0.427 m or 16.8 in ID) using a chemical method: absorption of CO_2 from air into solutions of either neat or doped (i.e., containing physical property modifiers) 0.1 mol/L NaOH. By applying a direct or decoupled methodology to obtain area data and explicitly investigating the effects of liquid viscosity and surface tension, as well as an array of geometric features, the shortcomings of the previously discussed studies are addressed. The general project objectives are summarized below.

- Evaluate the reaction kinetics of the CO_2-NaOH system using a wetted-wall column;

- Determine suitable chemical reagents to modify the surface tension and viscosity of the caustic solutions and characterize the kinetic impact (if any) of these additives;

- Expand the database of the Separations Research Program at the University of Texas at Austin by measuring the hydraulic performance and mass transfer area of various structured packings as a function of liquid load, liquid viscosity, and surface tension;

9

- Develop an understanding of the fluid mechanics associated with structured packing operation and utilize this knowledge in conjunction with the data to develop a global model that captures the experimental findings and adequately represents the mass transfer area of a broad range of structured packings and gas-liquid systems.

Chapter 2: Mass Transfer

This chapter first introduces the basic theory of mass transfer and summarizes several fundamental mass transfer models that have been proposed. The more advanced concept of mass transfer with chemical reaction is presented. The chemical system specific to this work (CO_2-NaOH) and the associated approximations and limiting conditions are also discussed.

2.1 INTRODUCTION TO MASS TRANSFER

Mass transfer consists of the migration of a component through a single phase or from one phase to another. The classic scenario of gas absorption into liquid is fundamental to the present work, and as such, this process is conveniently referred to in the subsequent theoretical discussion. In this simple case, a gas (CO_2) and a liquid are in contact (Figure 2.1).
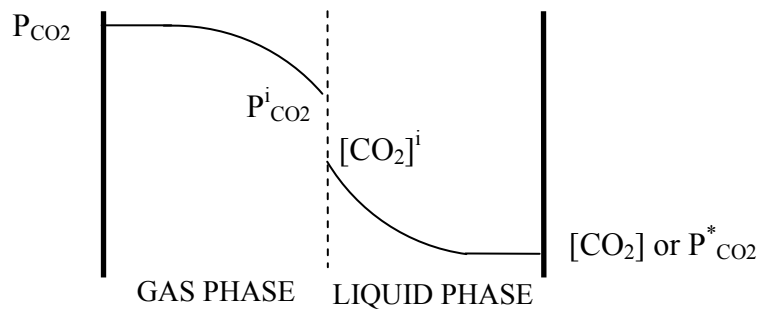
Figure 2.1. Illustration of concentration profiles for CO_2 absorption into liquid.

The flux of CO_2 (N_{CO2}) can be expressed in several equivalent manners:

$$N_{CO_2} = K_G \left(P_{CO_2} - P_{CO_2}^* \right) \qquad (2.1a)$$

$$N_{CO_2} = k_G \left(P_{CO_2} - P_{CO_2}^i \right) \tag{2.1b}$$

$$N_{CO_2} = k_L^0 \left([CO_2]^i - [CO_2] \right) = \frac{k_L^0}{H_{CO_2}} \left(P_{CO_2}^i - P_{CO_2}^* \right) \tag{2.1c}$$

In the above set of equations, the superscripts i and * respectively denote the interface and equilibrium partial pressures or concentrations. In equation 2.1c, the CO_2 partial pressure and concentration have been related by a distribution coefficient (H_{CO2}). Equation 2.2 is true of all molecular transport processes (momentum, mass, and heat) (Geankoplis, 2003).

$$\text{rate of transport} = \frac{\text{driving force}}{\text{resistance}} \tag{2.2}$$

Equations 2.1a-c can be interpreted from this perspective, with the "resistance" being associated with the mass transfer coefficients and the "driving force" being associated with the partial pressure or concentration gradients. The mass transfer coefficients can conveniently be considered in series resistance form, where the overall resistance ($1/K_G$) is the sum of the gas-side ($1/k_G$) and liquid-side (H_{CO2}/k_L^0) resistances.

$$\frac{1}{K_G} = \frac{1}{k_G} + \frac{H_{CO_2}}{k_L^0} \tag{2.3}$$

2.2 FUNDAMENTAL MASS TRANSFER MODELS

Various theories have been proposed to explain the phenomenon of mass transfer in detail. These models are briefly summarized below, in the context of a gas (CO_2)-liquid system.

2.2.1 Film Theory

Film theory (Lewis and Whitman, 1924) is the oldest and most basic mass transfer model. Four zones are assumed wherever a liquid and gas are in contact (Figure 2.2). First, there are the bulk fluid bodies, which are uniform due to rapid mixing by convection. The other two regions are on each immediate side of the interface and consist of stationary gas and liquid films, where only steady-state molecular diffusion is assumed to be occurring.
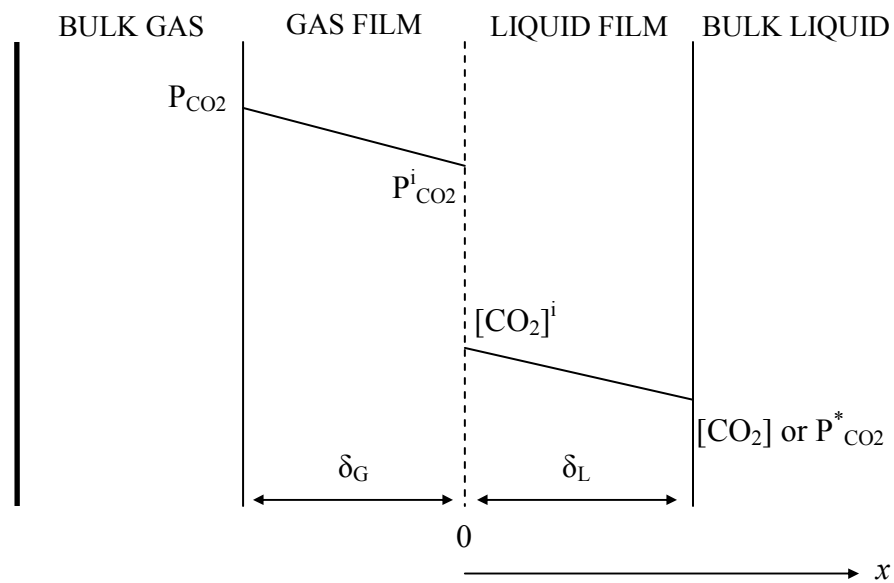
Figure 2.2. Film representation of physical absorption of CO_2 into liquid.

The differential equation for mass transfer can be written as:

$$D_{CO_2,L} \frac{d^2[CO_2]}{dx^2} = 0 \qquad (2.4)$$

$$[CO_2] = [CO_2]^i @ x = 0 \qquad (2.4a)$$

13

$$[CO_2] = [CO_2] @ x = \delta_L \qquad (2.4b)$$

After applying the appropriate boundary conditions (equations 2.4a and 2.4b), the CO_2 flux is given by:

$$N_{CO_2} = D_{CO_2,L} \frac{[CO_2]^i - [CO_2]}{\delta_L} \qquad (2.5)$$

Equation 2.6 readily follows from equations 2.1c and 2.5.

$$k_L^0 = \frac{D_{CO_2,L}}{\delta_L} \qquad (2.6)$$

As can be seen, film theory predicts the liquid-film mass transfer coefficient (k_L^0) to be directly proportional to the diffusion coefficient ($D_{CO2,L}$). Most experimental evidence, in contrast, suggests k_L^0 to exhibit a trend with $D_{CO2,L}$ that is closer to a square root dependence (Geankoplis, 2003). Thus, the practical applicability of film theory is obviously limited. Despite being physically unrealistic, it is nevertheless recognized as being useful for illustrative purposes (Bird et al., 2002).

2.2.2 Penetration Theory

Penetration theory (Higbie, 1935) assumes that liquid molecules are continuously shuttled between the bulk and the gas-liquid interface. Every molecule that is brought to the interface is exposed to mass transfer for a given duration of time (t). It is an unsteady-state theory, and so, the differential mass transfer equation is written as follows:

$$D_{CO_2,L} \frac{\partial^2 [CO_2]}{\partial x^2} = \frac{\partial [CO_2]}{\partial t} \qquad (2.7)$$

14

The liquid-film mass transfer coefficient predicted by penetration theory is shown in equation 2.8.

$$k_L^0 = 2\sqrt{\frac{D_{CO_2,L}}{\pi t}}$$

(2.8)

This theory provides an arguably more realistic picture of mass transfer than film theory, since it correctly matches the experimentally observed square root relation of the mass transfer and diffusion coefficients.

2.2.3 Surface Renewal Theory

Surface renewal theory (Danckwerts, 1951) is an extension of penetration theory. Rather than having a single contact time, it instead assumes the liquid elements to be exposed for varying periods of time. This distribution is interpreted in terms of the fraction of liquid surface renewed per time (s). The form of the liquid-film mass transfer coefficient (equation 2.9) is similar to that of penetration theory.

$$k_L^0 = \sqrt{D_{CO_2,L}\, s}$$

(2.9)

2.2.4 Eddy Diffusivity Theory

The most unfavorable aspect of either penetration or surface renewal theory is the complication that arises due to the incorporation of time. Eddy diffusivity theory, proposed by King (1966), is a model that predicts the "correct" relation of k_L^0 and $D_{CO2,L}$ without the introduction of a time variable (i.e., steady-state is assumed). The theory assumes diffusion to be the dominant process near the gas-liquid interface. As one

15

moves away from this interface toward the bulk liquid, the influence of convective fluid movement ("eddies"), denoted by e_d, becomes more and more significant. The differential material balance (equation 2.10) and predicted form of the liquid-film mass transfer coefficient (equation 2.11) are shown below.

$$\frac{\partial}{\partial x}\left[\left(D_{CO_2,L} + e_d x^2\right)\frac{\partial[CO_2]}{\partial x}\right] = 0 \qquad (2.10)$$

$$k_L^0 = \frac{2}{\pi}\sqrt{D_{CO_2,L} e_d} \qquad (2.11)$$

Glasscock (1990) demonstrated this solution to match the other theories within 5%.

2.3 MASS TRANSFER WITH CHEMICAL REACTION

Mass transfer with chemical reaction arises when the liquid contains a component that can react with the species diffusing from the gas. In this scenario, the absorption rate is enhanced beyond pure physical diffusion. Depending on the particular system, the rate can be classified as instantaneous, fast, intermediate, or slow. For an instantaneous system involving an irreversible reaction, the reacting species is consumed so quickly that the limiting factor is associated with its diffusion to the gas-liquid interface. In other words, the gas-film resistance completely dominates the mass transfer. For a fast system, the reacting species extends beyond the reaction interface into the liquid film, but its concentration goes to essentially zero before reaching the bulk liquid. An intermediate system is similar, except that the reacting species is not fully depleted in the liquid film and therefore its diffusion through the film is important as well. For a slow system, the

16

reacting species is able to diffuse entirely into the bulk liquid, which is where the reaction primarily occurs. For the purposes of the current work, the main regimes of concern are the fast and intermediate ones (Figure 2.3).
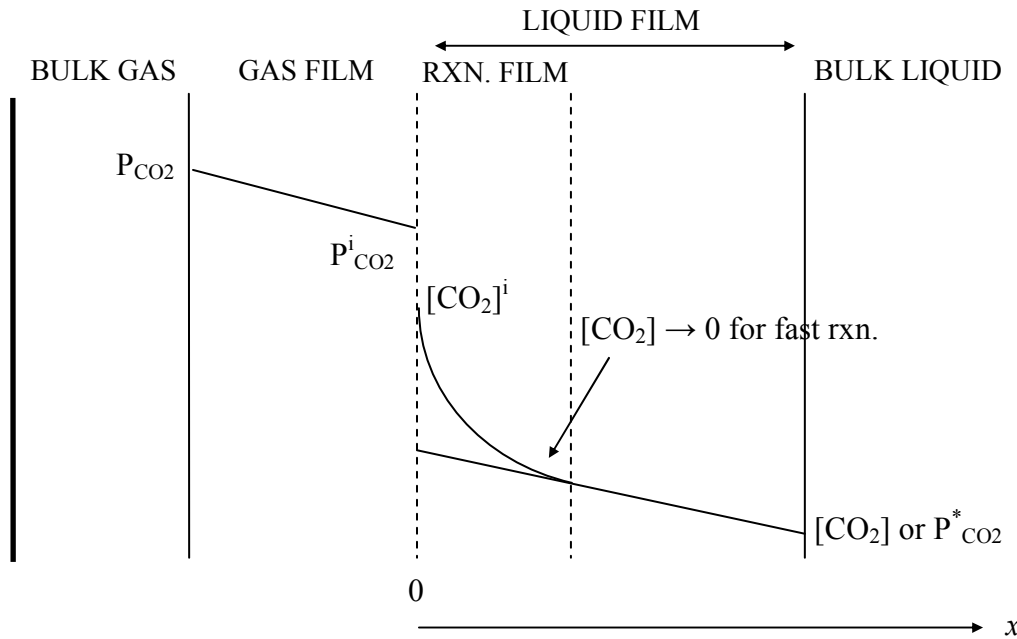
Figure 2.3. Film representation of absorption of CO$_2$ into liquid with chemical reaction.

The enhancement factor (E) is commonly encountered in scenarios involving absorption with chemical reaction. It reflects the increase in mass transfer due to the reaction relative to physical diffusion. An updated version of equation 2.1c that includes the enhancement factor is shown in equation 2.12. The parameters in this equation can be simplified into a single term, henceforth defined as k_g' (equation 2.13). Even though it is expressed in terms of a CO$_2$ partial pressure driving force (i.e., defined with gas-phase units), k_g' can, in a sense, be considered as a liquid-film mass transfer coefficient.

$$N_{CO_2} = \frac{E k_L^0}{H_{CO_2}} \left(P_{CO_2}^i - P_{CO_2}^* \right) \tag{2.12}$$

$$k_g{}' = \frac{E k_L^0}{H_{CO_2}} \tag{2.13}$$

The concept of k_g' has been utilized in past works (Cullinane, 2005; Dugas, 2009) as a convenient manner of analyzing and comparing the absorption performance of various CO_2-amine systems, since it allows for the presentation and relation of data without requiring knowledge of individual parameters like the Henry's constant (H_{CO2}). A revised form of the series resistance relation (equation 2.3) that includes k_g' is shown below.

$$\frac{1}{K_G} = \frac{1}{k_G} + \frac{1}{k_g{}'} \tag{2.14}$$

2.3.1 CO$_2$-NaOH Reaction Kinetics

The absorption of CO_2 into caustic (NaOH) solution, which typically falls into the category of mass transfer with fast chemical reaction, is of particular relevance to the present research. As such, the kinetic theory should be briefly discussed before proceeding. The reaction occurs in two steps:

$$CO_2(aq) + OH^- \leftrightarrow HCO_3^- \tag{2.15a}$$

$$HCO_3^- + OH^- \leftrightarrow CO_3^{2-} + H_2O \tag{2.15b}$$
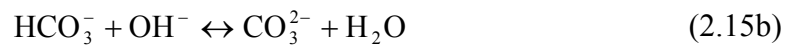
The rate of reaction 2.15b is much higher than that of reaction 2.15a. With sufficient free hydroxide, the concentration of bicarbonate (HCO_3^-) is negligible, and the overall reaction may be written as:

$$CO_2(aq) + 2OH^- \rightarrow CO_3^{2-} + H_2O \tag{2.16}$$
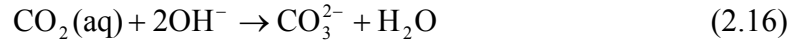
The reaction can be considered as practically irreversible, with a rate expression given by equation 2.17.

$$r = k_{OH^-}[OH^-][CO_2] \tag{2.17}$$

When CO_2 partial pressures are low and hydroxide ion is present in relative excess, the reaction can be treated as pseudo-first-order. The second-order rate constant (k_{OH^-}) and bulk hydroxide concentration can be combined into a pseudo-first-order rate constant (k_1). Equation 2.17 consequently simplifies to:

$$r \cong k_1[CO_2] \tag{2.18}$$

As a point of interest, the reaction of CO_2 with amines proceeds via an analogous mechanism (Wilson, 2004).

2.3.2 Pseudo-First-Order Reaction

The differential equation for mass transfer with the added dimension of chemical reaction (CO_2-NaOH) is shown in equation 2.19 under the assumption of pseudo-first-order conditions.

$$D_{CO_2,L} \frac{\partial^2[CO_2]}{\partial x^2} - k_1[CO_2] = \frac{\partial[CO_2]}{\partial t} \tag{2.19}$$

Bishnoi (2000) solved equation 2.19 and noted that the flux expression that ultimately results (equation 2.23) can be obtained regardless of the applied mass transfer theory (i.e., film theory, penetration theory, etc.). The solution using surface renewal theory was presented by Bishnoi and Rochelle (2000) and has been selected for display here. Equation 2.20 is obtained following application of the appropriate boundary conditions (equations 2.19a-c).

$$[CO_2] = [CO_2]^i @ x = 0 \tag{2.19a}$$

$$[CO_2] = 0 @ x = \infty \tag{2.19b}$$

$$[CO_2] = 0 @ t = 0 \tag{2.19c}$$

$$N_{CO_2} = k_L^0 \sqrt{1 + \frac{k_1 D_{CO_2,L}}{\left(k_L^0\right)^2}} \frac{\left(P_{CO_2}^i - P_{CO_2}^*\right)}{H_{CO_2}} \tag{2.20}$$

Equation 2.20 is notably relatable to equation 2.12 via the enhancement factor.

$$E = \sqrt{1 + \frac{k_1 D_{CO_2,L}}{\left(k_L^0\right)^2}} \tag{2.21}$$

The Hatta number (Ha) for pseudo-first-order reactions has been defined in various sources (Kucka et al., 2002; Haubrock et al., 2005):

$$Ha = \frac{\sqrt{k_1 D_{CO_2,L}}}{k_L^0} \tag{2.22}$$

For $Ha^2 \gg 1$, the Hatta number and enhancement factor are approximately equal and equation 2.20 can be simplified to:

$$N_{CO_2} \cong \frac{\sqrt{k_1 D_{CO_2,L}}}{H_{CO_2}} \left(P_{CO_2}^i - P_{CO_2}^* \right) \tag{2.23}$$

Combination of equations 2.12, 2.13, and 2.23 leads to the following theoretical expression for k_g':

$$k_g' = \frac{\sqrt{k_1 D_{CO_2,L}}}{H_{CO_2}} = \frac{\sqrt{k_{OH^-}[OH^-]D_{CO_2,L}}}{H_{CO_2}} \tag{2.24}$$

To legitimately interpret k_g' in this manner, Ha^2 must be large, and there must be minimal interfacial depletion of reactants. Haubrock et al. (2005), among others, quantified these requirements:

1. $Ha > 2$

2. $E_\infty / Ha > 5$

The enhancement factor for an instantaneous, irreversible reaction (E_∞) is expressed in equation 2.25.

$$E_\infty = 1 + \frac{D_{OH^-,L}[OH^-]H_{CO_2}}{D_{CO_2,L}P_{CO_2}^i} \tag{2.25}$$

The first criterion ensures that the "1 +" approximation is accurate. The second ensures that there is no interfacial depletion of reactants, which might arise due to (Bishnoi, 2000):

- An increase in CO_2 partial pressure at the interface.

- An increase in reaction kinetics (i.e., approach toward the instantaneous limit).

- A decrease in liquid-film mass transfer coefficients, whereby the transport of reactant to and removal of products from the interface becomes limited.

21

These criteria are discussed in the context of the experimental measurements in Chapter 4.

Chapter 3: Literature Review

A large amount of literature is available on the characterization of structured packing performance. The intent of this chapter is not necessarily to provide a comprehensive review of this vast library but rather to highlight some relevant studies – namely, on the topics of mass transfer area and hydraulics. Several investigations involving liquid flow over surfaces are first summarized. These investigations are beneficial to review in that they provide a detailed perspective of flow patterns not obtainable from macroscopic studies. The concept of rivulets also is the basis for some of the mechanistic mass transfer area models that are subsequently presented. A few studies that have employed more direct methodology to characterize the mass transfer area, as well as efforts that have sought to specifically evaluate the isolated impact of surface tension or viscosity, are discussed. Various hydraulic (pressure drop and hold-up) models are reviewed. Finally, a summary of the physical properties (liquid viscosity and surface tension) of several amine solvents is presented as well, in order to put the scope of the current project into context.

3.1 SURFACE FLOW STUDIES

3.1.1 Shi and Mersmann

The analysis of Shi and Mersmann (1985) was actually directed toward random packing, but the concepts logically extend to structured packing as well. The packing was considered to be composed of parallel, cylindrical flow channels. Liquid was assumed to flow in the form of uniformly distributed, freely spreading rivulets, which

partly wet the packing surface. The ratio of the wetted surface area to the total dry

packing area was reasoned to be directly dependent on rivulet width. Rivulet spreading

experiments on a 45°-inclined surface with dimensions of 400 mm (length) x 210 mm

(width) were conducted. Seven different plate materials and ten different solvent

systems, with viscosity and surface tension ranging respectively from around 1 to 21

mPa·s and 23 to 73 mN/m, were tested. Static systems were also examined to obtain a

relation between contact angle and film thickness. The data were used to fit theoretical

equations that had been proposed for the rivulet fluid mechanics under the assumption of

laminar flow. The result of this analysis was one of the earliest structured packing area

models (equation 3.1).

$$\frac{a_{\mathrm{w}}}{a_{\mathrm{p}}} = \frac{0.76 u_{\mathrm{L}}^{0.4} v_{\mathrm{L}}^{0.2}}{1 - 0.93\cos\gamma} \left(\frac{\rho_{\mathrm{L}}}{\sigma g}\right)^{0.15} \frac{a_{\mathrm{p}}^{0.2}}{\varepsilon^{0.6}} \tag{3.1}$$

Contact angle was correlated as having the strongest influence on the wetted area (a_{w}).

For reference, ceramics and stainless steel ranked on the low-end of the contact angle

spectrum (i.e., better wetting), whereas polypropylene and polytetrafluoroethylene were

on the high-end.

In the context of mass transfer, it is technically the effective area (a_{e}), rather than

the wetted area, that is of importance, since the latter incorporates "dead" or stagnant

zones not actively participating in mass transfer and neglects surfaces of liquid drops and

jets. To account for this difference, the authors proposed a small and strictly empirical

modification to equation 3.2:

$$\frac{a_e}{a_p} = a_f = \frac{0.76\,C_1\,d_{PE}^{1.1}\,u_L^{0.4}\,v_L^{0.2}}{1 - 0.93\cos\gamma}\left(\frac{\rho_L}{\sigma g}\right)^{0.15}\frac{a_p^{0.2}}{\varepsilon^{0.6}} \qquad (3.2)$$

3.1.2 McGlamery

McGlamery (1988) investigated the influence of surface topography on rivulet flow and mass transfer. Liquid film spreading experiments were performed on eight different stainless steel surfaces (660 mm x 126 mm), with viscosity and surface tension varying from roughly 1 to 11 mPa·s and 23 to 72 mN/m, respectively. Observations of the flow patterns over the textured surfaces, which could be categorized as flat (smooth), gauze, lanced, or embossed, were thoroughly documented. The main conclusions from the study were as follows:

- Roughness parallel to the flow direction reduced liquid spreading, whereas roughness normal to the flow path caused the liquid to drift laterally and therefore increased spreading.

- Depending on the surface texture, apparent contact angles could be larger (gauze or deep embossed surface) or smaller (lanced surface) than those on a flat surface. The contact angle data (measured via the sessile drop method), however, were acknowledged as being quite scattered due to both the surface topography and possible contamination. Furthermore, contact angles under conditions of flow were observed to be qualitatively lower than those under stationary conditions.

- Both roughness and perforations enhanced mass transfer. The enhancement from roughness was associated with increased turbulence, whereas the exact role of the perforations was not entirely clear.

- Solution of the Navier-Stokes equations under conditions of laminar flow did not adequately predict rivulet width.

3.1.3 Nicolaiewsky et al.

Nicolaiewsky et al. (1999) conducted rivulet flow studies on three stainless steel surfaces (smooth, perforated, or embossed) and on a ceramic surface. The tested fluids exhibited a surface tension range of 30.1 to 72.2 mN/m and an especially broad viscosity range of 0.75 to 125 mPa·s. The primary findings are summarized below:

- A higher viscosity both increased the thickness of liquid films and decreased the degree of spreading on the surfaces.

- Surface texture did not have a particularly noticeable impact on liquid spreading at a low viscosity, but greater spreading (associated with texture) was apparent at a viscosity in excess of 100 mPa·s.

- The correlated effect of contact angle on rivulet width (exponent of -0.26) was much weaker than that suggested by Shi and Mersmann (1985) (exponent of -1).

3.1.4 Cerro et al.

Cerro produced a series of publications in which the mechanics of film flow over structured-packing-like surfaces were characterized via both experiments and rigorous mathematical analyses.

In the first of these papers (Zhao and Cerro, 1992), the thickness profiles of different fluids over periodic surfaces (e.g., cylindrical rods, triangles, etc.) were evaluated. A theoretical equation for film thickness that was obtained via solution of the "classical" equations for flow on an inclined plate, such as might be demonstrated in a text like Bird et al. (2002), was presented and was termed the Nusselt film thickness (δ_{Nusselt}) – nomenclature that will be adopted by the present work as well.

$$\delta_{\text{Nusselt}} = \sqrt{\frac{3u_{\text{film}}\mu_{\text{L}}}{\rho_{\text{L}}g\sin\alpha}} = \sqrt[3]{\frac{3\mu_{\text{L}}}{\rho_{\text{L}}g\sin\alpha}\left(\frac{Q}{L_{\text{p}}}\right)} \qquad (3.3)$$

When the Nusselt film thickness was of the same order or larger than the amplitude of the solid surface structure, the film surface profile was flat, but at smaller thicknesses, the profile was observed to follow the contour or wavelength of the solid surface. Tests conducted with the surface most resembling structured packing always exhibited a flat film profile, although the authors speculated that thin-film conditions could be prevalent in sections of packing that were poorly irrigated. In nearly every case, the actual film thickness was larger and surface velocity was smaller than the corresponding Nusselt value. Three parameters were required to correlate the results: Nusselt film thickness, Reynolds number, and Capillary number.

27

Shetty and Cerro (1995) measured the thickness profiles of silicone oil on an inclined brass surface (510 mm x 178 mm) and compared them with numerical solutions. The results agreed well for both positive and negative plate angles (i.e., underside flow). Instabilities (i.e., surface waves and dripping of liquid off of the plate) were noted to develop at an inclination angle of -31° with respect to the vertical. These experiments were followed up in Shetty and Cerro (1998), using a corrugated stainless steel surface (432 mm x 203.2 mm). Films were observed to spread out on the upper side of the corrugated surface but reverted to rivulets when flowing on the underside, effectively causing spreading to stop after a few surface cycles. The authors acknowledged that the presence of adjacent corrugations (i.e., neighboring sheets in a packing bundle) were not accounted for and could play an important role in spreading, however.

3.1.5 Luo et al.

Luo et al. (2009) photographed the behavior of a water rivulet in a duct (120 mm x 16 mm x 215 mm) under conditions of countercurrent air flow. The range of liquid and gas rates was 0.2 to 1.4 cm^3/s and 0 to 1.7 m/s. The rivulet width was observed to be fairly independent of the gas, although it did exhibit a decrease on the order of 10 to 20% at the highest velocities. Furthermore, the gas rate effect appeared to be more pronounced at an inclination angle of 45° versus 60° (with respect to the horizontal). Increasing the angle from 30° to 60° resulted in a noticeable decrease in rivulet width, by about 30%.

3.1.6 Green

Green (2006) utilized x-ray computed tomography to generate 3-D images of stainless steel structured packing under irrigated conditions (with water). An example of one of these images is shown in Figure 3.1.
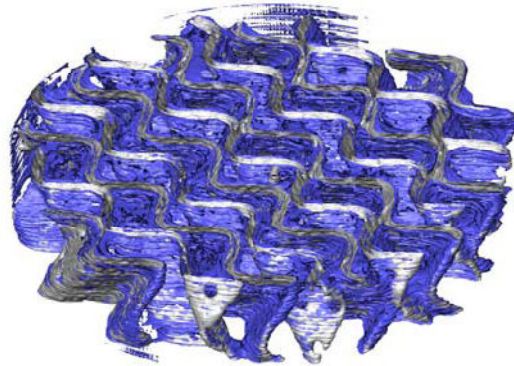
Figure 3.1. Image of Mellapak^{TM} 250Y at a liquid load of 36.6 m^3/m^2·h (15 gpm/ft^2), constructed by Green (2006). Wetted regions are indicated by blue.

Even under these moderate flow conditions, the packing was observed to be well coated, with films of liquid apparent on both the top and bottom sides of the sheets. Liquid menisci were visible in the packing channels and were speculated to be a function of water having a relatively high surface tension. The perforations were also found to be intermittently covered or bridged by liquid, suggesting that the missing surface area from the sheets due to these holes may not actually be too significant. While much useful information was obtained from these images, the speed and resolution of the measurement method was, unfortunately, not sufficient to be able to discern liquid film thicknesses or liquid dissociated from the packing surface (i.e., satellite droplets) with any precision.

3.1.7 Conclusions

The key observations and conclusions from the reviewed works are reiterated in the points below:

- Surface roughness or texture enhances mass transfer by increasing turbulence. It also can promote mass transfer by facilitating the spreading of liquid.

- An increase in liquid viscosity will result in films being thicker and spreading less.

- The liquid flow down the packing channels is not heavily influenced by the countercurrent gas. Both high gas velocities and steeper inclinations tend to decrease the spreading of the liquid.

- The structured packing surface is well wetted even under moderate flow conditions. Some flow on the underside of the packing sheets can be anticipated in addition to conventional flow over the top of the surface, but for the conventional channel geometries (45° or 60° with respect to the horizontal), this flow may not be entirely stable and may ripple or drop off of the surface. Liquid "bridges" and menisci are likely to form over the perforations and within the packing channels.

3.2 MECHANISTIC MASS TRANSFER AREA MODELS

The ordered layout of structured packing lends itself to a mechanistic analysis. Many mass transfer area correlations have been formulated in this manner, wherein fundamental principles or concepts have been applied in "building-up" the models. The

models of Rocha et al. (1996) and Billet and Schultes (1993), being perhaps the two most widely used correlations from the literature, are noteworthy and are discussed along with several other models of interest.

3.2.1 Separations Research Program (SRP)

Bravo et al. (1985), from the Separations Research Program (SRP) at the University of Texas at Austin, were among the first to offer a comprehensive mass transfer model for structured packing. Their work focused on Sulzer BX packing (finely woven gauze) and was based on experimental data with systems like *o/p*-xylenes and ethylbenzene/styrene, taken under total-reflux distillation conditions at atmospheric pressure or below. Correlations for the gas-film and liquid-film mass transfer coefficients were developed that many subsequent researchers have accepted as valid. The flow pathways through the packing were approximated as triangular or diamond-shaped channels, akin to a network of interconnected wetted-wall columns. Concepts such as "effective" gas and liquid velocities were introduced to account for the influence of the two phases on each other. Traditional relationships used to describe mass transfer in wetted-wall columns – namely, the correlation of Johnstone and Pigford (1942) for the gas-film mass transfer coefficient and penetration theory (Higbie, 1935) for the liquid-film mass transfer coefficient – were adapted to structured packing. Unfortunately, this early model was not especially relevant with respect to the mass transfer area, as it was argued that the gauze nature of the Sulzer BX packing would result in complete wetting

31

of the surface, such that $a_e = a_p$. An efficiency factor (β) was later proposed for sheet-metal packing in Fair and Bravo (1987):

$$a_e = \beta\, a_p \qquad (3.4)$$

This factor was empirically correlated with the approach to flooding in Fair and Bravo (1990).

$$\beta = 0.50 + 0.0058(\%\,\text{flood}) \qquad (3.5)$$

Equation 3.5 was stated to be valid for flooding percentages in the range of 0 to 85, with β being unity above 85% flooding.

Rocha et al. (1993, 1996) revised some of the ideas contained in the original SRP model. Central to this update was the contention that liquid hold-up should be intimately relatable to mass transfer efficiency, as well as to other factors such as pressure drop and flooding. The fractional area (a_f) was proposed as the product of F_{SE}, a factor accounting for variations in surface texture (0.35 for Mellapak packings), and F_t, a factor essentially related to hold-up. The fractional area model of Shi and Mersmann (1985), generalized slightly to allow for variable inclination angles, was assumed for the calculation of F_t.

$$a_f = F_{SE} F_t = F_{SE} \frac{29.12\, u_L^{0.4} v_L^{0.2} S^{0.359}}{(1 - 0.93\cos\gamma)(\sin\alpha)^{0.3}\, \varepsilon^{0.6}} \left(\frac{\rho_L}{\sigma g} \right)^{0.15} \qquad (3.6)$$

The contact angle was given by either equation 3.7a or 3.7b.

$$\cos\gamma = 5.211 \times 10^{-16.835\sigma} \quad \text{for } \sigma > 55 \text{ mN/m} \qquad (3.7a)$$

$$\cos\gamma = 0.9 \qquad\qquad \text{for } \sigma < 55 \text{ mN/m} \qquad (3.7b)$$

32

The mass transfer coefficients and effective phase velocities were given by equations 3.8-3.11. A factor that was defined to be slightly less than unity (C_E) was incorporated into the liquid-film mass transfer coefficient to account for regions in the packed bed not conducive to rapid surface renewal. Experiments showed this constant to typically be around 0.9 for structured packings.

$$k_G = \frac{0.054 D_G}{S} \left(\frac{(u_{Ge} + u_{Le}) \rho_G S}{\mu_G} \right)^{0.8} \left(\frac{\mu_G}{D_G \rho_G} \right)^{0.33} \qquad (3.8)$$

$$k_L^0 = 2\sqrt{\frac{D_L C_E u_{Le}}{\pi S}} \qquad (3.9)$$

$$u_{Ge} = \frac{u_G}{\varepsilon(1 - h_L)\sin\alpha} \qquad (3.10)$$

$$u_{Le} = \frac{u_L}{\varepsilon h_L \sin\alpha} \qquad (3.11)$$

The model was validated with mass transfer data (*HETP*) from various distillation studies (Table 3.1).

Table 3.1. Distillation databank used in Rocha et al. (1996).

Structured Packing	Specific area, a_p (m^2/m^3)	Chemical Systems
Flexipac-2	233	Cyclohexane/*n*-hexane
Gempak 2A	233	*o/p*-xylenes
Gempak 2AT	233	Ethylbenzene/styrene
Intalox 2T	213	Methanol/ethanol
Maxpak	229	Chlorobenzene/ethylbenzene
Mellapak 250Y	250	*i*-butane/*n*-butane
Mellapak 350Y	350	
Mellapak 500Y	500	
Sulzer BX	492	

3.2.2 Billet and Schultes

In the development of their correlation, Billet and Schultes (1993) started by proposing theoretical expressions for the liquid hold-up (equation 3.12) as well as for the liquid-film and gas-film mass transfer coefficients (equations 3.13 and 3.14), both of which were based on penetration theory.

$$h_L = \left(12 \frac{1}{g} \frac{\mu_L}{\rho_L} u_L a_p^2 \right)^{\frac{1}{3}} \tag{3.12}$$

$$k_L^0 = \frac{2}{\sqrt{\pi}} \sqrt{D_L \frac{u_L}{h_L l_\tau}} \tag{3.13}$$

$$k_G = \frac{2}{\sqrt{\pi}} \sqrt{D_G \frac{u_G}{(\varepsilon - h_L) l_\tau}} \tag{3.14}$$

A large database of absorption and desorption measurements involving approximately 70 different packings and 30 different chemical systems was then consulted. The packings were made from different materials (e.g., metal, ceramic, plastic, etc.) and were mostly of the dumped variety, but a few structured packings were also included. For reference, the features of the test systems are displayed below in Table 3.2 (liquid-phase controlled), Table 3.3 (gas-phase controlled), and Table 3.4 (mass transfer resistance in both phases).

Table 3.2. Physical properties of liquid-phase controlled systems used in Billet and Schultes (1993).

Chemical System	Liquid Density, ρ_L (kg/m^3)	Liquid Viscosity, μ_L (mPa·s)	Surface Tension, σ (mN/m)
Carbon dioxide / water	1003	1.14	74.0
Carbon dioxide / methanol	788	0.55	23.8
Carbon dioxide / buffer soln. (1)	1157	1.41	72.0
Carbon dioxide / buffer soln. (2)	1237	2.05	72.0
Carbon dioxide / 1.78 m NaCl	1040	1.08	76.0
Carbon dioxide-water / air	997	0.97	72.4
Carbon dioxide-air / water	998	1.00	72.7
Oxygen-water / air	996	0.94	72.0
Chlorine-air / water	997	0.98	72.0

Table 3.3. Physical properties of gas-phase controlled systems used in Billet and Schultes (1993).

Chemical System	Gas Density, ρ_G (kg/m^3)	Gas Viscosity, μ_G (mPa·s)	Surface Tension, σ (mN/m)
Air / water	1.188	0.018	72.5
Air / methanol	1.162	0.018	22.4
Air / benzene	1.162	0.018	27.4
Air / ethyl *n*-butyrate	1.162	0.018	21.8
Helium / water	0.159	0.020	71.3
Freon 12 / water	4.797	0.014	71.3
Ammonia-nitrogen / water	1.167	0.017	72.8
Ammonia-oxygen / water	1.291	0.021	72.2
Ammonia-air / 4% H2SO4 in water	1.180	0.018	59.4
Sulfur dioxide-air / 1.78 m NaOH	1.190	0.018	54.6
Sulfur dioxide-Freon 12 / 3 m NaOH	4.800	0.012	70.9
Chlorine-air / 2 m NaOH	1.150	0.018	70.9
Acetone-nitrogen / water	1.166	0.017	72.7

Table 3.4. Physical properties of systems with both liquid and gas-phase mass transfer resistance used in Billet and Schultes (1993).

Chemical System	Gas Density, ρ_G (kg/m³)	Gas Viscosity, μ_G (mPa·s)	Liquid Density, ρ_L (kg/m³)	Liquid Viscosity, μ_L (mPa·s)	Surface Tension, σ (mN/m)
Ammonia-air / water	1.188	0.018	999	1.03	72.7
Ammonia-propane / water	1.763	0.008	996	0.84	72.0
Ammonia-Freon 12 / water	4.929	0.011	998	0.96	72.4
Sulfur dioxide-air / water	1.150	0.018	989	0.98	70.0
Sulfur dioxide-oxygen / water	1.297	0.020	998	0.92	72.3
Acetone-air / water	1.162	0.018	997	0.86	72.1
Methanol-air / water	1.162	0.018	997	0.86	72.1
Ethanol-air / water	1.168	0.018	997	0.89	72.2
Carbon dioxide-air / 1 m NaOH	1.187	0.018	1043	1.25	75.0

Dimensional analysis showed that the data ($k_L{}^0 a_e$ and $k_G a_e$) were best fit by equations for the characteristic flow path length (l_τ) and fractional area in the following forms:

$$l_\tau = d_h = 4\frac{\varepsilon}{a_p} \tag{3.15}$$

$$a_f = 1.5\left(a_p d_h\right)^{-0.5}\left(\frac{u_L d_h}{\nu_L}\right)^{-0.2}\left(\frac{u_L^2 \rho_L d_h}{\sigma}\right)^{0.75}\left(\frac{u_L^2}{g d_h}\right)^{-0.45} \tag{3.16}$$

Viscosity was actually not varied much in any of the data sets that were used; the maximum viscosity was about 2 mPa·s. Surface tension values ranged from around 20 to 70 mN/m, but the majority of data collected were near 70 mN/m.

Billet and Schultes acknowledged that surface tension gradients along the height of the packed column could potentially affect the interfacial area and consequently discussed the incorporation of an additional layer of complexity to the model. For systems in which the surface tension does not change ("neutral") or increases ("positive")

along the top-to-bottom liquid flow path, equation 3.16 was accepted as valid. For "negative" systems, however, it was believed that the Marangoni effect – a phenomenon involving the flow of liquid away from regions of low surface tension – would need to be accounted for by multiplying equation 3.16 by an extra factor involving the Marangoni number, a ratio of surface tension forces to viscous forces.

The model was extended to conditions beyond the loading point in Billet and Schultes (1999). The database of measurements was expanded to include more test systems and packings, but the mass transfer area correlation presented in the 1993 publication was unchanged.

3.2.3 Delft

Predictive equations for both hydraulic and mass transfer performance were proposed as part of the Delft model (Olujic, 1997). The hydraulics were characterized by a rather complex set of equations (discussed in Section 3.5.3), but the mass transfer area was presumed to be a relatively simple function of liquid load (equation 3.17). Unique to this model was the explicit inclusion of a perforation factor, with Ω representing the fraction of packing surface area occupied by holes (usually 0.1 for perforated packings).

$$a_f = \frac{1 - \Omega}{1 + \dfrac{C_1}{u_L^{C_2}}} \tag{3.17}$$

The Delft correlation was updated to a modified version of the Onda et al. (1968) model in more recent publications (Olujic et al., 2001; Olujic et al., 2004).

$$a_f = (1 - \Omega)(a_f)_{Onda} \tag{3.18}$$

For reference, the Onda et al. model is shown in equation 3.19. This correlation was developed for random packings. Considering that the mass transfer area of structured packing is generally anticipated to be limited by its surface area and that the Onda et al. model prediction is capped by a fractional area limit of unity, however, it certainly can be thought of as having an inclination toward structured packing.

$$a_f = 1 - \exp\left[-1.45\left(\frac{\sigma_c}{\sigma}\right)^{0.75}\left(\frac{\rho_L u_L}{a_p \mu_L}\right)^{0.1}\left(\frac{u_L^2 a_p}{g}\right)^{-0.05}\left(\frac{\rho_L u_L^2}{\sigma a_p}\right)^{0.2}\right] \tag{3.19}$$

The σ_c term is defined as a material-specific critical surface tension and has a value of 75 mN/m for steel packings (Bravo and Fair, 1982).

3.2.4 Brunazzi et al.

Brunazzi et al. (1995), like Rocha et al. (1996), believed liquid hold-up to be at the center of the mass transfer problem. They utilized the geometric concepts in Shi and Mersmann (1985) and theorized that only the liquid hold-up and film thickness should be required to calculate the mass transfer area. Their model is shown in equation 3.20.

$$a_f = \frac{h_L}{\varepsilon}\frac{d_e}{4\delta_L} = \left(\frac{d_e}{4}\right)\left(\frac{h_L}{\varepsilon}\right)^{1.5}\left(\frac{\rho_L g \sin^2(\alpha)\varepsilon}{3\mu_L u_L}\right)^{0.5} \tag{3.20}$$

The Nusselt film thickness (equation 3.3) was assumed for the liquid film, and the equivalent diameter (d_e) had the same definition as the hydraulic diameter in the Billet and Schultes model (equation 3.15). Liquid hold-up was measured and was found to agree well with the correlation of Suess and Spiegel (1992), although the correlation was

noted to be slightly overpredictive at low liquid loads (below 6.75 m^3/m^2·h) and underpredictive at higher ones (above 6.75 m^3/m^2·h). Predicted values from the model compared favorably with experimental $K_G a_e$ data, obtained by absorbing 1,1,1-trichloroethane into a commercial solvent (Genosorb 300, with μ_L = 7.7 mPa·s and σ = 38.4 mN/m). A root-mean-square (RMS) error of 13.1% was calculated when Suess and Spiegel (1992) was used, and an error of 8.2% was calculated when their own experimental hold-up values were used.

3.2.5 Nawrocki et al.

Nawrocki et al. (1991) took an interesting approach by attempting to model the mass transfer area in a highly systematic fashion. The corrugated packing structure was simulated as a simple, ordered grid, and a 3-D liquid distribution matrix was created that enabled the computation of liquid flow at defined intersection points in the packing. Flow down a channel was assumed to necessarily be split into two rivulets at these regions: one proceeding down the original channel and the other flowing through the intersection point. Values for the split fraction were obtained from a fit of experimental liquid distribution data. Perforations were not accounted for in any manner. By utilizing the model for rivulet dimensions from Shi and Mersmann (1985) and keeping track of every meandering liquid stream, the wetted area could be calculated simply from the total surface area of the rivulets. Stagnant zones were assumed to be small, so that the effective and wetted areas were identical. No experimental validation was done, but the simulated values were found to agree well with the model of Onda et al. (1968).

39

3.2.6 Aroonwilas

Aroonwilas (2001) built upon the work of Nawrocki et al. (1991) by expanding on the complexity and constraints of the flow matrix. Depending on the particular geometry, a rivulet was potentially allowed to "skip" intersections, rejoining flow at a later point. The impact of perforations on flow pathways was factored in, although all liquid flow was still assumed to occur only on the upward-facing sides of the packing. Mass transfer data were collected for Gempak 4A, Mellapak 500Y, and Mellapak 500X structured packings using absorption of CO_2 into NaOH (1 to 2 mol/L) and into MEA (3 to 5.2 mol/L) in a 0.1 m ID acrylic column. Simulations were run that accepted inputs of gas and liquid feed conditions, initial liquid distribution pattern, number of packing elements, and geometric characteristics of the packing. These simulations were found to satisfactorily match the experimental results.

3.2.7 Ataki and Bart

Computational fluid dynamics (CFD) would seemingly lend itself to the characterization and modeling of the flow patterns within structured packing, and indeed, a number of efforts have attacked the problem in this manner. The work of Ataki and Bart (2006) is one investigation worth highlighting. The wetting of Rombopak 4M packing was simulated using a multi-phase flow volume-of-fluid (VOF) model in FLUENT under the assumptions of laminar liquid flow, no gas flow, and a constant static contact angle. The simulations showed that low viscosity liquids tended to bifurcate

upon reaching a packing sheet intersection, splitting into rivulets on the front and back of the sheets. A liquid with a high viscosity and contact angle, on the other hand, was more stable, remaining as a single rivulet. Visual experiments were carried out that affirmed the simulations. The effective area values that were obtained from the simulations were not fit too well by the Rocha et al. (1996) model (equation 3.6) initially, but after adjusting the surface enhancement factor (F_{SE}) to 0.604 and changing the exponent of the $(1 - 0.93\cos\gamma)$ contact angle term from 1 to 0.392, a much better correspondence was achieved. A correlation was also developed based on the CFD results. This is shown in equation 3.21.

$$a_f = 1.279 u_L^{0.372} \rho_L^{0.217} \mu_L^{0.0266} \sigma^{-0.243} \left(\cos\gamma\right)^{0.927} \tag{3.21}$$

A strong dependence on the contact angle was correlated, whereas the effect of viscosity was quite weak.

3.2.8 Conclusions

Many different approaches for modeling the mass transfer area of structured packing have been illustrated. However, it is important to recognize that a major aspect lacking from these studies was actual validation of the area. The correlation of Billet and Schultes (1993), for instance, was regressed from an extensive database of experimental measurements, but these consisted of overall mass transfer data ($k_L{}^0 a_e$ and $k_G a_e$) and required the assumption of certain forms for the mass transfer coefficients. One can easily envision the impact of different parameters (e.g., viscosity, surface tension, etc.) becoming confounded between the mass transfer coefficients and mass transfer area with

this approach, thereby making it difficult to trust the individual regressed models, even if the overall mass transfer performance is adequately predicted.

3.3 EXPERIMENTAL MASS TRANSFER AREA MEASUREMENTS

Strategies for obtaining standardized, comprehensive sets of mass transfer data have been discussed in Hoffman et al. (2007) and Rejl et al. (2009), although both works dealt exclusively with random packing. In general, investigations in the open literature that have focused on experimentally discerning or decoupling the mass transfer area are few and far between, especially when it comes to structured packing. Three known studies, in addition to the internal work associated with the SRP, are reviewed in the following sections. The basic idea is to take advantage of a chemical reaction, such that the flux becomes related solely to the effective area.

3.3.1 Henriques de Brito et al.

Henriques de Brito et al. (1994) were perhaps the first to report mass transfer area data for structured packing that had been determined independently of mass transfer coefficients. The kinetics of CO_2 absorption into fairly concentrated (1.6 to 2 mol/L) NaOH were measured in a wetted-wall column, and the results were incorporated into mass transfer area characterization studies of Mellapak 125Y, 250Y, and 500Y. Experiments were performed in a pilot-scale column equipped with a liquid distributor (527 points/m^2) over a range of liquid loads (12.3 to 71.5 m^3/m^2·h) and gas flow factors (0.85 to 3.25 (m/s)(kg/m^3)$^{0.5}$, or approximately 0.75 to 3 m/s in terms of superficial

velocities). Both the liquid-phase and gas-phase concentrations were measured, and the mass balance closure was around 20%. The liquid-phase analysis was assumed to be more trustworthy, though, and was exclusively used. Gas-side resistance was neglected in the calculations. An empirical relation was developed from the results:

$$a_f = 0.465 \ Re_L^{0.3} = 0.465 \left(\frac{\rho_L u_L}{\mu_L a_p} \right)^{0.3} \tag{3.22}$$

Even though density and viscosity were included as parameters in the model, these properties were never varied during the study. Interestingly, the correlation predicts fractional area values for water that are above unity even at low liquid loads and exceed two in some cases, which, as Murrieta et al. (2004) noted, is somewhat suspect. An anticipated decrease in fractional area with increasing geometric packing area (all other properties being equal) is also apparent. To rationalize these features, the authors suggested that mass-transfer-enhancing liquid flow instabilities (i.e., rippling or fragmentation into droplets) could be a factor. These would be more prominent in lower surface area packings like Mellapak 125Y, since the larger corrugation dimensions would necessarily imply longer film running lengths.

3.3.2 Weimer and Schaber

Weimer and Schaber (1997) measured the effective area of polypropylene and stainless steel versions of Mellapak 250Y. Their methodology consisted of absorbing CO_2 from air into solutions of NaOH or KOH with concentrations ranging from about 0.05 to 1 mol/L. The values obtained with KOH were slightly lower than those with

NaOH, which was presumably related to a discrepancy in the kinetics applied in the interpretation of the two systems. The KOH data were considered to be more appropriate to report, in the interest of being conservative. As might be expected, the stainless steel packing exhibited better wetting behavior than the plastic packing. The fractional area in this case increased from about 0.88 to 0.92 over a liquid load range of 15 to 30 $m^3/m^2 \cdot h$. The area also seemed to systematically increase with gas velocity (1 to 1.8 m/s), but the relative differences were not much larger than a few percent and were basically on the same order as the apparent error.

3.3.3 Dragan et al.

The effective area of Mellapak 750Y was evaluated by Dragan et al. (2000) in a 0.1 m (4 in) ID column. The test system involved the absorption of air-diluted CO_2 (5 to 10 mol %) into aqueous NaOH (0.5 or 1.0 mol/L). The liquid load and gas velocity were varied from 12.3 to 30.8 $m^3/m^2 \cdot h$ and 0.1 to 0.35 m/s respectively. Reported fractional area values were quite low, ranging from only 0.12 to 0.2. Like Henriques de Brito et al. (1994), the authors correlated the data as a Reynolds number-dependent equation (equation 3.23).

$$a_f = 0.1245 \, Re_L^{0.4} = 0.1245 \left(\frac{\rho_L d_p u_L}{\mu_L} \right)^{0.4} \qquad (3.23)$$

$$d_p = \frac{6(1-\varepsilon)}{a_p} \qquad (3.24)$$

3.3.4 Separations Research Program (SRP)

Packing characterization experiments are routinely conducted by the SRP. A 0.427 m (16.8 in) ID column with approximately 3 m (10 ft) of packing is used. Mass transfer area measurements are made by absorbing CO_2 from ambient air into 0.1 mol/L NaOH; the protocol is extensively covered in the next chapter. Typical liquid load and gas velocity operational limits are 2.5 to 75 $m^3/m^2 \cdot h$ and 0.6 to 1.5 m/s, respectively. A portion of the database was shown in Wilson (2004), but prior to this current body of work, no attempt has been made to publish the data generated from this apparatus or rigorously model the results.

3.3.5 Conclusions

For quick reference, the main features of the studies covered above have been summarized in Table 3.5. The breadth of data available in the open literature clearly needs to be expanded. Even including the SRP database, there is a need to test not just more packings, but specifically packings with geometric configurations other than the standard "Y" or 45°-inclination variety. None of the above studies ventured beyond the physical properties of water, so more work certainly can be done in this regard. Data quality is an issue too and is another aspect that could be improved in some of the cited studies. For instance, gas-film resistance was typically neglected, which may not necessarily have been a good assumption with the more concentrated caustic systems. Looking at specific examples, the high mass transfer area values obtained by Henriques de Brito (1994) were already called into question. For Dragan et al. (2000), it would be

logical to worry about wall effects being significant based on the column size that was

used.

Table 3.5. Sources of experimental mass transfer area data for structured packing.

Source	Structured Packing(s)	Chemical System	Liquid (L) and Gas (u_G) Loads	Column ID / Packing Height
Henriques de Brito et al. (1994)	Mellapak 125Y – 500Y (a_p = 125 – 500 m²/m³)	1 mol % CO_2 1.6 – 2 mol/L NaOH	L: 12 – 72 m³/m²·h (5 – 30 gpm/ft²) u_G: 0.75 – 3 m/s	0.295 m (11.6 in) / 0.42 m (1.4 ft)
Weimer and Schaber (1997)	Mellapak 250Y (a_p = 250 m²/m³)	Ambient air 0.05 – 1 mol/L KOH	L: 15 – 30 m³/m²·h (6 – 12 gpm/ft²) u_G: 1 – 1.8 m/s	0.242 m (9.5 in) / 2 m (6.6 ft)
Dragan et al. (2000)	Mellapak 750Y (a_p = 750 m²/m³)	5 – 10 mol % CO_2 0.5 – 1 mol/L NaOH	L: 12 – 31 m³/m²·h (5 – 13 gpm/ft²) u_G: 0.1 – 0.35 m/s	0.1 m (4 in) / 0.518 m (1.7 ft)
SRP (Wilson, 2004)	10+	Ambient air 0.1 mol/L NaOH	L: 2.5 – 75 m³/m²·h (1 – 30 gpm/ft²) u_G: 0.6 – 1.5 m/s	0.427 m (16.8 in) / 3 m (10 ft)

3.4 EFFECT OF LIQUID PROPERTIES ON MASS TRANSFER AREA

While models like Rocha et al. (1996) and Billet and Schultes (1993) drew upon large databanks of solvent systems exhibiting variable viscosity and surface tension values, no attempt was made to isolate the roles of these properties. Only a handful of studies have tried to discern the individual impact of viscosity or surface tension on the effective area. Most of these investigations are unfortunately limited to random packing, which might be expected to display different trends from structured packing, and not all employed the decoupled strategy that was described in the previous section. Nevertheless, they are worth reviewing for the qualitative ideas that they present.

3.4.1 Liquid Viscosity

3.4.1.1 Rizzuti et al.

Rizzuti et al. (1981) utilized the absorption of CO_2 into a buffer solution of 1 mol/L K_2CO_3/$KHCO_3$, with variable quantities of $KAsO_2$, to measure mass transfer area. The absorption apparatus was a 3.7 cm ID glass tube packed with glass Raschig rings (1 cm nominal size). Sugar was used to modify the viscosity over a relatively narrow range: approximately 0.9 to 1.55 mPa·s. Rizzuti et al. found there to be a direct relation between effective area and viscosity (exponent of 0.7). The sugar was presumed to have no effect on the reaction kinetics. The findings of Vázquez et al. (1989, 1997b) appear to refute this assumption, however, which casts some doubt on these results.

A slightly broader viscosity range (1.24 to 2.3 mPa·s) was examined in a follow-up study by Rizzuti and Brucato (1989). The same chemical system was used, although

48

the packed column was slightly larger than the previous one (8 cm ID). This time, two

distinct viscosity-related trends were observed. Effective area increased with viscosity at

first, up to a value of around 1.54 mPa·s. After this point, though, an inverse relationship,

coupled with a stronger viscosity effect, was seen. The authors suspected the reduction

of area at higher viscosities was caused by liquid bridging within the packing but were

unable to verify this hypothesis.

3.4.1.2 Nakajima et al.

Nakajima et al. (2000) also studied viscosity effects. The effective area of glass

Raschig rings (7 mm) was evaluated via a CO_2-NaOH absorption process in a glass

column (7.8 cm ID). Liquid was distributed at 33 points over the cross-section of the

column. Viscosity was regulated over the range of 0.95 to 4.5 mPa·s by the addition of

sugar. No mention was made of the kinetic impact of sugar, but as with the work of

Rizzuti et al. (1981, 1989), it is suspected that the results could have been confounded by

its presence. At lower gas velocities, interfacial area increased with liquid viscosity

initially, reached a maximum at about 2 mPa·s, and subsequently decreased upon further

increase of the viscosity. In contrast, at greater gas velocities, an inverse trend was

observed over the entire viscosity range. The authors postulated two mechanisms by

which viscosity could influence the generation of area. First, an increase in viscosity

would be expected to increase liquid retention in the packing and thus, wettability. An

elevated viscosity could, however, also reduce rippling and turbulence at the gas-liquid

interface and result in more liquid-phase stagnation. The reason that transitional behavior

49

was not observed in the latter case was because the high gas rates ensured appreciable liquid hold-up, such that the retention-related benefits associated with an increase in viscosity were masked. In contrast, the lower hold-up in general for the lower gas rate experiments enabled the initial "boost" from viscosity to have a measurable effect.

3.4.1.3 Nakov

Nakov (2000) studied the influence of viscosity in eight different "honeycomb"-type structured packings made of plastic and ceramic. The absorption column was rectangular (174 x 224 mm) and was equipped with a high density liquid distributor (10000 points/m^2). Absorption of NH_3 in aqueous H_2SO_4 was used as the test system, with sugar being employed to alter the viscosity. Liquid viscosity and density respectively varied from 1 to 10.3 mPa·s and 1000 to 1274 kg/m^3. Gas velocity was held constant at 1 m/s. Viscosity had a direct and rather strong impact on effective area at lower liquid loads (7 to 15 m^3/m^2·h). Above this limit, though, the fractional area appeared to asymptote at unity, regardless of viscosity.

3.4.2 Surface Tension

3.4.2.1 Sedelies et al.

Sedelies et al. (1987) employed an air-aqueous Na_2SO_3 system to characterize the effective area of polypropylene pall rings (25 mm) in a pilot-scale packed column. To test the impact of surface tension, surfactant (Tween® 20) was added to solutions, resulting in surface tension values of 35 mN/m. Unfortunately, massive foam formation

occurred, which severely limited the feasibility of the studies. The data that the authors managed to collect indicated no statistically confirmable influence of surface tension.

3.4.3 Conclusions

The key conclusions gleaned from the experiments discussed above have been compiled in Table 3.6. The results are confusing, to say the least. The relation between liquid viscosity and effective area cannot necessarily be summarized with a single label, but rather, may be a function of multiple factors, such as gas velocity or liquid load. This variability could explain why the mass transfer area models in the literature present such different, conflicting views. Not much can be said about surface tension, apart from the fact that to this point, it has seemed to draw less individual focus than viscosity.

Table 3.6. Literature studies focusing on effects of liquid viscosity or surface tension on mass transfer area.

Source	Packing	Chemical System	Viscosity (mPa·s)	Surface Tension (mN/m)	Findings / Conclusions
Rizzuti et al. (1981)	Random	Pure CO_2 1 mol/L K_2CO_3/$KHCO_3$ (with $KAsO_2$)	0.9 – 1.55 (sugar)	N/A	$a_e \sim \mu_L^{0.7}$
Rizzuti and Brucato (1989)	Random	Pure CO_2 1 mol/L K_2CO_3/$KHCO_3$ (with $KAsO_2$)	1.24 – 2.3 (sugar)	N/A	Direct relation of a_e and μ_L for $\mu_L < 1.5$ mPa·s Inverse relation for $\mu_L > 1.5$ mPa·s
Nakajima et al. (2000)	Random	2.5 mol % CO_2 0.8 – 1 mol/L NaOH	0.95 – 4.5 (sugar)	N/A	Low u_G: direct-to-inverse transition in relation bet/ a_e and μ_L at 2 mPa·s High u_G: always inverse relation
Nakov (2000)	Structured	NH_3 0.3 – 1.5 N H_2SO_4	1 – 10.3 (sugar)	N/A	Strong and direct effect of μ_L only at lower liq. loads (7 – 15 m³/m²·h)
Sedelies et al. (1987)	Random	Air Na_2SO_3	N/A	35 (Tween® 20)	Foaming issues and no conclusive influence of σ

52

3.5 SUMMARY OF MASS TRANSFER AREA MODELS

The mass transfer area models presented in the previous sections are compiled in Table 3.7 for convenient reference.

Table 3.7. Summary of referenced mass transfer area models.

Source	Fractional Area Model	Eqn.	Packing Basis
Shi and Mersmann (1985)	$a_f = \dfrac{0.76 C_1 d_{PE}^{1.1} u_L^{0.4} \nu_L^{0.2}}{1 - 0.93\cos\gamma}\left(\dfrac{\rho_L}{\sigma g}\right)^{0.15} \dfrac{a_p^{0.2}}{\varepsilon^{0.6}}$	(3.2)	Random
Rocha et al. (1996)	$a_f = F_{SE}\dfrac{29.12\, u_L^{0.4} \nu_L^{0.2} S^{0.359}}{(1-0.93\cos\gamma)(\sin\alpha)^{0.3}\,\varepsilon^{0.6}}\left(\dfrac{\rho_L}{\sigma g}\right)^{0.15}$	(3.6)	Structured
Billet and Schultes (1993)	$a_f = 1.5(4\varepsilon)^{-0.5}\left(\dfrac{4\varepsilon}{a_p}\cdot\dfrac{u_L}{\nu_L}\right)^{-0.2}\left(\dfrac{4\varepsilon}{a_p}\cdot\dfrac{u_L^2\rho_L}{\sigma}\right)^{0.75}\left(\dfrac{a_p}{4\varepsilon}\cdot\dfrac{u_L^2}{g}\right)^{-0.45}$	(3.16)	Random + Structured
Onda et al. (1968)	$a_f = 1 - \exp\left[-1.45\left(\dfrac{\sigma_c}{\sigma}\right)^{0.75}\left(\dfrac{\rho_L u_L}{a_p\mu_L}\right)^{0.1}\left(\dfrac{u_L^2 a_p}{g}\right)^{-0.05}\left(\dfrac{\rho_L u_L^2}{\sigma a_p}\right)^{0.2}\right]$	(3.19)	Random
Olujic et al. (2004)	$a_f = (1-\Omega)(a_f)_{Onda}$	(3.18)	Structured
Brunazzi et al. (1995)	$a_f = \left(\dfrac{d_e}{4}\right)\left(\dfrac{h_L}{\varepsilon}\right)^{1.5}\left(\dfrac{\rho_L g\sin^2(\alpha)\varepsilon}{3\mu_L u_L}\right)^{0.5}$	(3.20)	Structured
Ataki and Bart (2006)	$a_f = 1.279 u_L^{0.372}\rho_L^{0.217}\mu_L^{0.0266}\sigma^{-0.243}(\cos\gamma)^{0.927}$	(3.21)	Structured
Henriques de Brito et al. (1994)	$a_f = 0.465\left(\dfrac{\rho_L u_L}{\mu_L a_p}\right)^{0.3}$	(3.22)	Structured
Dragan et al. (2000)	$a_f = 0.1245\left[\dfrac{\rho_L u_L}{\mu_L}\cdot\dfrac{6(1-\varepsilon)}{a_p}\right]^{0.4}$	(3.23)	Structured

54

3.6 SUMMARY OF HYDRAULIC MODELS

3.6.1 Stichlmair et al.

Stichlmair et al. (1989) developed a generalized model for packed columns (random and structured), applicable over the full range of hydrodynamic conditions (i.e., dry to flooding). The basis of their approach was the particle model, in which the gas is assumed to flow around packing particles possessing a certain characteristic dimension. Liquid acts to increase this dimension and reduce the bed void fraction by adhering to the particle surface.

A correlation for the dry pressure drop (equation 3.25) was proposed based on the Ergun equation for packed beds.

$$\frac{\Delta P_{dry}}{Z} = f_0 \left[\frac{1-\varepsilon}{\varepsilon^3} \right] \frac{\rho_G u_G^2}{d_p} \tag{3.25}$$

$$f_0 = \frac{C_1}{Re_G} + \frac{C_2}{Re_G^{0.5}} + C_3 \tag{3.26}$$

$$Re_G = \frac{d_p u_G \rho_G}{\mu_G} \tag{3.27}$$

C_1, C_2, and C_3 are packing-specific constants. The introduction of liquid was theorized to affect the effective structure of the bed, modifying the parameters of porosity (ε), particle diameter (d_p) (given by equation 3.24), and friction factor (f_0). Incorporation of these changes led to an equation for the ratio of irrigated-to-dry pressure drop ($\Delta P/\Delta P_{dry}$).

$$\frac{\Delta P}{\Delta P_{dry}} = \left[\frac{1 - \varepsilon \left(1 - \frac{h_L}{\varepsilon} \right)}{1 - \varepsilon} \right]^{\frac{2+c}{3}} \left(1 - \frac{h_L}{\varepsilon} \right)^{-4.65} \tag{3.28}$$

$$c = \frac{-\dfrac{C_1}{Re_G} - \dfrac{C_2}{2 \, Re_G^{0.5}}}{f_0} \tag{3.29}$$

Equation 3.28 was asserted to be valid all the way through the loading point (i.e., the hydraulic region near flooding where the gas-liquid interaction starts to become especially strong). A correlation for hold-up below the loading point (equation 3.30) was provided that was validated with air/water data but was stated to be applicable for viscosities up to 5 mPa·s.

$$h_0 = 0.555 N_{Fr}^{\frac{1}{3}} \tag{3.30}$$

$$N_{Fr} = u_L^2 \frac{a_p}{g \varepsilon^{4.65}} \tag{3.31}$$

Above the loading point, hold-up was given by equation 3.32. The forces on the liquid (i.e., gas friction and the static pressure gradient produced by the pressure drop) have been combined in a dimensionless pressure drop term, $\Delta P/(Z\rho_L g)$.

$$h_L = h_0 \left[1 + 20 \left(\frac{\Delta P}{Z \rho_L g} \right)^2 \right] \tag{3.32}$$

An accurate value for the liquid hold-up was noted to be very important to the quality of the predicted pressure drop.

3.6.2 Rocha et al. (SRP)

As was mentioned in the discussion of the mass transfer area models, Rocha et al. treated structured packing as a network of wetted-wall columns and theorized that the effective area, pressure drop, and hold-up should all be related. The dry pressure drop (equation 3.33) was calculated from a conventional friction factor equation, with the friction factor being correlated from dry data for two packings.

$$\frac{\Delta P_{dry}}{Z} = \frac{0.177\rho_G}{S\varepsilon^2(\sin\alpha)^2}u_G^2 + \frac{88.774\mu_G}{S^2\varepsilon\sin\alpha}u_G \tag{3.33}$$

The irrigated pressure drop was based on a generic channel model (equation 3.34).

$$\frac{\Delta P}{Z} = \frac{\Delta P_{dry}}{Z}\left(\frac{1}{1-C_1 h_L}\right)^5 \tag{3.34}$$

The liquid hold-up was believed to be describable in terms of the liquid film thickness on the packing surface. The static hold-up contribution, which was later neglected for simplicity, was based on the static film studies performed by Shi and Mersmann (1985), and the operating contribution was based on the Nusselt film thickness (equation 3.3), modified to incorporate an effective liquid velocity (equation 3.11) and an effective gravity. The notion of effective gravity (g_{eff}) was proposed from a rationale that the liquid flowing down through the packing (via gravity) would be opposed by liquid buoyancy, vapor pressure drop, and drag on the liquid from the vapor, and was defined on the basis of this force balance:

$$g_{eff} = g\left[\left(\frac{\rho_L - \rho_G}{\rho_L}\right)\left(1 - \frac{\Delta P/Z}{\left(\Delta P/Z\right)_{flood}}\right)\right] \tag{3.35}$$

Systems with low phase density differences would be expected to be more prone to flooding, and equation 3.35 is indeed equipped to handle this fact, with g_{eff} approaching zero in this limit. Experimental (air-water) data were utilized in conjunction with the above concepts to develop a predictive correlation for hold-up (equation 3.36).

$$h_{\mathrm{L}} = \left(4\frac{F_{\mathrm{t}}}{S}\right)^{\frac{2}{3}}\left(\frac{3\mu_{\mathrm{L}}u_{\mathrm{L}}}{\rho_{\mathrm{L}}(\sin\alpha)\varepsilon g_{eff}}\right)^{\frac{1}{3}} \qquad (3.36)$$

The partial-wetting factor (F_{t}) was implicitly defined in equation 3.6. A consistent value of 1025 Pa/m was used by Rocha et al. for the flooding pressure drop in equation 3.35, which while not rigorously correct, simplified the analysis greatly and still yielded an adequate fit of the results. With the dry pressure drop and hold-up correlations established, the constant (C_1) in equation 3.34 was fit (again, using air-water data), and the final equation for pressure drop was obtained:

$$\frac{\Delta P_{dry}}{Z} - \frac{\Delta P}{Z}\left[1 - (0.614 + 71.35S)h_{\mathrm{L}}\right]^5 = 0 \qquad (3.37)$$

Overall, the approach of Rocha et al. was quite mechanistic and logical, but a good amount of empiricism (e.g., equations 3.33 and 3.37) was nevertheless still incorporated. The somewhat complex intertwining of pressure drop and hold-up within the model can also make its solution more difficult than some of the alternative hydraulic correlations.

3.6.3 Olujic et al. (Delft)

Of the hydraulic models reviewed here, the Delft model presented in Olujic et al. (2004) has by far the largest set of associated equations. The model employed some of

the same ideas as Rocha et al., such as effective gas and liquid velocities (albeit with slightly different definitions), and added a few other terms as well. These terms are presented in the equations below.

$$u_{Ge} = \frac{u_G}{(\varepsilon - h_L)\sin\alpha} \tag{3.38}$$

$$u_{Le} = \frac{u_L}{\varepsilon h_L \sin\alpha_L} \tag{3.39}$$

The liquid flow path was not considered to necessarily follow along the packing corrugation angle. Thus, an effective liquid flow angle was introduced:

$$\alpha_L = \arctan\left[\frac{\cos(90-\alpha)}{\sin(90-\alpha)\cos\left[\arctan\left(\frac{B}{2h}\right)\right]}\right] \tag{3.40}$$

Reynolds numbers based on effective (Re_{Ge}) and relative (Re_{Grv}) velocities were defined:

$$Re_{Ge} = \frac{\rho_G u_{Ge} d_{hG}}{\mu_G} \tag{3.41}$$

$$Re_{Grv} = \frac{\rho_G (u_{Ge} + u_{Le}) d_{hG}}{\mu_G} \tag{3.42}$$

Several geometry-based terms were also established. The packing channel dimensions (S, B, h) were related in a triangular fashion:

$$S = \sqrt{\frac{B^2}{4} + h^2} \tag{3.43}$$

59
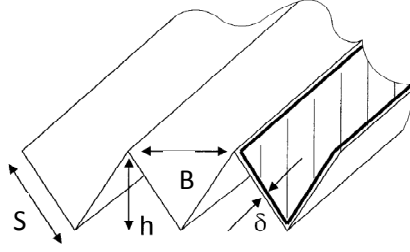
Figure 3.2. Packing channel dimensions. Slightly modified version of image from Olujic et al. (1999).

The specific area of the packing was not assumed to be the nominal (i.e., vendor-specified) area but rather, was defined using the channel dimensions.

$$a_p = \frac{4S}{Bh} \tag{3.44}$$

The fraction of the gas flow channel cross-section occupied by the liquid film was given by φ.

$$\varphi = \frac{2S}{B + 2S} \tag{3.45}$$

The hydraulic diameter of the triangular gas flow channel was specified as:

$$d_{hG} = \frac{\dfrac{(Bh - 2\delta_L S)^2}{Bh}}{\left[\left(\dfrac{Bh - 2\delta_L S}{2h}\right)^2 + \left(\dfrac{Bh - 2\delta_L S}{B}\right)^2\right]^{0.5} + \dfrac{Bh - 2\delta_L S}{2h}} \tag{3.46}$$

The Nusselt film thickness (equation 3.3) was assumed applicable for the liquid film.

Under dry conditions, equation 3.46 reduces to a much simpler form:

$$d_{hG,dry} = \frac{2Bh}{B + 2S} \tag{3.47}$$

60

The pressure drop prediction was predicated on the fundamental notion that gas-liquid interactions (GL), gas-gas interactions (GG), and directional changes (DC) would all contribute. The associated interaction coefficients and friction factors were respectively denoted by ζ and ξ.

$$\frac{\Delta P}{Z} = \frac{\Delta P_{GL} + \Delta P_{GG} + \Delta P_{DC}}{Z} = \frac{\left(\zeta_{GL} + \zeta_{GG} + \zeta_{DC}\right)}{Z} \cdot \frac{\rho_G u_{Ge}^2}{2} \tag{3.48}$$

$$\zeta_{GL} = \varphi \xi_{GL} \frac{Z}{d_{hG} \sin\alpha} \tag{3.49}$$

$$\xi_{GL} = \left\{ -2\log_{10}\left[\frac{\left(\frac{\delta_L}{d_{hG}}\right)}{3.7} - \frac{5.02}{Re_{Grv}}\log_{10}\left(\frac{\left(\frac{\delta_L}{d_{hG}}\right)}{3.7} + \frac{14.5}{Re_{Grv}}\right)\right]\right\}^{-2} \tag{3.50}$$

$$\zeta_{GG} = (1-\varphi)\xi_{GG} \frac{Z}{d_{hG} \sin\alpha} \tag{3.51}$$

$$\xi_{GG} = 0.722(\cos\alpha)^{3.14} \tag{3.52}$$

$$\zeta_{DC} = n_{pe}\left(\xi_{bulk} + \psi\xi_{wall}\right) \tag{3.53}$$

$$\psi = \frac{2h_{pe}}{\pi d_c^2 \tan\alpha}\left(d_c^2 - \frac{h_{pe}^2}{\tan^2\alpha}\right)^{0.5} + \frac{2}{\pi}\arcsin\left(\frac{h_{pe}}{d_c \tan\alpha}\right) \tag{3.54}$$

$$\xi_{bulk} = 1.76(\cos\alpha)^{1.63} \tag{3.55}$$

$$\xi_{wall} = \frac{4092u_L^{0.31} + 4715(\cos\alpha)^{0.445}}{Re_{Ge}} + 34.19u_L^{0.44}(\cos\alpha)^{0.779} \tag{3.56}$$

An enhancement factor (F_{load}) was incorporated to account for the pressure drop behavior in the loading region.

$$\left(\frac{\Delta P}{Z}\right)_{\text{load}} = \left(\frac{\Delta P}{Z}\right) F_{\text{load}} \tag{3.57}$$

$$F_{\text{load}} = 3.8 \left(\frac{F_G}{F_{G,\text{lp}}}\right)^{\frac{2}{\sin\alpha}} \left(\frac{u_L^2}{\varepsilon^2 g d_{hG}}\right)^{0.13} \tag{3.58}$$

The gas flow factor at the loading point was given by:

$$F_{G,\text{lp}} = \left[0.053\varepsilon^2 g d_{hG} \left(\frac{\rho_L - \rho_G}{\rho_G}\right)\left(u_L \sqrt{\frac{\rho_L}{\rho_G}}\right)^{-0.25} (\sin\alpha)^{1.24}\right]^{0.57} \sqrt{\rho_G} \tag{3.59}$$

The Delft model can be considered as very rational in its treatment of the pressure drop, but it is a little inconvenient that so many specific equations were deemed necessary to characterize the problem.

3.6.4 GPDC

The generalized pressure drop correlation (GPDC) method enables (in theory) packing pressure drop to be universally represented on a graphical basis as a function of a flow parameter (F_{lv}) and capacity parameter (*CP*). The most up-to-date version of the GPDC for structured packings was published by Kister et al. (2007) and has been reproduced in Figure 3.3.
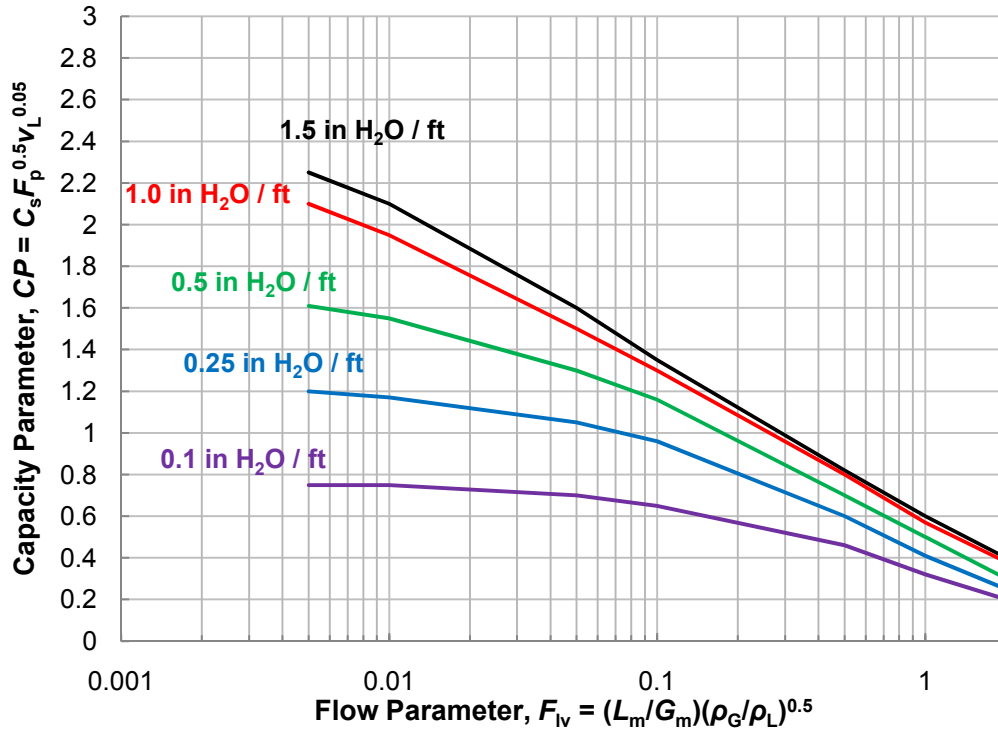
Figure 3.3. GPDC chart for structured packing.

The chart coordinates are given by equations 3.60 and 3.61.

$$F_{lv} = \left(\frac{L_m}{G_m} \right) \left(\frac{\rho_G}{\rho_L} \right)^{0.5} \tag{3.60}$$

$$CP = C_S F_P^{0.5} v_L^{0.05} \tag{3.61}$$

The flow parameter is representative of the ratio of liquid and vapor kinetic energies. The capacity parameter itself consists of a packing factor (F_P), dependent on packing size and shape, and a C-factor (C_S), which represents the ratio of vapor momentum and gravity forces on the liquid in the column (equation 3.62). The form of equation 3.61 is based off of English units, with C_s in ft/s, F_p in ft^{-1}, and v_L in centistokes.

$$C_S = u_G \left(\frac{\rho_G}{\rho_L - \rho_G} \right)^{0.5} \tag{3.62}$$

3.6.5 Suess and Spiegel (Hold-up)

Suess and Spiegel (1992) focused on obtaining pre-loading hold-up measurements in structured packing and specifically evaluated the influence of packing inclination angle and liquid viscosity. Given that these factors were of much interest in the context of the present work, an examination of their study is believed to be worthwhile, even though it is somewhat less comprehensive than the hydraulic models covered in the previous sections. The hold-up of three packings (Mellapak 250Y, Mellapak 500Y, and Mellapak 250X) was measured in a transparent PVC column with an inside diameter of 1 m (3.3 ft) using a gamma ray imaging technique. Liquid load was varied from 5 $m^3/m^2{\cdot}h$ all the way up to 200 $m^3/m^2{\cdot}h$. The packing angle was concluded to have a negligible effect on hold-up. Viscosity (up to 30 mPa·s) was found to affect hold-up with a 0.25 power dependence. For liquid loads below 40 $m^3/m^2{\cdot}h$, the hold-up (on a percent basis) was correlated in the following form:

$$h_L\left(\%\right)=0.0169a_p^{0.83}L^{0.37}\left(\frac{\mu_L}{\mu_{w,0}}\right)^{0.25} \tag{3.63a}$$

The liquid load term (L) in equation 3.63a is in units of $m^3/m^2{\cdot}h$, and the reference viscosity ($\mu_{w,0}$) denotes the viscosity of water at 20°C (approximately 1.002 mPa·s). A different correspondence with liquid load was observed above 40 $m^3/m^2{\cdot}h$. The calculated hold-up for this case is shown in equation 3.63b.

$$h_L\left(\%\right)=0.0075a_p^{0.83}L^{0.59}\left(\frac{\mu_L}{\mu_{w,0}}\right)^{0.25} \tag{3.63b}$$

3.6.6 Summary

The primary equations (i.e., dry and irrigated pressure drop) associated with the Stichlmair et al. (1989), Rocha et al. (1993), and Olujic et al. (2004) hydraulic models are summarized in Table 3.8.

Table 3.8. Summary of referenced hydraulic (pressure drop) models.

Source	Pressure Drop Model	Eqn.	Packing Basis
Stichlmair et al. (1989)	$$\frac{\Delta P_{dry}}{Z} = \left(\frac{f_0}{\varepsilon^3}\right)\left(\frac{\rho_G u_G^2 a_p}{6}\right)$$	(3.25)	Random + Structured
	$$\frac{\Delta P}{\Delta P_{dry}} = \left[\frac{1-\varepsilon\left(1-\dfrac{h_L}{\varepsilon}\right)}{1-\varepsilon}\right]^{\frac{2+c}{3}} \left(1-\frac{h_L}{\varepsilon}\right)^{-4.65}$$	(3.28)	
Rocha et al. (1993)	$$\frac{\Delta P_{dry}}{Z} = \frac{0.177\rho_G}{S\varepsilon^2(\sin\alpha)^2}u_G^2 + \frac{88.774\mu_G\,u_G}{S^2\,\varepsilon\sin\alpha}$$	(3.33)	Structured
	$$\frac{\Delta P_{dry}}{Z} - \frac{\Delta P}{Z}\left[1-(0.614+71.35S)h_L\right]^5 = 0$$	(3.37)	
Olujic et al. (2004)	$$\frac{\Delta P}{Z} = \frac{(\zeta_{GL} + \zeta_{GG} + \zeta_{DC})}{Z}\cdot\frac{\rho_G u_{Ge}^2}{2}$$	(3.48)	Structured
	$$\left(\frac{\Delta P}{Z}\right)_{load} = \left(\frac{\Delta P}{Z}\right)\left[3.8\left(\frac{F_G}{F_{G,lp}}\right)^{\frac{2}{\sin\alpha}}\left(\frac{u_L^2}{\varepsilon^2 g d_{hG}}\right)^{0.13}\right]$$	(3.57)	

66

3.7 PHYSICAL PROPERTIES OF AMINE SOLUTIONS

Given that a key objective of this project is the development of a mass transfer area model that is specifically capable of modeling the performance of aqueous amines in a CO_2 capture system, an assessment of the physical properties of these solvents is worthwhile, in order to gain an idea of the necessary breadth of experimental conditions. Particular solvents of interest include:

- 7 m (30 wt %) MEA (monoethanolamine);

- 11 m (40 wt %) MEA;

- 8 m PZ (piperazine) at a loading of 0.4;

- Potassium-promoted PZ (5 m K^+ / 2.5 m PZ);

- 4 mol/L MDEA (methyldiethanolamine) / 0.6 mol/L PZ;

- 4.8 m AMP (2-amino-2-methyl-1-propanol);

- 8 m 2-PE (2-piperidineethanol);

- 6 m AEP (1-(2-Aminoethyl)piperazine);

- 12 m EDA (ethylenediamine);

- 10 m DGA (diglycolamine);

- 7.7 m HEP (*n*-(2-hydroxyethyl)piperazine).

As a reminder, the molal (m) concentrations of the amine solvents presented throughout this document refer to a basis of moles of solute per kilogram of water.

3.7.1 MEA

Weiland et al. (1998) measured the viscosity of several aqueous amines at 25°C and loadings up to 0.5, with loading referring to a CO_2-enriched solution and henceforth defined on a basis of mol CO_2/mol alkalinity unless otherwise indicated. Among the examined solvents were 30 and 40 wt % MEA, which exhibited a minimum viscosity of 2.52 mPa·s (30 wt % MEA, unloaded) and a maximum of 6.73 mPa·s (40 wt % MEA, 0.5 loading). The authors combined their data with results from other sources to develop a correlation for viscosity dependent on amine mass %, temperature, and loading.

Vázquez et al. (1997a) measured the surface tension of unloaded MEA (30 and 40 wt %) from 25 to 50°C. The surface tension of the MEA solutions decreased from approximately 60 to 55 mN/m over this temperature range.

3.7.2 PZ

Freeman et al. (2010) reported the viscosity of concentrated (7 m to 10 m) PZ solutions at 40°C and a loading of 0.4. The viscosity of 8 m PZ at these conditions was roughly 11 mPa·s.

The surface tension of 8 m PZ (0.3 loading) at ambient conditions (20°C) has been measured by the Rochelle group at the University of Texas at Austin using both a ring tensiometer and a pendant drop technique, but the results have not been formally published. Values from the former method were around 60 mN/m, whereas those from the latter were slightly higher than water (77 mN/m). The inconsistency between the two procedures could have been related to the cleanliness of the ring or pendant drop needle.

68

Derks et al. (2005) made surface tension measurements of aqueous PZ at 20 and 40°C, as well, but only worked with dilute solutions (0.5 to 1.5 mol/L). The surface tension was similar to water and decreased slightly (68.5 to 67.6 mN/m at 40°C) with the addition of PZ.

3.7.3 Potassium-promoted PZ

Cullinane (2005) evaluated the viscosity of 5 m K^+ / 2.5 m PZ blends from 25 to 70°C and at a constant loading of 0.667, defined here as mol CO_2/(mol K^+ + mol PZ). The viscosity was 2.77 mPa·s at 40°C and varied from 4.15 to 1.42 mPa·s over the whole temperature spectrum.

3.7.4 MDEA/PZ

Paul and Mandal (2006a, 2006b) generated viscosity (15 to 60˚C) and surface tension (20 to 50˚C) data for a variety of unloaded MDEA/PZ solutions, ranging from a 27/3 wt % blend (roughly translating to 2.3 mol/L MDEA / 0.4 mol/L PZ) to a 18/12 wt % blend (1.5 mol/L MDEA / 1.4 mol/L PZ). The total MDEA/PZ concentration was always kept at 30 wt %. Paul and Mandal did not examine the particular combination of interest (4 mol/L MDEA / 0.6 mol/L PZ) but did propose a viscosity correlation based on concentration and temperature that could possibly be extrapolated. No correlation was given for surface tension, but based on the presented results, a value between 50 and 60 mN/m might be inferred for the aforementioned MDEA/PZ blend.

3.7.5 AMP

The viscosity of 4.8 m AMP (roughly 8 mol %) at 40°C was reported in Rochelle et al. (2009) over loadings from 0.15 to 0.58; values increased from 2.73 to 4.10 mPa·s. Viscosity data for AMP were published by Henni et al. (2003) as well, for unloaded solutions from 25 to 70°C. 4.8 m AMP was not explicitly tested but was encompassed within the range of concentrations; its viscosity could be estimated as 3.8 to 1.0 mPa·s over the aforementioned temperatures and about 2.2 mPa·s at 40°C specifically.

Vázquez et al. (1997a) measured the surface tension of aqueous AMP in addition to MEA. The surface tension of 4.8 m AMP decreased from 43.41 to 40.43 mN/m from 25 to 50°C.

3.7.6 Other Solvents

The viscosity of the remainder of listed solvents has been measured by the Rochelle group at 40°C (Rochelle et al., 2009). For 8 m 2-PE, viscosity varied from 11.42 to 23.47 mPa·s over a loading range from 0.21 to 0.61. 6 m AEP was characterized up to a loading of 0.36 and exhibited viscosity values from 10.27 (unloaded) to 26.2 mPa·s (the curves for 2-PE and AEP in the referenced report were actually switched). The viscosity of 12 m EDA increased from 4.59 to 14.15 mPa·s as the CO_2 loading increased from 0.1 to 0.49. 10 m DGA (not shown in the referenced citation but measured in conjunction with these solvents) was characterized from a loading of 0.2 to 0.49. Viscosity changed from 5.86 to 8.78 mPa·s over this range. 7.7 m HEP was

measured to have a viscosity of 13.24 mPa·s at a loading of 0.01 and a viscosity of 18.8 mPa·s at a loading of 0.27.

3.7.7 Conclusions

A synopsis of the physical property data is provided in Table 3.9. Gaps in information are evident, especially with respect to loading effects. At the concentrations of interest, MEA appears to be the amine closest to water in terms of both viscosity and surface tension (approximately 1 mPa·s and 72 mN/m at ambient conditions for water), although AMP and potassium-promoted PZ do not deviate too much on a viscosity basis and PZ is not far off on a surface tension basis. The viscosity of the amine solvents can, for the most part, be considered to fall within about a factor of ten of that of water. Likewise, the surface tension of these solvents is smaller by two-fold at most. Based on these general observations, an experimental design consisting of a viscosity range from 1 to 10 mPa·s and a surface tension range from 30 to 72 mN/m would seem to be sufficient to characterize the majority of relevant amines.

Table 3.9. Sources of physical property data for amine solutions.

Solvent	T (°C)	Loading	Viscosity (mPa·s)	Surface Tension (mN/m)	Source
7 m MEA	25	0 – 0.5	2.52 – 3.82		Weiland et al. (1998)
	25 – 50	Unloaded		60.41 – 56.36	Vázquez et al. (1997a)
11 m MEA	25	0 – 0.5	3.41 – 6.73		Weiland et al. (1998)
	25 – 50	Unloaded		58.74 – 54.67	Vázquez et al. (1997a)
8 m PZ	40	0.4	11		Freeman et al. (2010)
	20	0.3		60 – 77	The University of Texas at Austin
5 m K⁺ / 2.5 m PZ	25 – 70	0.667	4.15 – 1.42		Cullinane (2005)
MDEA / PZ (27/3 – 18/12 wt %)	15 – 60	Unloaded	4.007 – 0.871 (27/3 wt % blend)		Paul and Mandal (2006b)
	20 – 50	Unloaded		55.66 – 50.78 (27/3 wt % blend)	Paul and Mandal (2006a)
4.8 m AMP (8 mol %)	40	0.15 – 0.58	2.73 – 4.10		Rochelle et al. (2009)
	25 – 70	Unloaded	3.8 – 1.0 (interpolated)		Henni et al. (2003)
	25 – 50	Unloaded		43.41 – 40.43	Vázquez et al. (1997a)
8 m 2-PE	40	0.21 – 0.61	11.42 – 23.47		Rochelle et al. (2009)
6 m AEP	40	0 – 0.36	10.27 – 26.2		Rochelle et al. (2009)
12 m EDA	40	0.1 – 0.49	4.59 – 14.15		Rochelle et al. (2009)
10 m DGA	40	0.2 – 0.49	5.86 – 8.78		The University of Texas at Austin
7.7 m HEP	40	0.01 – 0.27	13.24 – 18.8		Rochelle et al. (2009)

Chapter 4: Experimental Methods

The experimental equipment, methods, and materials used in this work are described in this chapter. The primary equipment consisted of a wetted-wall column and a pilot-scale packed column. Supplementary equipment was required to analyze the inorganic carbon (CO_3^{2-}) content and physical properties (surface tension, viscosity, and density) of samples.

4.1 WETTED-WALL COLUMN (WWC)

A wetted-wall column (WWC) was used for CO_2 absorption rate measurements. The apparatus was originally built by Mshewa (1995) and has been most recently used by Cullinane (2005) and Dugas (2009) to measure the kinetics of CO_2-amine systems.

4.1.1 Equipment Description

The WWC (Figure 4.1) was constructed from a stainless steel tube of 1.26-cm OD and had an exposed length of 9.1 cm. Liquid was pumped up through the inside, emerging at the top and overflowing down the outside in a smooth, thin film. The specified contact area of 38.52 cm^2 was calculated from a summation of the tube body and tip, where the liquid overflow was assumed to be hemispheric in form. The column was enclosed in a glass tube (2.54-cm OD), forming the reaction chamber. This chamber was further enclosed in a second thick-walled glass cylinder (10.16-cm OD) in which paraffin oil was circulated to maintain a constant, uniform temperature in the reaction chamber.

73
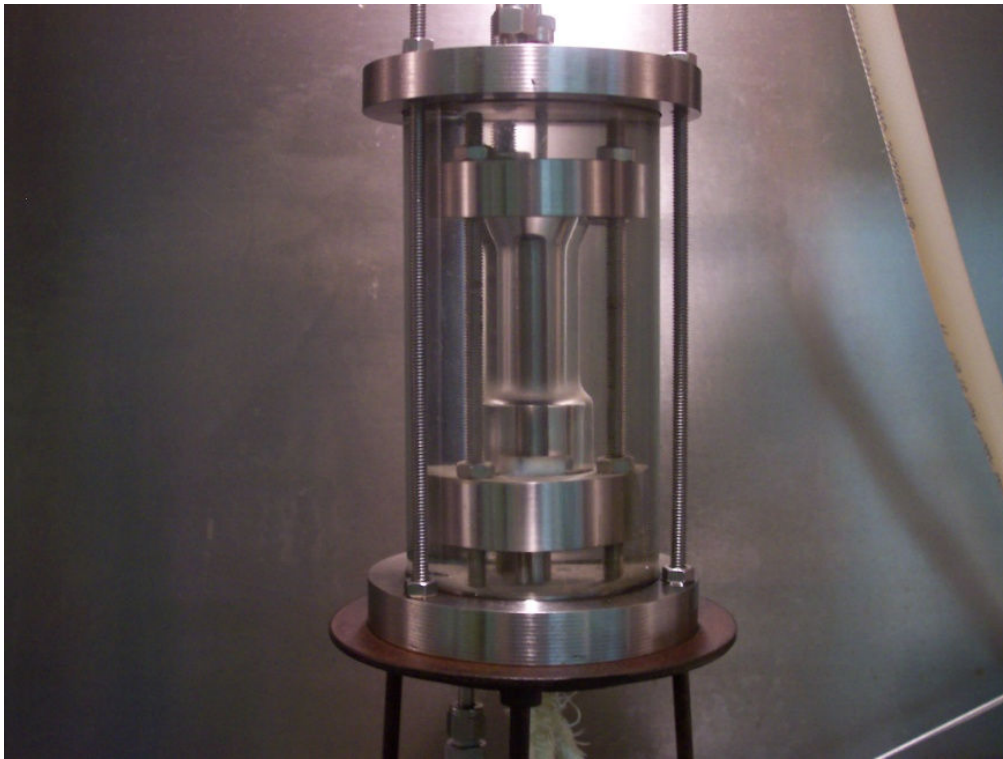
Figure 4.1. Photograph of WWC (above) and reaction chamber schematic (below).
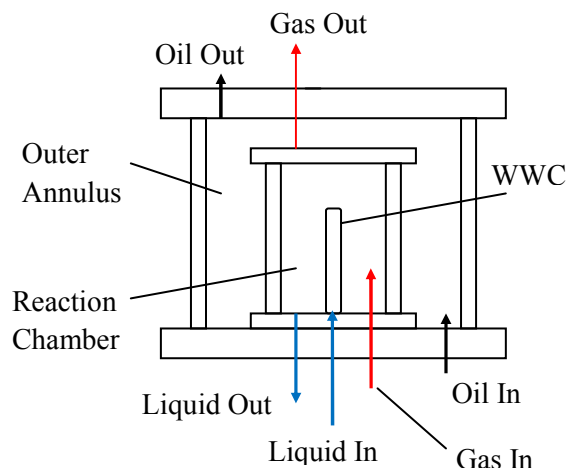
Figure 4.2 illustrates the entire experimental set up. The system was constructed using 1/4-in OD stainless steel tubing and Swagelok® fittings. A cloth fiber wrapping was used to insulate the tubing. Gas was supplied from both a N_2 Dewar and a cylinder

74

of N_2 with 5000 ppm$_v$ CO_2. Flow rates were controlled using Brooks Instrument Series 5850 mass flow controllers that were connected to a master control box (UT #406554). A 15 sLpm (standard L/min) controller (S/N 9103HC037044/001) and a 2 sLpm controller (S/N 9310HC038406/002) were respectively used for the N_2 and CO_2/N_2. The controllers were calibrated via the soap bubble displacement procedure described by Goff (2005). The mixed gas stream was pre-heated and saturated via bubbling through a water-filled stainless steel cylinder that was immersed in a temperature bath (Grant Heating Bath). The gas passed through a second temperature bath (Fisher Scientific Isotemp 3016H) before entering at the bottom of the reaction chamber and flowing upward in a countercurrent contacting process. The gas was introduced through a single inlet point that was encased in a funnel-shaped Teflon ring, intended to prevent the liquid and gas from mixing. The tubing size was reduced to 1/8-in OD for short sections immediately preceding and following the reaction chamber. A needle valve located downstream allowed for pressurization of the chamber. The gas traveled through a drying system consisting of a condenser (500 cm^3 Erlenmeyer flask submerged in an ice bath) and a glass tube (2.54-cm OD) packed with glass wool and anhydrous $CaSO_4$ before finally entering an infrared gas analyzer (Horiba PIR-2000, later replaced by Horiba VIA-510). CO_2 concentration was displayed as a voltage reading on a computer in real-time (graphical and spreadsheet formats) by means of PicoLog software, distributed by Pico Technology. The software was configured to record data at one second intervals.

A 1000 cm^3 stainless steel reservoir accounted for the majority of liquid hold-up in the system. The liquid was pumped (Cole-Parmer Micropump) in a closed loop through the same heating bath (Fisher Scientific Isotemp 3016H) as the gas. A rotameter was used to monitor the flow rate. The rotameter was calibrated with water by Cullinane (2005). The same calibration (reproduced below, where x refers to the rotameter setting and T_{ref} refers to a reference temperature of 25°C) was used in the current work.

$$Q\left(cm^3/s\right) = \left(0.4512x - 0.2901\right) \cdot \sqrt{\frac{(7.83 - \rho_{L,T_{ref}})}{(7.83 - 0.997)\rho_{L,T_{ref}}}} \cdot \sqrt{\frac{7.83 - \rho_L^2}{7.83 - \rho_{L,T_{ref}}^2}} \qquad (4.1)$$

An in-line septum near the pump suction allowed for the injection of additional liquid into the system, either to purge entrained bubbles during start-up or to maintain liquid inventory and prevent gas from entering the liquid line during operation. Samples for CO_2 content analysis could also be withdrawn through the septum. The liquid temperatures at the inlet and outlet of the reaction chamber were measured by Type-J thermocouples (±2.2°C). The thermocouples were calibrated against a thermometer in a temperature bath.
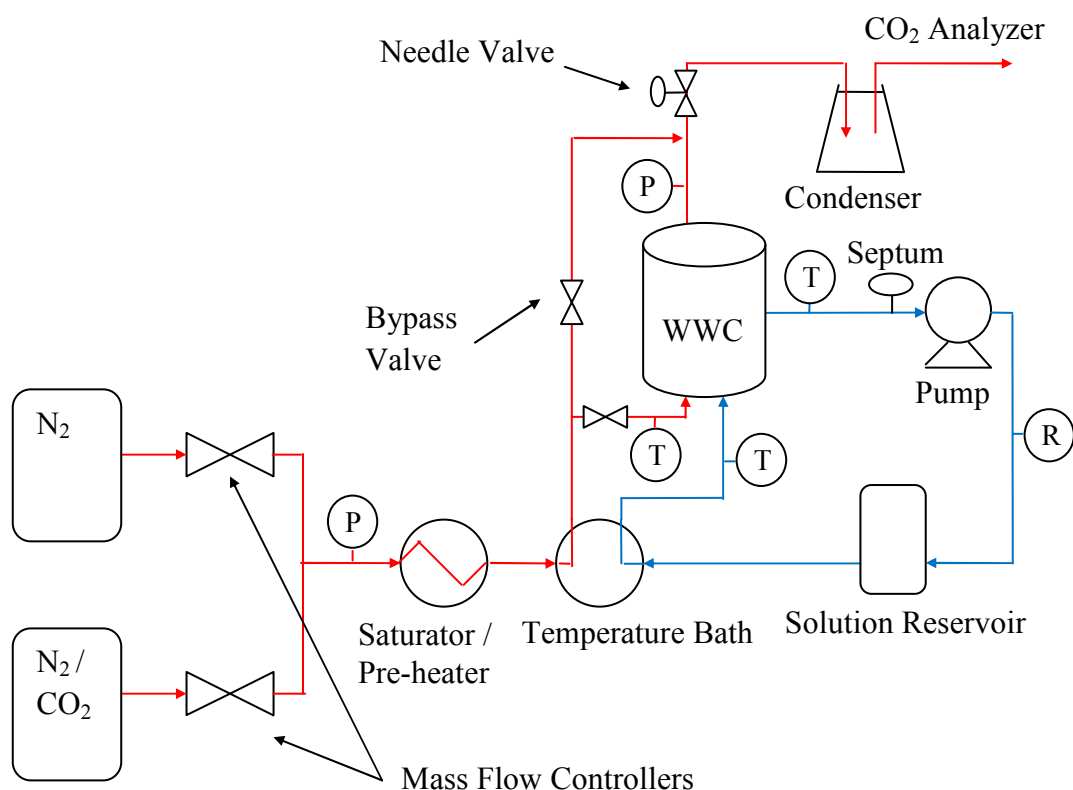
Figure 4.2. Schematic of WWC system. P: pressure gauge, T: thermocouple, R: rotameter.

4.1.2 Experimental Protocol

In a typical experiment, the solution reservoir was filled with 0.1 mol/L NaOH solution. The liquid was circulated at a constant rate (2-4 cm^3/s), and its temperature was allowed to stabilize. A gas stream with a known CO_2 concentration (based on the mass flow controller settings) was sent directly to the Horiba analyzer through the bypass line to create a calibration point relating CO_2 concentration to voltage. Once steady state was reached, indicated by a constant voltage reading, the bypass was closed, and the gas was instead directed through the reaction chamber. On achievement of steady state, the system was switched back into bypass mode, and a new inlet CO_2 concentration was run.

This alternating process was repeated several times in a given experiment; five different CO_2 concentrations were typically investigated, in randomized order. The bypass mode points were used to generate a calibration curve, which was subsequently utilized to interpret the absorption data. Operation in this internally calibrated manner was useful because it eliminated the need to do an absolute calibration of the Horiba analyzer.

A surfactant (TERGITOL^{TM} NP-7) and a polymer (POLYOX^{TM} WSR N750) were used respectively to modify the surface tension and viscosity of the caustic solutions in the WWC. For the experiments involving these agents, the desired mixture was prepared prior to filling the reservoir. The procedure from then on was identical to that outlined above.

4.1.3 Data Analysis

The performance of the WWC was modeled by series resistance (equation 2.14). The overall mass transfer coefficient (K_G) was determined from the CO_2 flux and the partial pressure driving force (equation 4.2). The ideal gas law was assumed to be applicable. P^*_{CO2} is zero because of the irreversibility of the CO_2-NaOH reaction – hence the simplified form of the log-mean partial pressure term.

$$K_G = \frac{N_{CO_2}}{\left(P_{CO_2} - P^*_{CO_2}\right)_{LM}} = \frac{N_{CO_2}}{P(y_{CO_2 \, in} - y_{CO_2 \, out})} \ln\left(\frac{y_{CO_2 \, in}}{y_{CO_2 \, out}}\right) = \frac{G}{RTa_{WWC}} \ln\left(\frac{y_{CO_2 \, in}}{y_{CO_2 \, out}}\right)$$

(4.2)

The gas-film mass transfer coefficient (k_G) was a function of physical properties and was calculated using a correlation specific to the WWC (equation 4.3) that was developed by

Bishnoi (2000) via absorption of SO_2 into 0.1 mol/L NaOH, an entirely gas-film controlled process. The gas-phase diffusion coefficient was estimated using the Chapman-Enskog equation (Bird et al., 2002) for a CO_2-N_2 system.

$$k_G = 1.075 \left(\frac{u_G \, d_{WWC}^2}{h_{WWC} \, D_{CO_2,G}} \right)^{0.85} \left(\frac{D_{CO_2,G}}{RTd_{WWC}} \right) \tag{4.3}$$

Experimental k_g' values from the WWC were obtained by solving equation 2.14 for k_g' and were compared with calculated values (equation 2.24).

$$\frac{1}{K_G} = \frac{1}{k_G} + \frac{1}{k_g'} \tag{2.14}$$

$$k_g' = \frac{\sqrt{k_{OH^-}[OH^-]D_{CO_2,L}}}{H_{CO_2}} \tag{2.24}$$

Equation 2.24 was evaluated using the correlations of Pohorecki and Moniuk (1988) for the reaction rate constant (k_{OH^-}) (equation 4.4), diffusion coefficient ($D_{CO2,L}$) (equation 4.5), and Henry's constant (H_{CO2}) (equation 4.6).

$$\log_{10}\left(\frac{k_{OH^-}}{k_{OH^-}^\infty} \right) = 0.221I - 0.016I^2 \tag{4.4}$$

$$\log_{10} k_{OH^-}^\infty = 11.895 - \frac{2382}{T} \tag{4.4a}$$

$$D_{CO_2,L} = \frac{D_{CO_2,w}\mu_w}{\mu_L} \tag{4.5}$$

$$\log_{10} D_{CO_2,w} = -8.1764 + \frac{712.5}{T} - \frac{2.591 \times 10^5}{T^2} \tag{4.5a}$$

79

The viscosity correlation for water used in the present research (equation 4.5b) was developed using data from the National Institute of Standards and Technology (NIST) (webbook.nist.gov), with a fitted form analogous to that proposed by Seeton (2006).

$$\mu_{\mathrm{w}} = 0.02414 \cdot 10^{\left(\frac{247.8}{T-140}\right)} \tag{4.5b}$$

The viscosity correlation for caustic solution (equation 4.5c) was obtained from a separate publication by Moniuk and Pohorecki (1991).

$$\log_{10}\mu_{\mathrm{L}}\,(\mathrm{mPa\cdot s}) = \frac{878.159}{T} - 3.0254 + 0.1103\left([\mathrm{OH}^-] + 2[\mathrm{CO}_3^{2-}]\right) + 0.08947\left(\frac{[\mathrm{CO}_3^{2-}]}{0.5[\mathrm{OH}^-] + [\mathrm{CO}_3^{2-}]}\right)$$

$$\tag{4.5c}$$

$$H_{\mathrm{CO}_2} = \frac{1}{H_{\mathrm{CO}_2-\mathrm{PM}}}; \quad \log_{10}\left(\frac{H_{\mathrm{CO}_2-\mathrm{PM}}}{H_{\mathrm{CO}_2,\mathrm{w\text{-}PM}}}\right) = -\sum I_i h_i \tag{4.6}$$

$$\log_{10}H_{\mathrm{CO}_2,\mathrm{w\text{-}PM}} = 9.1229 - \left(5.9044\times10^{-2}\right)T + \left(7.8857\times10^{-5}\right)T^2 \tag{4.6a}$$

The Henry's constant in Pohorecki and Moniuk (1988) was actually a solubility (units of kmol/m^3·bar) or in other words, was defined inversely to the Henry's constant referred to in the current work (e.g., in equation 2.24) and in many other instances. The "PM" symbol has been used to denote this distinction. In evaluating the summation in equation 4.6, two electrolyte compounds had to be considered: NaOH and Na$_2$CO$_3$ (Danckwerts, 1970). The Na$^+$ ions associated with OH$^-$ and those with CO$_3^{2-}$ were treated separately for the purpose of the ionic strength calculation, with the total sum always being equal to the starting concentration (i.e., 0.1 mol/L).

$$\sum I_i h_i = I_{\mathrm{NaOH}}\left(h_{\mathrm{Na}^+} + h_{\mathrm{OH}^-} + h_{\mathrm{CO}_2}\right) + I_{\mathrm{Na}_2\mathrm{CO}_3}\left(h_{\mathrm{Na}^+} + h_{\mathrm{CO}_3^{2-}} + h_{\mathrm{CO}_2}\right) \tag{4.6b}$$

The Henry's constant contributions of Na^+, OH^-, and CO_3^{2-} were provided respectively as 0.091 L/mol, 0.066 L/mol, and 0.021 L/mol. A range of values for the CO_2 contribution was given over temperatures from 0.2 to 60°C (Barrett, 1966). The CO_2 contribution was correlated in the form of equation 4.6c.

$$h_{CO_2} = \left(4.364 \times 10^{-7}\right) \cdot \left[T(^\circ C)\right]^3 - \left(3.297 \times 10^{-5}\right) \cdot \left[T(^\circ C)\right]^2 + \left(1.204 \times 10^{-4}\right) \cdot \left[T(^\circ C)\right] - 6.847 \times 10^{-3}$$

(4.6c)

Two different approaches were viable for the determination of the experimental k_g'. Values could be extracted on a point-by-point basis, with an individual K_G, k_G, and k_g' being associated with every CO_2 partial pressure condition (generally 5 within a given experiment). Alternatively, a single K_G value could be obtained from the slope of a plot of CO_2 flux against log-mean partial pressure ($P_{CO2,LM}$), with the intercept forced through zero (see equation 4.7). This in turn could be used to calculate an "overall" k_g' for the experiment.

$$N_{CO_2} = K_G \left(P_{CO_2} - P_{CO_2}^*\right)_{LM} = K_G P_{CO_2,LM}$$

(4.7)

The latter method has been favored by past WWC users like Cullinane (2005) and Dugas (2009). Dugas justified this approach, stating that absorption or stripping points near equilibrium (zero driving force) would be subject to greater relative error, thereby creating inconsistencies in the point-by-point basis. The CO_2-NaOH experiments in this work, however, were not operated in the same fashion as CO_2-amine tests. Conditions were strictly absorption-based, and the data were clustered closer to each other than to the zero point, which made it somewhat illogical to extrapolate to this limit. Furthermore,

the assumption of one k_G value was not entirely accurate, because a constant total gas flow rate (i.e., constant k_G) was not maintained in early-phase experiments. For these reasons, the point basis was considered to be more favorable. Ultimately, though, a statistical F-test with the baseline (0.1 mol/L NaOH) data showed there to be no difference between the two methods, which was not surprising given that the overall mean for each group was the same. The results from one case are shown for illustration.

$K_G = 3.91 \times 10^{-10}$ kmol/m²·Pa·s

$k_G = 21.7 \times 10^{-10}$ kmol/m²·Pa·s

$k_g' = 4.77 \times 10^{-10}$ kmol/m²·Pa·s

y = 3.91E-10x
R² = 9.96E-01
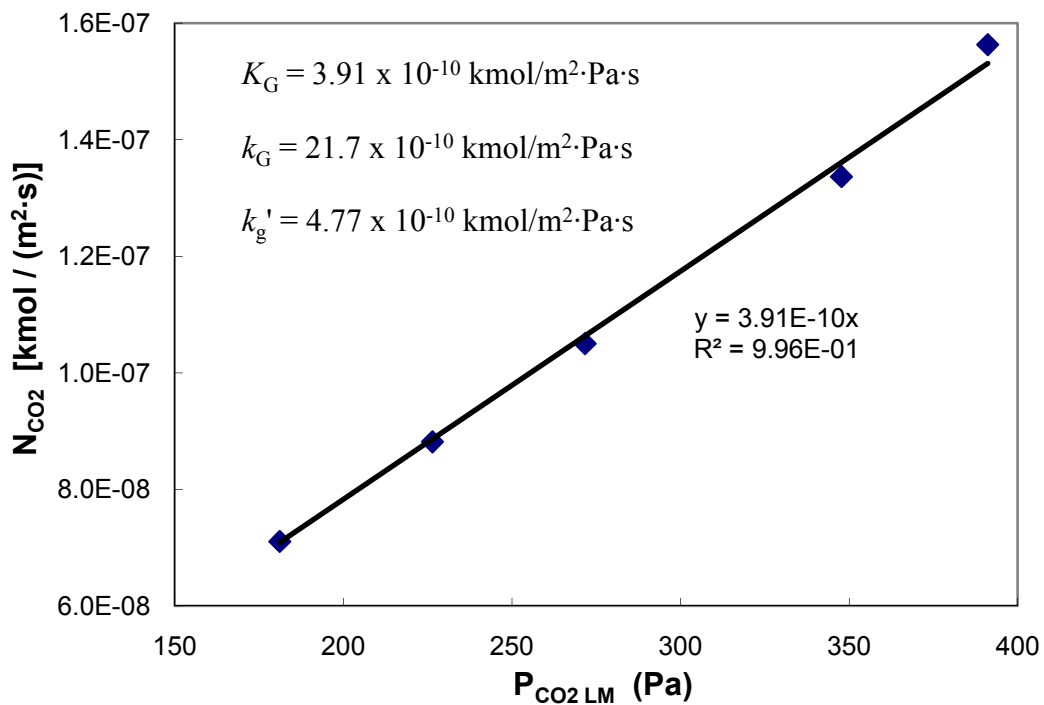
Figure 4.3. Determination of k_g' using slope method for K_G (0.1 mol/L NaOH, 32°C).

Table 4.1. Determination of k_g' from individual K_G and k_G points (0.1 mol/L NaOH, 32°C).

$P_{CO2\ LM}$ (Pa)	K_G x 10^{10} (kmol/m²·Pa·s)	k_G x 10^{10} (kmol/m²·Pa·s)	k_g' x 10^{10} (kmol/m²·Pa·s)
181	3.92	21.7	4.78
226	3.89	21.7	4.74
272	3.87	21.7	4.71
348	3.84	21.7	4.67
391	4.00	21.7	4.90
AVERAGE	3.90	21.7	4.76

4.1.4 Experimental Concerns

To ensure the WWC data were of satisfactory quality, experiments had to be designed such that:

- The reaction kinetics were the limiting factor for mass transfer in the liquid film.

- Interfacial depletion of hydroxide ion was minimal.

- The CO_2 removal was statistically appreciable.

- Gas-side resistance was minimal.

The first factor was not an issue; Ha^2 was always on the order of 10^2 in the WWC, with k_L^0 estimated from the theories of Pigford (1941), Hobler (1966), and Bird et al. (2002). The equations for calculating k_L^0 are not reproduced here but can be found in Pacheco (1998) or Cullinane (2005). Pacheco made k_L^0 measurements in the WWC via desorption of CO_2 from water and ethylene glycol and found the data to match the theory within 15%. The theory was presumed to be applicable for the calculation of k_L^0 in this work, which ranged from 0.007-0.014 cm/s. The second condition basically required that CO_2 partial pressures not be excessive, which created an interesting trade-off with the third

criterion, since higher partial pressures would necessarily imply greater (i.e., more statistically favorable) absolute CO_2 removal across the reaction chamber. Finally, a low gas-film resistance was desirable in order to minimize any potential disconnect between the measured flux and k_g', since an empirical correlation (equation 4.3) with inherent error was being used to calculate k_G. The gas-film resistance could essentially be controlled via the superficial gas velocity through the system.

Gas-phase backmixing in the reaction chamber was not believed to be a concern. The Péclet number (Pe_G) is commonly referred to in the characterization of gas flow patterns, with an increasing Pe_G corresponding to a transition from backmixing to plug-flow conditions (Shetty et al., 1992). For a rough definition of these limits, backmixing might be expected to be prevalent for $Pe_G < 1$, and plug-flow might be safely assumed for $Pe_G > 10$. The gas-phase Péclet number for the WWC (defined in equation 4.8) was on the order of 10^2, so the presumption of plug-flow behavior was thought to be valid.

$$Pe_G = \frac{u_G d_{WWC}}{D_{CO_2,G}} \qquad (4.8)$$

The operational limits that were ultimately settled on consisted of gas flow rates ranging from 4.2 to 4.7 sLpm (later set constant at 4.5 sLpm) and CO_2 partial pressures from 130 to 600 Pa (with total pressures ranging from 15 to 70 psig). Interfacial depletion of hydroxide was estimated to be no greater than 3%, thereby ensuring minimal deviation from the pseudo-first-order assumption (see Appendix C for example calculation). The gas-film resistance and CO_2 removal across the reaction chamber ranged from approximately 10 to 25%. Both parameters were found to vary in tandem,

which seemed logical in the context of residence time. For example, a lower gas velocity would be associated with a greater gas-film resistance but would also result in the gas spending more time in the reaction chamber, thereby allowing for more removal of CO_2.

4.1.5 Equipment Modifications

Several adjustments were made to the experimental apparatus over the course of the present work. These changes were not believed to cause any discrepancies in the data but were nevertheless thought to be worthwhile to report – particularly the last point.

- The mass flow controllers were periodically re-calibrated to ensure that they were functioning properly.

- The gas analyzer used for the majority of experiments was the Horiba PIR-2000. The range of the analyzer was adjustable (0.05, 0.15, or 0.25 vol %), with an expected repeatability of ±0.5% of full scale. The flow rate into the PIR-2000 was initially not rigorously measured, but a rotameter was later installed to ensure the machine was receiving the "proper" sample rate (500 cm^3/min). The PIR-2000 was replaced by the VIA-510 for the last few experiments that were performed (3/27/07 and beyond). The VIA-510 was digital and possessed several new features – a built-in rotameter, an expanded analytical range (0.05, 0.1, 0.5, or 1 vol %, with ±0.5% repeatability) and zero/span settings for the purpose of absolute calibration – but was still operated in identical fashion to the PIR-2000.

- Both the inlet and outlet liquid temperatures were measured at first. No significant temperature change across the reaction chamber was ever observed

(0.1°C difference, if any, for temperatures around 30°C). The outlet thermocouple was eventually moved to the gas-side of the system to enable the gas stream temperature to periodically be checked, and subsequent liquid temperature values were based solely off of the inlet.

- Shortly after completing the tests with POLYOX WSR N750, film stability issues arose. A stable liquid film could not be maintained (i.e., rivulet flow and dry patches), even after extensive washes with water, soap solution (generic detergent and Alconox® detergent), and mild acid/base (HNO_3/NaOH) solutions. Contamination of the WWC surface (i.e., via polymer adsorption) was suspected. Since gentle rinsings seemed to be ineffective at removing whatever was adhered to the surface, the apparatus was disassembled, and the surface was carefully cleaned with a cloth and a scouring pad. No immediate effect was noticed, but after continuing to run significant quantities of water through the WWC, satisfactory film conditions were eventually restored.

  During this downtime, the o-rings in the system were replaced. The rubber gaskets that were used to create a seal with the thick-walled glass cylinder were found to have severely eroded and were replaced with two concentric o-rings. After reassembly, an air-tight seal could not be maintained at the gas-side connection above the upper flange of the glass cylinder (near the weld point), which affected the oil flow in the outer annulus. The insertion of an intermediary nylon washer at this connection point (constructed by the machine shop in the chemical engineering department at the University of Texas at Austin) fixed this

86

problem. The hourglass-shaped reaction chamber unfortunately was cracked in this process, so a new piece was built. Figure 4.4 compares the dimensions of the two chambers, which were practically identical. To verify that the flow behavior of the gas (i.e., gas-film mass transfer coefficient) had not appreciably changed, Dugas (2009) measured the absorption of CO_2 into 2 m PZ. The data were found to comply with the "original" gas-film mass transfer coefficient correlation (equation 4.3). A baseline (CO_2-NaOH) experiment was also conducted to confirm this similitude. Similar k_g' values as in the past were obtained.
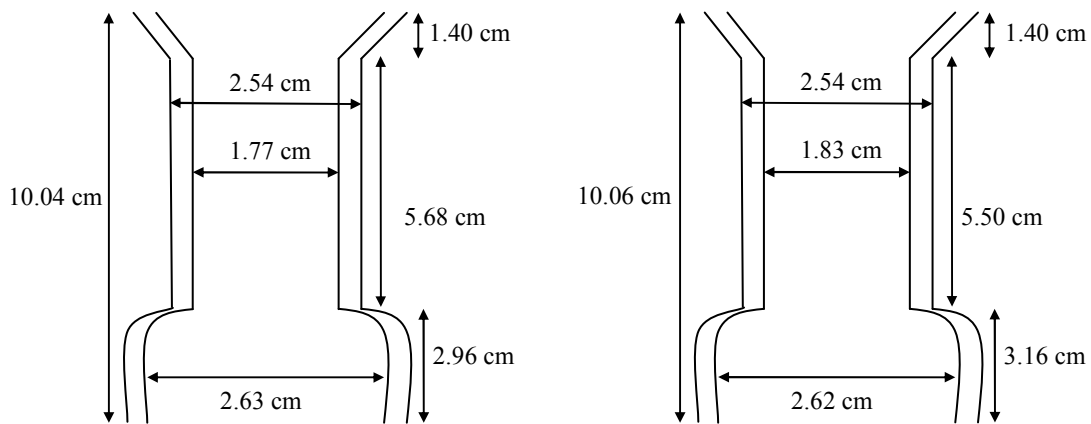
Figure 4.4. "Old" (left) and current (right) WWC reaction chamber dimensions.

4.2 PACKED COLUMN

A pilot-scale packed column was used to characterize the mass transfer and hydraulic performance of structured packing. Lewis and Seibert, researchers affiliated with the Separations Research Program (SRP) at the University of Texas at Austin, began conducting preliminary experiments with this system in 2002 and established the

foundation for the experimental methodology utilized in subsequent tests. Wilson (2004) used the equipment to evaluate the mass transfer area of several random and structured packings prior to the present work.

4.2.1 Equipment Description

The column was located in the outdoor area of the SRP facility and had an outside diameter of 0.46 m (18 in), an inside diameter of 0.427 m (16.8 in), and a total height of approximately 7.62 m (25 ft). A photograph of the column is shown in Figure 4.5, and a schematic of the whole system is presented in Figure 4.6. The column body, piping, and valves were all constructed from plastic (PVC).

Figure 4.5. Photograph of packed column apparatus.
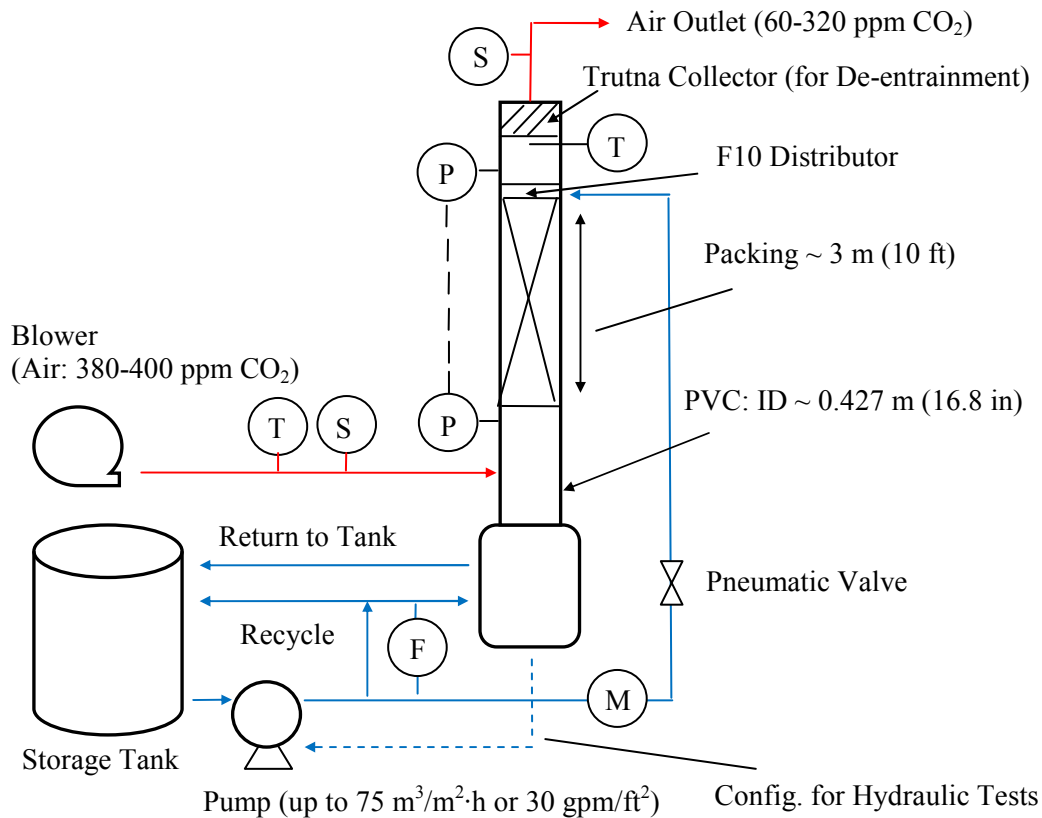
Figure 4.6. Schematic of packed column experimental system. P: pressure transmitter, T: thermocouple, M: Micromotion, S: CO$_2$ sampling point, F: filter.

A 30 kW (40 hp) blower with a variable-speed motor drive was used to supply ambient air to the column, which was introduced via a duct with an outside diameter of 0.203 m (8 in) into the side of the column (below the packed bed). The air flow rate was monitored by an annubar flow meter (Dietrich Standard, model #DCR15), which was basically an averaging pitot tube. The annubar was inserted into a run of schedule 80 steel piping with a diameter of 0.102 m (4 in). The length of straight piping before and after the annubar was 4.3 m (14 ft) and 1.2 m (4 ft), respectively, and the piping was reduced from and expanded to a diameter of 0.203 m (8 in) beyond these limits. Two Rosemount differential pressure transmitters were utilized in the flow measurement. One

was employed to monitor the static pressure (model #3051S1TG2H2E11F1AB4A0190) and was calibrated for 1020 kPa (150 psi); the other was directly associated with the annubar (model #3051S1CD1A2F12A1AB2D2) and was calibrated for 6215 Pa (25 in H_2O).

A centrifugal pump capable of discharging 0.57 m^3/min (150 gpm) was used to transport liquid to the top of the column from a 1.3 m^3 (350 gal) storage tank located near the column base. Liquid flow rate was regulated with a variable-speed drive on the pump and was measured using a Micromotion coriolis meter. A portion of the flow from the storage tank was typically diverted and recycled back to the tank, in order to operate in a more favorable drive-speed region of the pump. The recycled liquid could either be passed through a bag filter for removal of solids like gravel or sent straight to the tank. (The filter section was closed off whenever antifoam (Dow Corning® Q2-3183A), which was necessary in some trials, was present. Since the antifoam is technically a suspension, there was concern that it could become trapped in the filter). A pneumatic valve could be opened or closed to allow or block liquid flow to the column. The liquid at the top was distributed using a pressurized fractal distributor with 108 drip points/m^2 (10 points/ft^2) – henceforth referred to as the F10 distributor – that was positioned within 12 cm (5 in) of the packing. A Trutna collector was located in the column segment above the distributor. This multi-plated device prevented liquid from reaching the column exhaust by knocking it out and allowing it to drain back into the storage tank. The approximate liquid inventory in the system could be gauged via a level transmitter installed on the column sump (up to 63.5 cm or 25 in). A void height of approximately 1.8 to 2.1 m (6 to 7 ft)

91

between the bottom of the packed bed and liquid in the sump was typical during operation.

Pressure drop through the packing was determined using parallel differential pressure transmitters (Rosemount), calibrated for low (up to 750 Pa or 3 in H_2O) and high (up to 6215 Pa or 25 in H_2O) measurements. The temperature of the gas in the inlet ductwork and at the outlet of the column was measured with thermocouples, and the liquid temperature was monitored at the Micromotion meter. The temperature (T_{corr}) used in the calculation of k_g' was an average of these values, with the liquid weighted more heavily (i.e., gas temperatures first averaged, then averaged with the liquid). This practice was based purely on experience and was found to do a better job of reconciling the mass transfer area data at ambient temperature extremes (i.e., summer vs. winter) than simply using the liquid temperature. The "corrected" temperature was on average within 3°C of the liquid temperature, so the applied correction was not extremely drastic. The gas-phase CO_2 concentration of either the inlet or outlet air was measured using an infrared analyzer (Horiba VIA-510) that was calibrated with zero (N_2) and span gases (450 ppm$_v$ CO_2/N_2). The reading range of the Horiba was 0.05% CO_2 by volume, with a reproducibility of ±0.5% of full scale. A vacuum pump (Air Dimensions Inc., Micro Dia-Vac® pump) was used for the sampling of the air. Control of the major pieces of equipment (i.e., pump, blower, pneumatic valve, etc.) was done via DeltaV software from Emerson.

Approximately 3 m (10 ft) of packing was used in every experiment. Individual bales were 21 to 21.6 cm (8.25 to 8.5 in) in height and about 42 cm (16.5 in) in diameter.

Each element was equipped with wiper bands, intended to direct liquid away from the column wall and back into the packing bulk. The elements from Sulzer Chemtech were all bound with two wiper band strips, whereas the prototype packing (P500) that was tested had only one strip. During packing changeouts, the column was separated at its flanged joints via a chain pulley system. The old packings were removed near the column base, and the new ones were dropped in from the top. During installation, elements were rotated 90° relative to each other, a universally recommended practice to facilitate liquid distribution.

4.2.2 Protocol for Hydraulic Experiments (Pressure Drop and Hold-up)

Hydraulic studies were conducted with either process water or water containing property-modifying additives but never with any caustic in the system. The no-caustic policy was instituted to ensure the air sampling line at the top of the column would not become contaminated around the flood point, as well as for general safety reasons. As a consequence, the hydraulic conditions for the mass transfer experiments were perhaps not wholly comparable to the hydraulic data, since higher pressure drops were sometimes observed for the mass transfer tests under identical circumstances. This discrepancy was possibly caused by $NaOH/Na_2CO_3$ salts resulting in a small degree of foaming but was not believed to be especially significant, particularly from a qualitative perspective.

In a typical hydraulic run, the storage tank was first filled with water. The water was pumped from the tank to the column sump but was not allowed to return; the sump was filled until near-overflow. The liquid line valves were then configured to circulate

liquid between the sump and column, with the storage tank excluded from the loop, and the pump was turned on (60% VSD). The pneumatic valve controlling flow to the column was closed, but the pump was left running to keep the liquid lines as primed as possible. The blower was turned on (200 ACFM), and the liquid level in the sump was allowed to stabilize for 5 to 10 minutes to establish a baseline liquid-level reading. The pneumatic valve was subsequently opened. A constant liquid load was set, and the air flow rate was incremented until near-flooding or flooding conditions were reached, generally indicated by a pressure drop of around 815 Pa/m (1 in H_2O/ft) or higher. The liquid hold-up was measured at the same time as the pressure drop. Hold-up measurements utilized the level transmitter installed on the sump and were determined from the sump geometry (approximately 0.57 m or 22.6 in ID) and the difference between the current and baseline liquid levels (equation 4.9).

$$h_{\mathrm{L}} = \frac{d_{\mathrm{sump}}^{2} \cdot (\text{Current level} - \text{Calculated baseline level}) - V_{\mathrm{F10}} - V_{\mathrm{pipe}}}{d_{\mathrm{c}}^{2} Z} - h_{\mathrm{L,entrance/end}}$$

(4.9)

Evaporation, as well as physical loss of liquid through the column exhaust, would be expected to reduce the total liquid volume in the system and would cause the actual or current baseline level to be lower than when it was first established. These losses were accounted for via an evaporation calculation (based on inlet/outlet humidity) that automatically decremented the initial input over time. This tracking of the baseline level was perhaps the most prominent source of error in the hold-up measurement, as there was usually a discrepancy (typically no more than 1.3 cm or 0.5 in) between the calculated

value (i.e., initial input – calculated loss) and the value observed upon re-establishment of the baseline, following a set of measurements. In addition to the volumetric difference, several other factors were included in equation 4.9, such as the estimated hold-up in the F10 distributor (V_{F10} = 0.001 m^3 or 0.04 ft^3) and in the un-primed (or dry) sections of piping in the system. As an aside, a fractal distributor, unlike other distributors such as trough types, can be expected to exhibit a relatively constant liquid hold-up regardless of liquid load. This feature was advantageous in this context and was part of the reason why the F10 distributor was selected over alternative options. An effort was also made to account for minor hold-up contributions from entrance and end effects, although the value that was assumed ($h_{L,entrance/end}$ = 0.003) was basically negligible.

A step-by-step operating procedure for the hydraulic experiments is provided in Appendix A.1.2.

4.2.3 Protocol for Mass Transfer Experiments

The storage tank was charged with 0.75 m^3 (200 gallons) of process water, metered through the Micromotion device. Approximately 3.7 kg (8.05 lbs) of solid NaOH pellets were added to the tank to create a 0.1 mol/L solution. This quantity was slightly greater than the theoretical calculation would suggest and was deduced based on experience with the system. The solution was circulated through the recycle loop shown in Figure 4.6; the pneumatic valve and filter line were closed during this time. The pellets were given at least an hour to dissolve, after which the pneumatic valve was opened to allow for flow through the packing. The solution was allowed to mix at 24.4-

36.6 $m^3/m^2 \cdot h$ (10-15 gpm/ft^2) for 1.5 hours – enough to ensure a minimum of 5 to 6 inventory turnovers. The packing was then pre-wet at a relatively high liquid load (61.1 $m^3/m^2 \cdot h$ or 25 gpm/ft^2) – a standard practice in industrial applications – for at least 5 minutes. In situations where foaming was a concern, this was sometimes lowered to 48.8 $m^3/m^2 \cdot h$ (20 gpm/ft^2). A sample was taken from the column sump and titrated with phenolphthalein against an acid standard (0.1 mol/L HCl) to verify that the NaOH concentration was indeed around 0.1 mol/L prior to starting the experiment. The titrated concentration was generally within 5% of 0.1 mol/L.

The blower was set at one of three air rates: 0.6, 1, or 1.5 m/s (180, 300, or 450 ACFM), although one run at 2.3 m/s (700 ACFM) was also conducted as a check on gas-side resistance. Liquid load was incremented or decremented over a maximum range of 2.4-73.2 $m^3/m^2 \cdot h$ (1-30 gpm/ft^2). The mass transfer area was calculated based on the CO_2 removal from the air. Each condition was given at least 10 minutes to reach steady state, indicated by relatively constant readings across the various process parameters (CO_2 concentration, flow rate, temperature, etc.). Pressure drop was not allowed to exceed 815 Pa/m (1 in H_2O/ft) to ensure that all measurements were in the pre-loading region. Data at these conditions were thought to be more operationally relevant (and more reproducible) than data in the flooding region, and furthermore, the multitude of potential issues associated with flooding, such as contamination of the air sampling line with caustic solution, wetting of the Trutna de-entrainment device (see Section 4.2.7), or even expulsion of caustic out of the column exhaust, were avoided. After taking a satisfactory number of points, the air rate was changed to a different value, and the procedure was

96

repeated. As with the hydraulic experiments, detailed operational protocol can be found in Appendix A.1.3.

4.2.4 Solution Preparation with Additives

Tests at low surface tension (TERGITOL NP-7) or enhanced viscosity (POLYOX WSR N750) required some modification to the preparation procedure. For the cases where both hydraulic and mass transfer area data were desired at these conditions, the same liquid inventory was used in order to minimize the generated waste. The hydraulic experiment was always performed first. A small quantity of make-up water was then added to the system to account for expected solvent losses, and the mass transfer test was subsequently conducted.

Preparation with TERGITOL NP-7 was straightforward; both the surfactant and antifoam were added to the storage tank simultaneously and were given adequate time to mix in.

Preparation with POLYOX was a bit more complicated. The storage tank was first filled with 0.75 m^3 (200 gallons) of water. The water was circulated between the sump and tank (*not* through the packing) at a fairly low rate (50-55% VSD), and the POLYOX was gradually added in 0.45 to 0.68 kg (1 to 1.5 lb) increments over a period of 1 to 1.5 hours; this was found to be an effective dissolution method. Mixing at a low rate helped to minimize foaming, but a small amount of antifoam (< 5 g) was sometimes added if foaming was problematic. Generally, at least 4 hours were needed for the POLYOX to dissolve. Afterward, the solution was circulated through the entire system

to achieve a homogenous mixture. The solution viscosity was analyzed with a rheometer (described in Section 4.3.3). Samples were taken from at least two locations (e.g., sump and pump suction port) as a consistency check. If the viscosity was not as intended, appropriate adjustments were made – either by discarding some inventory and adding dilution water or dissolving more POLYOX in the system – until the target viscosity was achieved. Equation 4.10, developed from bench-scale measurements (Figure 4.7), was used to guide the solution preparation, with the mass fraction (w) defined on a percentage basis in this case:

$$\mu_L \left(mPa \cdot s \right) = 1.7924 \exp^{1.3182\,w} \tag{4.10}$$
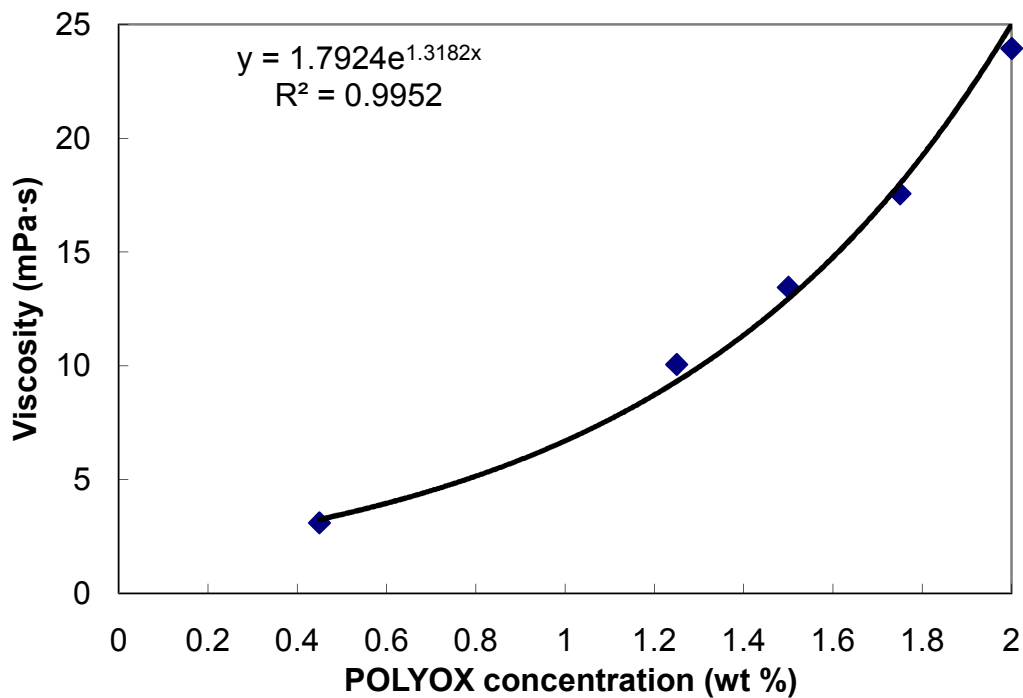
Figure 4.7. Correlation of POLYOX WSR N750 weight percent with solution viscosity at 25°C.

The solution viscosity during an experiment was calculated from a correlation. The viscosities of a few representative samples were measured over the experimental temperature range, and the data were used to develop a temperature-dependent equation specific to the experiment. An exponential fit was chosen for this purpose. The analysis from one case is shown in Figure 4.8 for illustration.
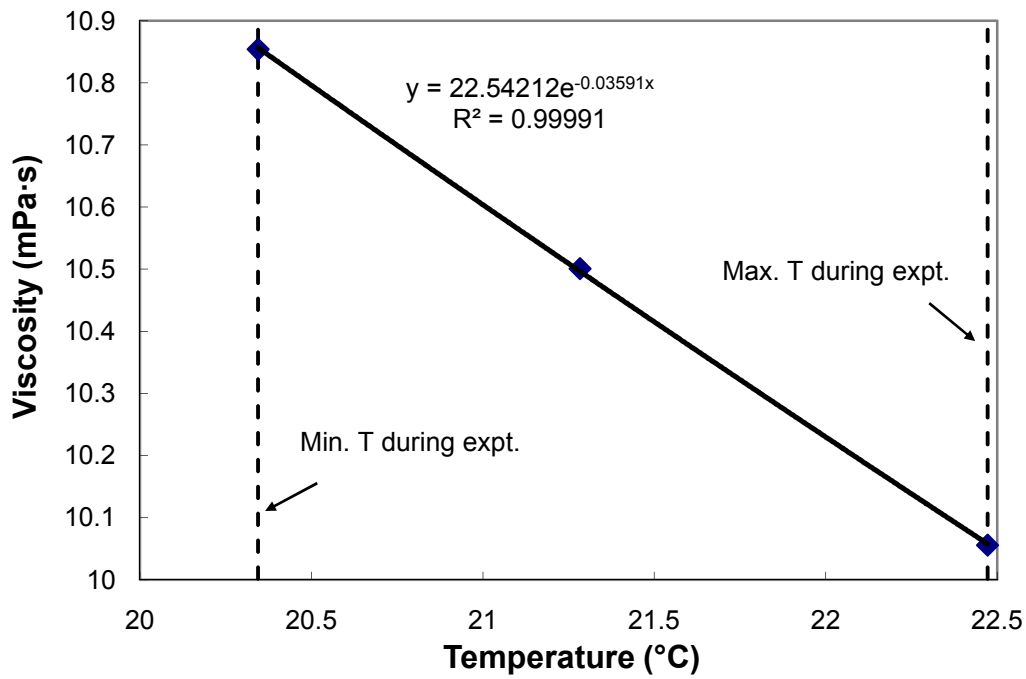
Figure 4.8. Correlation of viscosity with temperature for SRP experiment 0908.

4.2.5 Data Analysis (Mass Transfer Experiments)

The differential mass balance associated with absorption in a packed column is given by equation 4.11.

$$u_G \frac{\mathrm{d}y}{\mathrm{d}z} = (K_G a_e)(RT)(y^* - y) \tag{4.11}$$

The packed column experimental system was regarded as dilute, and a CO_2 equilibrium partial pressure of zero was assumed (again, due to the irreversibility of the CO_2-NaOH reaction). The effect of the temperature gradient across the column on the gas flow rate was neglected, as was the impact of humidification. The gas velocity (u_G) and volumetric mass transfer coefficient ($K_G a_e$) were considered to be constant. Under these conditions, integration of equation 4.11 over the packed bed height (Z) yields the following expression for the volumetric mass transfer coefficient:

$$K_G a_e = \frac{u_G}{ZRT} \ln\left(\frac{y_{CO_2,in}}{y_{CO_2,out}}\right) \tag{4.12}$$

The series resistance relation (equation 2.14) was applicable to the packed column as well. Gas-film resistance was intentionally limited by using dilute caustic solution (0.1 mol/L) and operating at relatively high superficial air velocities. This resistance was calculated from the correlation of Rocha et al. (1996) to account for 1-2% of the overall mass transfer resistance on average; measurements consisting of the absorption of SO_2 into caustic solution have supported this estimate. The $1/k_G$ term in equation 2.14 was neglected, and K_G was therefore assumed to be equal to k_g'. The effective area (a_e) could subsequently be isolated in equation 4.12 by dividing through by k_g'.

$$a_e = \frac{u_G \ln\left(\frac{y_{CO_2,in}}{y_{CO_2,out}}\right)}{ZK_G RT} \approx \frac{u_G \ln\left(\frac{y_{CO_2,in}}{y_{CO_2,out}}\right)}{Zk_g' RT} = \frac{u_G \ln\left(\frac{y_{CO_2,in}}{y_{CO_2,out}}\right)}{ZRT} \cdot \frac{H_{CO_2}}{\sqrt{k_{OH^-}[OH^-]D_{CO_2,L}}}$$

$$\tag{4.13}$$

4.2.6 Experimental Concerns

The primary concerns associated with the hydraulic measurements were related to operational issues, rather than to the actual experimental design. To minimize inaccuracies, care had to be taken to ensure:

- No condensation or entrained liquid was present in the pressure transmitter lines.

- The calculated baseline liquid level closely mirrored the actual value.

Liquid occasionally found its way into the pressure transmitter tubing, particularly when operating at high liquid loads or around the flood point. This issue was addressed by routinely checking and purging these lines. Correctly tracking the time-based depletion in the baseline reading was quite imperative to the integrity of the hold-up measurements, because the baseline was typically only established once for each liquid load condition (i.e., every 30 to 60 minutes). If necessary, the input humidity values could be adjusted to force the evaporation calculation to better synchronize with the actual observed solvent loss rate. For instance, the relative humidity at the outlet might be reduced from 100% to 80% if the calculated baseline level was found to be appreciably lower than the actual level observed upon re-establishment of the baseline.

The concerns previously discussed for the WWC (Section 4.1.4) were also pertinent to the mass transfer tests in the packed column. The large Ha^2 criterion was comparatively weaker, due to k_L^0 being greater. The mass transfer coefficient was estimated from the correlation of Rocha et al. (1996). Ha^2 was 12 in the absolute worst case, but it was at least 30 for 95% of the recorded data points. Interfacial depletion of hydroxide was not an issue, because the CO_2 partial pressures were at ambient level.

Given these circumstances, achieving a statistically adequate removal of CO_2 was important, which is partly why the system was designed with 3 m (10 ft) of packing. The other reason for the bed depth was to reduce entrance and end effects, which could be quite significant for shorter beds. Wall effects, entrance effects that might be associated with the splashing of liquid on to the packing from the distributor, and end effects that might be associated with the dripping of liquid from the bottom of the packing on to the pool in the column sump were neglected in the mathematical interpretation of the data. Still, such effects must be recognized as a potential issue. A relevant discussion is presented in Section 6.10.2. The Trutna collector appeared to have a relatively high geometric area, but its impact on CO_2 removal was not considered since it was not presumed to be significantly wetted under the pre-loading conditions of the mass transfer experiments. Bulk consumption of hydroxide was much more significant here than in the WWC and was critical to monitor, since allowing the hydroxide level to get too low could potentially be problematic for the kinetics. The inventory was never depleted by more than 40% within an experiment, as determined by total inorganic carbon (TIC) analysis (see Section 4.3.1).

A strict design of experiments was not adhered to. That is, the packings and physical conditions (i.e., low surface tension or high viscosity) ideally should have been tested in random order, with a designated scenario (e.g., M250Y baseline) being used a center-point. Furthermore, the test points, which were generally always run in incrementing sequence, should have been randomized. The former was impractical due to the time constraints associated with turning over the column, as well as the solution

102

preparation and disposal (with TERGITOL NP-7 or POLYOX). The latter was also impractical, because the range of operational conditions for a given packing was not necessarily known beforehand. Jumping around, with large, sudden increments or decrements, would greatly extend the duration of experiments, too, due to the additional time that would be required to reach steady state.

4.2.7 Equipment Modifications

Minor repairs/modifications that were performed over the lifetime of the project included:

- Installation of a new entrainment drain line and Trutna collector in the top segment of the column (10/25/07).

- Replacement of the thermocouple measuring the outlet gas temperature, which lost functionality (4/9/09).

- Repair of cracks in the nozzles or column shell itself, which necessitated the use of PVC glue (10/29/07) or in one extreme case, the welding of a plastic frame over the damaged area (4/30/09). The integrity of the repairs was affirmed via pressure testing.

The installation of a leak-check system was by far the most significant improvement made (1/24/08). Issues were on occasion discovered with the air sampling system, wherein either the vacuum pump had failed or the plastic tubing lines had become punctured. This resulted in the leakage of ambient air into the sampled exhaust, which if left uncorrected, drastically affected the apparent CO_2 removal and hence the

interpreted mass transfer area. The leak-check set-up utilized the zero-point calibration gas (N_2) to identify any air contamination between the sampling point and the Horiba gas analyzer. The incorporation of this test into the experimental procedure is discussed as part of the step-by-step instructions in Appendix A.1.3.

4.3 SUPPORTING METHODS AND EQUIPMENT

4.3.1 Total Inorganic Carbon (TIC) Analysis

To account for bulk hydroxide depletion, the CO_2 content of samples from the WWC and packed column experiments was analyzed via a total inorganic carbon (TIC) analytical method analogous to the one used by past experimentalists (Cullinane, 2005; Hilliard, 2008; Dugas, 2009) to characterize the CO_2 loading of amine solutions. This depletion was not especially significant in the case of the WWC (less than 5%), but it was for the packed column (30-40%). The TIC apparatus consisted of a rotameter, several vertically-mounted glass tubes in series, and finally, the Horiba PIR-2000 analyzer. The first tube was designed with a frit and an extra horizontal port (plugged with a septum) to allow for the injection of liquid. The remaining tubes were drying columns packed with glass wool and anhydrous $Mg(ClO_4)_2$. Approximately 0.5 to 1.0 cm^3 of 30 wt % H_3PO_4 solution (drained and replenished periodically) was maintained in the first chamber, and N_2 gas was bubbled through. Samples were injected into the acid, and the CO_3^{2-} in solution was liberated as gaseous CO_2, which was subsequently swept to the Horiba analyzer by the N_2 carrier gas. The injected masses were recorded, and every sample was tested at least three times to verify reproducibility. The liberated CO_2 appeared as a

voltage pulse in PicoLog, and the area of this peak (integrated via the trapezoidal rule) was associated with an unknown CO_2 (or equivalently, CO_3^{2-}) concentration. To complete the analysis, a calibration relating area with moles of CO_2 was necessary. This was developed by injecting varying quantities of a $Na_2CO_3/NaHCO_3$ buffer solution containing 1 mg C/cm^3, or approximately 1 mg C/g (1000 ppm$_w$ C). The OH^- concentration of a given sample could be back-calculated based on the initial concentration and the reaction stoichiometry, since 2 OH^- ions had to react for every CO_3^{2-} ion produced.

Analysis of neat NaOH samples was straightforward, but the solutions containing surfactant or polymer could be more problematic due to foaming. This issue was mitigated somewhat by mixing antifoam in with the acid and operating at a lower gas flow rate. None of the additives contained inorganic carbon, and therefore, the treatment of the data was identical to that of the neat samples.

4.3.2 Goniometer (Surface Tension and Contact Angle)

The goniometer apparatus (ramé-hart Inc., model #100-00) was used to make surface tension and contact angle measurements. It was owned and overseen by the Willson research group at the University of Texas at Austin (CPE 3.432) and was comprised of an adjustable Teflon stage, a syringe support arm, a computer-linked camera for live image display, and a light source (Figure 4.9). A syringe assembly (ramé-hart Inc., part #100-10-20) consisting of a plastic screw-type body, glass chamber,

and stainless steel needle was used to dispense solution. The needle that was typically used was 22-gauge (0.7112 mm OD) in size.
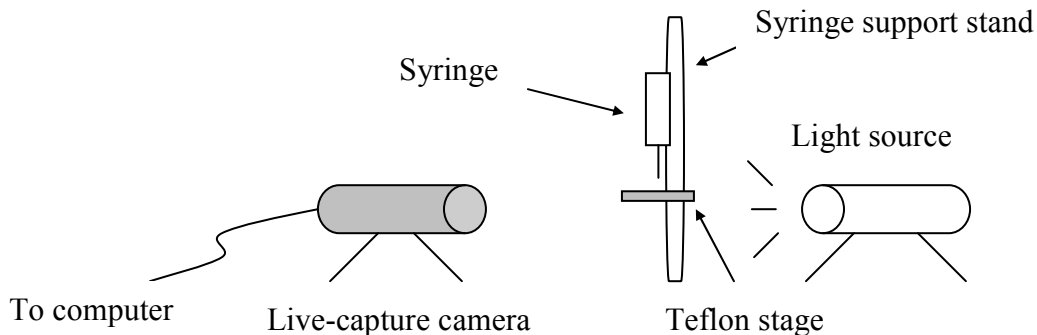
Figure 4.9. Schematic of goniometer set-up.

Surface tension measurements were made via the pendant drop method. The syringe was filled with liquid and suspended vertically, with the needle tip in view of the camera. A drop was slowly dispensed, and a computer image was saved at the near-breaking point of the droplet, where gravity and surface tension forces should have been in balance. FTA32 Video 2.0 software (freely distributed by First Ten Angstroms, Inc.) was used to calculate the surface tension based on the droplet profile. The drop dimensions were calibrated using the needle diameter as a reference point. This method yielded surface tensions for water (either distilled/deionized or HPLC grade) that were 5-10% higher than the accepted value (78-80 mN/m vs. 72.7 mN/m, from Haar et al. (1984)). Tests with ethylene glycol (48.4 mN/m) and propanol (22.4 mN/m) (Jasper, 1972) revealed a similar offset. A simple linear calibration (equation 4.14) based on these data was consequently applied to all measurements.

$$\sigma(\text{calibrated, mN/m}) = 0.9117\sigma(\text{measured, mN/m}) + 1.8074 \qquad (4.14)$$

Every sample was tested at least five times (i.e., five different dispensed droplets). A water standard was always tested together with unknowns to ensure the 5-10% "offset" was still being exhibited. Overall, the pendant drop analysis was simple to perform and yielded highly reproducible results. The inability to make measurements at temperatures other than ambient was perhaps its one weakness. This was not particularly worrisome, though, because surface tension is a fairly weak function of temperature. For instance, from 20 to 40°C, the temperature range roughly pertinent to the packed column, the surface tension of water only decreases from 72.7 to 69.6 mN/m (Haar et al., 1984). The surface tension during experiments involving TERGITOL NP-7 or POLYOX WSR N750 was approximated as being equal to the value measured at room temperature. For illustrative purposes, a snapshot of an analyzed water droplet in FTA32 Video 2.0 is shown in Figure 4.10.
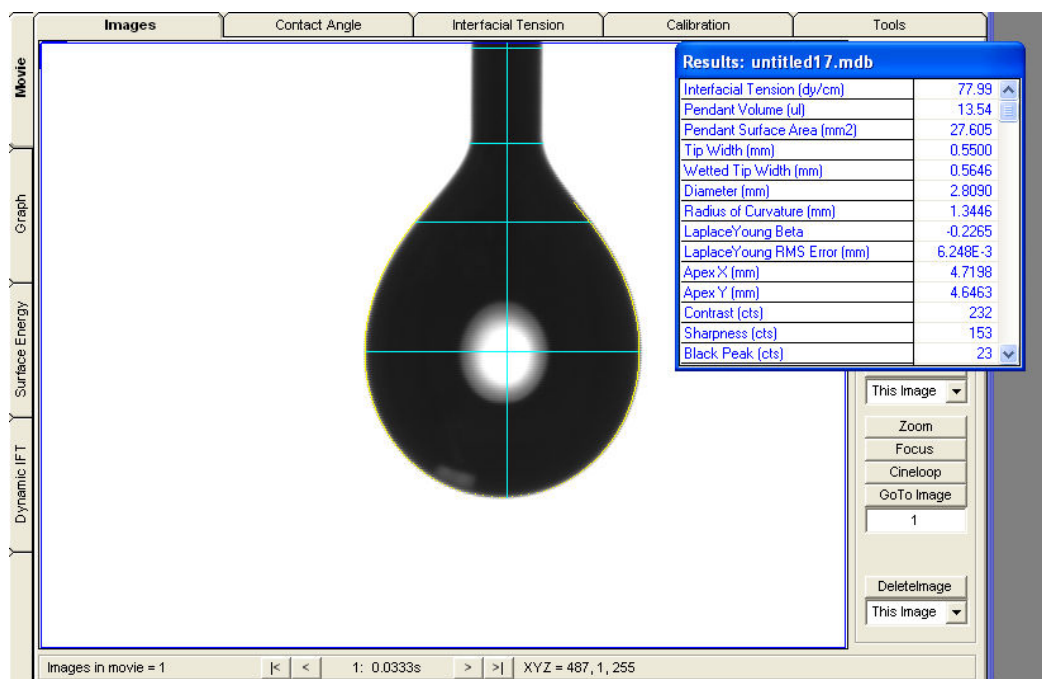
Figure 4.10. Image of pendant drop (water) analyzed in FTA32 Video 2.0.

Contact angle was measured via the sessile drop method. A smooth piece of stainless steel was used as the surface of interest. (Measurements with a flat piece of sheet metal sharing the same features as Mellapak^{TM} structured packing were initially attempted but were found to be unreliable due to the dimpled surface.) Preparation of the surface involved a thorough rinsing with Alconox solution, acetone, and distilled water, followed by drying in a clean oven. After the surface was allowed to cool, measurements were conducted immediately to minimize the potential for surface contamination. Analysis was done via DROPimage software that was installed on the goniometer computer. A 5 mm^3 (5 μL) droplet was dispensed on the surface, and a completely level baseline was established within the DROPimage window – if necessary, by adjusting the tilt of the Teflon stage. The droplet was framed, and its contact angle and dimensions

were output by the program. Contact angles were evaluated quickly (within 30 secs) after deposition, before significant evaporation could occur. For illustrative purposes, a snapshot of a water droplet is displayed in Figure 4.11.
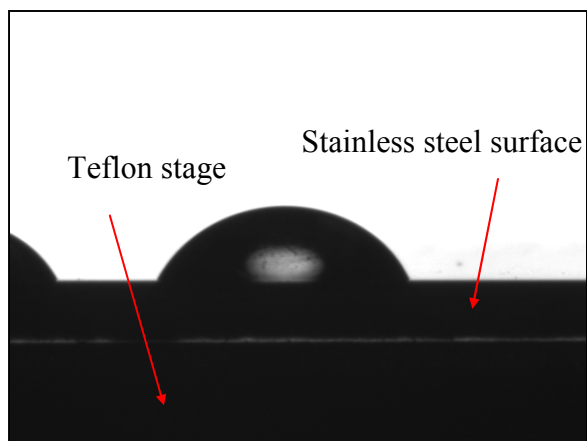
Figure 4.11. Image of sessile drop (water) on stainless steel surface.

Step-by-step instructions for both the surface tension and contact angle measurements can be found in Appendix A.2.

4.3.3 Rheometer (Viscosity)

A Physica MCR 300 rheometer (Anton Paar, USA) equipped with a cone-plate spindle (CP 50-1) was used for viscosity measurements. It was maintained by Dr. Keith Friedman and shared with the undergraduate chemical engineering fundamentals laboratory (ChE 253M) at the University of Texas at Austin (CPE 1.420). Temperature was regulated (±0.1°C) with a Peltier unit (TEK 150P-C) and a Julabo F25 water bath unit (for counter-cooling). After appropriately setting up the system (see Appendix A.3 for operating instructions), 700 mm^3 (700 µL) of sample was deposited on the rheometer platform, and the analysis was performed. The spindle was rotated at a specified angular

velocity, and the torque required to turn it was measured; viscosity was calculated based on these parameters and the system geometry (i.e., cone radius and angle). Profiles consisted of a logarithmically ramped or decremented shear rate (100-500 s^{-1}), with a minimum of 10 points taken at 15 second intervals. The shear rate range was tailored to the anticipated conditions in the packed column, calculated under the assumptions of a Nusselt film thickness and a no-slip boundary layer. Measurements at shear rates higher than 500 s^{-1} were considered to be misleading, due to the increasingly non-Newtonian (shear thinning) behavior of the POLYOX solutions.

4.3.4 Density Meter

A Mettler Toledo DE40 density meter was used to measure the densities of solutions. The instrument consisted of an oscillating U-shaped glass tube. The oscillation frequency of the tube was related to the density of solution contained inside. The apparatus was highly accurate (±0.0001 g/cm^3) and simple to operate. The machine was purged with water and then acetone prior to analyzing the sample of interest.

4.4 CHEMICALS AND MATERIALS

The NaOH [1310-73-2] used in WWC experiments was purchased from Fisher Scientific (certified grade, 0.1005-0.0995 N). The Department of Physics at the University of Texas at Austin supplied the N_2 [7727-37-9], which was greater than 99% pure. The 5000 ppm$_v$ CO_2 [124-38-9] was procured from Praxair. The $CaSO_4$ (mesh size

of 8) [7778-18-9] exhibited a blue-to-purple color change depending on its saturation and was obtained from W.A. Hammond Drierite Company Ltd.

The NaOH pellets used for the packed column tests were reagent grade and were purchased from PHARMCO-AAPER (98.5%) (primary source) or EMD Chemicals Inc. (97.0%) (alternate source). The difference in caustic solution preparation relative to the WWC was a matter of convenience and was not believed to adversely affect the comparability of the experiments. Both the titration HCl (reagent grade) [7647-01-0] and phenolphthalein solution [77-09-8] were obtained from Ricca Chemical Company. The concentrated HCl (38%, CMOS grade) utilized for neutralization was from J.T. Baker. The N_2 and 450 ppm_v CO_2 cylinders were supplied by Praxair.

The acid solution used in TIC analyses was prepared from a stock solution of 85 wt % o-H_3PO_4 [7664-38-2] that was purchased from Fisher Scientific. The Na_2CO_3/$NaHCO_3$ [497-19-8 / 144-55-8] standard solution was obtained from Ricca Chemical Company. The $MgClO_4$ [10034-81-8] was purchased from Fisher Scientific.

TERGITOL NP-7 [127087-87-0], a nonionic nonylphenol ethoxylate-based surfactant, was initially supplied by Dow (sample quantity) and then later procured from Sigma-Aldrich. POLYOX WSR N750 [25322-68-3], which was basically poly(ethylene oxide) with a molecular weight of 300,000, was obtained from Dow (via ChemPoint). The antifoam agent (Q2-3183A), a silicone dispersion consisting of small quantities of octylphenoxy polyethoxy ethanol, polyether polyol, and treated silica, was supplied by Dow Corning® (via UNIVAR).

Chapter 5: Wetted-Wall Column Results

The experiments conducted using the wetted-wall column (WWC) are summarized in this chapter. Justification for the use of the kinetic correlations of Pohorecki and Moniuk (1988), rather than alternatives in the literature, is first offered, and then the WWC results are discussed. The absorption rate of CO_2 in 0.1 mol/L NaOH (base case) was measured. The effect of surfactant (surface tension reducer) and polymer (viscosity enhancer) on this rate was also investigated. The data were found to match the values predicted from literature models within 10%.

5.1 KINETIC MODELS

The kinetics of CO_2 absorption into aqueous hydroxide solutions have been examined in numerous literature studies (Pinsent et al., 1956; Nijsing et al., 1959; Hikita and Asai, 1964; Pohorecki and Moniuk, 1988; Kucka et al., 2002). The kinetic model (k_{OH^-}) of Pohorecki and Moniuk was specifically selected as the basis for this investigation for several reasons. Of the cited sources, it was the only one that contained the NaOH concentration of interest (0.1 mol/L) in its experimental range. The tested temperatures (18 to 41°C) were more pertinent than those examined in some of the other studies. In addition, Pohorecki and Moniuk provided a comprehensive set of equations for not only k_{OH^-} but also the other k_g'-implicit parameters (H_{CO2} and D_{CO2}), along with densities and viscosities (Moniuk and Pohorecki, 1991). This transparency eliminated discrepancies that could have arisen when attempting to compare calculated k_g' values with experimental ones. The Pohorecki and Moniuk correlations have historically been

112

used by the Separations Research Program for packing area characterization studies, and it was convenient to continue the present work along these lines. Finally, the quality of the Pohorecki and Moniuk models has been singled out by various sources (Haubrock et al., 2005; Hoffman et al., 2007; Rejl et al., 2009).

5.2 BASE CASE

Baseline experiments consisting of the absorption of CO_2 into 0.1 mol/L NaOH were performed to verify the model of Pohorecki and Moniuk (1988). The results were interpreted in terms of a normalized k_g' (experimental k_g' / "Pohorecki" k_g') and are plotted as a function of log-mean CO_2 partial pressure (Figure 5.1), liquid flow rate (Figure 5.2), and temperature (Figure 5.3). The data seem to be randomly distributed for the most part. The fact that no systematic dependence on partial pressure or flow rate was observed serves to affirm that pseudo-first-order conditions were satisfied. While a second-order effect of temperature is perhaps identifiable in Figure 5.3, the trend was not thought to be significant, and the Pohorecki correlation was not believed to be in need of a temperature-based modification. Application of such a correction would not be trivial, considering that k_g' actually contains three terms with fairly strong temperature dependences: k_{OH-}, $D_{CO2,L}$, and H_{CO2}. The WWC temperature range (27-35°C) was selected with outdoor conditions in mind. Control with the heating baths became troublesome below 27°C, which is why lower temperatures were not investigated.
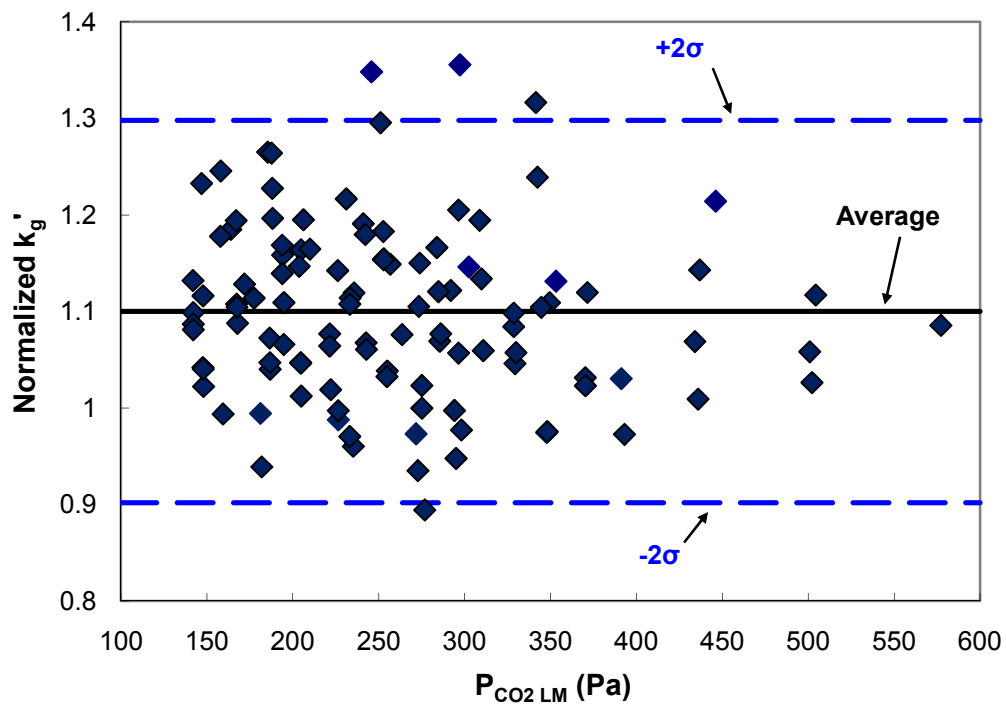
Figure 5.1. Normalized k_g' of base case (0.1 mol/L NaOH) as a function of CO_2 partial pressure.
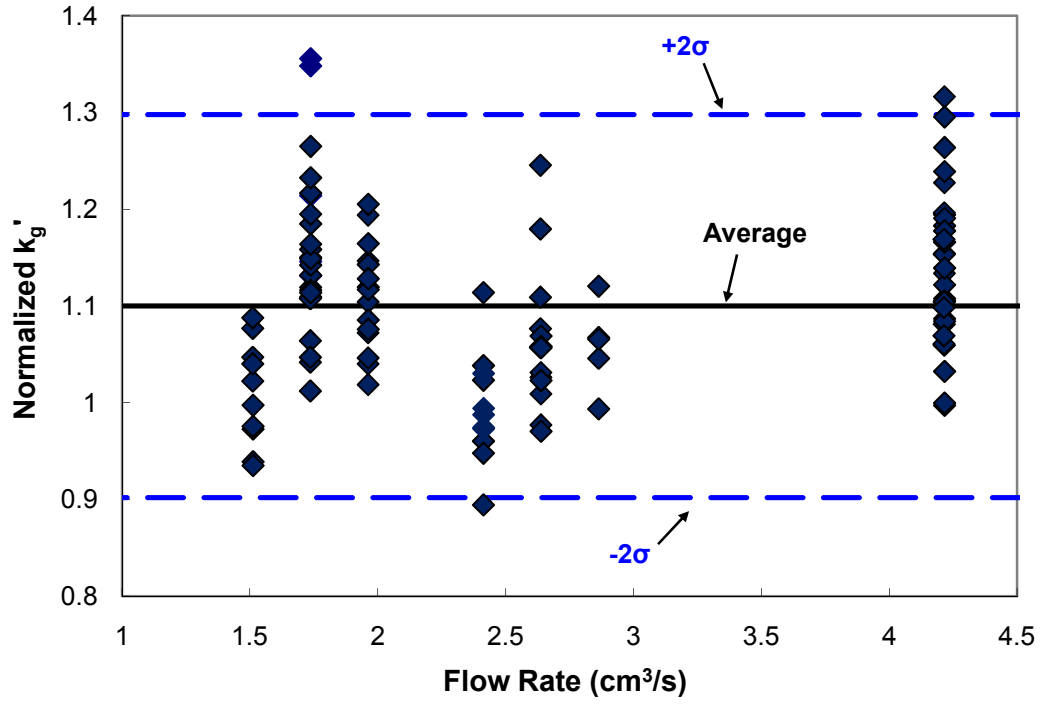
Figure 5.2. Normalized k_g' of base case (0.1 mol/L NaOH) as a function of liquid flow rate.
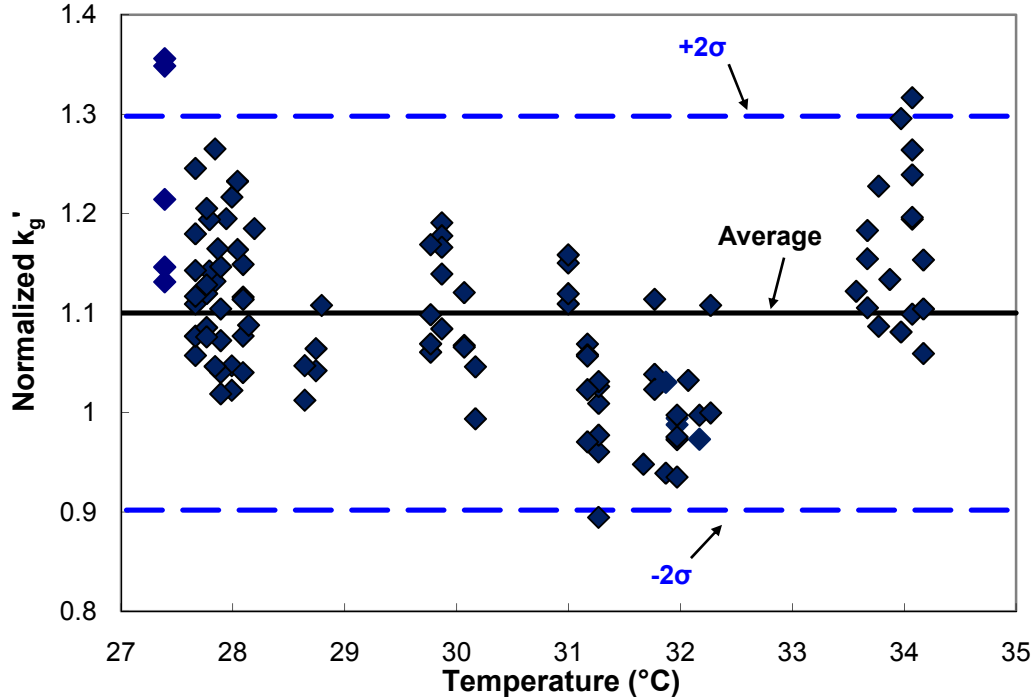
Figure 5.3. Normalized k_g' of base case (0.1 mol/L NaOH) as a function of temperature.

The average normalized k_g' was 1.10 ± 0.09. While the data and the Pohorecki k_g' were in reasonable agreement, the results appear to be systematically 10% greater than the model. Pohorecki and Moniuk found it necessary to apply a correction for bulk-to-interface hydroxide depletion for their experiments in the dilute region ($I \leq 0.5$ mol/L). This depletion was estimated to be as high as 25% at the lowest investigated concentration (0.1 mol/L) and was addressed somewhat simplistically by assuming an average bulk/interface hydroxide concentration in the calculations. A comparison of their k_{OH^-} correlation with their actual results shows the low-end points (0.1 mol/L) to be underpredicted (in agreement with our findings), whereas the more concentrated solutions are fit better (Figure 5.4).

116
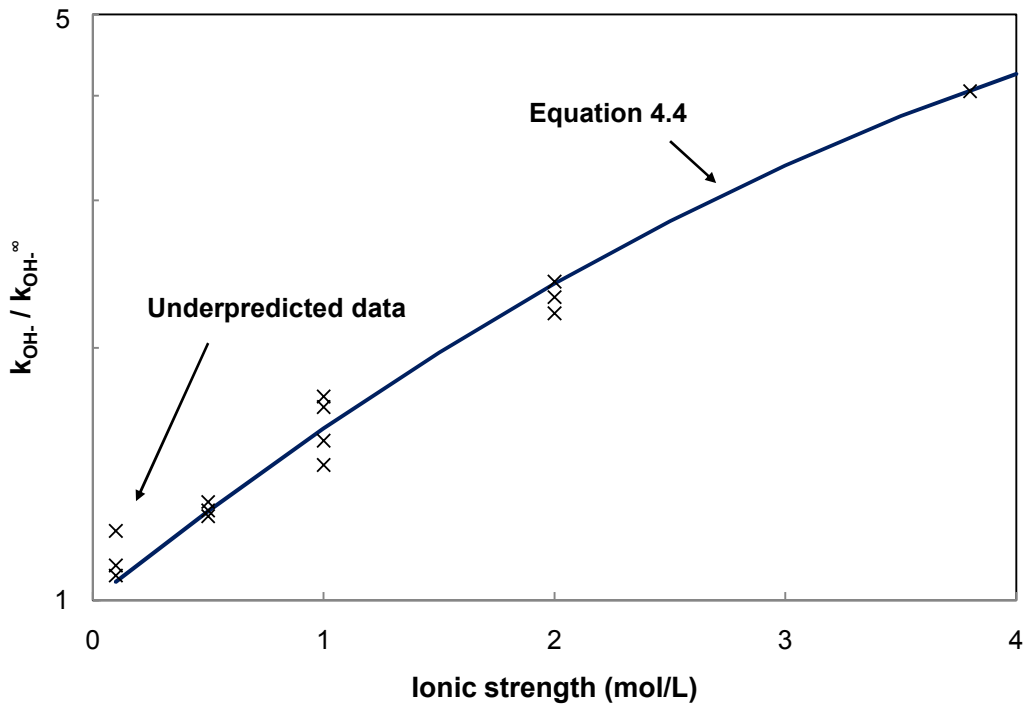
Figure 5.4. Kinetic measurements of CO_2-NaOH system at 20°C, reproduced from Pohorecki and Moniuk (1988).

More scatter in the results is evident with decreasing ionic strength as well, implying that greater error may have been inherently associated with these conditions. The apparently faster rates in the WWC compared to the laminar jet absorber of Pohorecki and Moniuk could also possibly have been a function of liquid film rippling on the WWC surface enhancing the mass transfer. This explanation is not very probable, though. First, the film appeared quiescent for all of the tested flow rates, and furthermore, wave formation would only be anticipated for vertical running lengths much longer than the one here (9.1 cm) (Sherwood et al., 1975).

One could argue based on the WWC data that the Pohorecki k_g' was in need of a small (10%) corrective factor. Nevertheless, the discrepancy was not believed to be

sufficient to dismiss the model, given the experimental standard deviation (also around 10%) and the satisfactory handling of temperature variation. The Pohorecki k_g' was presumed to be acceptable for the interpretation of the packing area measurements. The consequences of this decision must be stressed. The fact that the mass transfer area is inversely related to k_g' (see equation 4.13) means the "selection" of k_g' has a significant impact on the analysis – not necessarily qualitatively but at the very least quantitatively. This issue is given more thought in Section 6.10.1.

5.3 SURFACTANT SYSTEM

Several water soluble surfactants (DOWFAX[TM] C6L, TRITON[TM] X-114, TERGITOL[TM] TMN-6, TERGITOL[TM] TMN-100X, and TERGITOL[TM] NP-7) were considered for the purpose of reducing surface tension. These surfactants were recommended by a Dow representative on account of their stability under acidic/basic conditions. TERGITOL NP-7 appeared to result in the least amount of foaming and was ultimately chosen above the other surfactants because of this characteristic. It was slightly more potent than the alternatives as well, requiring a concentration of 125 ppm$_v$ to lower surface tension to 30-35 mN/m.

Foaming was, nevertheless, still a significant issue with TERGITOL NP-7, especially in the packed column, and consequently, Dow Corning[®] Q2-3183A antifoam was used for foam mitigation. A preliminary caustic scrubbing experiment in the packed column was performed by Kettner (2006), in which 125 ppm$_v$ of TERGITOL NP-7 and 150 mg/L of antifoam were used. No major operational issues were reported. When this

same system was tested in the WWC, though, film stability problems were observed, evidenced either by rippling in the film or dry spots on the column. A stable film was ultimately found to be maintainable by using less antifoam (50 mg/L) and operating at a high liquid flow rate (greater than 4 cm^3/s). Schultheiss (2006) subsequently tested this solution in the packed column and discovered that foaming remained under control even with the reduced antifoam concentration. Hence, the blend of 125 ppm$_v$ of TERGITOL NP-7 and 50 mg/L antifoam was used in all WWC experiments and the majority of packed column experiments at low surface tension. For the latter, elevated antifoam concentrations (generally no higher than 100 mg/L) were on occasion used for two reasons. First, the antifoam seemed to lose effectiveness over time, not only in terms of aging but also during operation, and tests in the later stage of the present project in particular were run longer to obtain more comprehensive data sets. Second, as mentioned earlier, hydraulic and mass transfer tests were run with the same liquid inventory to minimize waste, which resulted in the carry-over of antifoam between experiments. Ideally, WWC experiments should have been conducted to coincide exactly with the concentrations used in the packed tower, but it did not seem likely that there would be an appreciable difference in kinetic (k_g') behavior over the range of "actual" antifoam concentrations. The WWC results with 125 ppm$_v$ TERGITOL NP-7 and 50 mg/L antifoam were presumed to be universally applicable.

The results from the WWC tests at low surface tension are displayed in Figure 5.5. For comparison, the neat 0.1 mol/L NaOH data obtained over the same timeframe are shown as well.
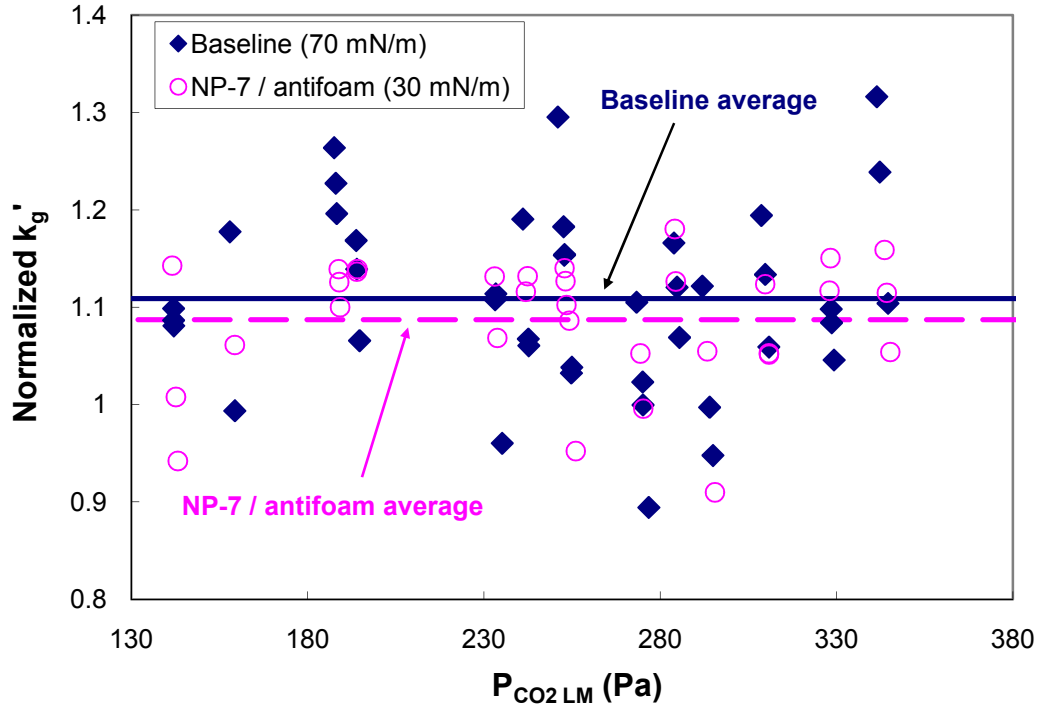
Figure 5.5. Normalized k_g' of base case (0.1 mol/L NaOH) and surfactant system (0.1 mol/L NaOH + 125 ppm$_v$ TERGITOL NP-7 + 50 mg/L Q2-3183A antifoam).

The average normalized k_g' for the surfactant system (1.09 ± 0.07) was quite similar to the base case. A null hypothesis test (Z-test with a pooled variance) with a 95% confidence interval was applied and revealed there to be no statistically significant difference between the base case and surfactant system results. Thus, the TERGITOL NP-7 and antifoam were concluded to have no impact on the kinetics, and the Pohorecki k_g' was deemed to be appropriate for use in the analysis of the mass transfer experiments at low surface tension as well.

The influence of surfactants on mass transfer across gas-liquid interfaces has been investigated in numerous studies in the literature. Results have varied wildly. For example, Burnett, Jr. and Himmelblau (1970) investigated an ammonia-water system and

found that absorption rates could either increase (soluble surfactant) or decrease (insoluble surfactant). The general consensus, however, seems to be that surfactants tend to inhibit mass transfer. Two causes for this reduction have been proposed: the dampening or elimination of interfacial turbulence (i.e., rippling) and the formation of a physical barrier hindering transfer (Emmert and Pigford, 1954; Burnett, Jr. and Himmelblau, 1970; Nguyen Ly et al., 1979). The latter premise implies that a surfactant-related resistance term, in addition to the gas-side and liquid-side resistances, should be incorporated into the overall resistance. While the magnitude of this resistance is likely a function of not only surfactant concentration but also specific surfactant type, making it difficult to quantify, the barrier contribution has been concluded to be negligible relative to the impact from rippling in a number of sources (Emmert and Pigford, 1954; Sherwood et al., 1975). Consequently, it is neglected in the present work. As was explained in Section 5.2, rippling was not anticipated to be a factor (with or without surfactant) in the WWC set-up on account of the short tube length. Hence, both surfactant-associated mechanisms proposed above were ruled out. A third issue warranting consideration was the potential impact of the surfactant and antifoam on local ion concentrations. This effect could have been important had the additives been charged species, but they were nonionic, so this concern was dismissed as well. Having discounted all of these factors, the comparable k_g' results for the baseline and surfactant seemed reasonable.

5.4 POLYOX SYSTEM

POLYOX[TM] WSR N750 was used as a viscosity enhancer. Since the maximum concentration used was fairly low (1.25 wt %), significant changes to the rate constant (k_{OH^-}) or CO_2 solubility (H_{CO2}) were not anticipated. In dilute, mixed solutions of electrolytes and organics (or nonelectrolytes), Rischbieter et al. (1996) noted that the impact of both components on gas solubility can be represented by the Sechenov relation (i.e., salting-out effect), shown in generic form below. Solubility is related to the concentration of species in solution ([S]) by a constant (K_s). The subscript 0 refers to a pure solution.

$$\log\left(\frac{H_G}{H_{G,0}}\right) = K_s[S] \tag{5.1}$$

Lohse et al. (1981) measured the solubility of CO_2 in aqueous solutions of poly(ethylene oxide) and poly(vinyl alcohol) and correlated the results in the same form as equation 5.1, with $K_s = 2.23 \times 10^{-4}$ L/g. The impact of 1.25 wt % POLYOX WSR N750 on CO_2 solubility (H_{CO2}) was calculated to be around 0.5% using this correlation – negligible relative to the electrolyte contribution already being accounted for with the Pohorecki model (equation 4.6).

Rischbieter et al. (1996) did not speculate on any kinetic effects, but in the context of the current work, the solubility relation was presumed to be extendable to the treatment of the rate constant (k_{OH^-}). That is, the polymer impact was associated with an electrolyte contribution or in other words, ionic strength. For 0.1 mol/L NaOH, the electrolyte ionic strength contribution to k_{OH^-} is rather small to begin with. For instance,

in equation 4.4, the summed temperature contribution (terms in equation 4.4a) is over two orders of magnitude larger than the summed ionic strength contribution at 25°C. The POLYOX WSR N750 impact was likely to be even weaker, so its presence was presumed to have no effect on k_{OH^-}.

In contrast with the other parameters implicit to k_g', one would anticipate the CO_2 diffusion coefficient ($D_{CO2,L}$) to be different for the viscous polymer solution. The relation proposed by Pohorecki and Moniuk assumes the diffusion coefficient to vary inversely (1:1) with viscosity. A ten-fold viscosity enhancement would therefore be expected to decrease k_g' by a factor of $\sqrt{10}$, or approximately 3. A rather unique feature of aqueous polymer solutions, however, was revealed upon review of the literature: limited influence on the diffusivity of small molecules like CO_2, even at high viscosity. Komiyama and Fuoss (1972) measured the conductivity of KCl in aqueous solutions of poly(vinyl alcohol) and found that even when viscosity was increased by over five orders of magnitude, conductance – a reflection of ionic mobility – only decreased by about 50%. They speculated that while the bulk viscosity of a solution might be enhanced by entanglement of long polymer chains, considerable freedom should still exist for the localized movement of chain segments and of small molecules around these segments. In other words, the local viscosity should be significantly lower than the bulk viscosity, and thus, the CO_2 diffusion rates in polymer solutions and in pure solutions should not differ too much. The findings of Osmers and Metzner (1972) and Lohse et al. (1981) were in support of this conclusion as well. In addition to their experiments involving solubility, Lohse et al. made CO_2 diffusion measurements on a wetted-wall column apparatus and

correlated their results in the form of equation 5.2. The subscripts 0 and P respectively refer to pure solution and polymer.

$$\frac{D_{CO_2,L}}{D_{CO_2,0}} = \left(\frac{\mu_L}{\mu_0}\right)^{-3.7\sqrt{\frac{M_0}{M_P}}} \tag{5.2}$$

Equation 5.2 indicates that for a given increase in viscosity, the corresponding impact on the diffusion coefficient will decrease with increasing molecular weight of polymer. For this reason, the fairly large POLYOX WSR N750 (molecular weight of 3×10^5) was selected so that minimal correction would be necessary. (Larger polymers on the order of 10^6 were considered as well but seemed to be more susceptible to undesirable shear thinning.) According to equation 5.2, a ten-fold viscosity enhancement with POLYOX WSR N750 should only decrease diffusion by about 6%.

The k_g' data at high viscosity are presented in Figure 5.6, with the neat 0.1 mol/L NaOH results obtained concurrently also displayed for comparison. The denominator for the viscous system was the Pohorecki k_g' with the diffusion coefficient modified in accordance with equation 5.2. The "pure" diffusion coefficient ($D_{CO2,0}$) was calculated on the basis of NaOH solution (not just water); in other words, it was the $D_{CO2,L}$ used for the baseline calculations (equation 4.5). These tests would have ideally been run with 50-100 mg/L antifoam in order to directly relate the WWC and packed column systems, but unfortunately, this was not done. Nevertheless, based on the surfactant system data, it did not seem probable that the inclusion of antifoam would have made any difference in the results.
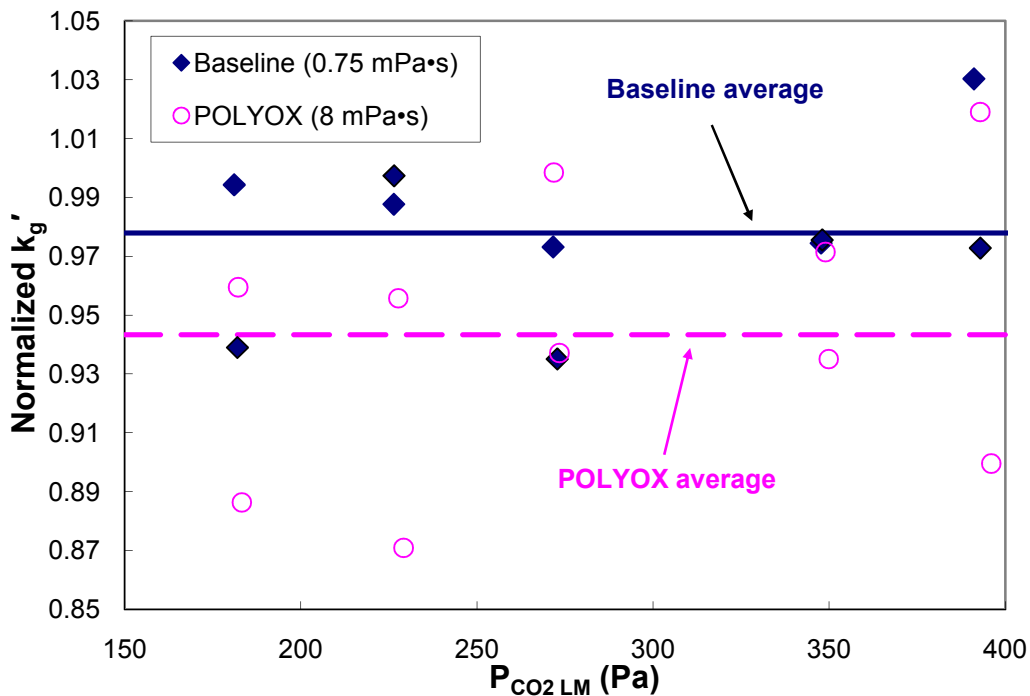
Figure 5.6. Normalized k_g' of base case (0.1 mol/L NaOH) and polymer system (0.1 mol/L NaOH + 1.25 wt % POLYOX WSR N750).

The average normalized k_g' was 0.94 ± 0.05. The modified k_g' model matched the data well and affirmed the bulk-vs.-local viscosity theory. A null hypothesis test with a 95% confidence interval (Z-test with a pooled variance) did, however, reveal that the normalized k_g' values for the base case and POLYOX system were statistically dissimilar, which raised the possibility of a small (less than 5%) bias in the interpretation of the packing area data. The slight overprediction of the Pohorecki-Lohse model could have been a function of the diffusion coefficient equation (equation 5.2) being extrapolated beyond its limits; the maximum molecular weight in the databank of Lohse et al. (1981) was 10^5. The polydispersity (i.e., molecular weight distribution) of POLYOX WSR

N750 could have been an issue too, but the variance between the samples was likely not large enough to appreciably affect the diffusion coefficient.

The normalized data in these particular baseline experiments were closer to unity than the past data. The newer Horiba VIA-510 was installed in place of the Horiba PIR-2000 prior to these experiments, so this difference may have been related to the instrument changeover.

5.5 SUMMARY OF RESULTS

The WWC results for the three tested systems (base case (0.1 mol/L NaOH), low surface tension (0.1 mol/L NaOH + 125 ppm$_v$ TERGITOL NP-7 + 50 mg/L Dow Corning Q2-3183A antifoam), and high viscosity (0.1 mol/L NaOH + 1.25 wt % POLYOX WSR N750)) are summarized in Table 5.1. The data from the baseline experiments performed concurrently with the TERGITOL NP-7 and POLYOX WSR N750 runs are also shown for reference. To reiterate, the model k_g' for the baseline and low surface tension systems was simply the Pohorecki k_g'. The model k_g' for the viscous system was the Pohorecki k_g' corrected with the Lohse diffusion coefficient.

The Pohorecki and Pohorecki-Lohse models matched the data within 10% and were believed to be acceptable for use with no further modifications. Because the fit was not perfect, small impacts of surface tension or viscosity in the packing area measurements could have effectively been obscured. For example, the normalized k_g' for the POLYOX system was about 5% lower than the concurrent base case value, which meant that the detection limit of a viscosity effect was on the order of 5%. If the

viscosity impact happened to be of this magnitude and affected the mass transfer area in a systematically opposite fashion as the applied k_g', then such an effect would go entirely unnoticed.

Table 5.1. Summary of WWC results (experimental conditions: 27-35°C, 0.11-0.32 m/s (gas), 1.5-4.2 cm³/s (liquid), 150-630 Pa CO_2 at inlet).

Test system	Approx. μ_L and/or σ	# of data pts.	Normalized k_g'	Normalized k_g' (base case)	Experiment dates
0.1 mol/L NaOH (all)	0.8 mPa·s 70 mN/m	111	1.10 ± 0.09	N/A	4/20/06 – 6/13/08
0.1 mol/L NaOH 125 ppm$_v$ TERGITOL NP-7 50 mg/L Dow Corning Q2-3183A antifoam	30 mN/m	32	1.09 ± 0.07	1.11 ± 0.09	9/22/06 – 11/2/06
0.1 mol/L NaOH 1.25 wt % POLYOX WSR N750	8 mPa·s	10	0.94 ± 0.05	0.98 ± 0.03	3/27/07 – 3/30/07

128

Chapter 6: Packed Column Results (Mass Transfer Area)

The structured packing effective area results are presented in this chapter. The development of a global model to represent the database is discussed, and this model is compared against several other correlations in the literature. Finally, analyses involving alternate interpretations of the data are provided.

The experimental data showed the mass transfer area to be most strongly related to packing surface area (125-500 m^2/m^3) and liquid load (2.5-75 $m^3/m^2\cdot$h or 1-30 gpm/ft^2). Surface tension (30-72 mN/m) had a weaker but significant effect. Gas velocity (0.6-2.3 m/s), liquid viscosity (1-15 mPa·s), and flow channel configuration had essentially no impact on the area. Surface texture (embossing) increased the effective area by 10% at most. The ratio of mass transfer area to specific area (a_e/a_p) was correlated within limits of ±13% for the entire experimental database. This global model is shown below:

$$\frac{a_e}{a_p} = a_f = 1.34\left[\left(\frac{\rho_L}{\sigma}\right)g^{1/3}\left(\frac{Q}{L_p}\right)^{4/3}\right]^{0.116}$$

The predicted fractional area can be seen to be a function of liquid density (ρ_L, in kg/m^3), surface tension (σ, in N/m or equivalently kg/s^2), the gravitational constant (9.81 m/s^2), and the flow rate per wetted perimeter (Q/L_p, in m^3/m·s).

6.1 MASS TRANSFER AREA EXPERIMENT: GENERAL COMMENTS

The mass transfer area results from a typical run with Sulzer Mellapak™ 250Y, a standard, high-capacity, structured packing, are shown in Figure 6.1. As might be anticipated, the effective area can be seen to increase with liquid load. The points also all overlay closely, despite being distinguished by three different air velocities. This result is further discussed in Section 6.4.
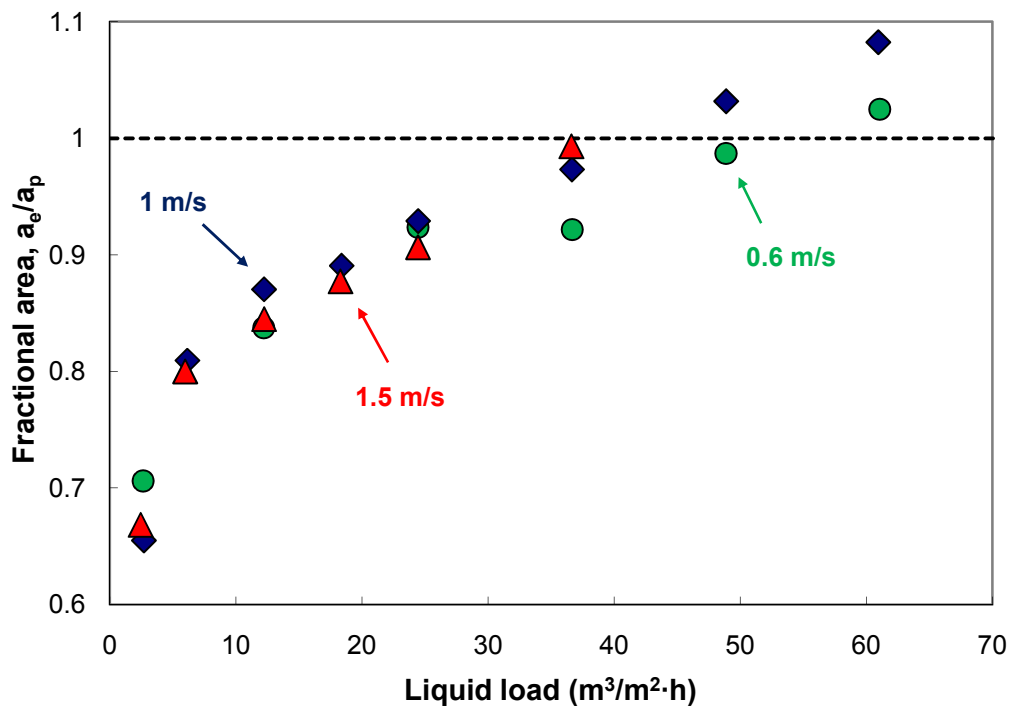
Figure 6.1. Mass transfer area of Mellapak 250Y ($a_p = 250$ m^2/m^3).

6.1.1 Liquid Distribution

As stated in the Experimental Methods, a pressurized fractal distributor with 108 drip points/m^2 was utilized for liquid distribution in every experiment. This density was believed to be sufficient to avoid maldistribution and other undesirable effects, based on

past distributor studies conducted by the Separations Research Program (SRP) at the University of Texas at Austin. In these tests, the mass transfer area of a prototype 500-series packing (a_p = 500 m^2/m^3) was evaluated via an earlier yet analogous version of the methodology used in the current work. Four distributors were compared: a fractal distributor with 430 points/m^2, a gravity-fed orifice pipe with 430 points/m^2, a trough drip tube with 145 points/m^2, and the fractal distributor with 108 points/m^2. The respective fractional areas (a_e/a_p) that were measured at a superficial gas velocity of 1 m/s and liquid load of 36.6 m^3/m^2·h (15 gpm/ft^2) were 0.57, 0.53, 0.58, and 0.54. The fact that the trough drip tube (intermediate drip point density) happened to yield the highest area or that the orifice pipe (highest drip point density) happened to yield the lowest area should not be over-interpreted; the differences between the distributors (less than 10%) were within the anticipated noise limits. Similar results were obtained at other gas and liquid loads as well. For the purpose of these packing characterization studies, the 108 point/m^2 fractal distributor was concluded to be just as effective as the much denser variants, which surely possessed enough drip points to eliminate any concerns over poor distribution. This assumption is echoed in the literature. Perry et al. (1990), for instance, reported a distribution density of 100 points/m^2 to work well for most packings.

6.1.2 Pre-wetting

The pre-wetting of packing prior to start-up is a common industrial practice. The idea is to maximize the packing efficiency by creating a surface conducive to liquid

spreading (i.e., liquid-liquid contact instead of liquid-solid contact). Pre-wetting was incorporated into the experimental protocol to relate the system performance as closely to industry as possible, but this practice could potentially obscure the true interaction of liquid load and effective area. The intent was to coat the packing surface, but if this liquid film were actually acting as a source of mass transfer, then at conditions of lower CO_2 removal (i.e., low liquid loads) especially, the measured area would be a reflection of both the liquid throughput and the stagnant liquid.

To investigate this effect, a simple saturation study was conducted. Caustic solution (0.1 mol/L NaOH) was prepared as in a typical mass transfer experiment, and the packing (Mellapak 2Y, $a_p = 205$ m^2/m^3) was pre-wetted at a liquid load of 61 m^3/m$^2 \cdot$h (25 gpm/ft^2) for 10 minutes. The pump was then shut down, and liquid was allowed to drain from the packing for 15 minutes. The blower was turned on and set at a superficial air velocity of 1 m/s (300 ACFM), and the approach of the outlet CO_2 concentration toward the inlet (ambient) level was monitored. Afterward, this same procedure was repeated, except with a drainage time of only 5 minutes. Figure 6.2 displays the results from these tests.
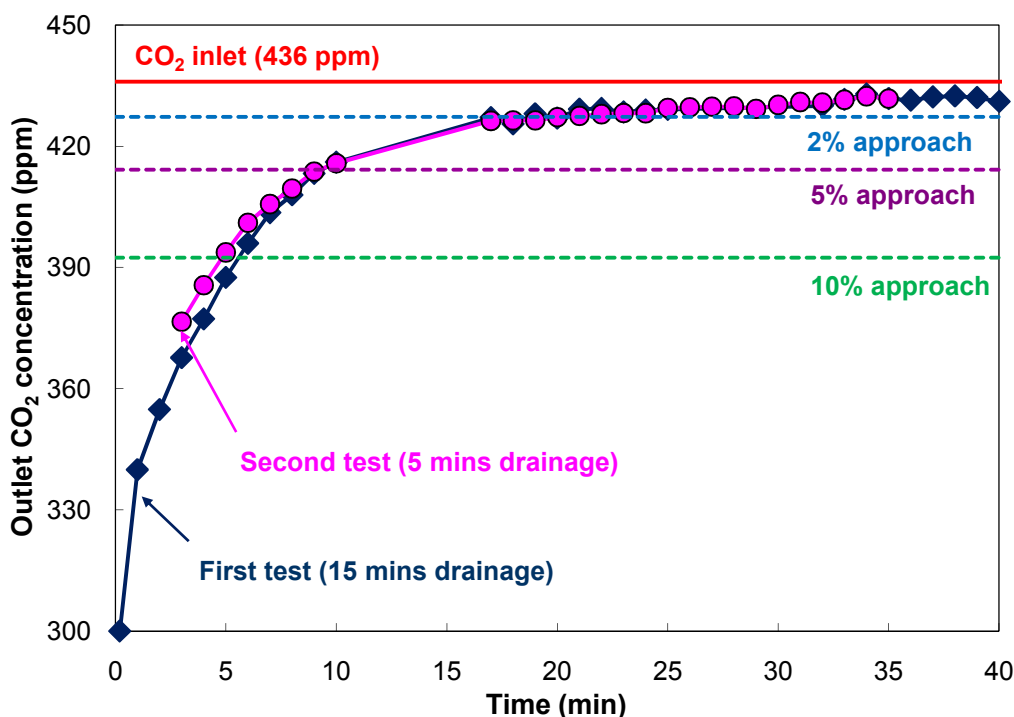
Figure 6.2. Pre-wetting film saturation data obtained with Mellapak 2Y ($a_p = 205$ m^2/m^3). Inlet CO$_2$ concentration was periodically confirmed, as reflected by gaps in the data (e.g., from 10 to 15 min).

Static hold-up is generally quite small in structured packing (Rocha et al., 1993), so it was not surprising that the two experiments gave similar results. In other words, the packing was expected to drain freely. The area above either curve can be roughly estimated as 1000 ppm CO$_2$·min. If a complete stoichiometric (2:1) reaction of OH$^-$ with CO$_2$ and a solution concentration of 0.1 mol/L are assumed, the associated liquid volume is 6.9 L, which translates to a static hold-up of 1.5%.

Much of the active hydroxide was consumed within the first 10 minutes; the outlet CO$_2$ concentration was already within about 5% of the inlet concentration by this point. A 2% approach to the inlet concentration was achieved after about 20 minutes. Since the liquid circulation was completely shut off, all of the CO$_2$ removal was

133

attributable to the pre-wetting process, so this exercise could in essence be considered a worst-case scenario. The results were incorporated into the experimental protocol. Conditions were usually given 10 minutes to reach steady state, but whenever transitioning from a high liquid load to a low one (e.g., pre-wetting to start-up), a longer period of time (20 minutes) was allowed to ensure the mass transfer contribution from the stagnant liquid was minimized. The vast majority of experiments were performed in order of increasing liquid load, but a few tests were done in decreasing order. In light of these findings, the latter practice should henceforth probably be ceased, in an effort to avoid hysteresis-related problems.

6.2 DATABASE OVERVIEW AND MODEL DEVELOPMENT

The entire database of mass transfer area measurements is shown in Figure 6.3 and can be found tabulated in Appendix B.3. Table 6.1 lists the packings included in this database, along with their relevant physical dimensions and approximate conditions at which they were tested. Experiments at low surface tension (30 mN/m) and high viscosity (10 mPa·s) were conducted using the same additives as tested in the WWC – that is, 125 ppm$_v$ TERGITOL NP-7 and 1.25 wt % POLYOX WSR N750, respectively. Intermediate viscosity (5 mPa·s) cases were run using a slightly lower concentration of POLYOX WSR 750 (0.85 wt %). This system was not explicitly investigated in the WWC but was assumed to adhere to the same model as the high viscosity scenario. The channel dimensions (see equation 3.43) were defined in the same triangular relation as in other publications like Olujic et al. (2004) and Side-Boumedine and Raynal (2005). The

134

perimeter per cross-sectional area (L_p/A) was specified in terms of the packing channel geometry (equation 6.1). This definition necessarily presumes there to be flow on the channel undersides, which is consistent with the observations of Shetty and Cerro (1995) and Green (2006).

$$\frac{L_p}{A} = \frac{4S}{Bh} \tag{6.1}$$

All packings were manufactured by Sulzer Chemtech (Mellapak^{TM} and MellapakPlus^{TM}), with the exception of Flexipac^{TM} 1Y (Koch-Glitsch Inc.) and the prototype 500-series packing. Every packing surface was perforated.

M250Y, M500Y, and F1Y were the only packings with channel dimensions listed in the literature. M250X, MP252Y, and M250YS were examined and were found to be very similar to M250Y in this regard, so the cited M250Y dimensions were presumed applicable for these packings. The channel dimensions for M125Y and M2Y in Table 6.1 were based solely on actual measurements. Void fraction can roughly be calculated on the basis of specific area and sheet thickness (t_{sheet}), which is usually around 0.1 mm (Pilling, 2008).

$$\varepsilon \cong 1 - \frac{a_p t_{sheet}}{2} \tag{6.2}$$

The void fractions for M125Y and M2Y (both about 0.99) were determined in this manner.
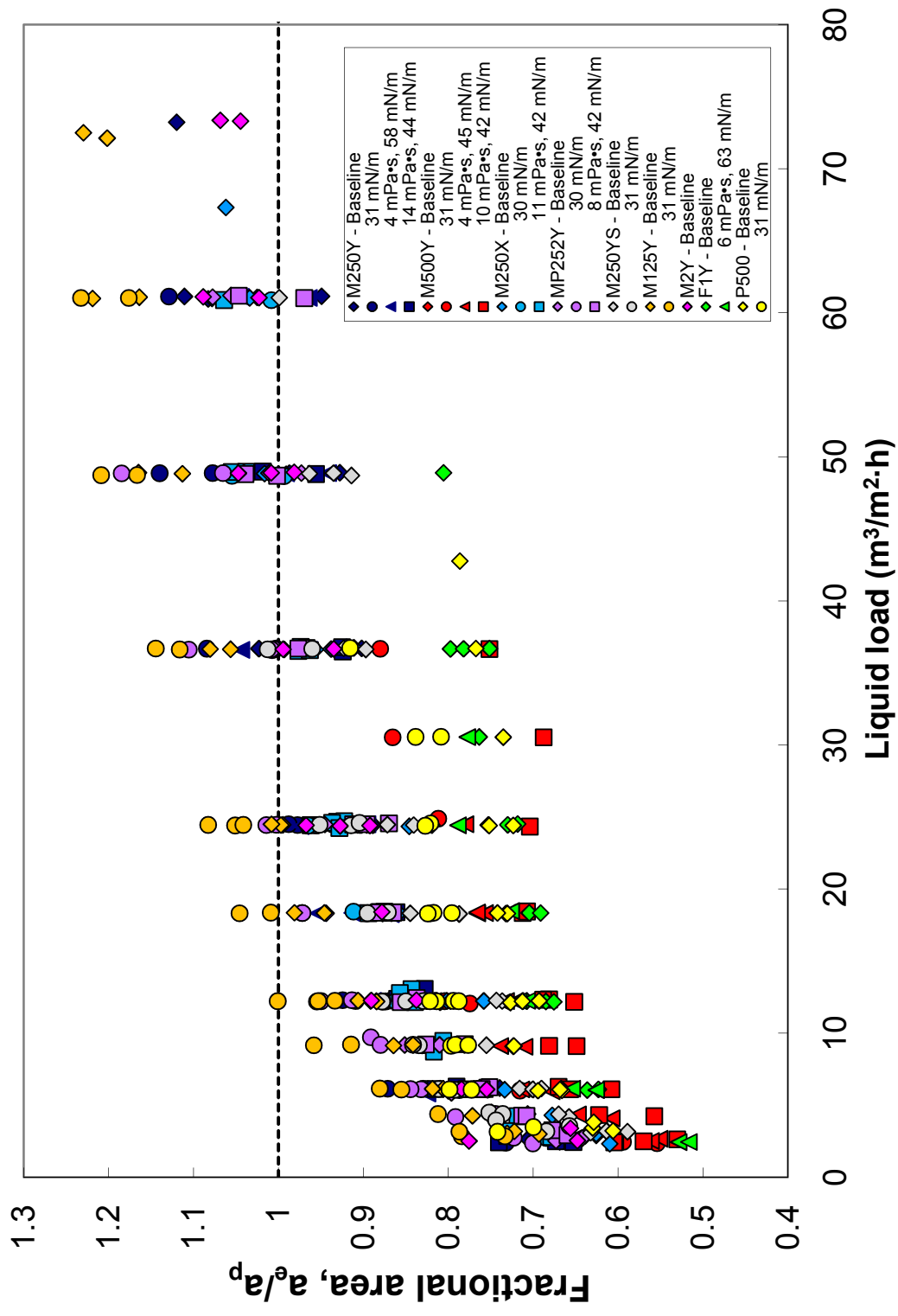
Figure 6.3. Structured packing mass transfer area database.

136

Table 6.1. Packings and experimental conditions included in mass transfer area database.

Packing	Specific area, a_p (m²/m³)	Corrugation angle, α (°)	Channel side, S (mm)	Channel base, B (mm)	Crimp height, h (mm)	Perimeter per xs-area, L_p/A (m/m²)	Void fraction, ε	Parameter source(s)	Conditions: μ_L^a (mPa·s) / σ^b (mN/m)
Mellapak 250Y (M250Y)	250	45	17	24.1	11.9	237	0.95	Petre et al. (2003)	1/73, 0.8/31, 4/58, 14/44
Mellapak 500Y (M500Y)	500	45	8.1	9.6	6.53	517	0.92	Aroonwilas (2001)	1/73, 0.9/31, 4/45, 10/42
Mellapak 250X (M250X)	250	60	17	24.1	11.9	237	0.98	a_p, α, ε: Suess and Spiegel (1992) Others: measured	1/73, 1/30, 11/42
MellapakPlus 252Y (MP252Y)	250	45	17	24.1	11.9	237	0.98	a_p, α, ε: Alix and Raynal (2008) Others: measured	0.8/71, 0.8/30, 8/42
Mellapak 250Y (smooth) (M250YS)	250[c]	45	17	24.1	11.9	237	0.95	ε: assumed same as M250Y Others: measured	1.1/73, 1/31
Mellapak 125Y (M125Y)	125	45	37	55	24.8	109	0.99	a_p, α: Spiegel and Meier (1988) Others: meas./calc.	0.9/72, 0.8/31
Mellapak 2Y (M2Y)	205	45	21.5	33	13.8	189	0.99	a_p: Pilling (2008) Others: meas./calc.	0.9/72
Flexipac 1Y (F1Y)	410	45	9	12.7	6.4	443	0.91	a_p: Hardy (2007) Others: Petre et al. (2003)	0.8/71, 6/63
Prototype 500 (P500)	500	45	8.1	9.6	6.53	517	0.92	Assumed same as M500Y	0.9/72, 0.9/31

[a] For base case (0.1 mol/L NaOH), calculated from correlation of Moniuk and Pohorecki (1991)
[b] For base case (0.1 mol/L NaOH), assumed same as water and calculated from fit of data in Haar et al. (1984)
[c] Denotes uncertainty in actual specific area

6.2.1 Material Balance

The overall CO_2 material balance for the database is shown in Figure 6.4. The values obtained from the liquid-phase analysis (TIC) are charted along the "CO_2 generated" axis, and those obtained from the gas phase (Horiba analyzer) are plotted along the "CO_2 absorbed" axis.
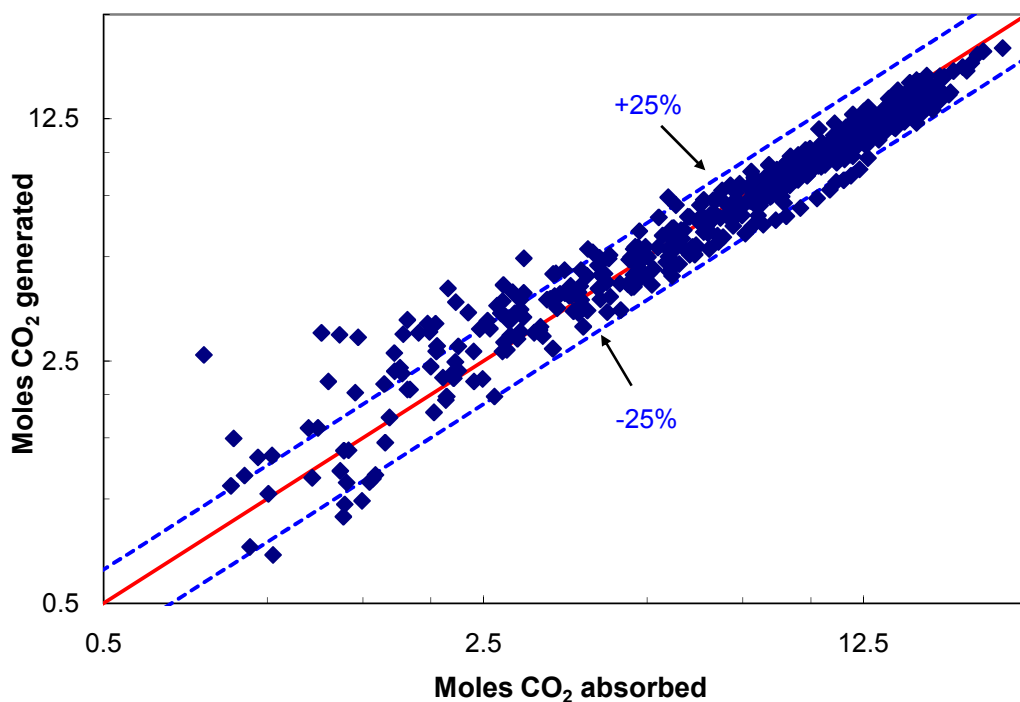
Figure 6.4. CO_2 material balance for packed column experiment.

The relative deviation between the two sources was generally less than 25%. The low-end of the parity plot can be seen to be the region of greatest disagreement, which may be a reflection of the poorer resolution of the TIC method at low CO_2 concentrations. No points were discarded on the basis of the material balance, although an argument perhaps could have been made for the omission of the major outliers. Several factors could have contributed to the overall discrepancy. On the gas side, the steady-state outlet CO_2

138

concentration was utilized to determine the moles of CO_2 that were absorbed. In other words, the transitional period prior to the establishment of stable conditions was not accounted for, which in most cases (i.e., decreasing CO_2 concentration associated with ramp-up in liquid load) meant that the calculated absorption was exaggerated. On the liquid side, the homogeneity of the samples obtained from the column sump at low liquid loads was an issue. At high loads, the system concentration was satisfactorily represented by the samples, since the combination of flow rate and time (10 minutes or more) was sufficient to result in good turnover. At very low loads, though, the solution in the sump, having just passed through the packing, was guaranteed to possess elevated levels of CO_3^{2-} (CO_2) and be a poor representation of the overall liquid inventory. Sample collection in these situations was typically delayed by several minutes to hopefully allow for better mixing, but this practice did not make much of a difference. In the TIC analysis, the samples taken at low liquid loads would often exhibit implausible CO_2 concentrations – that is, higher concentrations than those measured in samples taken later in time. These samples had to be discarded, so the CO_2 concentrations had to be estimated (via linear interpolation) in a number of cases. This fact clearly could have affected the liquid side of the material balance. Evaporation was not accounted for but could have also been a factor. Calculations based on the inlet and outlet air conditions showed that at most (i.e., assuming an outlet relative humidity of 100%), a water loss between 5 and 10% could generally be expected. (Ambient temperatures and humidities were obtained from http://www.weather.com/.)

There were potential flaws associated with using either the gas or liquid side to track the absorption of CO_2 or equivalently, depletion of hydroxide in the system over time. Since it was the composition of the liquid that was of interest, it seemed more sensible to apply the corresponding analytical method (TIC) for this purpose. While using the gas side to measure both the mass transfer and hydroxide depletion would perhaps allow for the analysis to be more intrinsically consistent, a large difference versus the TIC method would ultimately not be anticipated.

6.2.2 Global Model

Dimensionless numbers were used to correlate the packing area database. The modeling effort was solely concerned with liquid parameters, given the apparently limited influence of gas properties (again, to be discussed later). The effective area for structured packing is anticipated to primarily be attributable to liquid in contact with the packing surface, rather than free droplets (Weimer and Schaber, 1997), so the characteristic length was logically defined by a liquid film thickness. The resemblance of the flow channels to simple inclined plates suggested that it might be appropriate to apply the "classical" Nusselt film thickness (Bird et al., 2002) in the calculation of this parameter (equation 3.3).

$$\delta_{\text{Nusselt}} = \sqrt{\frac{3u_{\text{film}}\mu_{\text{L}}}{\rho_{\text{L}}g\sin\alpha}} = \sqrt[3]{\frac{3\mu_{\text{L}}}{\rho_{\text{L}}g\sin\alpha}\left(\frac{Q}{L_{\text{p}}}\right)} \qquad (3.3)$$

The liquid rate per wetted perimeter term (Q/L_{p}) is commonly encountered in fluid flow processes. The wetted perimeters for the packings in Table 6.1, as calculated from

equation 6.1, are notably almost equivalent to their nominal surface areas. In fact, some authors like Olujic et al. (2004) have actually assumed equation 6.1 to apply for the packing surface area rather than the standard vendor-specified value (e.g., 250 m^2/m^3 for M250Y). If information on packing channel dimensions is not available, the specific area could perhaps serve as a reasonable proxy for the wetted perimeter in equation 3.3. This point will be revisited shortly.

A summary of the dimensionless numbers commonly associated with fluid flow processes is presented in Table 6.2, with both the standard and expanded (i.e., with equation 3.3 substituted in) forms shown.

Table 6.2. Dimensionless numbers.

Dimensionless number	Force ratio: X/Y	Standard form	Nusselt-substituted form	Eqn.
Reynolds (Re_L)	Inertia / Viscosity	$\dfrac{\rho_L u_L \delta_L}{\mu_L}$	$\dfrac{\rho_L}{\mu_L} \dfrac{Q}{L_p}$	(6.3)
Capillary (Ca_L)	Viscosity / Surface Tension	$\dfrac{\mu_L u_L}{\sigma}$	$\dfrac{1}{\sigma}\left(\dfrac{\rho_L g \sin\alpha}{3}\right)^{1/3}\left(\mu_L \dfrac{Q}{L_p}\right)^{2/3}$	(6.4)
Weber (We_L)	Inertia / Surface Tension	$\dfrac{\rho_L u_L^2 \delta_L}{\sigma}$	$\dfrac{1}{\sigma}\left[\dfrac{\rho_L^4 g (\sin\alpha)}{3\mu_L}\left(\dfrac{Q}{L_p}\right)^5\right]^{1/3}$	(6.5)
Froude (Fr_L)	Inertia / Gravity	$\dfrac{u_L^2}{g\delta_L}$	$\dfrac{\rho_L \sin\alpha}{3\mu_L}\left(\dfrac{Q}{L_p}\right)$	(6.6)
Bond (Bo_L)	Gravity / Surface Tension	$\dfrac{\rho_L g \delta_L^2}{\sigma}$	$\dfrac{(\rho_L g)^{1/3}}{\sigma}\left[\dfrac{3\mu_L}{\sin\alpha}\left(\dfrac{Q}{L_p}\right)\right]^{2/3}$	(6.7)

141

The best fit of the database (based on R^2 values) was obtained from a regression in the form of equation 6.8. The constants and standard errors are shown in equation 6.8a. (The M250YS data were not included in the regression due to uncertainty regarding the actual specific area of this packing, as will be explained in Section 6.8.)

$$\ln a_{\mathrm{f}} = C_1 \ln(We_{\mathrm{L}}) + C_2 \ln(Fr_{\mathrm{L}}) + C_3 \tag{6.8}$$

$$\ln a_{\mathrm{f}} \pm 0.065; \ C_1 = 0.112 \pm 0.003; \ C_2 = -0.032 \pm 0.004; \ C_3 = 0.271 \pm 0.014$$

$$\tag{6.8a}$$

The Froude number coefficient was noticed to be one-third of the Weber number coefficient. (The ratio is admittedly not quite one-third based on the numbers in equation 6.8a, but it was nearly exact when this analysis was first performed, with a smaller database.) This correspondence was thought to possibly be significant, and so, a follow-up regression was performed where the Weber and Froude numbers were fixed in this ratio (equation 6.9).

$$\ln a_{\mathrm{f}} = C_1 \ln[(We_{\mathrm{L}})(Fr_{\mathrm{L}})^{-\frac{1}{3}}] + C_2 \tag{6.9}$$

$$\ln a_{\mathrm{f}} \pm 0.065; \ C_1 = 0.116 \pm 0.002; \ C_2 = 0.292 \pm 0.009 \tag{6.9a}$$

Equation 6.9 represents the pinnacle of this work: a global correlation of the mass transfer area database. The final form of the model, obtained upon conversion of equation 6.9 into power law form, is displayed in equation 6.10.

$$a_{\mathrm{f}} = 1.34\left[(We_{\mathrm{L}})(Fr_{\mathrm{L}})^{-\frac{1}{3}}\right]^{0.116} \tag{6.10}$$

The $(We_L)(Fr_L)^{-1/3}$ grouping is shown expanded in equation 6.11.

$$(We_L)(Fr_L)^{-1/3} = \left(\frac{\rho_L}{\sigma}\right)g^{1/3}\left(\frac{Q}{L_p}\right)^{4/3} = \left(\frac{\rho_L}{\sigma}\right)g^{1/3}\left(\frac{Q}{A}\cdot\frac{Bh}{4S}\right)^{4/3} \tag{6.11}$$

In situations where the channel dimensions are not known or are perhaps not well defined, such as for novel packings like the Raschig Super-Pak family (Schultes and Chambers, 2007), use of the packing specific area (a_p) instead of the wetted perimeter (L_p) might be appropriate for the calculation of $(We_L)(Fr_L)^{-1/3}$.

For this experimental system (air-water), a correction to the gravitational constant (g) due to factors like gas density was not believed to be necessary, but the incorporation of an "effective gravity" term, such as that proposed by Rocha et al. (1993), could warrant consideration if applying equation 6.10 to other applications – for example, those at high pressure conditions.

Figure 6.5 is a dimensionless plot of the mass transfer area database, together with the model and dashed lines denoting two standard deviations (±13%). Interpretation of the standard deviation on a percentage basis was thought to be appropriate, considering the actual regressions were done in logarithmic form. The fit of the model was quite acceptable given the broad scope of conditions, which, as indicated in Table 6.1, consisted of packing sizes ranging from 125-500 m^2/m^3, liquid viscosity from roughly 1-15 mPa·s, and surface tension from 30-72 mN/m. The liquid load and specific area, reflected in the flow rate per wetted perimeter (Q/L_p) in equation 6.11, most strongly dictated the mass transfer area. This term can be considered as a generalized liquid load that enables the packings to be compared on a more common ground than the

conventional liquid load ($m^3/m^2 \cdot h$ or gpm/ft^2). While recasting the mass transfer area data (e.g., Figure 6.1) as a function of (Q/L_p) would be logical, many of the subsequent figures are nevertheless plotted in terms of liquid load, as it is a more relatable basis. In addition to the generalized liquid load, surface tension and liquid density were correlated as relevant parameters, although the density was never varied (the densities of the neat caustic solutions and those containing either surfactant or polymer were equivalent and are tabulated in Appendix B.1). Interestingly, the grouping of density, surface tension, and the gravitational constant in equation 6.11 somewhat resembles the capillary length (κ^{-1}), a characteristic dimension encountered in fluid mechanics (e.g., associated with the Young-Laplace equation).

$$\kappa^{-1} = \sqrt{\frac{\sigma}{\rho_L g}} \qquad\qquad (6.12)$$

Given that capillary bridges could hypothetically be prominent within structured packing (see Sections 6.3 and 6.5), the incorporation of density into the global correlation could have real physical significance. Gas velocity and liquid viscosity were notably absent from the model; both were concluded to have a negligible effect on area over the range of values tested. Also not included were terms involving the packing corrugation angle (M250X), element interface (MP252Y), and surface texture (M250YS), since none of these geometric features were found to appreciably affect the effective area. These results are all discussed in detail in the following sections.
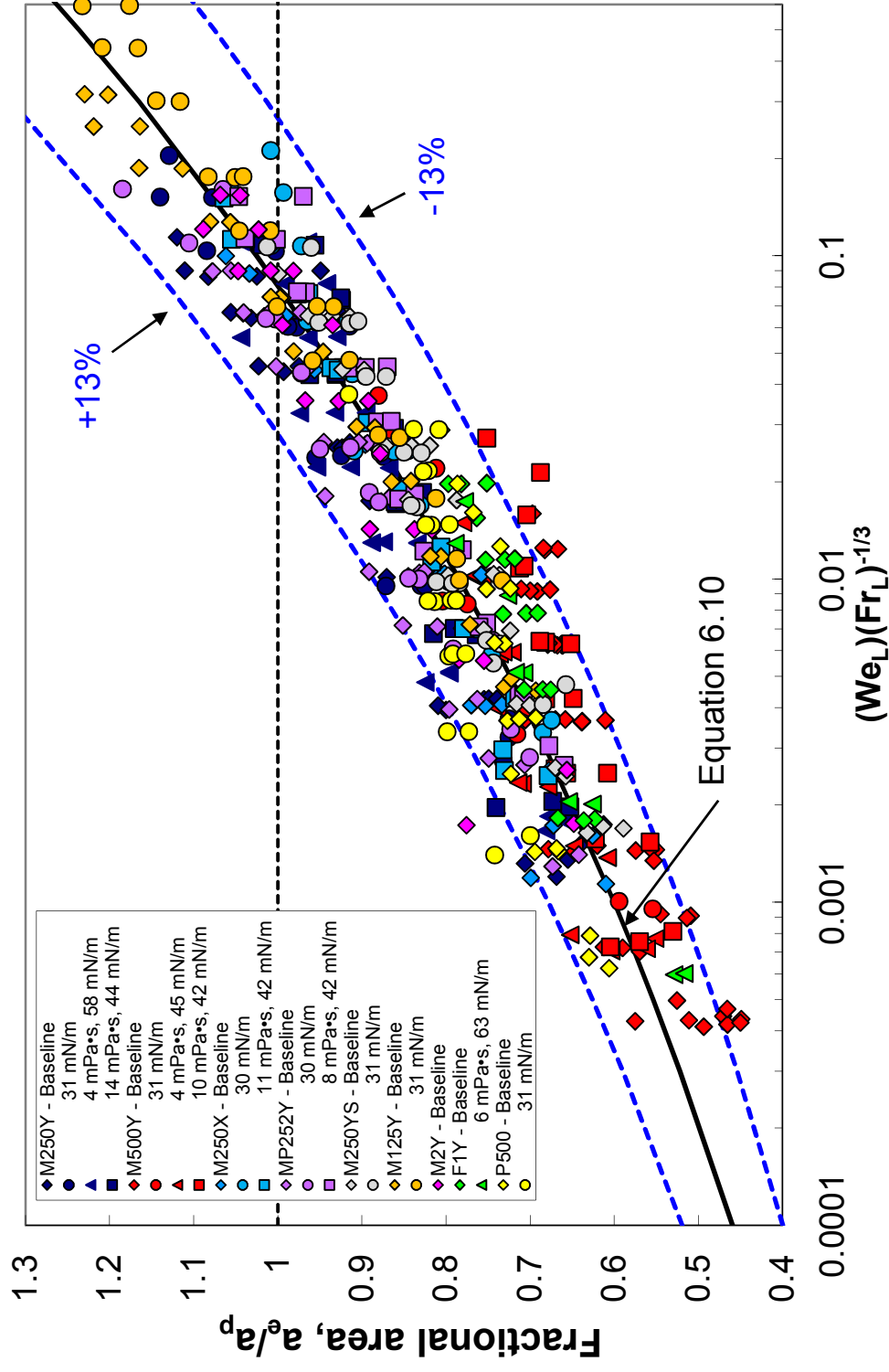
Figure 6.5. Structured packing mass transfer area database, shown on dimensionless basis and compared with global model (equation 6.10).

145

6.3 EFFECT OF LIQUID LOAD AND PACKING SIZE (M125Y/M250Y/F1Y/M500Y)

Four packings are displayed in Figure 6.6: M125Y, M250Y, F1Y, and M500Y. The strong influence of both liquid load (2.5-75 $m^3/m^2 \cdot h$) and packing geometric area (125-500 m^2/m^3) on the mass transfer area is illustrated. Every packing exhibited an increase in effective area with increasing liquid load. This was naturally attributable to a greater portion of the packing being wetted and therefore available to participate in the mass transfer process. Rivulet flow studies (McGlamery, 1988; Nicolaiewsky et al., 1999) would speculate that the effective area was governed by the ability of the liquid to spread within the individual flow channels. When considering both the relatively small geometric boundaries ($S < 40$ mm) and the surface tension results (see Section 6.5), though, the trend with liquid load was surmised to be dictated by the distribution of liquid to the channels themselves – not necessarily the degree of coverage within a singular channel.
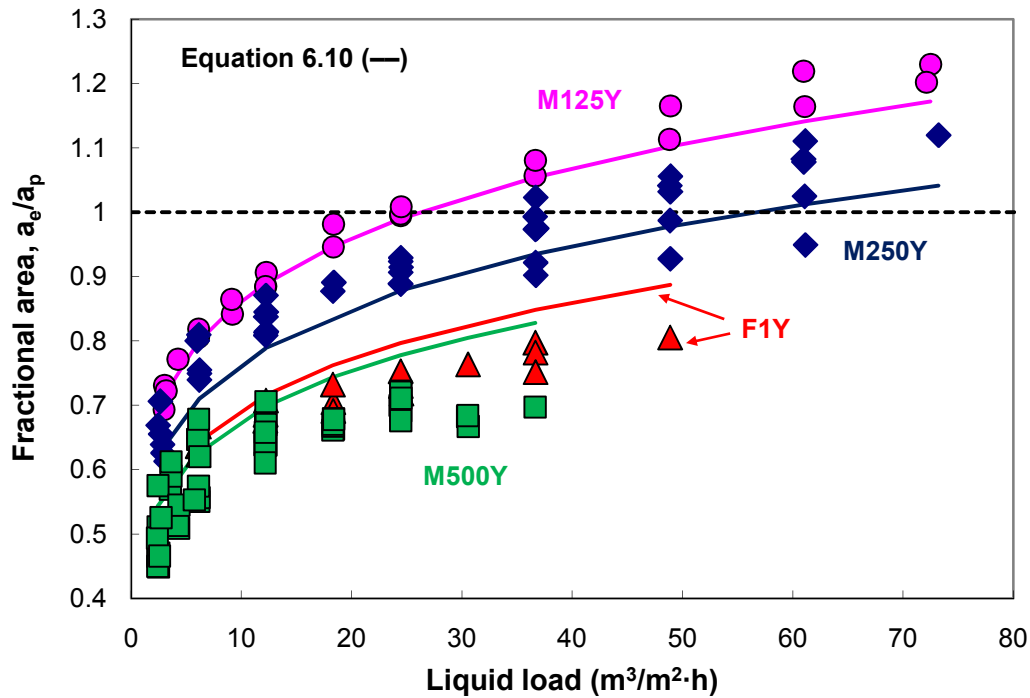
Figure 6.6. Mass transfer area of M125Y (a_p = 125 m^2/m^3), M250Y (a_p = 250 m^2/m^3), F1Y (a_p = 410 m^2/m^3), and M500Y (a_p = 500 m^2/m^3).

The standard M250Y packing performed well on a fractional area basis; measured values ranged from 0.65 to 1.12. Its specific area was clearly being well utilized, but as might be expected of a structured packing, little mass transfer seemed to occur beyond the packing surface. This behavior is in contrast with random packing, where the effective area often exceeds the nominal area, sometimes by more than 50% (Wilson, 2004). The fact that M125Y exhibited an even higher (10%) fractional area than M250Y, approaching a value of 1.3 at the high-end loads, was quite striking. M125Y, being a coarser packing, would experience a greater relative impact of factors like end or wall effects. These factors could very well have contributed to the observed deviation, but without having much supporting data or a rigorous model for these phenomena, applying

a correction to the results was not fully justifiable. The implications of doing so are nevertheless very much worth discussing (see Section 6.10.2), as a subtraction of end and wall effects would force the upper fractional area values of not only M125Y but also packings like M250Y closer to unity and therefore yield more sensible results from a physical perspective. Considering the data at face value for the moment, the fractional area efficiency of structured packings as they become coarser can be seen to tend toward that of random packings. Henriques de Brito et al. (1994) speculated that low a_p packings could be more prone to liquid flow instabilities such as rippling or formation of satellite droplets due to longer film running lengths. These phenomena certainly could have contributed to the M125Y mass transfer area. The fractional area efficiency of the finer packings (F1Y and M500Y) was notably lower; both were found to plateau far below unity. The trend with liquid load also appears to differ from the coarser packings, in that a more distinct fractional area asymptote was reached at the highest liquid loads. F1Y and M500Y could have been less subject to mass-transfer-enhancing film instabilities, as might be theorized by Henriques de Brito et al. (1994), or the packings could have been limited by liquid distribution. Structured packing is naturally configured to self-distribute liquid, but compared with coarser packings, F1Y and M500Y could require a greater number of elements to become fully distributed, even with excellent initial distribution. Hence, a greater fraction of the bed would effectively be wasted. Capillary effects were believed to be the most reasonable explanation of the results, however. Essentially, the poorer efficiencies were thought to be attributable to detrimental liquid bridging and pooling between packing sheets akin to those observed by

148

Green (2006) in his x-ray imaging work, which could be a foreseeable problem for fine packings due to their constricted layout. The asymptotic behavior could be justified by this hypothesis too – a reflection of the packings becoming clogged near their upper capacity limits and therefore unable to benefit from additional liquid throughput.

6.3.1 Incorporation of Geometric Dimension

To demonstrate the ability of equation 6.10 to collapse the various data sets, the results in Figure 6.6 have been re-plotted in dimensionless form in Figure 6.7. (The flow rate per wetted perimeter values are also shown along the top axis for illustration.) Equation 6.10 captures the overall combination of liquid load and geometry well, but it misses subtle aspects like the tendency of F1Y and M500Y to flatten out. This is also evident from a plot of the residuals (Figure 6.8).
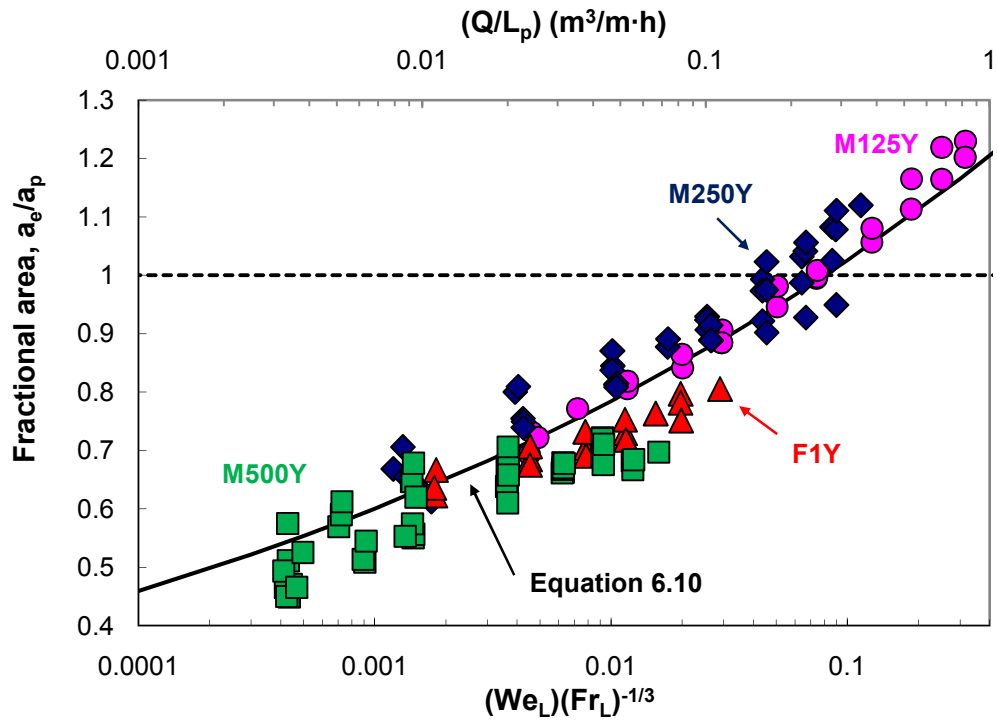
Figure 6.7. Representation of mass transfer area of M125Y ($a_p = 125$ m^2/m^3), M250Y ($a_p = 250$ m^2/m^3), F1Y ($a_p = 410$ m^2/m^3), and M500Y ($a_p = 500$ m^2/m^3) on dimensionless basis (bottom axis) and as a function of flow rate per wetted perimeter (top axis).

150
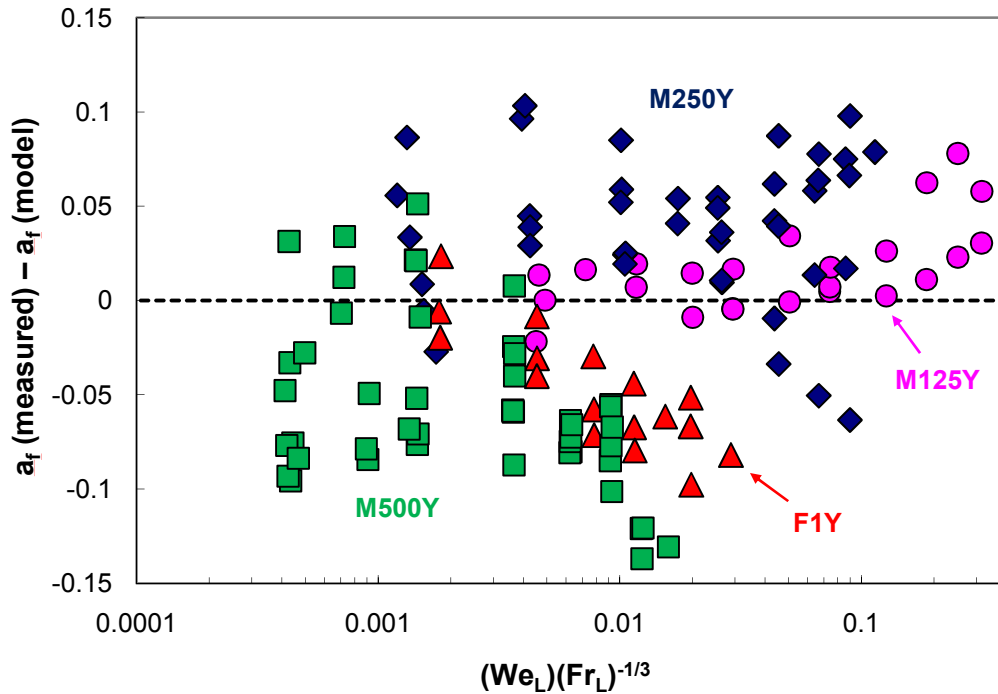
Figure 6.8. Area residuals of M125Y (a_p = 125 m^2/m^3), M250Y (a_p = 250 m^2/m^3), F1Y (a_p = 410 m^2/m^3), and M500Y (a_p = 500 m^2/m^3) as a function of $(We_L)(Fr_L)^{-1/3}$, with a_f (model) values from equation 6.10.

Thus, while the model is satisfactory in its current form, improvements can be made. Another parameter could be required to account for phenomena like liquid accumulation induced by the narrow, constricted sheets of the finer packings. Use of a geometric dimension would be logical for this purpose. Equation 6.13 is presented as an example, in which a dimensionless geometric term (*GD*), defined as the ratio of the column diameter to the packing channel side (d_c/S), has been added to the original regression. (A quadratic form for *GD* was found to work best, in terms of keeping the sum-of-squared errors minimal while also maintaining an equation with a limited number of terms.) The constants and standard errors from this analysis are provided in equation 6.13a.

$$\ln a_\mathrm{f} = C_1 \ln\left[(We_\mathrm{L})(Fr_\mathrm{L})^{-\frac{1}{3}}\right] + C_2\left[\ln(GD)\right]^2 + C_3 \qquad (6.13)$$

$$\ln a_\mathrm{f} \pm 0.059; \ C_1 = 0.104 \pm 0.002; \ C_2 = -0.011 \pm 0.001; \ C_3 = 0.363 \pm 0.011$$

$$(6.13a)$$

The residuals are improved with the addition of *GD* (Figure 6.9), which could theoretically be related to any of a number of factors, such as liquid distribution, entrance or end effects, or wall effects. The uncertainty regarding the actual significance of this parameter, together with its somewhat arbitrary definition and lack of validation (only a single column diameter was tested), mean that equation 6.13 must be considered with reservation, however. That is, the addition of a geometric term should be recognized to offer potential improvement to the model but not really be justifiable without further insight. Therefore, equation 6.10 is still endorsed as the primary model contributed by the present research.
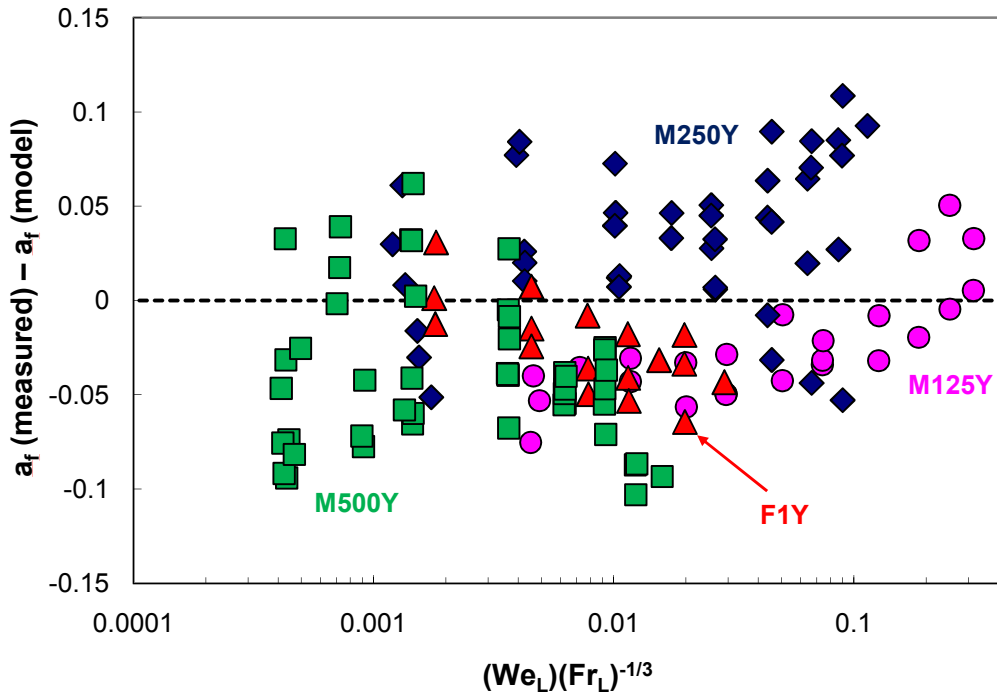
Figure 6.9. Area residuals of M125Y (a_p = 125 m^2/m^3), M250Y (a_p = 250 m^2/m^3), F1Y (a_p = 410 m^2/m^3), and M500Y (a_p = 500 m^2/m^3) as a function of $(We_L)(Fr_L)^{-1/3}$, with a_f (model) values from equation 6.13.

6.4 EFFECT OF AIR RATE

Multiple air velocities were run within a given experiment. The residuals of the experimental database as a function of air velocity are displayed in Figure 6.10. The predicted values from equation 6.13, rather than equation 6.10, have been used for this purpose, as they offer a slightly smoother interpretation of the results. The residuals were fit with a simple linear equation (equation 6.14), with the regressed constants shown in equation 6.14a.

$$a_f(\text{measured}) - a_f(\text{model}) = C_1 u_G + C_2 \qquad (6.14)$$

153

$$[a_f(\text{measured}) - a_f(\text{model})] \pm 0.046; \quad C_1 = 0.011 \pm 0.006; \quad C_2 = -0.011 \pm 0.007$$

$$(6.14a)$$
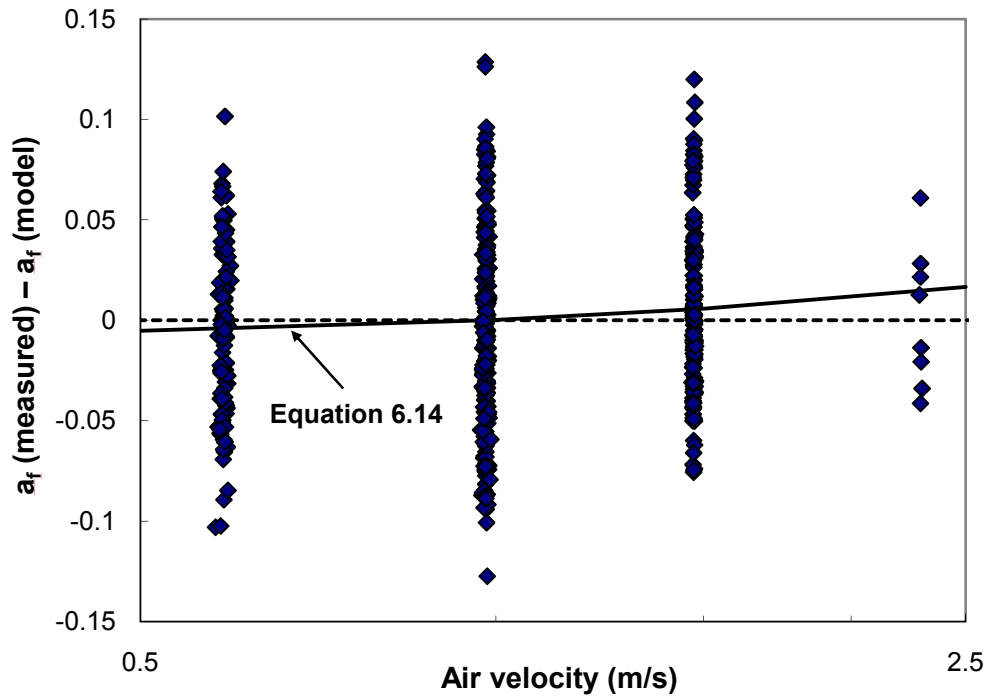
Figure 6.10. Area residuals of experimental database as a function of superficial air velocity, with a_f (model) values from equation 6.13.

One could possibly argue there to be an increasing trend with velocity. The impact was rather insignificant, though, and could, in fact, have been an artifact of factors like gas-side resistance or end effects. The measured mass transfer area in the present work was concluded to be insensitive to the air rate. This conclusion is consistent with many of the structured packing models in the literature (Wang et al., 2005). As such, it was considered acceptable to treat all of the data obtained at different air rates (for a given packing and liquid load condition) on equivalent terms and average them for clarity. Several of the plots that follow show results that have been consolidated in this manner.

154

6.5 EFFECT OF SURFACE TENSION (M250Y/M500Y/P500)

6.5.1 Contact Angle and Surface Tension

Many studies (Shi and Mersmann, 1985; McGlamery, 1988; Rocha et al., 1996) have considered contact angle to be a more relevant parameter to refer to than surface tension in the context of the effective area of packing. Hence, prior to presenting the results in this section, a clarifying discussion regarding surface tension and contact angle is in order. The contact angle is a three-phase property that represents the angle formed at the contact point of these phases. As shown in Figure 6.11, for a gas (G)-liquid (L)-solid (S) system, it is the angle (γ) formed through the liquid phase.
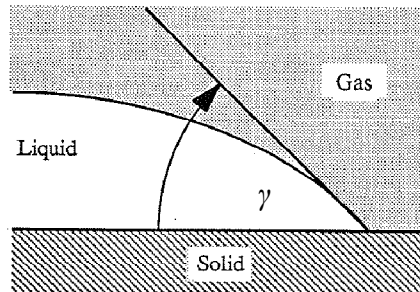
Figure 6.11. Illustration of the contact angle. Slightly modified version of image from McGlamery (1988).

A relation between the contact angle and the interfacial tensions of the three phases was derived by Young (1805), where the subscripts refer to the respective phases. The subscripts from the liquid-vapor interfacial tension ("surface tension") have been omitted in equation 6.15 to be consistent with the nomenclature used throughout this work.

$$\sigma\cos\gamma = \sigma_{SG} - \sigma_{SL} \tag{6.15}$$

155

The contact angle and surface tension will vary in tandem if the right-hand side of equation 6.15 is constant. Given that the solid-gas (stainless steel-air) and solid-liquid (stainless steel-dilute caustic) interactions were anticipated to be the same for every test system, this difference in interfacial tensions was believed to be fixed, and the contact angle and surface tension were expected to be correlated.

To verify this theory, contact angle measurements were conducted via the sessile drop technique on a flat, embossed piece of sheet metal (obtained from Sulzer) with the same characteristics as that of Mellapak packing. Because of the surface texture, however, vastly different contact angles could be obtained depending on the drop volume and placement. Therefore, the significance of these measurements was questionable. Since it was the relation between contact angle and surface tension that was of interest, rather than absolute contact angles, it was opted to instead perform these tests on a smooth (untextured) stainless steel surface and compare the contact angles to the surface tension values obtained from pendant drop analysis. Four data sets are presented in Figure 6.12. In each case, a baseline reading (either distilled/deionized water or 0.1 mol/L NaOH) was established along with the tested sample (0.1 mol/L NaOH containing either 125 ppm_v TERGITOL NP-7 + 50 mg/L antifoam or 1.25 wt% POLYOX with variable quantities of antifoam). Mean contact angle values (i.e., average of left and right) and approximate surface tension values (rounded) were used to generate the plot.
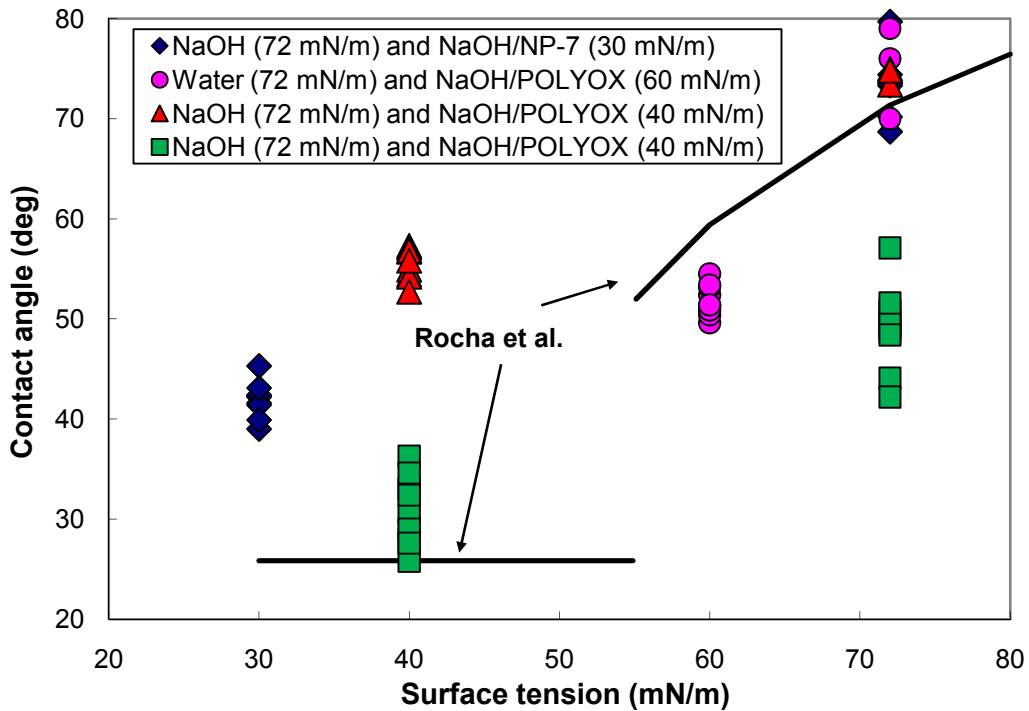
Figure 6.12. Contact angles on stainless steel surface.

The correlation between contact angle and surface tension that was presented in Rocha et al. (1996) is shown alongside the results for comparison.

$$\cos\gamma = 5.211 \times 10^{-16.835\sigma} \qquad \text{for } \sigma > 55 \text{ mN/m} \qquad (3.7a)$$

$$\cos\gamma = 0.9 \qquad \text{for } \sigma < 55 \text{ mN/m} \qquad (3.7b)$$

The agreement is reasonable in the high surface tension/contact angle region but not really at the low end, which is not surprising, given that equation 3.7b represents a broad generalization. The data are a bit scattered, but overall, a fairly direct scaling of contact angle with surface tension is apparent. For example, the high surface tension condition (72 mN/m) corresponded to a contact angle of 70°, and the low surface tension condition (30 mN/m) exhibited a contact angle of about 40°. The base case in the last data set had a

157

much lower contact angle than expected, but this depression carried through to the POLYOX results as well, resulting in a similar relative decrease as a function of surface tension as that in the other scenarios. The offset may have been related to the cleanliness of the surface in that particular instance. Nicolaiewsky and Fair (1999) performed a far more extensive set of contact angle measurements on structured-packing-like surfaces than those conducted here and also found there to be good correlation of the surface tension and contact angle for a given surface. Figure 6.13 is shown to illustrate, where the data for two shallow embossed, corrugated ("SEC"), stainless steel surfaces (45° and 60°) presented in the publication (Figure 6) have been reproduced.
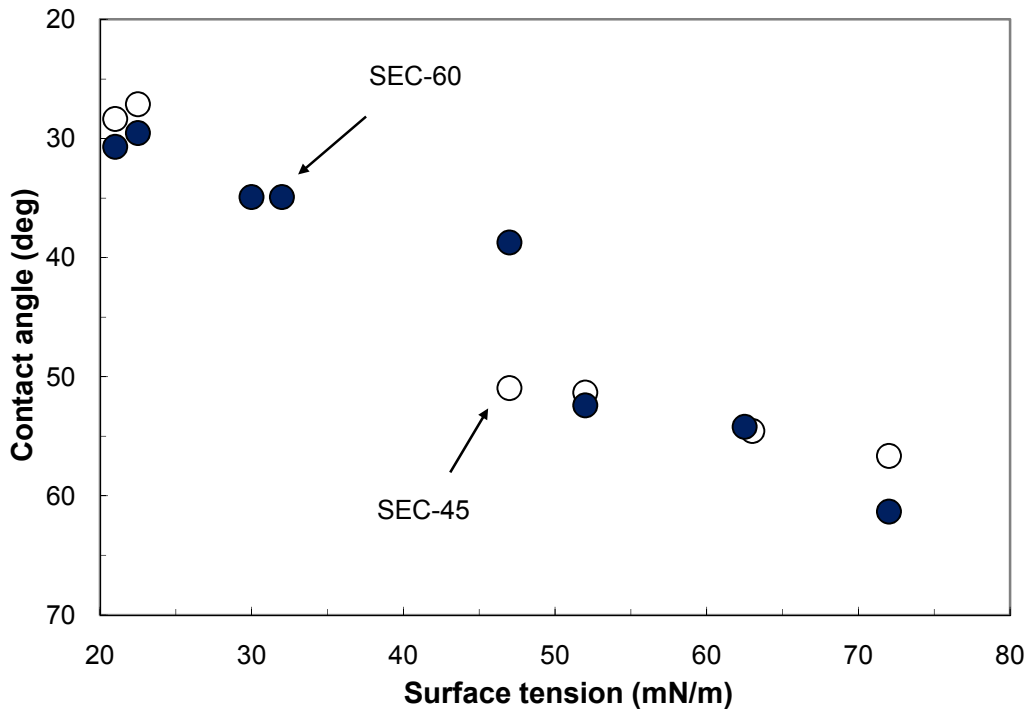
Figure 6.13. Contact angle and surface tension data for two shallow embossed, corrugated ("SEC"), stainless steel surfaces (45° and 60°), reproduced from Nicolaiewsky and Fair (1999).

158

Hence, while it is true that contact angle may be a more fundamental property than surface tension, both parameters were presumed to basically have the same meaning for the purpose of the current work. Surface tension was the more convenient parameter to relate to and reproducibly measure and hence, report.

In this context, the limitations of the global correlation (equation 6.10) must also be stressed. Stainless steel structured packings possessing fairly common inherent geometries (see equation 3.43) were solely examined. Thus, the correlation would not necessarily be expected to apply to other materials, such as plastic or ceramic, due to differences in wetting behavior compared with stainless steel, or to packings like Raschig Super-Pak, which resemble structured packing but lack a well defined channel geometry.

6.5.2 Surface Tension Results

Extensive tests showed that the mass transfer area was always enhanced by a reduction in surface tension (30 mN/m), regardless of packing geometry. A greater impact of surface tension on finer packings (500-series) relative to coarser ones (250-series and lower) was observed. The effective area was higher by 15-20% on average for the former, whereas the increase was 10% or less for the latter. The data sets for M250Y (Figure 6.14) and M500Y/P500 (Figure 6.15) are shown for example. The error bars associated with the M250Y and M500Y baseline data have been included to help put the surface tension effect into perspective. The standard deviation in the measurements can be seen to be around 5%, which was typical and was on the order of what an error propagation analysis (see Appendix D) might suggest.

159
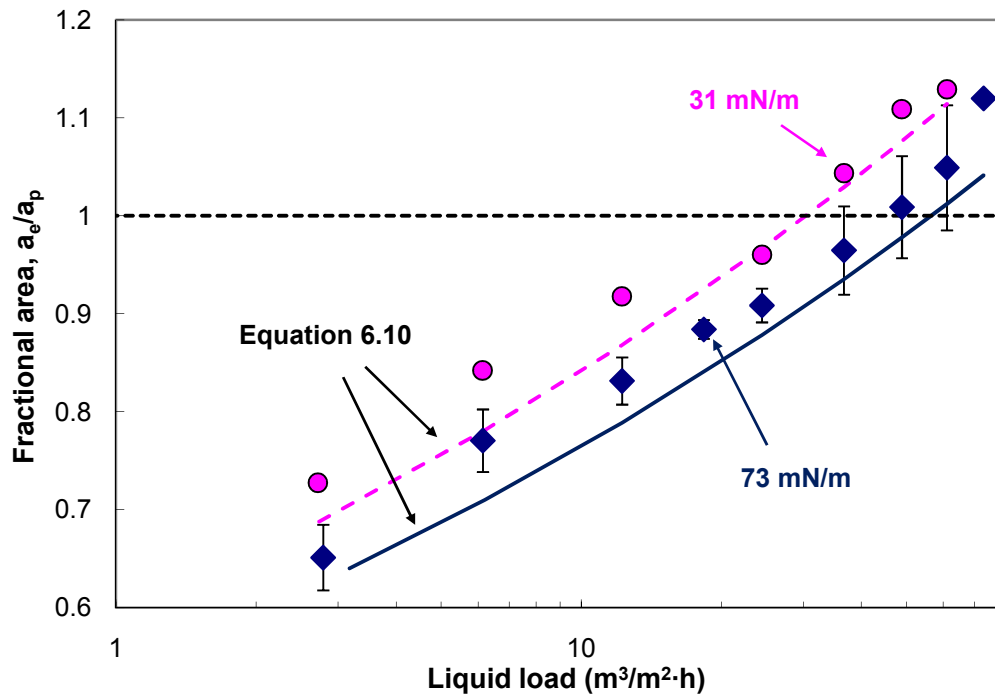
Figure 6.14. Mass transfer area of M250Y ($a_\mathrm{p} = 250$ m^2/m^3) at baseline and low surface tension. Error bars denote one standard deviation.
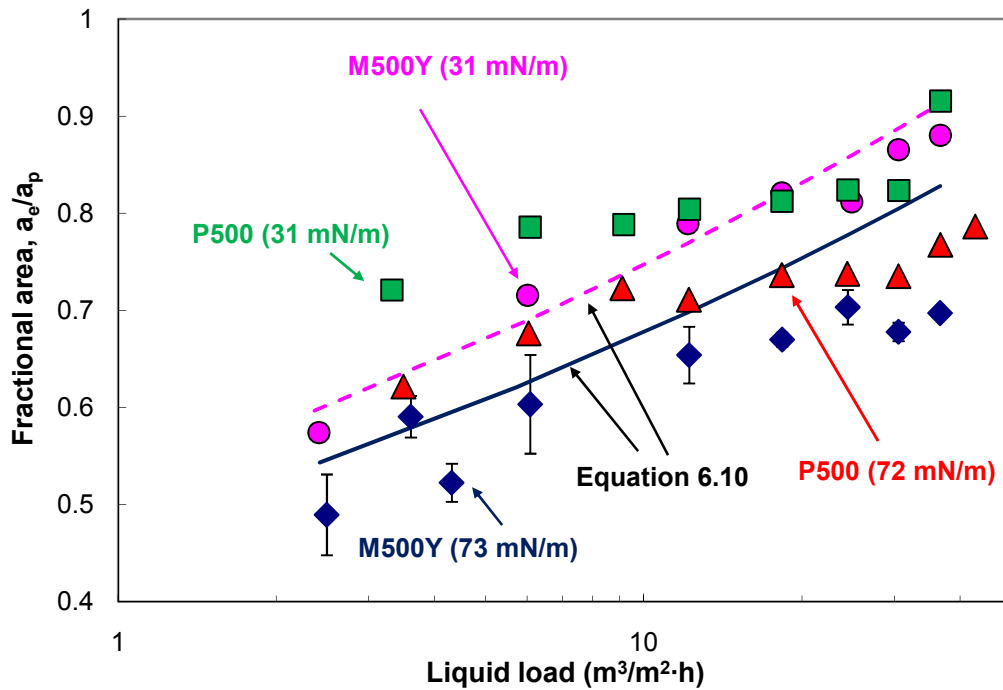
Figure 6.15. Mass transfer area of M500Y and P500 ($a_p = 500$ m^2/m^3) at baseline and low surface tension. Error bars denote one standard deviation.

The P500 experiment was performed as a follow-up to the M500Y test, to verify that there was indeed a stronger linkage of surface tension with high surface area packings. The impact was smaller than the one observed with M500Y, due to the P500 baseline points being slightly higher, but was still more significant than the difference observed with all other packings. Hence, the unique effect of surface tension was thought to be affirmed. It is unclear why P500 outperformed M500Y for the base case but then overlapped at low surface tension. The geometry (e.g., surface texture) of P500 may have been less conducive to undesirable liquid bridging but lost this advantage when the surface tension was reduced.

A lower surface tension (or lower contact angle) would intuitively be associated with better liquid spreading. If spreading were a valid explanation for the increase in wetted area, though, then a bigger deviation from the base case at low liquid loads (i.e., 10 $m^3/m^2 \cdot h$ and below) would be expected, due to surface coverage limitations. Such separation was not reflected in the data. The improvement in mass transfer area was fairly constant for every packing as a function of liquid load, with the greatest departure actually occurring at the upper capacity limit of the 500-series packings. This consistency suggests that the enhancement was attributable to a common mechanism other than liquid spreading, such as creation of satellite droplets or wave formation, or in other words, an augmentation of the underside instabilities observed by Shetty and Cerro (1995). This same idea was proposed in the previous section when discussing the M125Y results. Thus, it could be that increasing packing coarseness or decreasing surface tension destabilizes the liquid films on the packing surface. The additional 5-10% distinction between coarse and fine packings was believed to be related to capillary phenomena. The model is not sophisticated enough to account for this difference, since there is no direct linkage of surface tension and geometry in equation 6.10. Figures 6.16 and 6.17 serve to further illustrate this point.

162
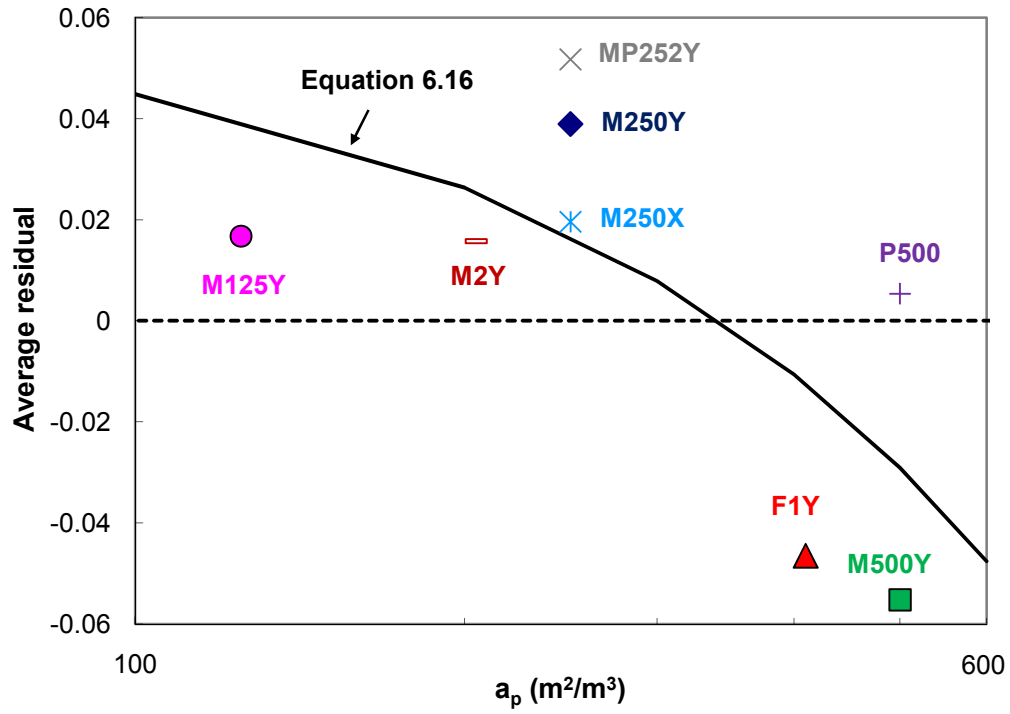
Figure 6.16. Average area residuals of packings at high surface tension as a function of packing size, with a_f (model) values calculated from equation 6.10.
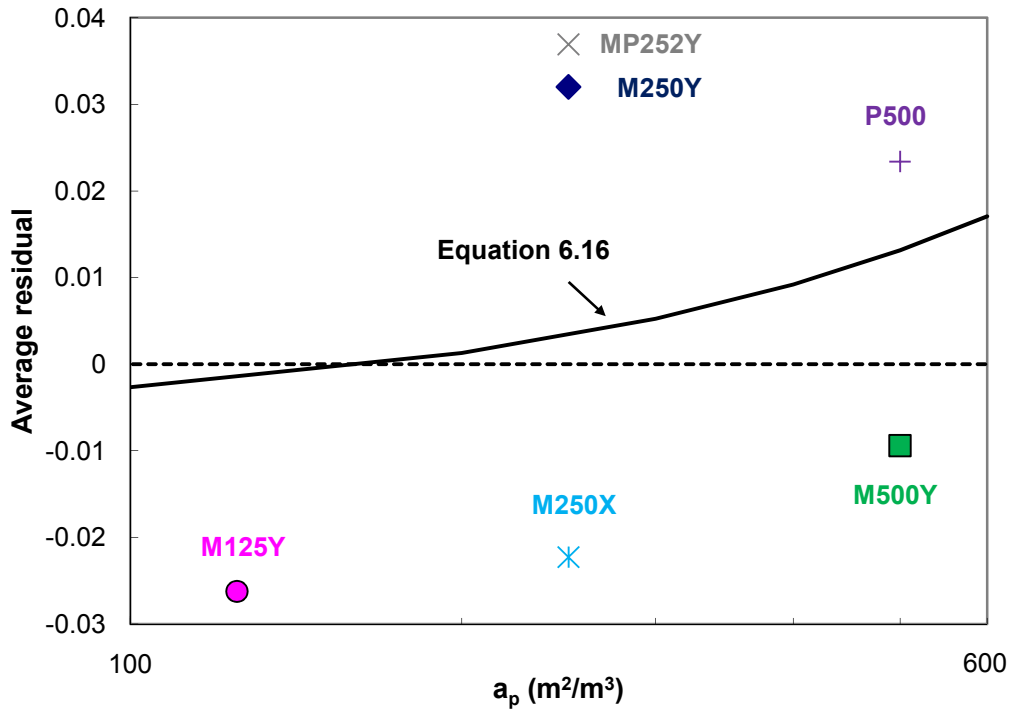
Figure 6.17. Average area residuals of packings at low surface tension as a function of packing size, with a_f (model) values calculated from equation 6.10.

An average residual for each packing is displayed in the two figures. This average residual was simply the mean of the residuals for either the baseline (Figure 6.16) or at low surface tension (Figure 6.17), where the predicted values were calculated from equation 6.10. The rationale for plotting the results in this manner was to more clearly differentiate the alignment of the packings, which could be somewhat lost in a plot of the full database. The linear fit of the data in Figure 6.16 is given by equation 6.16, and the associated constants are in equation 6.16a.

$$\left[a_f\left(\text{measured}\right) - a_f\left(\text{model}\right)\right]_{\text{avg}} = C_1 a_p + C_2 \tag{6.16}$$

$$\left[a_f\left(\text{measured}\right) - a_f\left(\text{model}\right)\right]_{\text{avg}} \pm 0.030; \ C_1 = -1.8 \times 10^{-4} \pm 8.04 \times 10^{-5}; \ C_2 = 0.063 \pm 0.027$$

$$\tag{6.16a}$$

164

A systematic downward trend is evident, and it can be seen that the mass transfer area of the coarser and finer packings is respectively underpredicted and overpredicted at high surface tension. At low surface tension (Figure 6.17), the data appear to be more evenly distributed around zero. The fit is provided by equations 6.16 and 6.16b.

$$\left[a_f\left(\text{measured}\right) - a_f\left(\text{model}\right)\right]_{\text{avg}} \pm 0.031; \ C_1 = 3.95 \times 10^{-5} \pm 9.04 \times 10^{-5}; \ C_2 = 0.007 \pm 0.031$$

(6.16b)

The form of equation 6.10 was basically a compromise between the two observed surface tension effects (10% for most packings and 15-20% for the high surface packings) and thus, compensated both ends of the spectrum. Had each of these distinct effects truly been captured, then there would not be such a uniform distribution in Figure 6.17.

This issue could perhaps be corrected with the incorporation of an additional parameter. The M250Y and M500Y data have been plotted as a function of the flow rate per wetted perimeter (or generalized liquid load) in Figure 6.18. As can be seen, the effect of surface tension is not strictly related to (Q/L_p), since there is some overlap in the two data sets. Hence, simply including a cross term between the two parameters would not necessarily solve the problem. The alignment of the low surface tension M500Y data set with the M250Y results may indicate that the fluid flow in these cases is closer to ideality (i.e., Nusselt film conditions), either due to the open structure of the packing (M250Y) or the lack of capillary formations (M500Y at low surface tension), than for the M500Y base case.

165
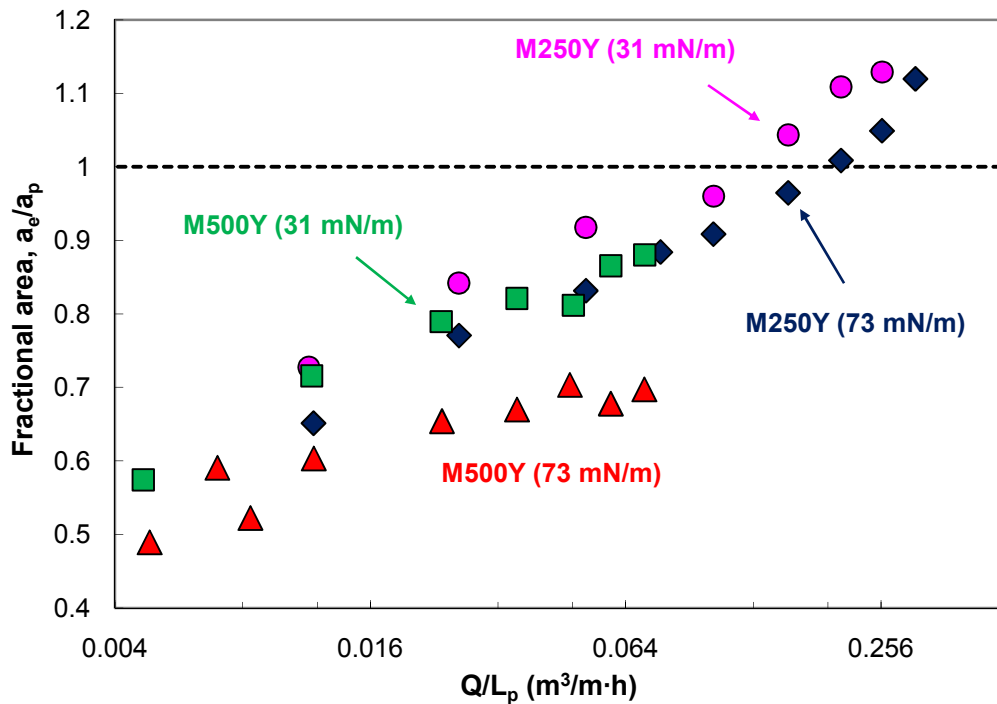
Figure 6.18. **Mass transfer area of M250Y ($a_p = 250$ m^2/m^3) and M500Y ($a_p = 500$ m^2/m^3) at baseline and low surface tension as a function of flow rate per wetted perimeter.**

6.5.3 Foaming

The antifoam that was used in the experiments with TERGITOL NP-7 and POLYOX was, for the most part, effective in controlling foam in the packed column, but it was not entirely successful in eliminating it. Foaming was primarily dictated by the liquid load, which limited the operational range of the "doped" caustic solutions relative to the base case, and was identified by at least one of these operational indicators:

- Visual cues, such as bubble formation within the packing (observed through the column viewing windows);

166

- A large spike in pressure drop, which would on occasion subside, presumably due to the collapse of the foam;

- Instability (oscillations) in the pressure drop or blower air rate, where it became quite difficult to control the system set-point.

The effect of the oscillations on the apparent mass transfer performance was interesting. Given the direct relation of the mass transfer area on gas velocity (equation 4.13), variability in the recorded data was anticipated depending on the time frame, but the area that was measured whenever these instabilities occurred was always much lower than would be expected. This point is illustrated in Figure 6.19, using the low surface tension (31 mN/m) P500 data as an example.
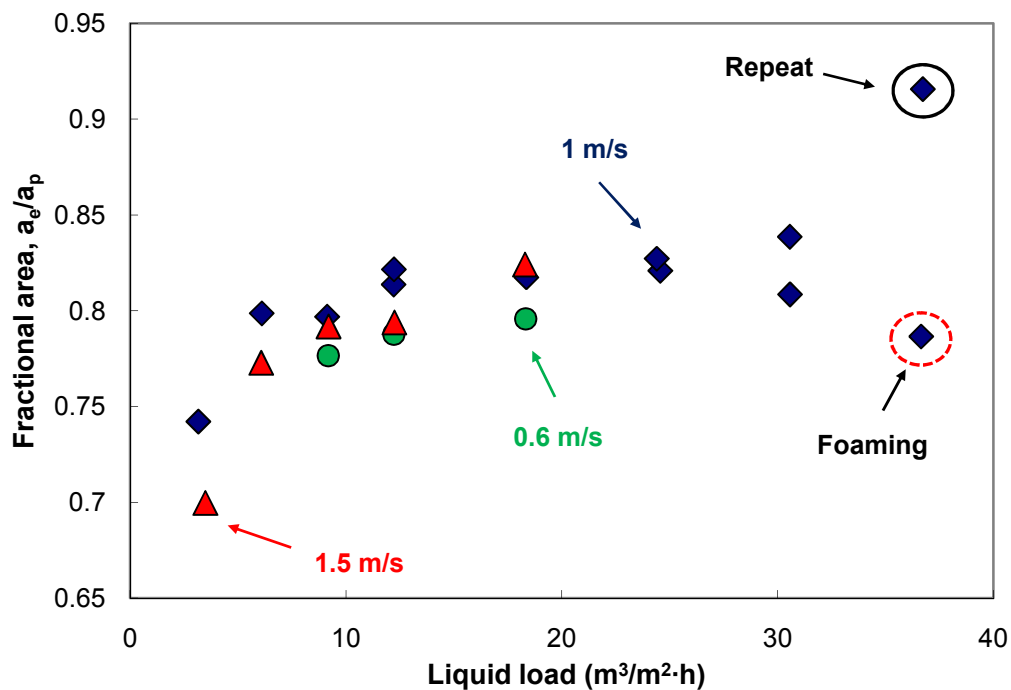
Figure 6.19. Mass transfer area of P500 ($a_p = 500$ m^2/m^3) at low surface tension.

The dash-circled point at the highest liquid load corresponds to a foaming condition. Considering the trend of the data at lower liquid loads and the repeat point (solid-circled) that was taken after a small amount of antifoam was added to the system, the impact of foaming is quite evident. The drop-off in area was not likely due to inaccuracies in the air rate measurement alone. The foam could have caused axial mixing issues or hindered the contact of the liquid with the packing surface. All data that were "contaminated" by foam were ultimately discarded from consideration. Naturally, one might be concerned about foam having more than simply a once-in-a-while impact, but the lack of evidence really would not support this inference. In other words, even for the foaming-prone systems, the data obtained under most circumstances were believed to be of acceptable quality.

6.6 EFFECT OF LIQUID VISCOSITY

The experimental design consisted of three liquid viscosity conditions: baseline or low (1 mPa·s), intermediate (5 mPa·s), and high (10 mPa·s). Viscosity could not be increased without also changing surface tension because POLYOX WSR N750 affects both parameters. For the moderate viscosity solutions, surface tension was measured in the range of 45-60 mN/m, and for the high viscosity solutions, surface tension was around 40 mN/m. To remove the expected effect of surface tension from the analysis, the residuals, rather than the raw data, have been plotted (Figure 6.20). The line through the residuals is given by equation 6.17, and the regressed constants are shown in equation 6.17a.

$$a_f(\text{measured}) - a_f(\text{model}) = C_1 \mu_L + C_2 \tag{6.17}$$

$$[a_f(\text{measured}) - a_f(\text{model})] \pm 0.046; \ C_1 = -0.001 \pm 0.001; \ C_2 = 0.005 \pm 0.003$$

$$\tag{6.17a}$$

The statistics were not supportive of any meaningful trend. Viscosity was concluded to have no impact on the mass transfer area over the range of tested values.
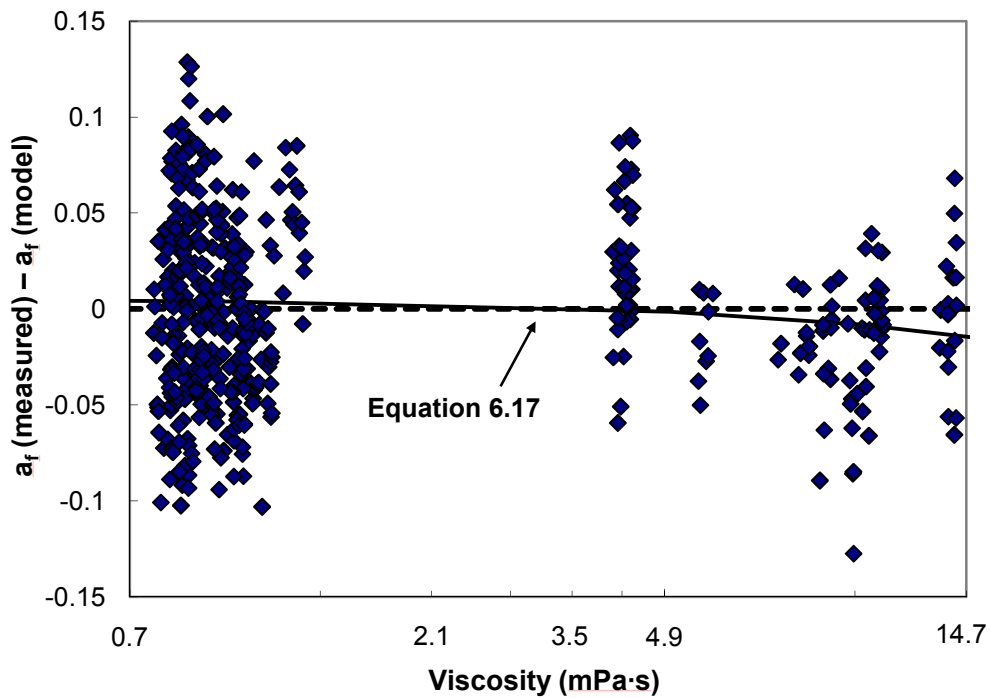
Figure 6.20. Area residuals of experimental database as a function of liquid viscosity, with a_f (model) values from equation 6.13.

Nicolaiewsky et al. (1999) presented a summary of the predicted impact of viscosity on the mass transfer area, as proposed by various literature models. Differing and even contradictory relations are evident. Given this variance of opinion, the lack of observed effect in this work was not overly surprising. Intuitively, the elevated viscosities would result in slightly thicker liquid films on the packing surface. In the

idealized scenario of a smooth, inclined plate, this change would raise the gas-liquid contact line further above the surface but would not necessarily affect the surface area, in concurrence with the experimental findings. In practice, though, rivulet flow experiments, such as those performed by Shi and Mersmann (1985) and Nicolaiewsky et al. (1999) would suggest viscosity influences spreading and hence the mass transfer area. The viscosity ranges in these studies were notably more expansive than the one investigated in the present work (1 to 15 mPa·s); Nicolaiewsky et al. (1999) examined some systems with viscosities greater than 100 mPa·s. As such, the possibility that viscosity could become significant at higher values cannot be discounted. The tested range may not have been broad enough to appreciably affect the spreading of liquid relative to the width of the packing flow channels.

As a final comment, the film saturation test described in Section 6.1.2 was not attempted under viscous conditions, but one could envision the film contribution requiring more time to dissipate due to the slower drainage of liquid. In other words, even though the experimental protocol (i.e., allowing 10 minutes for steady-state) was not modified for these circumstances, perhaps it should have been. While the establishment of the baseline liquid level in the hydraulic tests was definitely observed to take a little longer at high viscosity, nothing that would be indicative of this issue was observed for the mass transfer area measurements. The CO_2 outlet concentrations that were recorded were not changing or fluctuating any more in the viscous cases than in the other experiments.

6.7 EFFECT OF CHANNEL GEOMETRY (M250Y/M250X/MP252Y)

6.7.1 Effect of Corrugation Angle (M250Y/M250X)

The M250Y, M250X, and MP252Y mass transfer area data are shown in Figure 6.21. M250X had steeper flow channels (60°) than M250Y (45°) but otherwise was geometrically equivalent. Its measured area appears to be lower than M250Y but by less than 5% – insufficient to be distinguished from the experimental noise. Consequently, the two packings were concluded to have the same effective area. While this result would seemingly contradict past investigations (Olujic et al., 2000; Fair et al., 2000) that reported a 20 to 30% decrease in mass transfer performance when shifting from a 45° to a 60° inclination, the literature studies were interpreted on an *HETP* basis and therefore could be more reflective of the mass transfer coefficient than the effective area. Olujic et al. (2000) found that Montz B1-250 (45°) had a 20% lower *HETP* than Montz B1-250.60 (60°). However, the model of Rocha et al. (1996) would also predict the 45° packing to have a 15 to 20% greater gas-film mass transfer coefficient (k_G). Hence, the poorer *HETP* of Montz B1-250.60 could have been entirely attributable to a lower mass transfer coefficient, which would imply that the wetted areas of the Montz packings were similar – just as the results in Figure 6.21 would indicate.
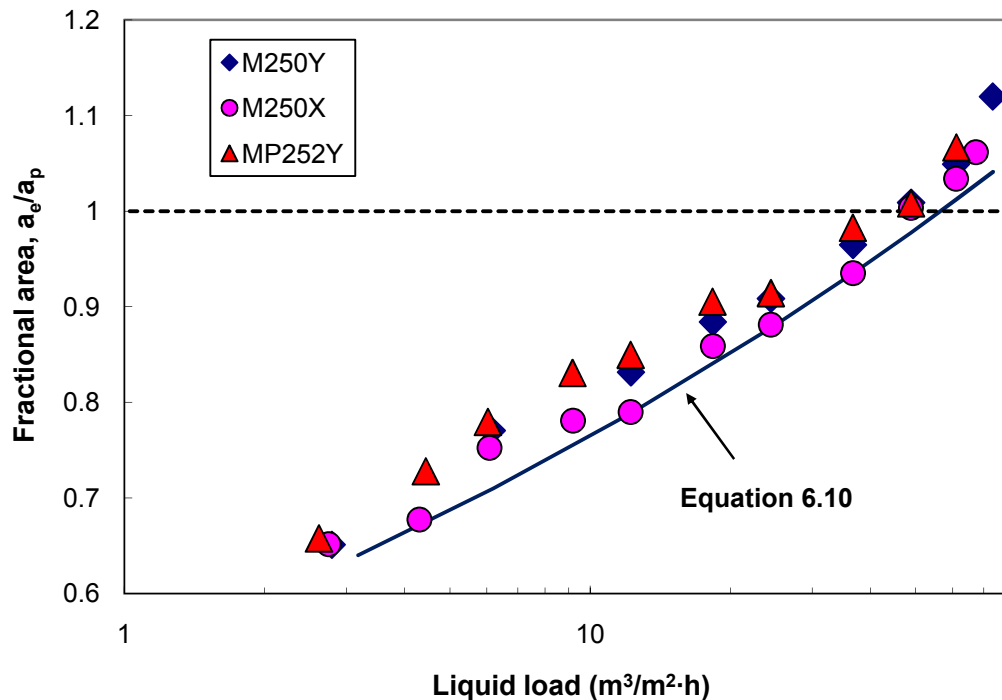
Figure 6.21. Mass transfer area of M250Y, M250X, and MP252Y (a_p = 250 m^2/m^3).

6.7.2 Effect of Element Interface (M250Y/MP252Y)

The interface between packing elements, often referred to as the joint, is known to exhibit a much higher fractional liquid hold-up than the element itself (Suess and Spiegel, 1992; Green et al., 2007) and is identified as the location where flooding is first initiated. High-capacity packings have been introduced to counteract this problem and expand the operational limits of conventional packing (Moser and Kessler, 1999; Olujic et al., 2001). The idea is to basically bend the sheets near the joint from the standard 45° inclination to a vertical (90°) orientation in order to facilitate a smoother flow transition. Our particular high-capacity packing (MP252Y) resembled M250Y except for the aforementioned modification, which occurred at the top/bottom 1.25-cm of each 21-cm tall element. The

172

channel dimensions (*S, B, h*) were measured to be the same as for M250Y, and the specific area was assumed to be 250 m^2/m^3 as well. (Alix and Raynal (2008) notably listed slightly different dimensions for MP252Y than the values in Table 6.1, but even if their numbers were used, the calculated wetted perimeters of MP252Y and M250Y would still be within 3% of each other.) The M250Y and MP252Y data were practically indistinguishable, which would suggest that the joint does not tangibly contribute to the mass transfer area. The fact that the majority of data was collected far from the loading region, where one would not expect there to be a great deal of gas-liquid turbulence or mixing between elements, could explain the lack of a joint effect. That is, the two packings could possibly only deviate (in terms of mass transfer area) near flooding, where M250Y might be anticipated to exhibit greater mass transfer (at the expense of pressure drop) because of its more abrupt joint transition.

6.8 EFFECT OF TEXTURE (M250Y/M250YS)

M250YS was an untextured (smooth) version of M250Y. The two packings were otherwise geometrically identical and were both assumed to have a specific area of 250 m^2/m^3. Figure 6.22 displays the mass transfer area results for the packings.

173
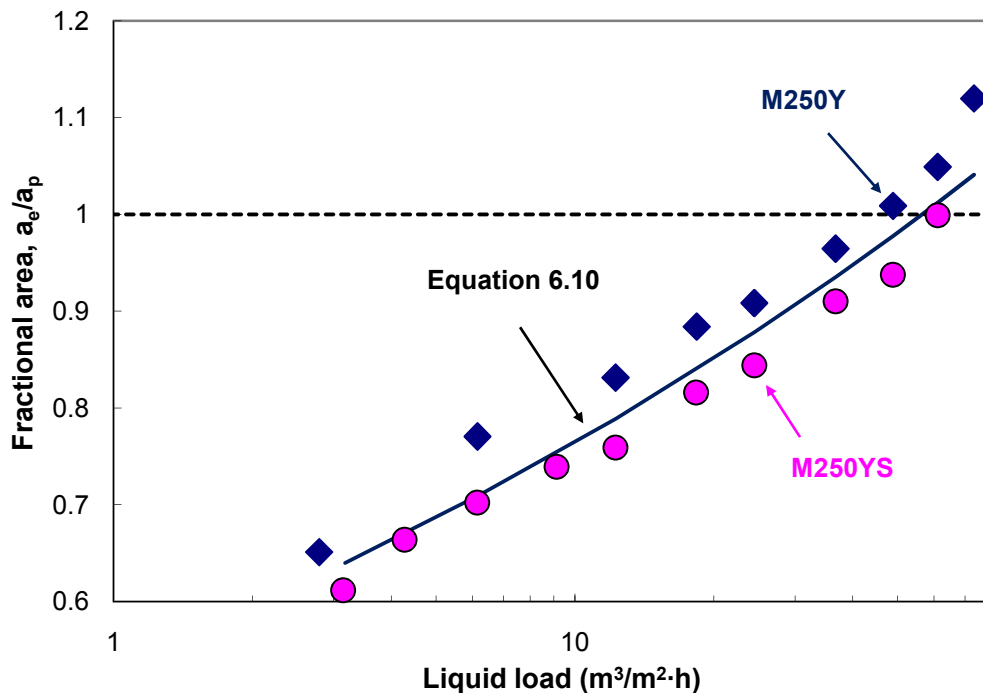
Figure 6.22. Mass transfer area of M250Y and M250YS ($a_p = 250$ m^2/m^3).

McGlamery (1988) speculated that surface texture could increase mass transfer via two mechanisms: greater liquid spreading and enhanced turbulence. While the M250YS points were lower than the M250Y points, the difference between the two data sets was constant (10%) over the investigated liquid loads, which, based on prior arguments, would favor turbulence as the explanation when interpreting the results.

Alternatively, because the surface of M250YS was not embossed, it possibly had a lower specific area than M250Y by 10%. In this case, one might conclude the impact of texture on the effective area to be negligible. As will be discussed in the next chapter, the hydraulic results would favor this theory. Given that the evidence is not absolute, however, it appears that the only definite conclusion that can be made is that texture has at most a weak effect on the mass transfer area.

174

6.9 COMPARISON WITH LITERATURE MODELS

6.9.1 Aqueous Systems

In Figure 6.23, equation 6.10 is compared with a few commonly cited literature models for the case of M250Y at baseline (i.e., water-like) conditions. The experimental data (averaged) are also displayed for reference. The models are reproduced below from Chapter 3. Each is also identified alongside the packing family for which it was intended.

Rocha et al. (1996) (structured):

$$a_{\mathrm{f}} = F_{\mathrm{SE}} \frac{29.12\, u_{\mathrm{L}}^{0.4} v_{\mathrm{L}}^{0.2} S^{0.359}}{(1 - 0.93\cos\gamma)(\sin\alpha)^{0.3}\, \varepsilon^{0.6}} \left(\frac{\rho_{\mathrm{L}}}{\sigma g} \right)^{0.15} \tag{3.6}$$

Billet and Schultes (1993) (structured + random):

$$a_{\mathrm{f}} = 1.5(a d_{\mathrm{h}})^{-0.5} \left(\frac{u_{\mathrm{L}} d_{\mathrm{h}}}{v_{\mathrm{L}}} \right)^{-0.2} \left(\frac{u_{\mathrm{L}}^2 \rho_{\mathrm{L}} d_{\mathrm{h}}}{\sigma} \right)^{0.75} \left(\frac{u_{\mathrm{L}}^2}{g d_{\mathrm{h}}} \right)^{-0.45} \tag{3.16}$$

Onda et al. (1968) (random):

$$a_{\mathrm{f}} = 1 - \exp\left[-1.45 \left(\frac{\sigma_{\mathrm{c}}}{\sigma} \right)^{0.75} \left(\frac{\rho_{\mathrm{L}} u_{\mathrm{L}}}{a_{\mathrm{p}} \mu_{\mathrm{L}}} \right)^{0.1} \left(\frac{u_{\mathrm{L}}^2 a_{\mathrm{p}}}{g} \right)^{-0.05} \left(\frac{\rho_{\mathrm{L}} u_{\mathrm{L}}^2}{\sigma a_{\mathrm{p}}} \right)^{0.2} \right] \tag{3.19}$$

Brunazzi et al. (1995) (structured):

$$a_{\mathrm{f}} = \frac{h_{\mathrm{L}}}{\varepsilon} \frac{d_{\mathrm{e}}}{4\delta_{\mathrm{L}}} = \left(\frac{d_{\mathrm{e}}}{4} \right) \left(\frac{h_{\mathrm{L}}}{\varepsilon} \right)^{1.5} \left(\frac{\rho_{\mathrm{L}} g \sin^2(\alpha)\varepsilon}{3\mu_{\mathrm{L}} u_{\mathrm{L}}} \right)^{0.5} \tag{3.20}$$

Henriques de Brito (1994) (structured):

$$a_f = 0.465 \left(\frac{\rho_L u_L}{\mu_L a_p} \right)^{0.3} \tag{3.22}$$

Present work (structured):

$$a_f = 1.34 \left[\left(\frac{\rho_L}{\sigma} \right) g^{1/3} \left(\frac{Q}{L_p} \right)^{4/3} \right]^{0.116} \tag{6.10}$$

A value of 0.35 for the F_{SE} term in equation 3.6 was specified for Mellapak packings in Rocha et al. (1996). This value was presumed applicable for the purpose of this analysis.
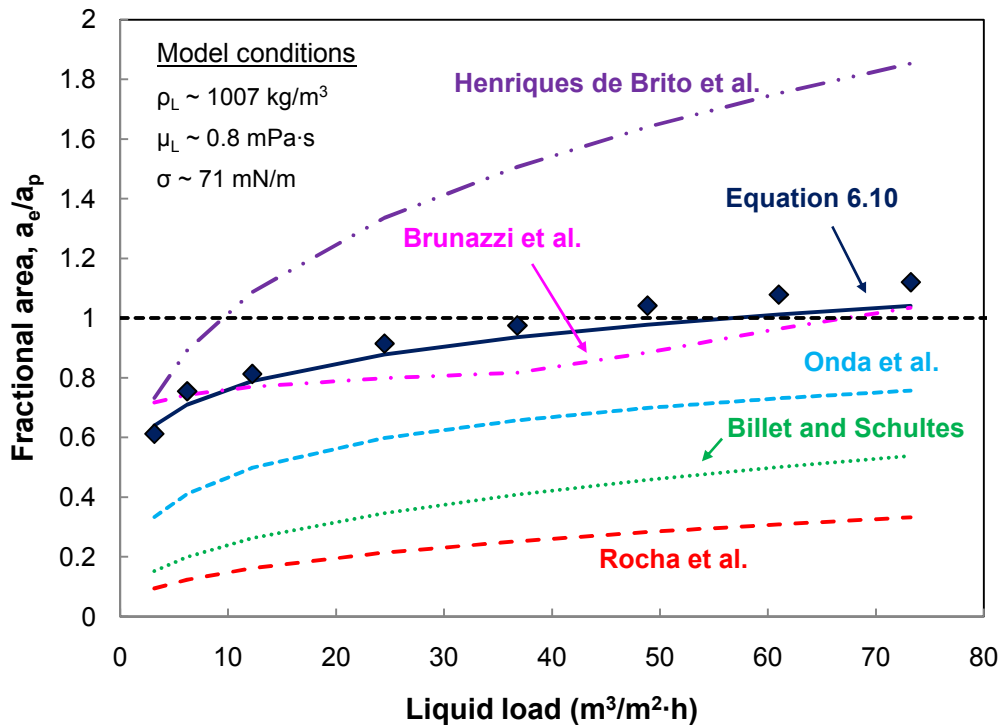
**Figure 6.23. Mass transfer area of M250Y ($a_p = 250$ m^2/m^3) compared with predicted values from models.**

The fit of the literature correlations is overall quite poor. Brunazzi et al. provides the best match of the results, but as will soon be demonstrated, is not nearly as successful at other

conditions or with other packings. The small bump in the curve around 40 m^3/m$^2\cdot$h is due to the discontinuity in the Suess and Spiegel (1992) model implicit in Brunazzi et al. Onda et al. offers the next closest fit, which is interesting given that it is actually intended for random packings. As was stated in Section 3.2.3, however, its application toward structured packings does make some sense due to its imposed limit of unity on the fractional area. With a fairly open packing like M250Y, one would expect the majority of the surface to be well utilized at high liquid loads, near the packing capacity limit. The three remaining models represent two physically unrealistic extremes in this regard. Henriques de Brito et al. predicts fractional areas in significant excess of unity, approaching a value of two near 80 m^3/m$^2\cdot$h. Rocha et al. and Billet and Schultes, on the other hand, predict areas that are unreasonably low. For Rocha et al., at least, this poor accuracy could be partly due to a reliance on distillation data, which generally consist of very low surface tension systems. This weighting could have caused an overly exaggerated surface tension bias or alternatively, an underestimation of the wetting ability of water. As a final note, most of the correlations exhibit comparable trends with liquid load, so there is at least some agreement in that respect.

Similar issues to those discussed above are apparent even with packings other than M250Y. Comparisons at baseline conditions for M500Y (Figure 6.24) and M125Y (Figure 6.25) are shown for illustration.

177
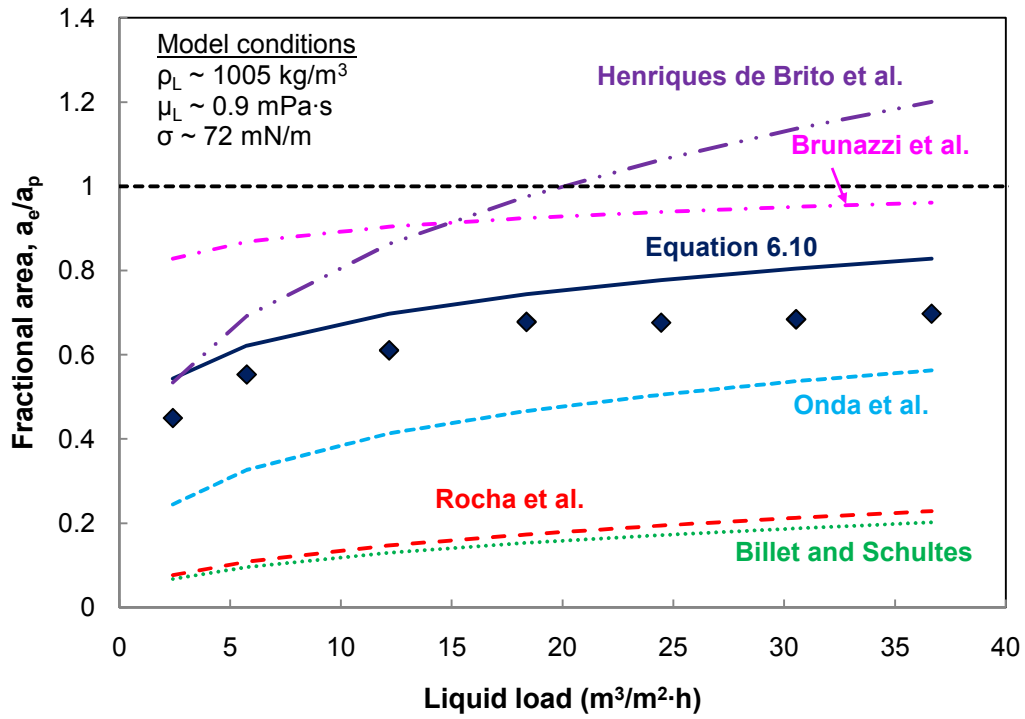
Figure 6.24. Mass transfer area of M500Y ($a_p = 500$ m^2/m^3) compared with predicted values from models.
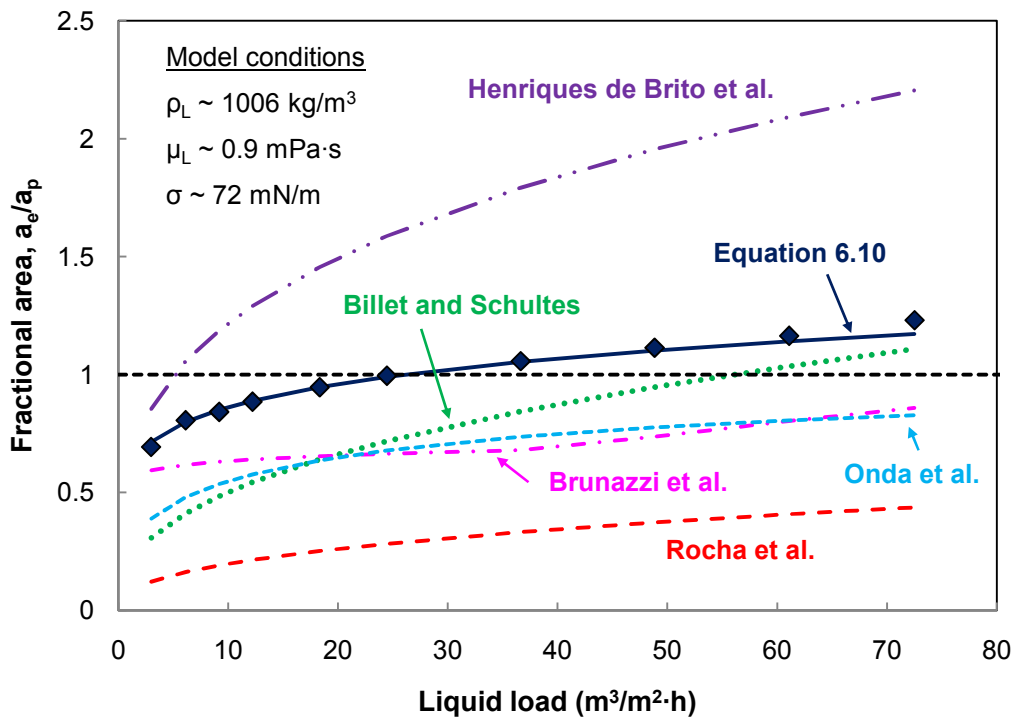
Figure 6.25. Mass transfer area of M125Y ($a_p = 125$ m^2/m^3) compared with predicted values from models.

The performance of the models is exhibited at low surface tension (Figure 6.26) and high viscosity (Figure 6.27). At low surface tension, the fit of Rocha et al. notably becomes better than at high surface tension. This result is discussed further in the next section. The strong (and opposite) viscosity dependences of Rocha et al. and Henriques de Brito et al. are apparent in Figure 6.27, with the two curves essentially flip-flopping their positions from the base case. In general, while some of the literature correlations appear to work on occasion (e.g., Brunazzi et al. for M250Y baseline, Billet and Schultes for M250Y high viscosity), the models cannot be relied on over a broad range of conditions.
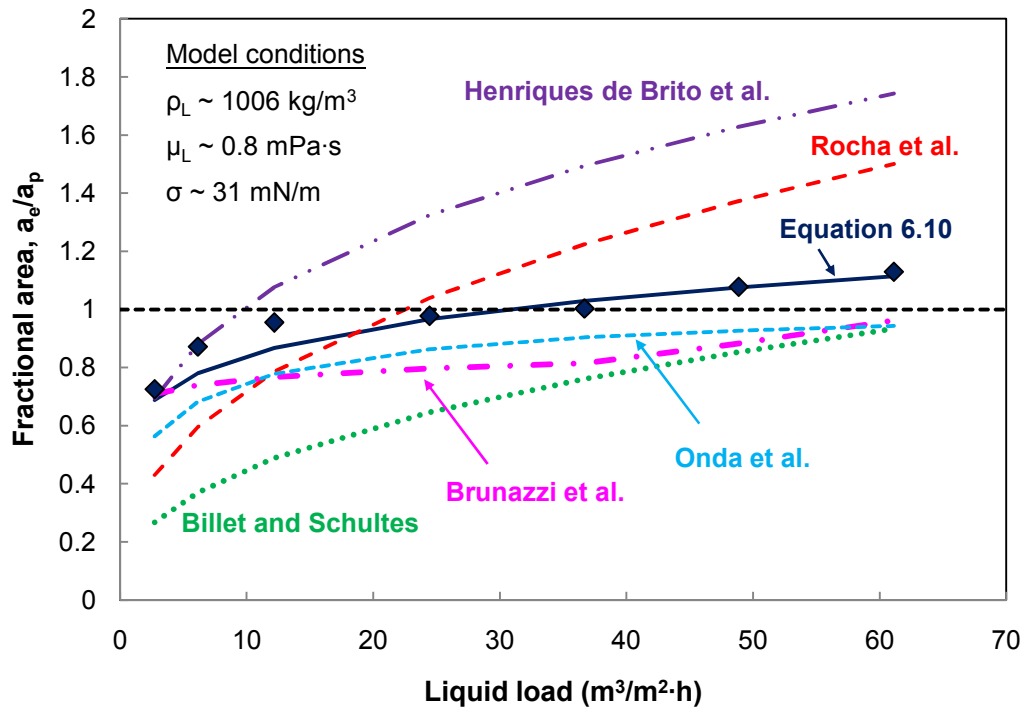
Figure 6.26. Mass transfer area of M250Y ($a_p = 250$ m^2/m^3) compared with predicted values from models at low surface tension.
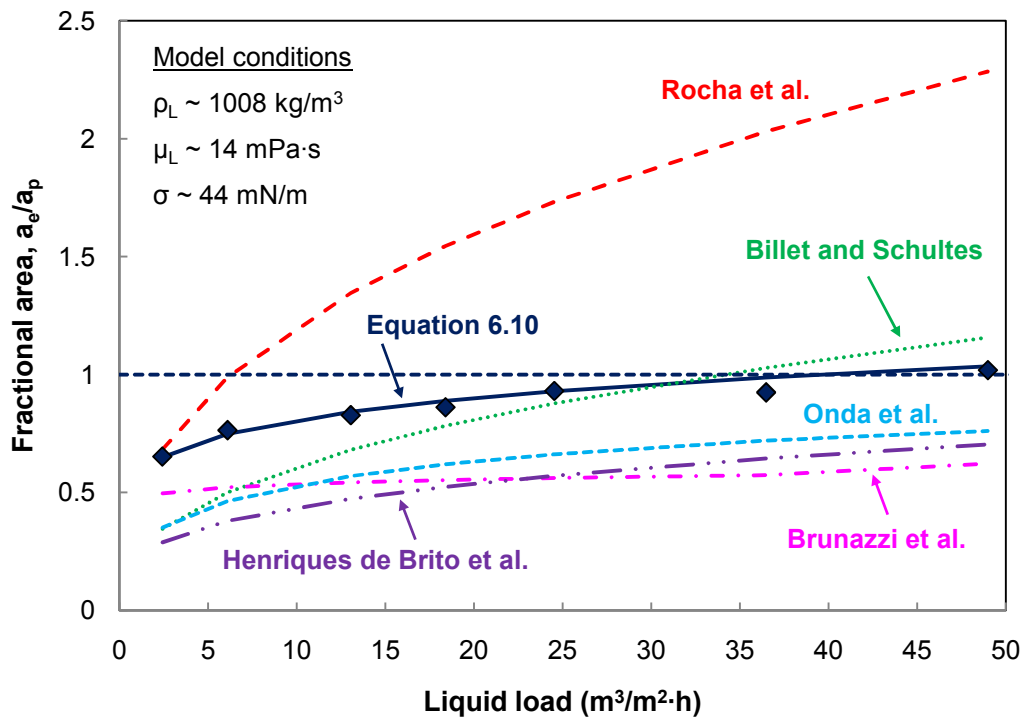
Figure 6.27. Mass transfer area of M250Y ($a_p = 250$ m^2/m^3) compared with predicted values from models at high viscosity.

As a final exercise, the models have been extrapolated to an infinitely large liquid load (2500 m^3/m^2·h) in Figure 6.28. All of the curves with the exception of Onda et al. tend toward infinity, which suggests that even though the models may be applicable over a practical liquid load range, their underlying forms may be somewhat disjointed from the true physics of the packed column system.
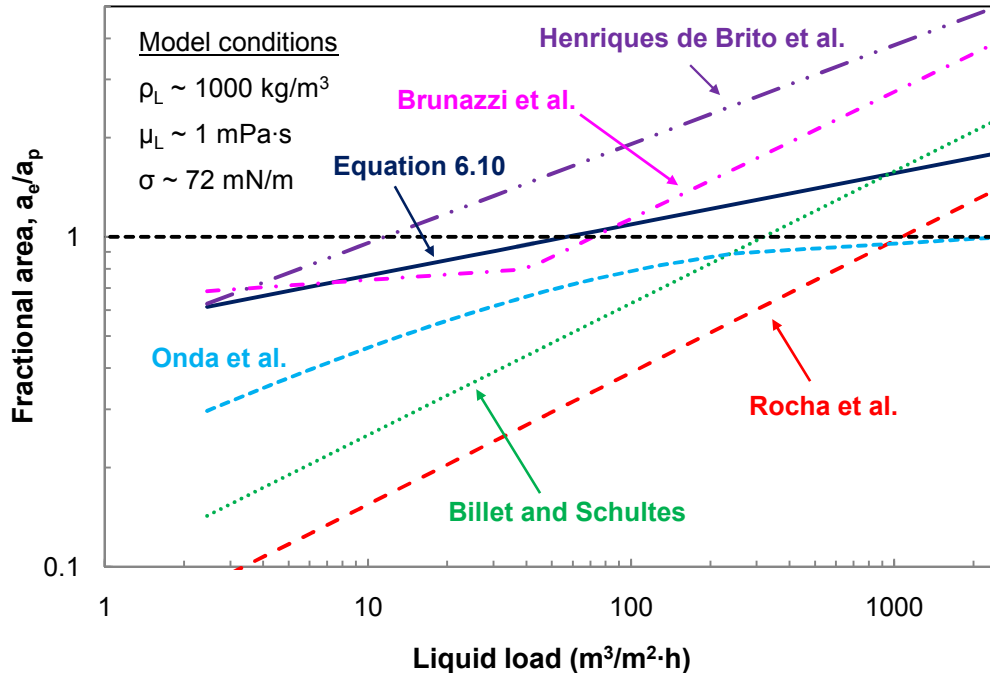
Figure 6.28. Mass transfer area of M250Y (a_p = 250 m^2/m^3) compared with predicted values from models, extrapolating out to infinite liquid load limit.

6.9.2 Hydrocarbon Systems

In the previous section, the literature models (Rocha et al. (1996) and Billet and Schultes (1993) in particular) were demonstrated to be quite poor in their handling of aqueous systems. An important objective of the present research was to address these shortcomings and establish a model suitable for aqueous solvents. Ideally, though, this model would be universal, capable of bridging the apparent gap between aqueous systems and other systems, like hydrocarbons. To test this objective, equation 6.10 was evaluated at conditions reported in a distillation study (cyclohexane/*n*-heptane) conducted by the SRP (Olujic et al., 2000). The highest pressure scenario (414 kPa) deviated most

from water and was selected to offer the most rigorous assessment of the model. Liquid load ranged from 2.5 to 50 m^3/m^2·h, and the relevant physical properties (averaged at the column bottom) were: ρ_L = 561 kg/m^3, μ_L = 0.16 mPa·s, and σ = 8 mN/m. Figure 6.29 compares equation 6.10 with the literature correlations for this distillation condition and for water. For this analysis, the assumed properties of water were: ρ_L = 1000 kg/m^3, μ_L = 1 mPa·s, and σ = 72 mN/m. The mass transfer area of the cyclohexane/n-heptane system was predicted to be 20% higher than the area with water for M250Y. This prediction was a somewhat liberal extrapolation of the 10% effect observed during the low surface tension experiments, which only went down to about 30 mN/m, but at the very least, the predicted fractional area values were plausible, ranging from 0.74 to 1.18. Similar conclusions can be drawn from the comparisons with M500Y (Figure 6.30) and M125Y (Figure 6.31). Obviously, because no data exist (either here or in the literature) where the effective area has been independently measured at a very low surface tension (below 30 mN/m), it is impossible to say whether or not equation 6.10 is truly correct under these circumstances. Still, one cannot deny that the global correlation offers physically reasonable predictions for both aqueous and hydrocarbon systems and therefore appears to be more flexible than Rocha et al. and Billet and Schultes, which certainly do not handle the former well. Nevertheless, because equation 6.10 was developed using aqueous systems, it remains best suited for applications of this nature. As with any model, caution should be exercised when extrapolating beyond the databank upon which it was based.
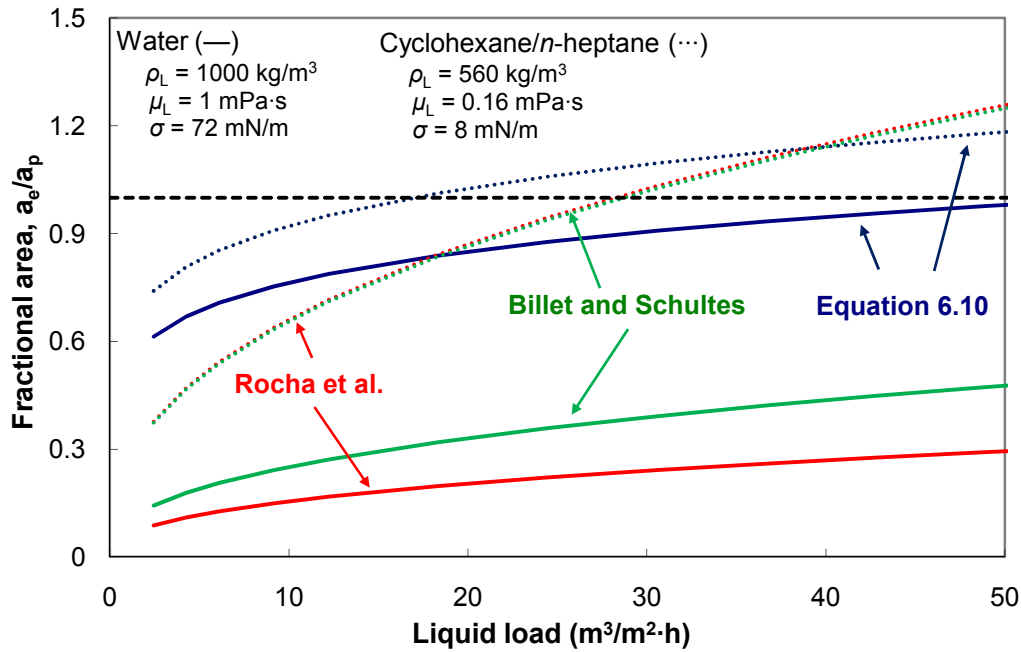
Figure 6.29. Predicted mass transfer area of M250Y ($a_p = 250$ m²/m³) from various models. Lines denote water (—) or cyclohexane/n-heptane system at 414 kPa (···).
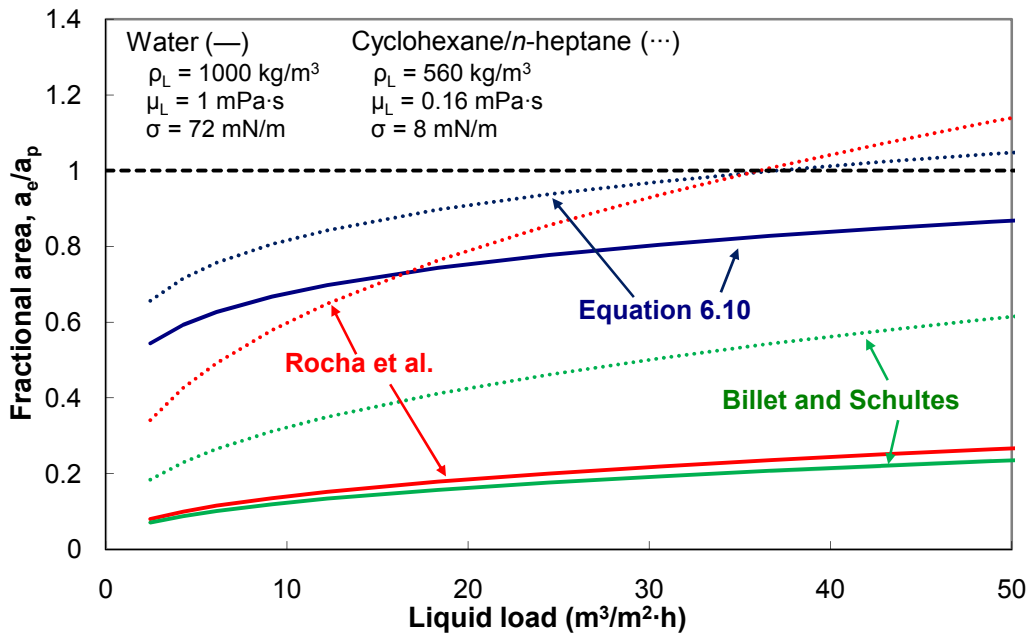
Figure 6.30. Predicted mass transfer area of M500Y ($a_p = 500$ m²/m³) from various models. Lines denote water (—) or cyclohexane/n-heptane system at 414 kPa (···).

184
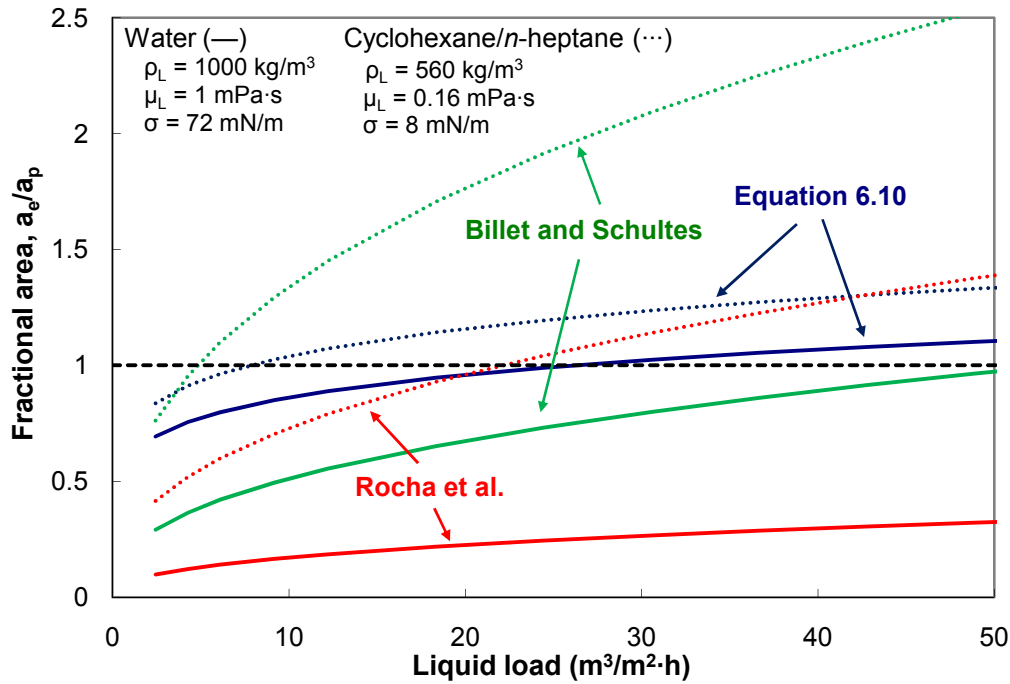
Figure 6.31. Predicted mass transfer area of M125Y ($a_p = 125$ m^2/m^3) from various models. Lines denote water (—) or cyclohexane/n-heptane system at 414 kPa (⋯).

For the M250Y scenario, the close convergence of the two literature models for cyclohexane/n-heptane was perhaps indicative of a common or similar databank basis for this specific case. (Note that the same overlap was not observed for M500Y or M125Y.) Also worth pointing out was the much better agreement of the models with equation 6.10 (relative to the water scenario), particularly at moderate liquid loads (25 to 50 m^3/m^2·h). Thus, while the use of the Rocha et al. or Billet and Schultes correlations for the analysis of aqueous systems is not recommended, they could actually be acceptable when applied toward distillation-type systems.

6.10 ALTERNATE INTERPRETATIONS

The entire analysis thus far was performed under the assumption that the k_g' models from the literature were valid and that the packing was the lone source of mass transfer in the system. This treatment of the data was believed to be legitimate, but had either or both of these assumptions not been true, then the interpretation would clearly be different. These hypothetical scenarios are investigated further in this section.

6.10.1 Modified k_g'

The WWC measurements exhibited rates (k_g') that were marginally different than those predicted by the literature models. The average normalized k_g' values were higher in the cases of the baseline (1.1) and TERGITOL NP-7 (1.09) systems and were slightly lower for the POLYOX system (0.94). The fractional area measurements were modified accordingly with these numbers, to quantify exactly how the database would change. (The 0.94 factor was applied to both the intermediate and high viscosity scenarios, even though it was only the latter that was tested in the WWC.) The updated effective area correlation (equation 6.18) and database (Figure 6.32) are shown below. The dashed lines denote two standard errors (±18%).

$$a_f = 1.26\left[\left(We_L\right)\left(Fr_L\right)^{-\frac{1}{3}}\right]^{0.114} \tag{6.18}$$
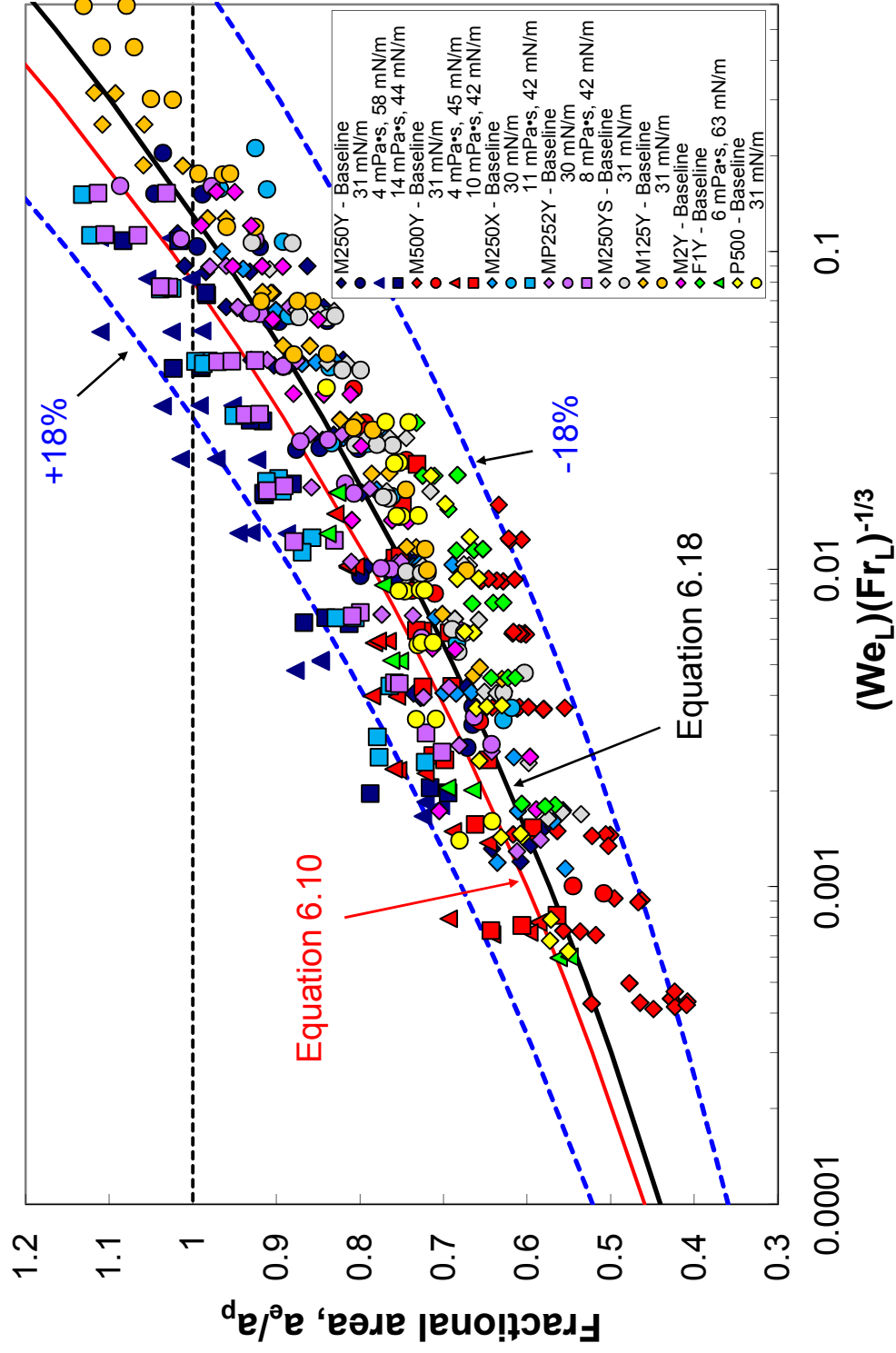
Figure 6.32. Structured packing mass transfer area database after incorporation of k_g' modification, shown on dimensionless basis and compared with global models (equations 6.10 and 6.18).

187

The fit is obviously poorer than before (see Figure 6.5), due to the induced separation of the viscous systems from the other data sets. While this interpretation of the results would suggest that a different dimensionless grouping (i.e., one with a viscosity term included) should be utilized to collapse the database, the $(We_L)(Fr_L)^{-1/3}$ basis still does a decent job of unifying the data (limits of less than 20%). Thus, if the WWC results had indeed been handled incorrectly in the original analysis, the consequences from a quantitative perspective can be seen to not be extremely substantial.

6.10.2 Entrance, End, and Wall Effects

The contributions of secondary phenomena like end and wall effects were not incorporated into the results, but these certainly could have enhanced the mass transfer occurring in the system, thereby leading to a skewed interpretation. The potential implications of three such issues are discussed.

The "splash" zones at the top (liquid impact on the packing surface) and bottom (liquid impact on the pool in the sump) of the packed column were both possible sources of mass transfer. Yeh (2002) studied liquid-phase mass transfer in spray contactors. For the case of spray impacting a solid surface, the number of liquid-phase transfer units was correlated in the following form:

$$N_L = 0.0026 u_{L,imp}^{0.7} u_{L,spray}^{-0.2} \tag{6.19}$$

The two velocity terms in equation 6.19, referring to the liquid velocity at the impact point ($u_{L,imp}$) and from the spray source ($u_{L,spray}$), were defined in units of cm/s. For this analysis, the impact velocity was obtained from a conversion of potential energy to

kinetic energy. The distributor-to-packing distance was never greater than about 12 cm (5 in). This distance was not recorded in every test, though, so for these instances, a 12 cm separation (worst case) was assumed, equating to a $u_{L,imp}$ of 153 cm/s. The spray velocity was calculated based on the liquid load and the specifications of the fractal distributor: drip point density of 108 drip points/m^2 (10 points/ft^2) and approximate drip point diameter of 6 mm. The number of liquid-phase transfer units can also be generically expressed as:

$$N_L = \frac{k_L^0 a}{Q} \tag{6.20}$$

Equations 6.19 and 6.20 can be rearranged to solve for the area associated with the impact at the top of the column.

$$a_{imp,top} = 0.0026 u_{L,imp}^{0.7} u_{L,spray}^{-0.2} \left(\frac{Q}{k_L^0} \right) \tag{6.21}$$

For simplicity, a constant value of 0.01 cm/s was used for k_L^0. This estimate was based on the predicted values for the mass transfer coefficients of droplets in Yeh (2002). It also happened to be of the same order of magnitude as the anticipated liquid-film mass transfer coefficients in the WWC and in structured packing.

The number of transfer units associated with spray impact into a liquid was found by Yeh (2002) to be of comparable magnitude to that for liquid-solid impact and was correlated in a similar form:

$$N_L = 0.0056 u_{L,imp}^{0.5} u_{L,spray}^{-0.5} \tag{6.22}$$

The impact velocity at the pool surface was approximated similarly as before, with the drop-off being calculated from the difference between the maximum distance (2.1 m or about 7 ft for a near-empty sump) and the liquid level in the sump (generally around 25 cm or 10 in). The spray velocity was simply the liquid superficial velocity.

The column wall was a potential mass transfer source as well. The surface was treated as fully wetted at all liquid loads and was assumed to extend slightly beyond the boundaries of the packed bed, to a total length of about 4.6 m (15 ft). This equated to an area of 6.2 m^2.

The results of the analysis for M125Y, M250Y, and M500Y are shown in Table 6.3. The values in the table are calculated from actual baseline conditions involving these packings.

Table 6.3. Mass transfer area contributions from entrance/end/wall effects and packing.

Packing	Approx. liquid load (gpm/ft^2 or m^3/m$^2 \cdot$h)	$a_{imp,top}$ (m^2)	$a_{imp,bottom}$ (m^2)	a_{wall} (m^2)	$a_{packing}$ (m^2)	a_{sum} / $a_{packing}$ (%)	a_f	$a_{f,mod}$
	1 or 2.4	0.05	0.6	6.2	39	17.6	0.69	0.57
M125Y	10 or 24.4	0.3	1.6	6.2	57	14.2	0.99	0.85
	30 or 73.2	0.6	2.8	6.2	70	13.7	1.23	1.06
	1 or 2.4	0.05	0.6	6.2	69	9.9	0.61	0.55
M250Y	10 or 24.4	0.3	1.6	6.2	103	7.9	0.91	0.84
	30 or 73.2	0.7	2.8	6.2	127	7.6	1.12	1.03
	1 or 2.4	0.04	0.5	6.2	92	7.3	0.45	0.42
M500Y	10 or 24.4	0.2	1.6	6.2	139	5.8	0.68	0.64
	15 or 36.6	0.3	2.0	6.2	143	5.9	0.70	0.66

The total area contributions (a_{sum}) from the entrance/end/wall effects could be significant relative to the packing. M125Y, having the lowest absolute area, is impacted the greatest, with the adjusted fractional area ($a_{f,mod}$) being close to 20% lower in the worst-case scenario. As would be anticipated, a higher liquid load translates to a larger "splash"

190

contribution, although the relative impact on the fractional area actually decreases along these lines. The values at a given liquid load are the same for every packing, because there was no packing-dependent component in the spray effect calculations. The wall effects in particular are believed to be somewhat exaggerated, but any overcompensation in this regard could effectively serve to account for other potential contributing factors, such as the mass transfer area from the rivulets and droplets falling off of the bottom of the packing (prior to hitting the liquid pool), that were omitted from the analysis. Even if the calculations in Table 6.3 are all slightly inflated, they at least demonstrate that both the sump and wall likely warrant more concern than the top region of the column.

The analysis outlined in Table 6.3 was applied to the entire database. The area associated with the secondary effects was subtracted from the raw measurements, and these new data were regressed in the same form as the original global model (equation 6.23). The modified database is shown in Figure 6.33. The dashed lines denote two standard errors (±13.5%).

$$a_{\mathrm{f}} = 1.20 \left[(We_{\mathrm{L}})(Fr_{\mathrm{L}})^{-\frac{1}{3}} \right]^{0.109} \tag{6.23}$$
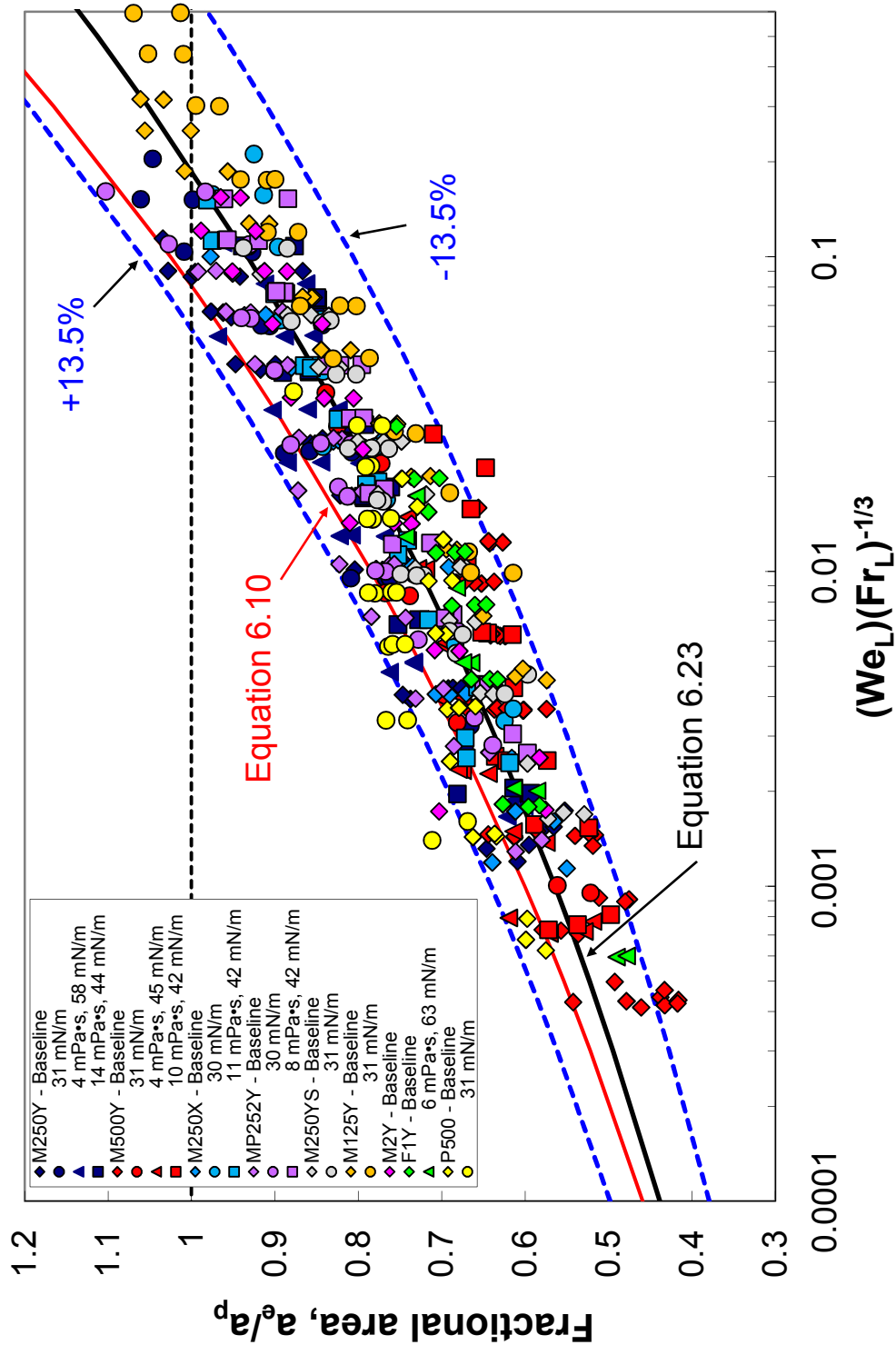
Figure 6.33. Structured packing mass transfer area database after removal of wall and end effects, shown on dimensionless basis and compared with global models (equations 6.10 and 6.23).

192

The result of the corrections was essentially a flattening of the overall trend with $(We_L)(Fr_L)^{-1/3}$. The M500Y data were not moved much, whereas the M125Y data were noticeably shifted down. Within a given data set, though, the slope with liquid load actually increased, due to the points at high liquid loads being less affected than the ones at lower loads. The fractional area values were all reduced to around 1.1 or less, which one might argue is more sensible than some of the raw values that were obtained (upwards of 1.3), in the context of the expected performance limitations of structured packing. The most interesting consequence of this exercise was that the high surface area packing points (F1Y and M500Y), which previously were observed to tail-off from the rest of the results, appeared to blend in better. This feature is more easily seen in a plot of the residuals (Figure 6.34).
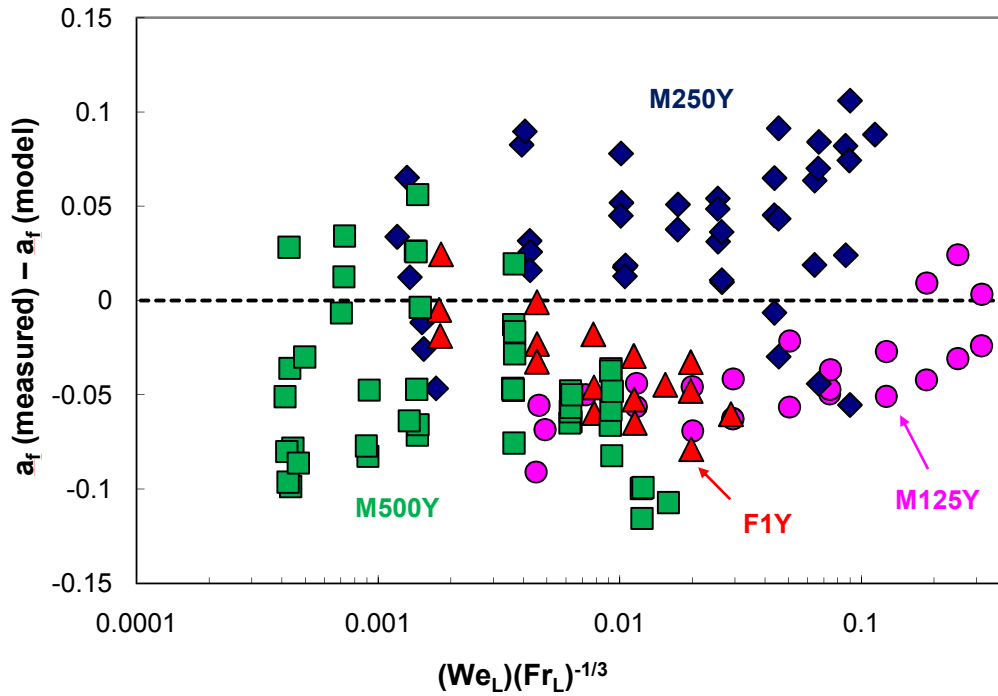
Figure 6.34. Area residuals for experimental database as a function of $(We_L)(Fr_L)^{-1/3}$, with a_f (model) values from equation 6.23.

Recall that the residuals with the original model (Figure 6.8) showed a trend with packing size, with the majority of F1Y and M500Y points falling below the zero line and the M250Y and M125Y points predominantly residing above it. This bias seems to have been eliminated somewhat. A regression with a quadratic geometric dimension (GD), as was introduced in Section 6.3.1, term was subsequently performed (equation 6.13). The constants and standard errors are provided in equation 6.13b.

$$\ln a_f = C_1 \ln \left[(We_L)(Fr_L)^{-1/3} \right] + C_2 [\ln(GD)]^2 + C_3 \qquad (6.13)$$

$\ln a_f \pm 0.068; \ C_1 = 0.108 \pm 0.002; \ C_2 = -0.001 \pm 0.001; \ C_3 = 0.187 \pm 0.013$

(6.13b)

194

The *GD* parameter is not at all significant in this case, indicating that the inclusion of secondary effects basically accomplished the same purpose as the addition of the geometric dimension. This treatment has a much more logical basis, though, and thus, the *GD* analysis (and the associated model defined by equation 6.13a) presented earlier should probably be disregarded in light of this analysis. The dimensionless $(We_L)(Fr_L)^{-1/3}$ grouping on its own would seem to be sufficient to capture the database. One might question why equation 6.23 is not the finalized mass transfer area correlation, since it is literally a more robust version of equation 6.10. While this modified correlation may indeed be more realistic, one must be aware that it was based on an approximate analysis and represents a work-in-progress, whereas equation 6.10 undeniably represents the raw data.

As a final comment, preliminary mass transfer area tests have been conducted that have monitored the difference between the ambient CO_2 level and the level immediately preceding the packed bed. These tests have indicated there to be upward of a 20 to 30% mass transfer contribution from the sump (Perry et al., 2010). This result is quite striking and is a little difficult to comprehend, and one must bear in mind that the protocol is still being refined and that the sump characterization study is a work in progress. Still, the possibility that the raw measurements obtained in the present work could be in need of some refinement with respect to end and wall effects is certainly legitimate.

.

Chapter 7: Packed Column Results (Hydraulics)

Hydraulic data, obtained primarily to supplement the effective area results, are presented in this chapter. An overview of general hydraulic (pressure drop and liquid hold-up) features is first offered. The experimental data, categorized on the basis of packing size, geometric configuration, surface tension, and viscosity, are then discussed. Last, the predictive capabilities of several hydraulic models in the literature are evaluated.

As expected, both pressure drop and hold-up increased with packing size and liquid load, with the former relation being in relatively direct proportion. The pre-loading pressure drop increased by upwards of a factor of three over the range of operational liquid loads, and as much as a five- to ten-fold increase in hold-up was observed. The geometric channel configuration significantly affected the pressure drop. Changing from a 45° to 60° channel, for instance, decreased pressure drop by more than a factor of two and increased capacity by about 20%. The packing texture (smooth vs. embossed) resulted in a 15 to 20% difference in pressure drop and hold-up (lower for smooth), although this was believed to be related to geometric area rather than the actual surface features. Surface tension (30-72 mN/m) had no appreciable impact on the pre-loading pressure drop of M250Y and M500Y and a relatively small effect on the liquid hold-up (15-30%). Increasing the liquid viscosity (1-15 mPa·s) only slightly elevated the pre-loading pressure drop (5-10%) but had a major effect on the hold-up, doubling it in the case of the 250-series packings (M250Y/M250X/MP252Y). Both the decrease in surface tension and increase in viscosity were observed to reduce the capacity of packings by up to 20%, but it was not entirely clear whether this was due to the physical

196

property changes themselves or to foaming. The impact of mere irrigation of the packing on the hydraulics was striking relative to the fairly marginal influence of surface tension and viscosity. Neither a relation between the mass transfer area and hydraulic results, nor a consistent connection between the two hydraulic parameters themselves (pressure drop and hold-up), was discernible from the data.

The examined hydraulic models were adequate under dry conditions but were not particularly successful with either the prediction of the pre-loading pressure drop or the behavior in the loading region under irrigated conditions. Several of the models relied on an implicitly calculated liquid hold-up for their prediction of pressure drop, and the incorporation of an external value for the hold-up (either a calculated or experimental value) tended to yield an improvement in this prediction.

7.1 HYDRAULICS EXPERIMENT: GENERAL OVERVIEW

To demonstrate the standard trends observed in any given air-water hydraulic experiment, the pressure drop results from a typical run (with M250Y) are shown (Figure 7.1). The gas flow factor (F_G) is a convenient independent variable since it is theoretically meaningful (Bernoulli equation) and allows for the incorporation of temperature effects (via gas density).

$$F_G = u_G \sqrt{\rho_G} \qquad (7.1)$$
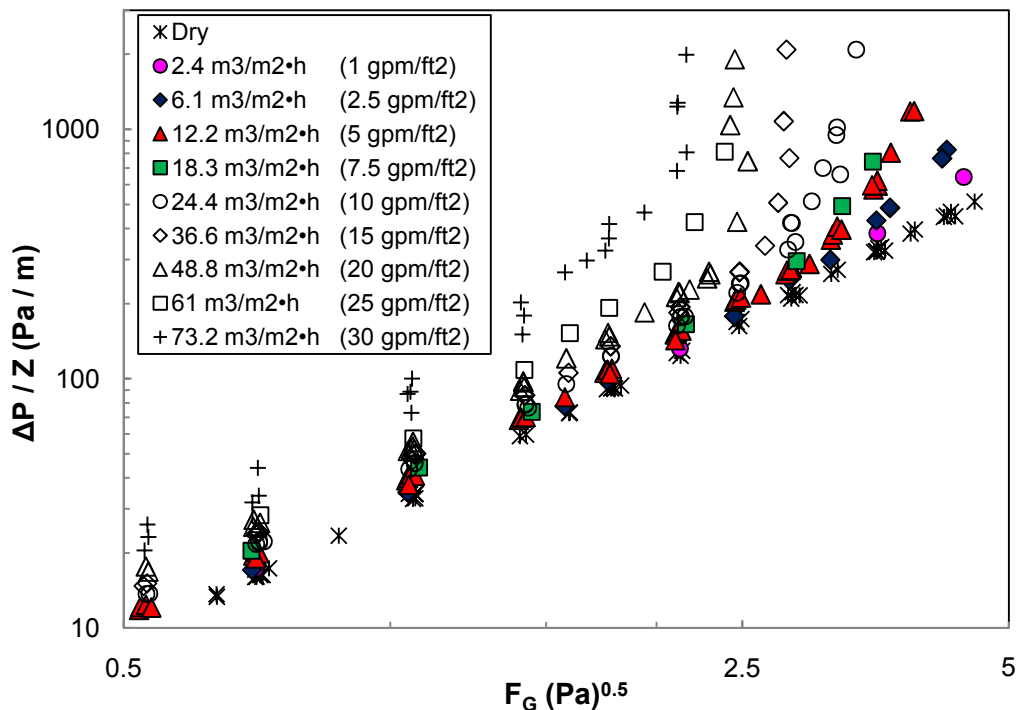
Figure 7.1. Pressure drop of M250Y with air-water system.

Two distinct regions are identifiable. In the pre-loading region, there is a steady exponential increase in pressure drop with the gas rate. This should be a squared relation based on the Bernoulli equation, but frictional effects result in the power being slightly lower – around 1.8 to 1.9. The loading region represents the condition where this dependence begins to sharply increase, with flooding technically occurring when this power approaches a limit of infinity. At a given gas flow factor, the pressure drop can be seen to increase with liquid load, and greater separation between the data sets is apparent in the limit of higher loads.

Similar trends apply for liquid hold-up. The fractional hold-up plotted in Figure 7.2 is simply the ratio of liquid volume in the packing to the volume of the packing itself.
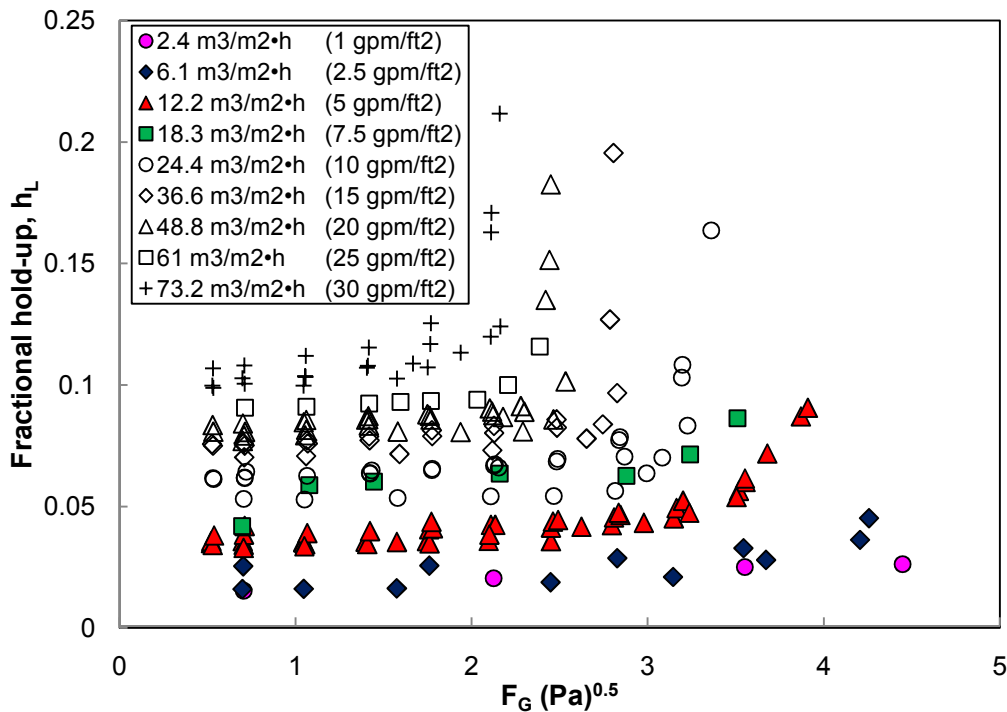
Figure 7.2. Hold-up of M250Y with air-water system.

The gas and liquid have limited interaction in the pre-loading region. The consequence is that liquid hold-up is fairly constant. In contrast, at the onset of loading and beyond, a dramatic increase in hold-up is evident. The pre-loading hold-up is seen to fall in the range of 1 to 10% over the tested liquid loads. This was generally true for every packing that was studied, and so, it is probably safe to assume a value of this magnitude if an on-the-fly estimate is so desired. Akin to pressure drop, an increasing trend with liquid load at a constant gas flow factor is apparent, but the effect actually seems to diminish in this case, with the data sets becoming more compacted. For instance, the hold-up roughly doubles from 12.2 to 24.4 $m^3/m^2 \cdot h$ (5 to 10 gpm/ft^2), but not nearly the same increase is seen when going from 24.4 to 48.8 $m^3/m^2 \cdot h$ (10 to 20 gpm/ft^2). At low liquid loads, one could envision the hold-up to be primarily associated with the access of liquid to the

199

packing channels and crevices, whereas the contribution to hold-up at high loads could be a simple function of increasing film thickness. The former mechanism would perhaps be expected to be more significant than the latter – hence the greater initial dependence that was observed.

As can be surmised from Figures 7.1 and 7.2, the quantity of data associated with the hydraulic tests was quite large, making the presentation and relation of the results in a condensed yet meaningful manner rather difficult. To handle this dilemma, the data were normalized against M250Y, a logical center-point in terms of both specific area (125-500 m^2/m^3) and geometry (M250X, MP252Y, M250YS). Pressure drop was normalized by a correlation for the dry M250Y pressure drop (equation 7.2), obtained from a fit of the raw data in power law form (Figure 7.3).

$$\frac{\Delta P_{dry,M250Y}}{Z} = 30.924 F_G^{1.8555} \qquad (7.2)$$
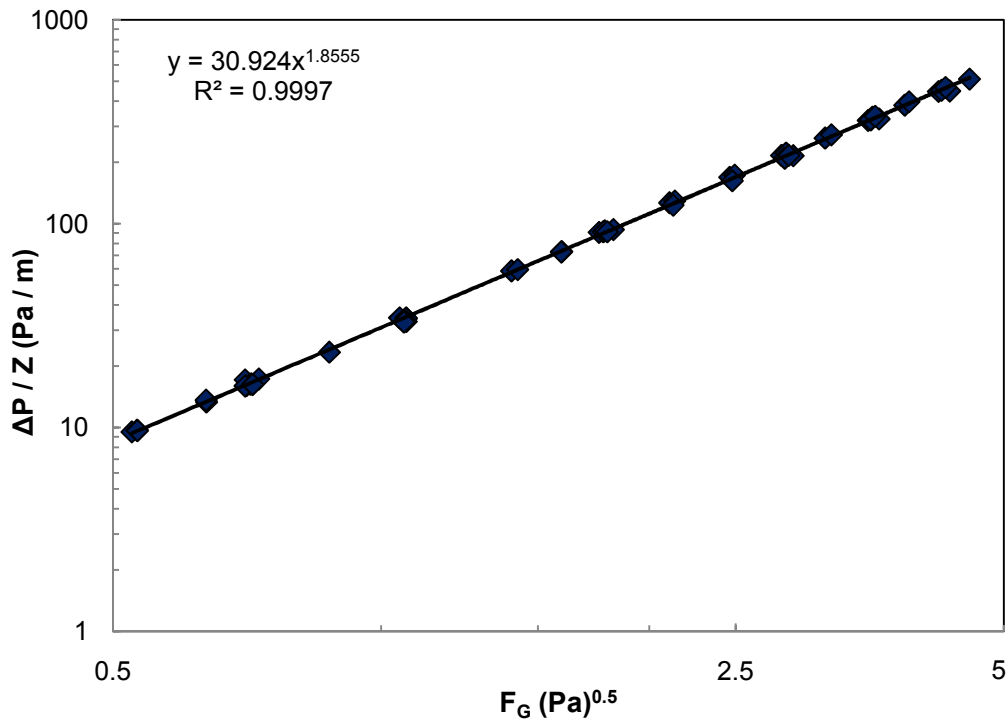
Figure 7.3. Dry pressure drop of M250Y.

Hold-up was normalized by a correlation for the baseline (water) M250Y hold-up at a vapor flow factor of approximately 0.7 $Pa^{0.5}$ – a relatively low flow rate to guarantee that the system was in the pre-loading region.

$$h_{\text{L base,M250Y}}(\%) = 0.7975L^{0.6028} \qquad (7.3)$$
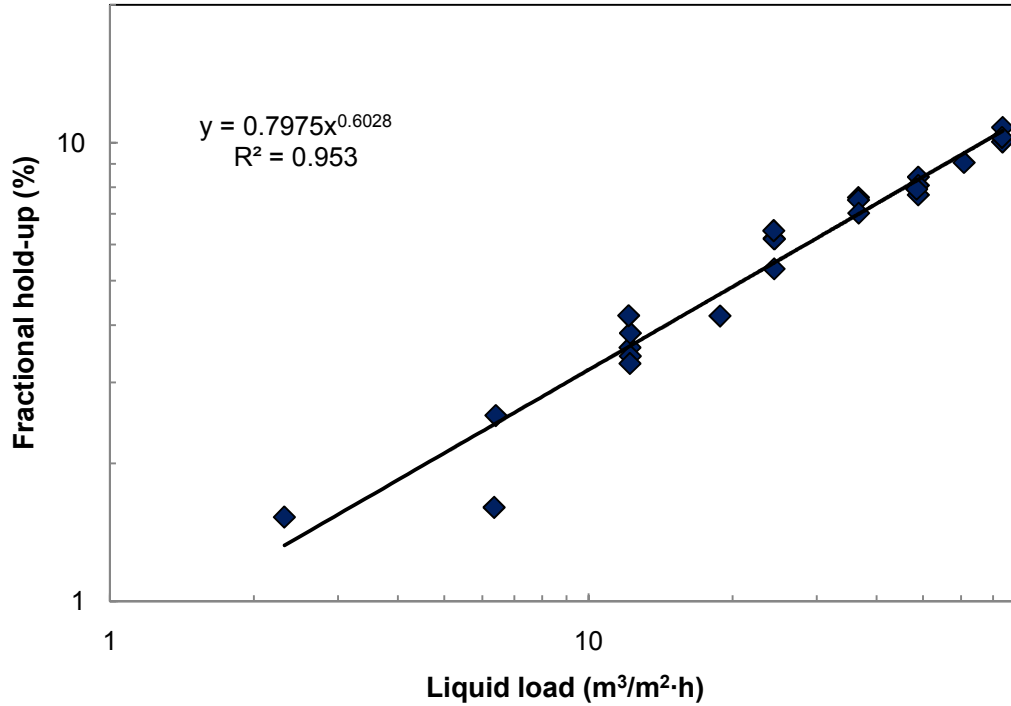
Figure 7.4. Hold-up of M250Y at a gas flow factor of 0.7 Pa$^{0.5}$.

In many of the cases below, results for a representative set of conditions are shown, since it was considered redundant to present every data point that was acquired.   The full database can be found tabulated in Appendix B.3.   An overview of the packings in the database and experimental conditions is provided in Table 7.1.

Table 7.1. Packings and experimental conditions included in hydraulics database.

Packing	Conditions: $\mu_L{}^a$ (mPa·s) / σ^b (mN/m)
Mellapak 250Y (M250Y)	0.8/71, 0.9/31, 6/60, 14/44
Mellapak 500Y (M500Y)	1/72, 0.9/30, 5/48, 10/44
Mellapak 250X (M250X)	1/72, 14/45
MellapakPlus 252Y (MP252Y)	0.9/72, 12/45
Mellapak 250Y (smooth) (M250YS)	1.1/73
Mellapak 125Y (M125Y)	0.9/72
Mellapak 2Y (M2Y)	1.1/73
Flexipac 1Y (F1Y)	Dry only
Prototype 500 (P500)	1/73

[a] For base case (water), calculated from equation 4.5b
[b] For base case (water), calculated from fit of data in Haar et al. (1984)

7.2 EFFECT OF PACKING SIZE (M125Y/M250Y/F1Y/M500Y)

Dry pressure drop data for four packings ranging in specific area from 125 to 500 m^2/m^3 are displayed in Figure 7.5. The relative values correspond perfectly with the packing sizes (i.e., M125Y ~ 0.5, M250Y ~ 1, M500Y ~ 2), which indicates that the dry results are further collapsible via a normalization by the specific area. This is demonstrated in Figure 7.6, with the general correlation given by equation 7.4.

203

$$\frac{\left(\Delta P / Z\right)_{dry}}{a_p} = 0.125 F_G^{1.84} \tag{7.4}$$
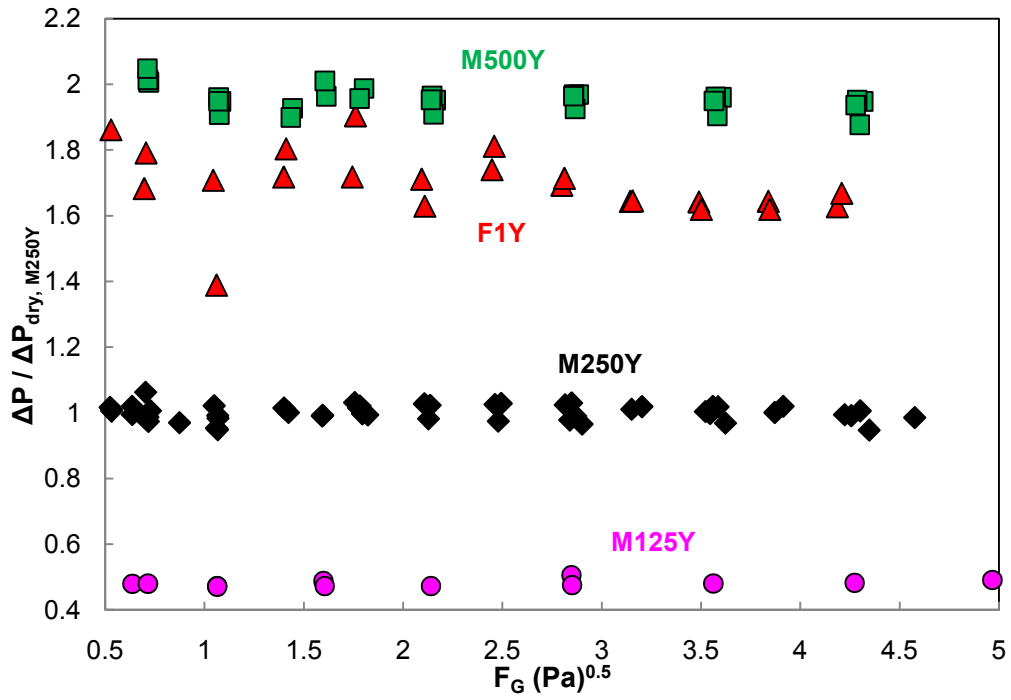
Figure 7.5. Normalized dry pressure drop of M125Y, M250Y, F1Y, and M500Y.
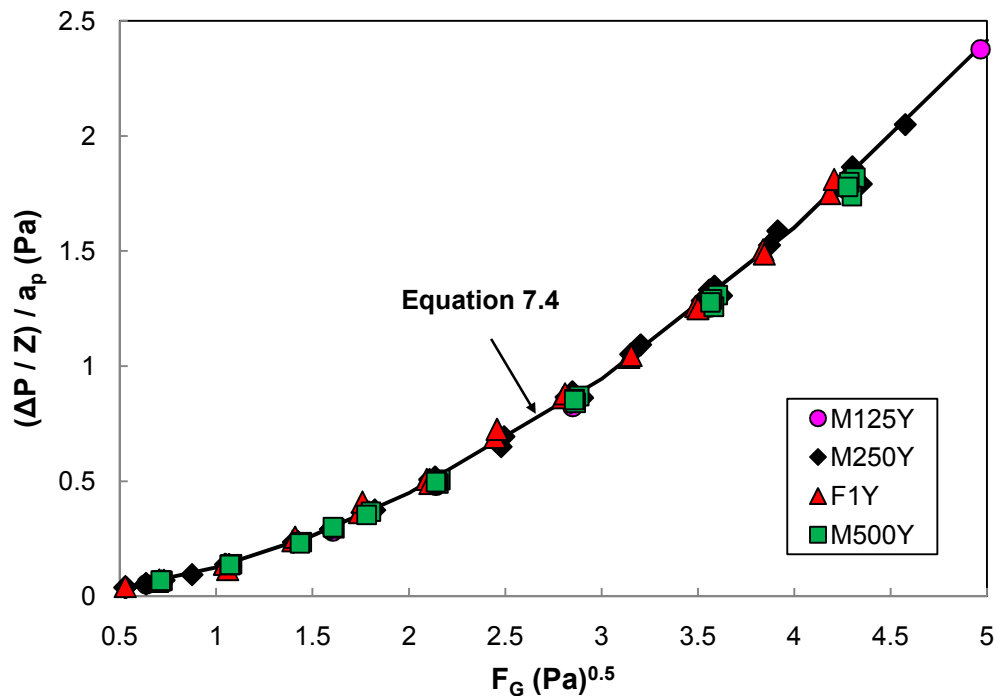
**Figure 7.6. Dry pressure drop of M125Y ($a_p = 125$ m^2/m^3), M250Y ($a_p = 250$ m^2/m^3), F1Y ($a_p = 410$ m^2/m^3), and M500Y ($a_p = 500$ m^2/m^3), normalized by packing specific area.**

Irrigated data (24.4 m^3/m^2·h or 10 gpm/ft^2) are shown in Figure 7.7. (F1Y was not included because irrigated data were not obtained with this packing.) The capacity difference between the packings is evident, with M500Y exhibiting a much earlier flooding onset ($F_G \sim 1.5$-1.7 Pa$^{0.5}$) compared to M125Y ($F_G \sim 3.5$ Pa$^{0.5}$). Two slightly separate flooding curves can be seen for M500Y, which is reflective of the fact that precise measurements around this point are difficult to obtain – at least, relative to pre-loading conditions. The deviation could have also been caused by contamination in the system resulting in a small degree of foaming and consequently causing the apparent packing capacity to be reduced. The pre-loading ratios for the packings are similar to those under dry conditions (M125Y ~ 0.6, M250Y ~ 1.3, M500Y ~ 3.4), but the

205

alignment is not as exact. The M250Y pressure drop is slightly higher than would be expected in comparison with M125Y, and the M500Y pressure drop deviates even more with respect to M250Y. This result makes sense, since the vapor flow through a packing like M500Y would be expected to be more strongly affected at a given liquid load than a packing like M125Y based on the available void space (0.92 for M500Y, 0.99 for M125Y).
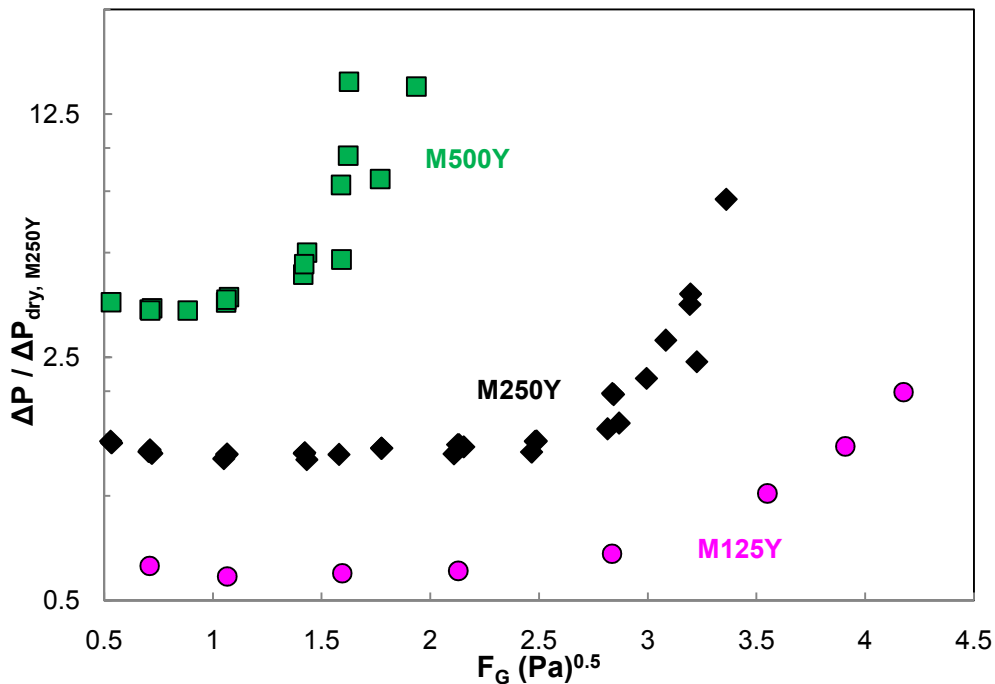

Figure 7.7. Normalized pressure drop of M125Y, M250Y, and M500Y at a liquid load of 24.4 $m^3/m^2 \cdot h$ (10 gpm/ft^2).

The corresponding hold-up measurements for the three packings are plotted in Figure 7.8. Whereas the pre-loading pressure drop ratios were found to increase with specific area, the hold-up ratios appear to decrease (M125Y ~ 0.6, M250Y ~ 1.1, M500Y ~ 1.75). This trend is examined in more detail in Figure 7.9, where the hold-up can be seen to

converge. This convergence would imply that there is an increasing dependence of hold-up on liquid load from M125Y to M500Y that could again be related to void space. In other words, M125Y, being the most "open" packing, could have the greatest capacity for liquid retention. Nevertheless, the filling of the packing with liquid still had less of an impact on the void region for vapor flow than the packing size itself, which is why the pressure drop did not increase with the comparative increase in hold-up.
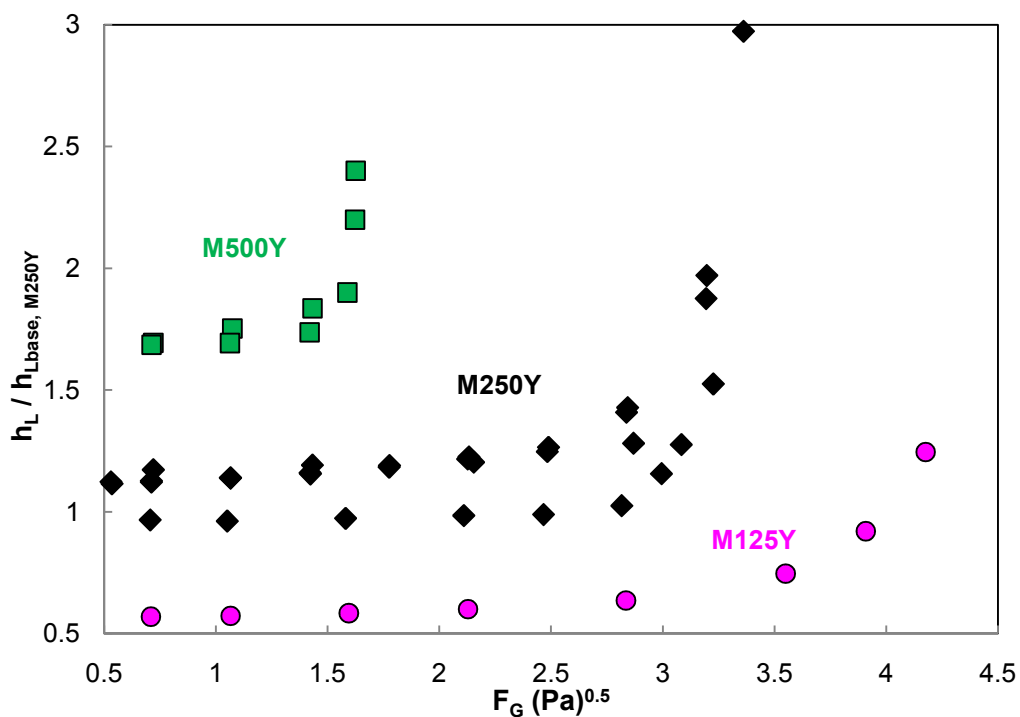

Figure 7.8. Normalized hold-up of M125Y, M250Y, and M500Y at a liquid load of 24.4 $m^3/m^2 \cdot h$ (10 gpm/ft^2).
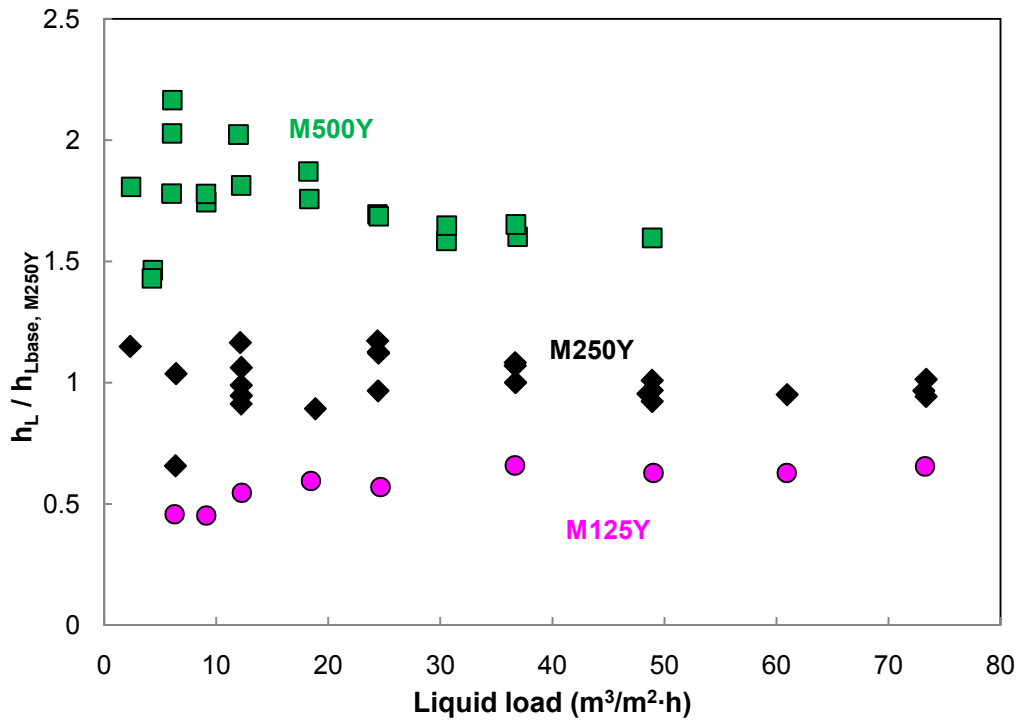
Figure 7.9. Normalized hold-up of M125Y, M250Y, and M500Y at a gas flow factor of 0.7 Pa$^{0.5}$.

7.3 EFFECT OF CHANNEL GEOMETRY (M250Y/M250X/MP252Y)

While M250Y, M250X, and MP252Y were found to exhibit nearly identical mass transfer areas, their pressure drop behavior was quite contrasting. Figure 7.10 shows the dry pressure drop of M250X and MP252Y to be 40% and 70% of that of M250Y. This approximate ratio is maintained even under irrigated (pre-loading) conditions (Figure 7.11), where the capacity of both M250X and MP252Y can be seen to be about 20% greater as well.
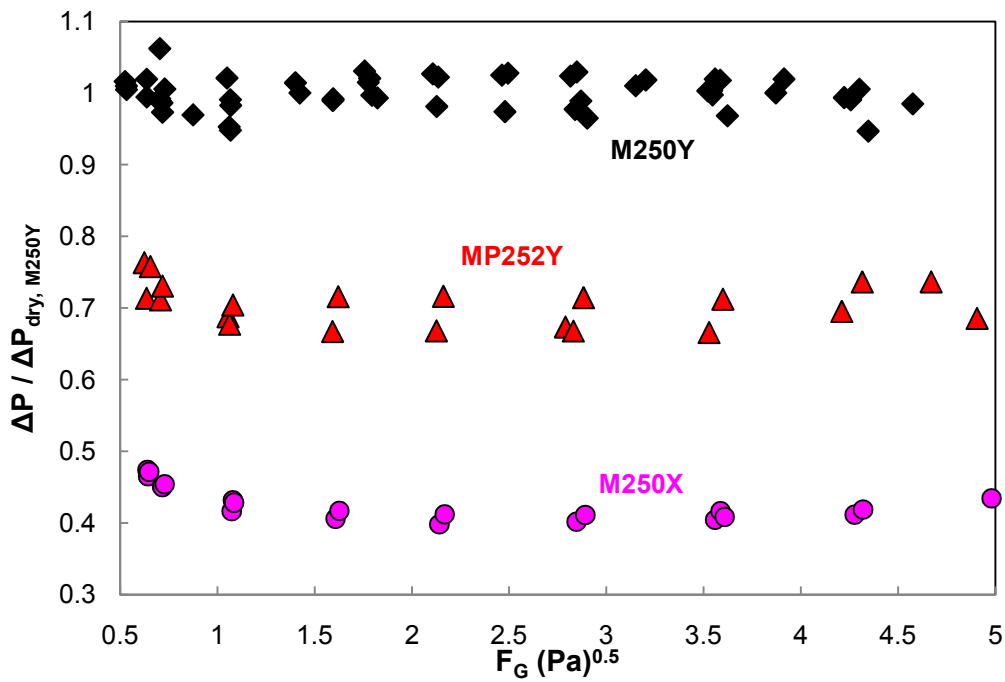
**Figure 7.10. Normalized dry pressure drop of M250Y, M250X, and MP252Y.**
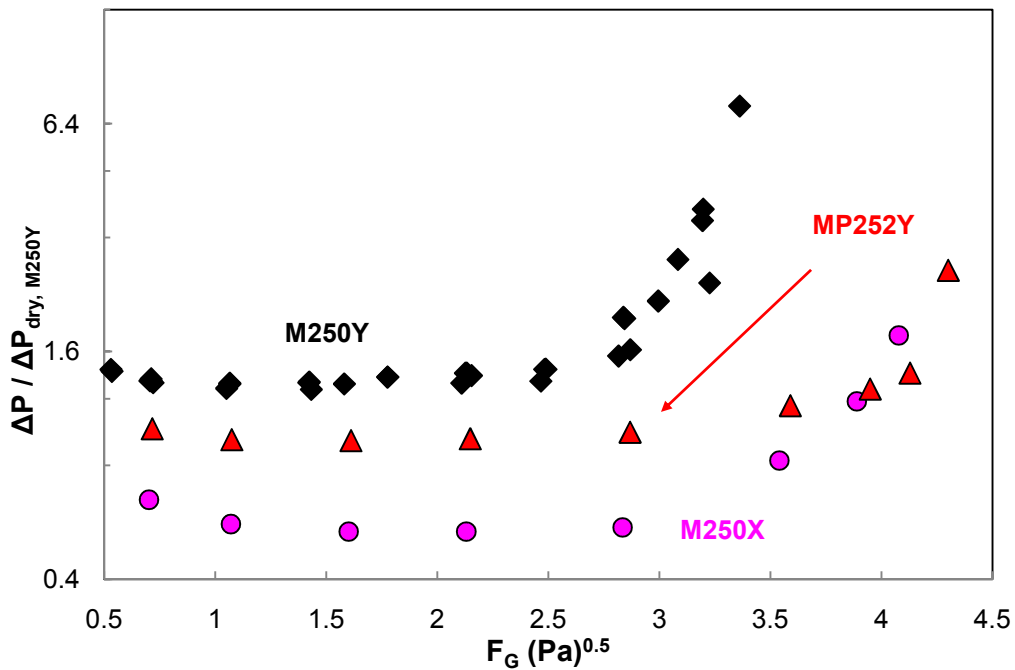
Figure 7.11. Normalized pressure drop of M250Y, M250X, and MP252Y at a liquid load of 24.4 m³/m²·h (10 gpm/ft²).

The notion that pressure drop, hold-up, and effective area should be intertwined in some manner is certainly logical and is the foundation of literature models like Rocha et al. (1993, 1996) and Brunazzi et al. (1995) but thus far, the theory has been applied with limited success. The experimental data have shown the mass transfer area to not be definitively impacted by gas velocity and therefore have not been supportive of any ties to pressure drop. Attempting to correlate the effective area with hold-up may be futile as well, given that viscosity was concluded to have no appreciable effect on the former but as will be demonstrated later, clearly affects the latter. A relation between pressure drop and hold-up has, nevertheless, been discernible – at least, with respect to the results involving different packing sizes. A comparison of the M250Y/M250X/MP252Y pressure drop data and hold-up data (Figure 7.12), though, reveals that there may not be a straightforward connection here either. The measured hold-ups for M250X and MP252Y appear to be lower than the M250Y hold-up at low liquid loads (less than 20 $m^3/m^2 \cdot h$). The data overlap at the higher loads, despite there being as much as a factor of two separation in the packing pressure drop (M250Y vs. M250X). The hold-up behavior could be a consequence of M250X and MP252Y being more amenable to the drainage of liquid – due to the flow channels being steeper, for example – but losing this advantage under the burden of high throughputs. Alternatively, the apparent deviation from M250Y at low liquid loads could merely be a function of the weaker statistical accuracy of the measurements at these conditions. Suess and Spiegel (1992) would agree with the latter theory, since their results with M250Y and M250X showed the corrugation angle to have a negligible influence on the hold-up.
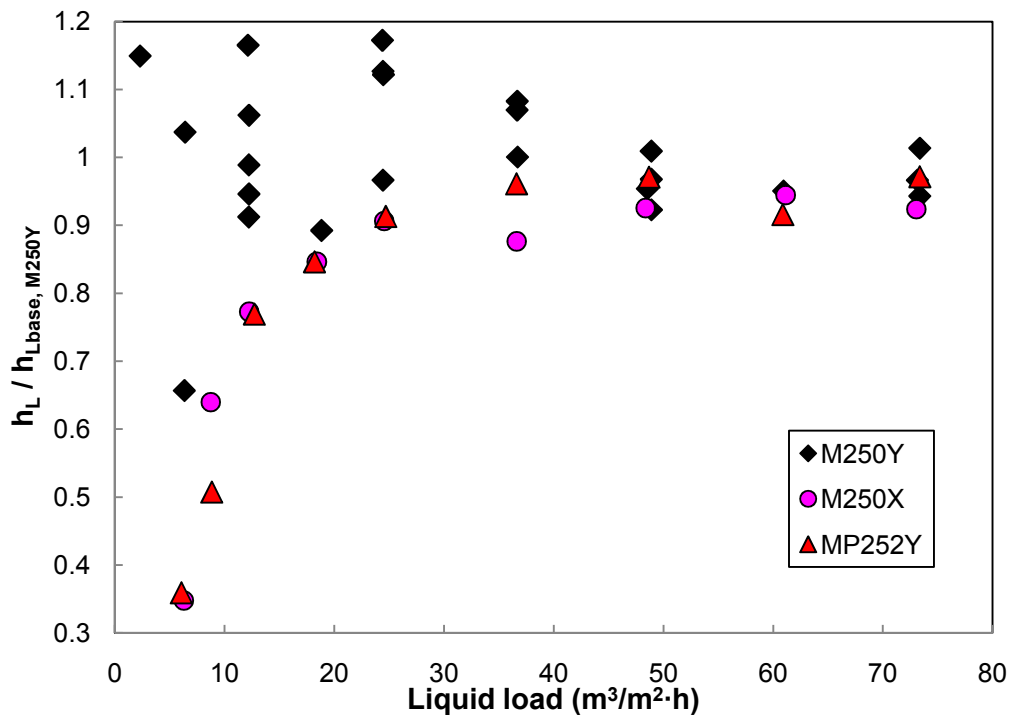
Figure 7.12. Normalized hold-up of M250Y, M250X, and MP252Y at a gas flow factor of 0.7 Pa[0.5].

The fact that M250Y, M250X, and MP252Y exhibited radically dissimilar pressure drops and yet had similar hold-up values might be considered counterintuitive. Pressure drop is a reflection of drag, which must necessarily be attributed to the liquid (opposition to the gas), and thus, the inclination might be to equate liquid volume fraction to pressure drop. Other contributing mechanisms aside from drag exist, though, such as kinetic losses associated with the directional changes in the gas flow. These losses would seem to be far more dominant than any liquid-related drag – at least, for the experimental conditions in the present work. In short, the channel configuration would appear to have a far greater impact on the vapor flow path (i.e., hydraulics) than on the liquid (i.e., wetted area or hold-up).

211

As a final topic of discussion, it obviously would not make sense to select M250Y over M250X or MP252Y on the criterion of effective area alone, on account of its significantly poorer hydraulic aspects. The M250X/MP252Y tradeoff is not as straightforward. Upon closer inspection of Figure 7.11, one can see that while the pressure drop for MP252Y is higher, it also seems to be slightly less sensitive in the loading region or in other words, more resistant to flooding. (This characteristic was apparent at other liquid loads as well.) Based on these findings, geometric designs not currently commercially available but seemingly worth pursuing might include a packing with channels steeper than 60° or possibly a hybrid 60°/smoothed joint packing ("MellapakPlus 252X"). Trade-offs associated with the gas-film mass transfer coefficient and axial mixing will, of course, need to be considered at some point. Furthermore, it is not clear when or if a drop-off in mass transfer area might begin to occur. The global area model (equation 6.10) would predict never, but it is hard to envision that performance would be good at the limit of a 90° inclination or basically a vertical channel, either on account of wettability issues or problems with gas and liquid distribution. The possibility that a single optimum angle might exist or that the optimum configuration might, in fact, be application-dependent is not unreasonable.

7.4 EFFECT OF TEXTURE (M250Y/M250YS)

The dry pressure drop of M250Y and that of its untextured counterpart (M250YS) are compared in Figure 7.13. The M250YS pressure drop is 15 to 20% lower. Frictional losses due to the embossing could perhaps account for this discrepancy. If these effects

were indeed significant, however, then the pressure drop would be anticipated to converge at higher liquid loads, since the increasing liquid film thicknesses (0.1 to 0.7 mm as predicted from equation 3.3) would potentially mask the surface microstructures (also estimated to be on the order of 0.1 mm). The pressure drop at 48.8 $m^3/m^2 \cdot h$ (20 gpm/ft^2) is shown in Figure 7.14. The same ratio as under dry conditions is evident, indicating that friction is not the sole explanation. Recall that in the discussion of the mass transfer results, two possible conclusions were offered regarding the embossing: it either provided a small turbulence-related (10%) benefit, or it had no effect aside from merely increasing the packing surface area by about 10%. Both pressure drop and hold-up were demonstrated earlier to scale fairly directly with packing size (Figures 7.7 and 7.8). The lower pressure drop and hold-up (Figure 7.15) exhibited by M250YS, coupled with the apparent invalidation of the "friction theory," would support the latter conclusion and imply that it has a 15 to 20% lower specific area than M250Y. Since the measured difference in mass transfer area between the two packings was only about 10%, this in turn would indicate the smooth packing to actually be more efficient than the standard textured version, which does not make much sense. Both size (10-15%) and some other phenomena (5-10%) – either friction or some other factor – could be contributing to the overall hydraulic discrepancy.
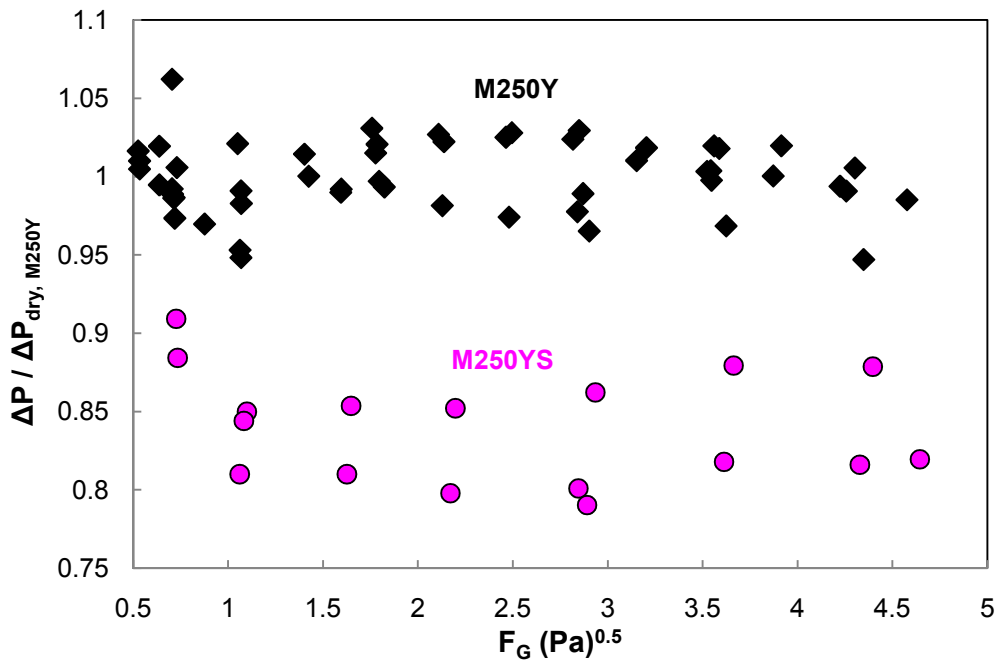
**Figure 7.13. Normalized dry pressure drop of M250Y and M250YS.**

Figure 7.14. Normalized pressure drop of M250Y and M250YS at a liquid load of 48.8 $m^3/m^2 \cdot h$ (20 gpm/ft^2).

214
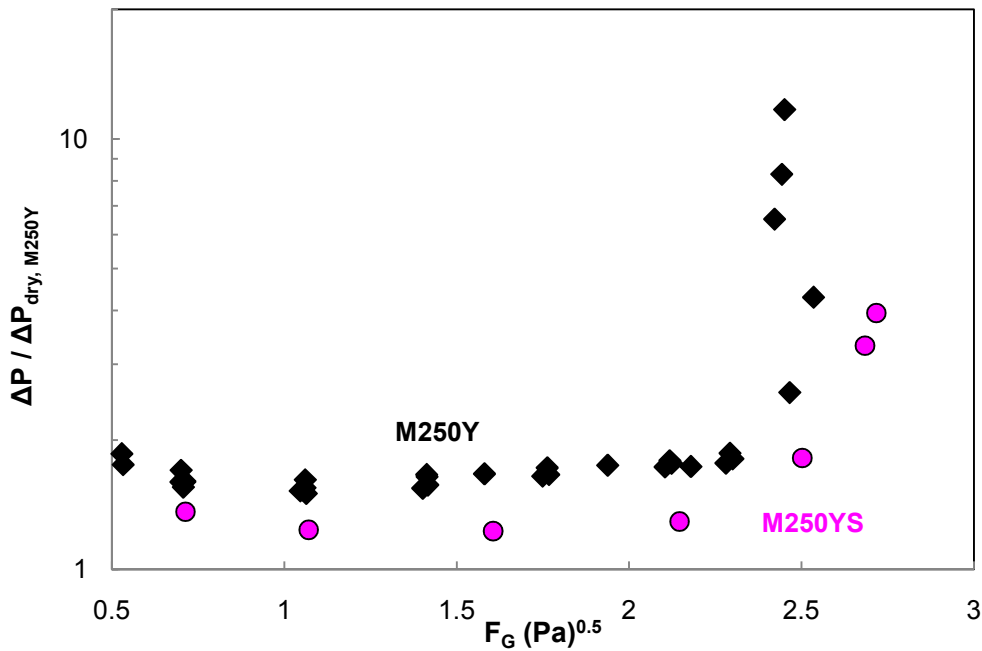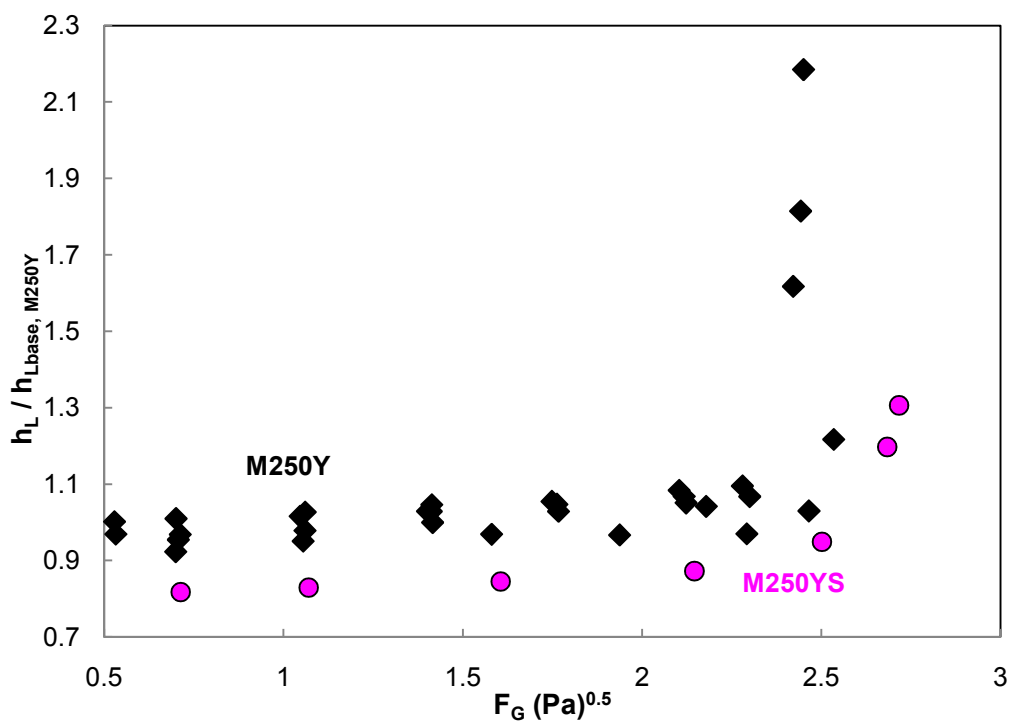
Figure 7.15. Normalized hold-up of M250Y and M250YS at a liquid load of 48.8 $m^3/m^2 \cdot h$ (20 gpm/ft^2).

7.5 EFFECT OF SURFACE TENSION (M250Y/M500Y)

The mass transfer data showed that the tested packings could be separated into two categories (500-series vs. all others) on the basis of surface tension. In an effort to better understand these results, the influence of surface tension on the hydraulic performance of two representative packings (M250Y and M500Y) was studied. The data for M250Y are displayed in Figure 7.16.
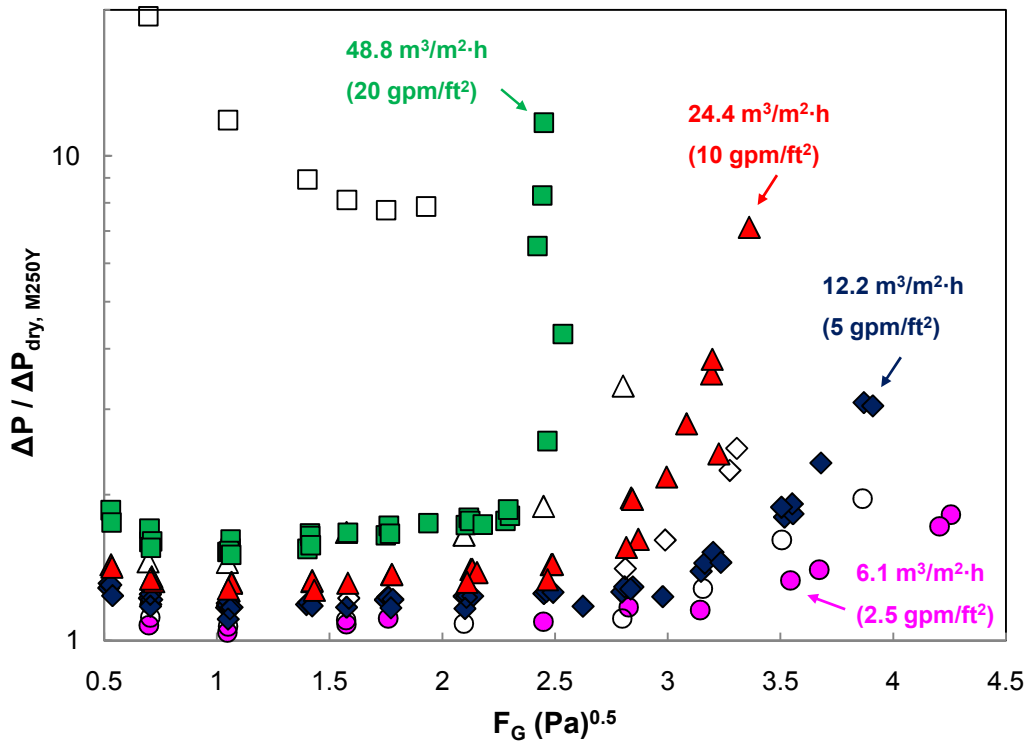
Figure 7.16. Normalized pressure drop of M250Y at baseline (72 mN/m, solid points) and low surface tension (30 mN/m, open points).

At the low liquid loads (6.1 and 12.2 m³/m²·h or 2.5 and 5 gpm/ft²), the baseline and low surface tension data do not appreciably differ in the pre-loading region. A more consistent deviation (10%) is noticeable at 24.4 m³/m²·h (10 gpm/ft²), with the low surface tension points exhibiting a slightly higher pressure drop. The results at 48.8 m³/m²·h (20 gpm/ft²) represent a unique shift in behavior related to foaming. The pressure drop at the lowest gas flow factor is much higher than would be expected, but the subsequent increase in flow rate has a far weaker impact on pressure drop than normal (i.e., significantly smaller exponent than 1.8 or 1.9), up until the flood point. This trend was always exhibited whenever foaming was prominent. In these situations, additional antifoam would often be mixed in to the system in an attempt to obtain

216

apparent non-foaming results or basically, data in adherence with "standard" trends (see Section 7.1), but this solution was not always effective, particularly at the more vigorous liquid loads like the 48.8 $m^3/m^2 \cdot h$ (20 gpm/ft^2) scenario displayed in Figure 7.16. Just as was the case for the mass transfer tests, the operational range for the surfactant system was more limited than the baseline range. While foam was seemingly only a factor at the highest liquid loads, one could certainly be concerned about it having an unnoticed impact at lower loads. The lack of any tell-tale signs was believed to be proof enough that no foaming was occurring in these well-behaved situations.

The M500Y results are plotted in Figure 7.17. The two systems appear to overlap closely in the pre-loading region (within 5%), akin to the M250Y data at 6.1 and 12.2 $m^3/m^2 \cdot h$ (2.5 and 5 gpm/ft^2).
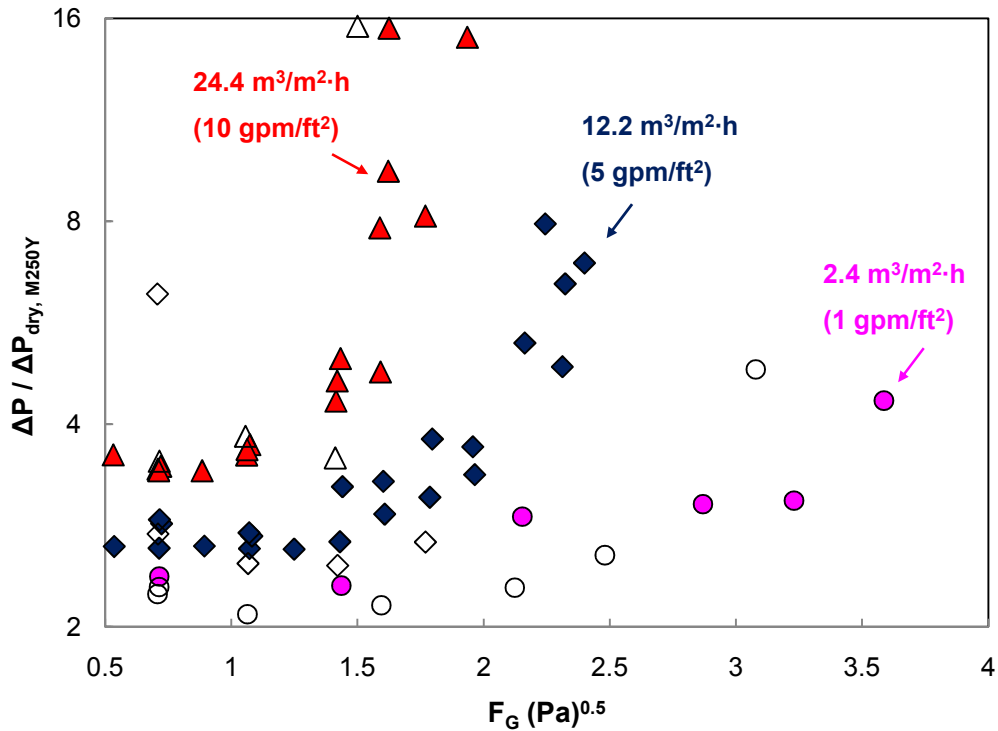
Figure 7.17. Normalized pressure drop of M500Y at baseline (72 mN/m, solid points) and low surface tension (30 mN/m, open points).

The majority of data sets – particularly those at low liquid loads, which were believed to be a bit more credible on account of there being a lower probability of foam – were consistent in showing no effect of surface tension. Thus, from a generalized perspective, the impact of surface tension on pressure drop would appear to be negligible or very minor, especially relative to the effect of irrigation. The pressure drop at 12.2 $m^3/m^2 \cdot h$ (5 gpm/ft^2) for M250Y, for instance, is 20 to 25% greater than the dry pressure drop, whereas the difference between the solid and open points at this condition is only about 5% at most. Pressure drop aside, a perhaps more relevant feature to consider is the influence of surface tension on capacity. The low surface tension data are more prone to flooding under every circumstance. This decreased capacity could be attributable to

218

foaming rather than an actual effect of surface tension, but hold-up was generally observed to spike in tandem with the pressure drop in these situations, which would support the notion that flooding was truly occurring. (A pressure drop surge induced by foam would not necessarily be accompanied by an increase in hold-up.)

Recall that in the discussion of the mass transfer area data, capillary phenomena were theorized to be responsible for the unique interaction of surface tension with the high surface area packings. The pressure drop results were not too useful in confirming or refuting this hypothesis, but the hold-up measurements were anticipated to provide better clarity. A reduction in surface tension was speculated to decrease hold-up appreciably for M500Y, due to the alleviation of bridged and pooled liquid. The hold-up data for M250Y and M500Y at liquid loads of 6.1, 12.2, and 24.4 $m^3/m^2 \cdot h$ (2.5, 5, and 10 gpm/ft^2) are displayed in Figures 7.18 through 7.20.
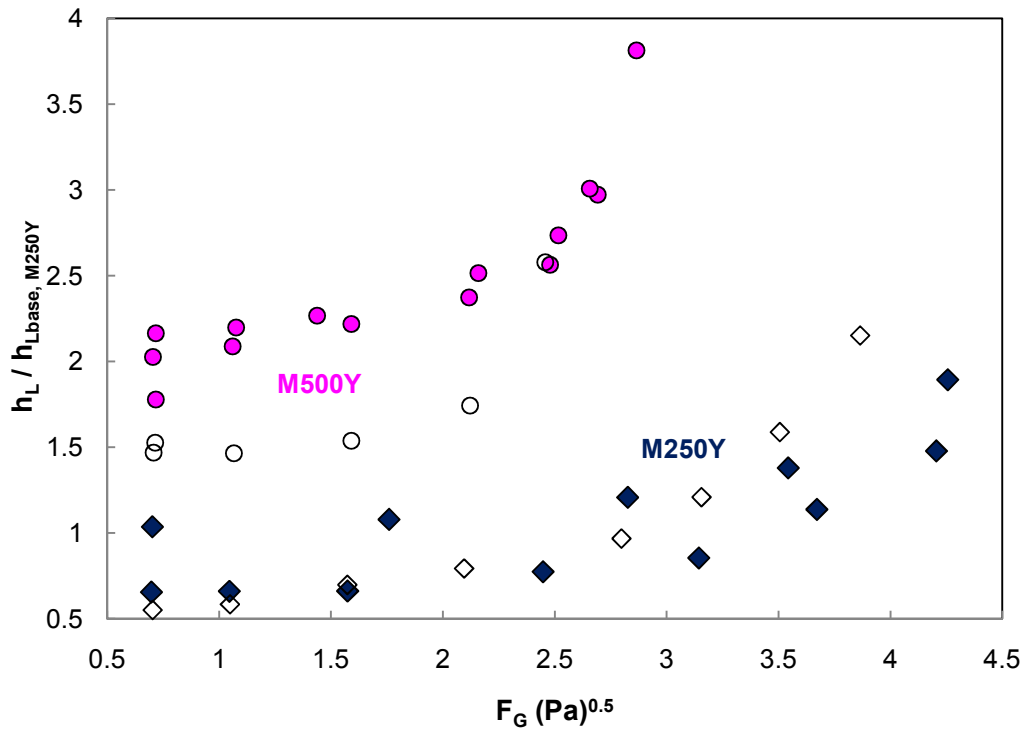
Figure 7.18. Normalized hold-up of M250Y and M500Y at a liquid load of 6.1 m³/m²·h (2.5 gpm/ft²) at baseline (72 mN/m, solid points) and low surface tension (30 mN/m, open points).
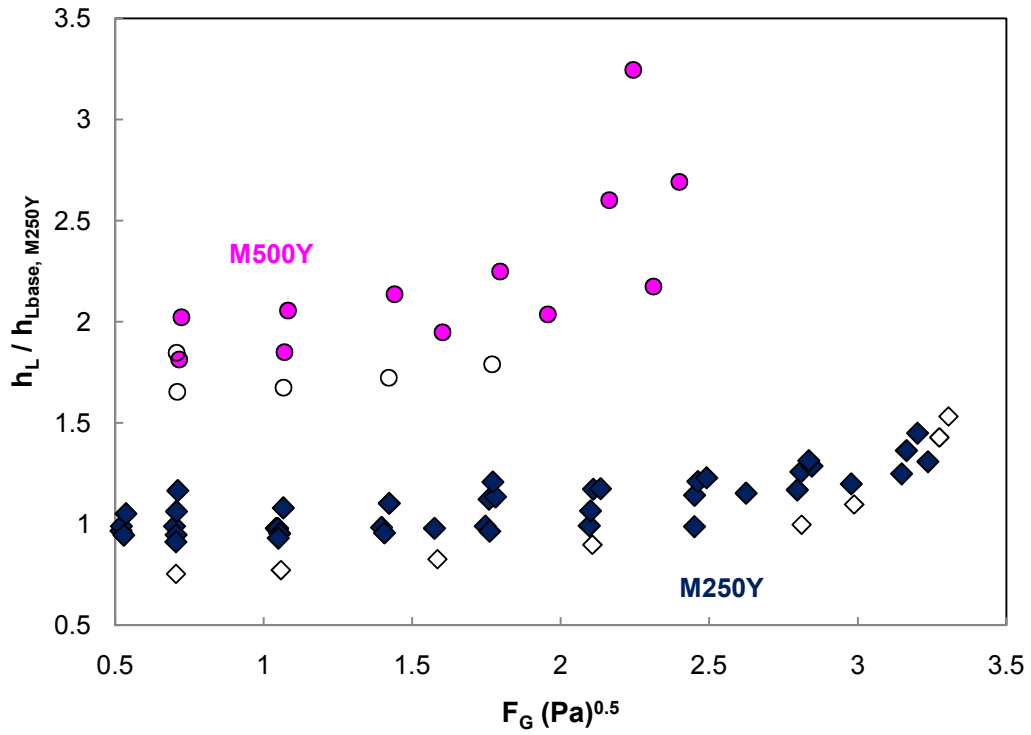
Figure 7.19. Normalized hold-up of M250Y and M500Y at a liquid load of 12.2 m³/m²·h (5 gpm/ft²) at baseline (72 mN/m, solid points) and low surface tension (30 mN/m, open points).
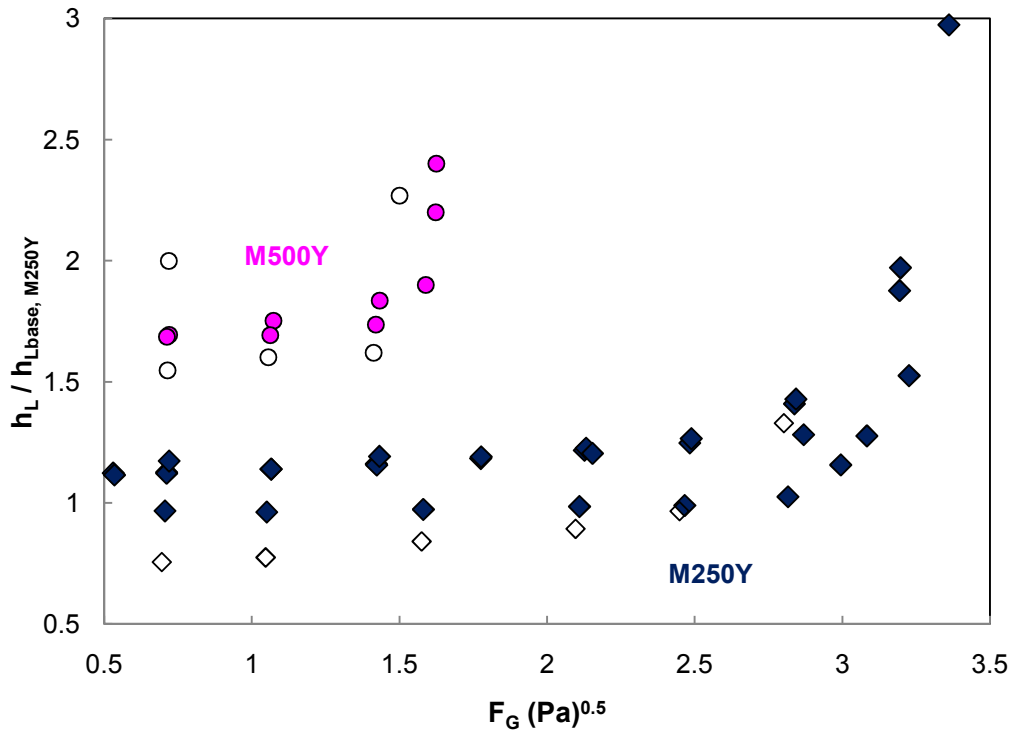
Figure 7.20. Normalized hold-up of M250Y and M500Y at a liquid load of 24.4 m³/m²·h (10 gpm/ft²) at baseline (72 mN/m, solid points) and low surface tension (30 mN/m, open points).

Unfortunately, not much information can be deciphered from these results either. For M500Y, the hold-up at low surface tension is lower (15-30%) than for the baseline at 6.1 and 12.2 m³/m²·h (2.5 and 5 gpm/ft²), but the same is true (20-30%) for M250Y at 12.2 and 24.4 m³/m²·h (5 and 10 gpm/ft²). Hold-up does seem to decrease with a reduction in surface tension, but in this case, M250Y actually exhibited a greater decrease on average than M500Y. This result does not necessarily disprove the capillary hypothesis, but it does indicate that the interaction of surface tension with packing mass transfer area cannot be rationalized in terms of just hold-up.

7.6 EFFECT OF LIQUID VISCOSITY (M250Y/M500Y/M250X/MP252Y)

The standard M250Y and M500Y packings were studied under baseline, intermediate viscosity (approximately 5 mPa·s), and high viscosity (approximately 10 mPa·s) conditions. Tests at high viscosity were in addition conducted with M250X and MP252Y to investigate the interaction of this parameter with geometric configuration. The baseline and high viscosity hydraulic data for these four packings at 12.2 m^3/m^2·h (5 gpm/ft^2) are respectively shown in Figure 7.21 (pressure drop) and Figure 7.22 (hold-up).
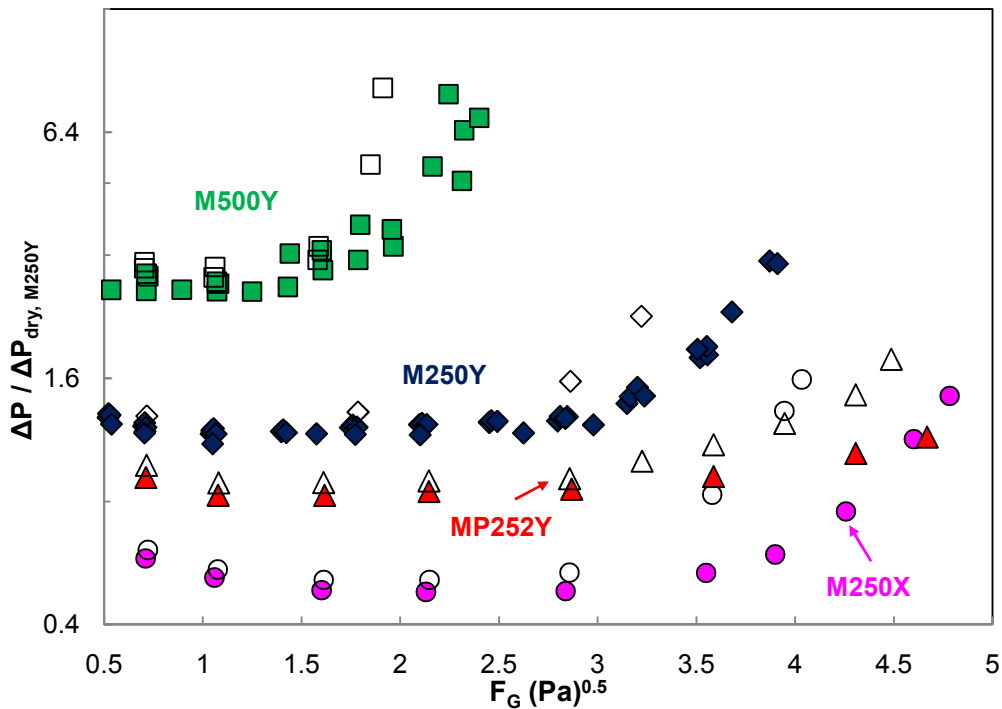

Figure 7.21. Normalized pressure drop of M250Y, M500Y, M250X, and MP252Y at a liquid load of 12.2 m^3/m^2·h (5 gpm/ft^2) at baseline (solid points) and high viscosity (open points). (See Table 7.1 for detailed physical conditions.)
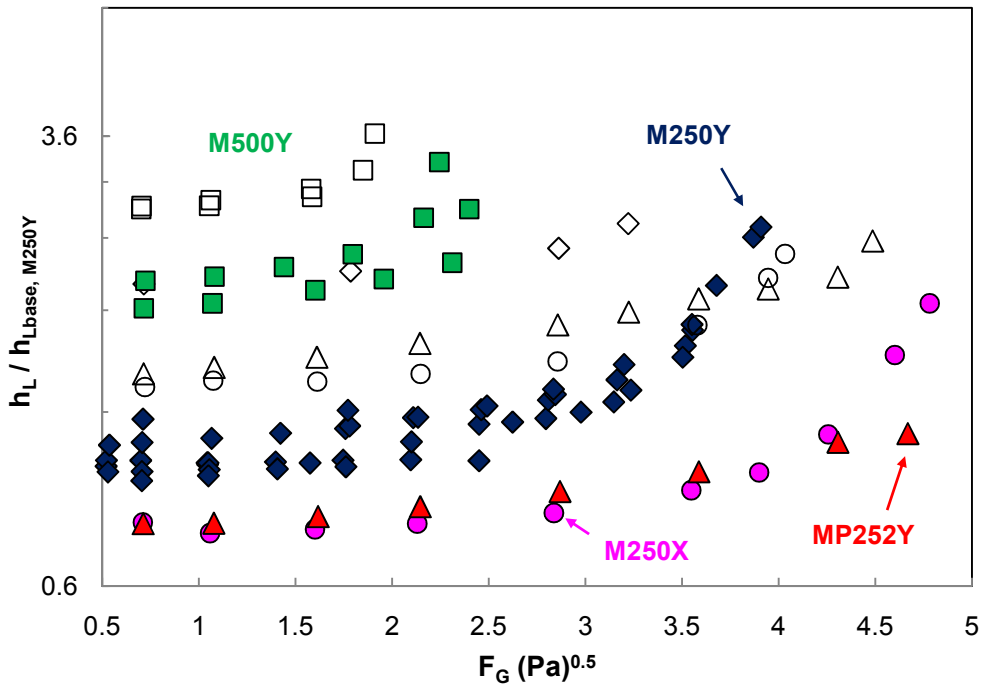
Figure 7.22. Normalized hold-up of M250Y, M500Y, M250X, and MP252Y at a liquid load of 12.2 m³/m²·h (5 gpm/ft²) at baseline (solid points) and high viscosity (open points). (See Table 7.1 for detailed physical conditions.)

The potential confounding of these results due to surface tension must be acknowledged, but given that its isolated impact seemed be either negligible (pressure drop) or minor relative to the viscosity-associated effect (hold-up), it was believed to be acceptable to evaluate the viscous system results at face value. A small (5 to 10%) but consistent impact of viscosity on the pre-loading pressure drop is evident. A decrease in capacity of around 20% on average is also noticeable. A large spike in hold-up can be seen to result from the elevation in viscosity – about a factor of two increase for the three 250-series packings. Interestingly, M500Y does not experience quite the same enhancement (only 30 to 50%), which, as has been repeatedly suggested, could be a consequence of there simply being less open space to fill. Various sources (McGlamery, 1988; Nicolaiewsky

224

et al., 1999) established that an enhancement in viscosity can be anticipated to result in thicker liquid films. An elevated pressure drop would therefore logically be associated with higher viscosity, based on the liquid occupying more of the available void space. The fact that only a 5 to 10% effect is apparent even with a ten-fold viscosity increase is striking and suggests that the liquid film comprises such a small portion of the packing flow channels that its thickness is basically irrelevant to the countercurrent gas stream – up until the loading region, at any rate. Here, the gas would be expected to become extremely sensitive to interference from the liquid, which is why it makes sense that packing capacity might suffer at a high viscosity. Alternatively, the observed capacity decrease could have been an artifact of foam, as was possibly suspected with the surfactant system.

7.7 EVALUATION OF HYDRAULIC MODELS

The development of a global hydraulic model from the data would be an extremely worthwhile endeavor but was considered to be outside the scope of the current work. At the very least, though, an assessment of several commonly referenced hydraulic models was thought to be useful. In many such correlations, liquid hold-up is implicit in the pressure drop calculation, and so, having an accurate value for this parameter is clearly crucial.

Iterative solutions were notably required for some of the models. The SOLVER function in Microsoft Excel$^{®}$ was implemented to solve these equations. Because the large databank required this process to be repeated for hundreds of cases, a simple macro

was created that on execution, automatically and repeatedly applied SOLVER. The code is included in Appendix E for reference.

7.7.1 Standalone Hold-up Models

7.7.1.1 Suess and Spiegel

The predictive capabilities of the pre-loading hold-up model of Suess and Spiegel (1992) as a function of packing size (Figure 7.23) and liquid viscosity (Figure 7.24) are presented alongside the pre-loading measurements ($F_G \sim 0.7$ Pa$^{0.5}$) obtained in this work. (The model did not include any influence of surface tension or corrugation angle, so comparative plots on these bases were not thought to be worthwhile.)
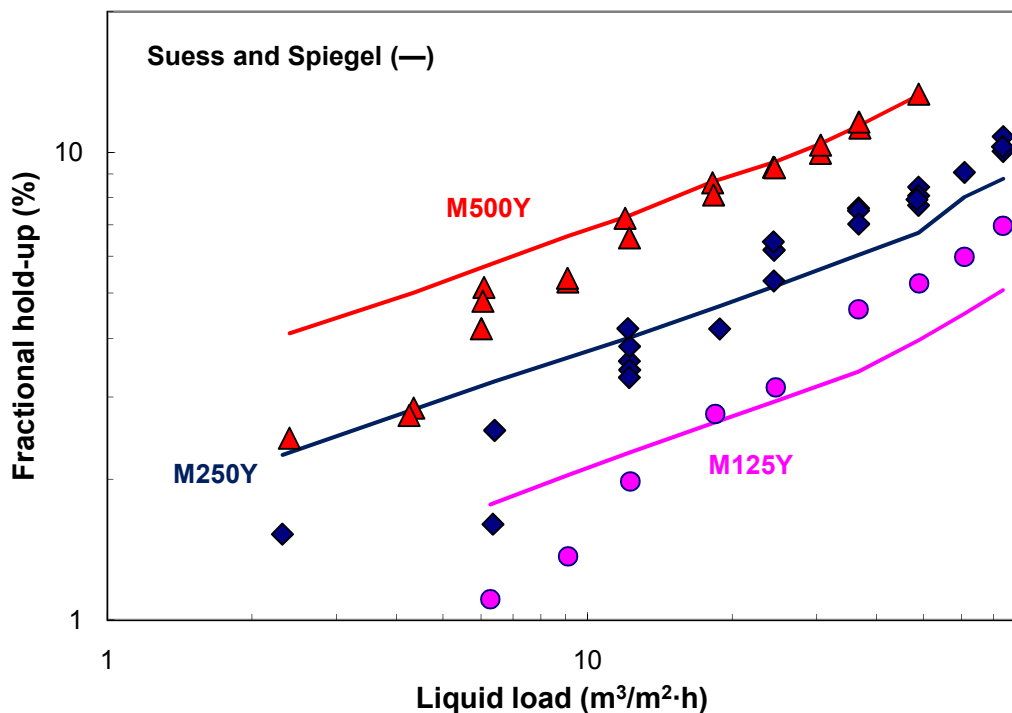

Figure 7.23. Hold-up of M125Y, M250Y, and M500Y at a gas flow factor of 0.7 Pa$^{0.5}$, compared with model of Suess and Spiegel (1992).
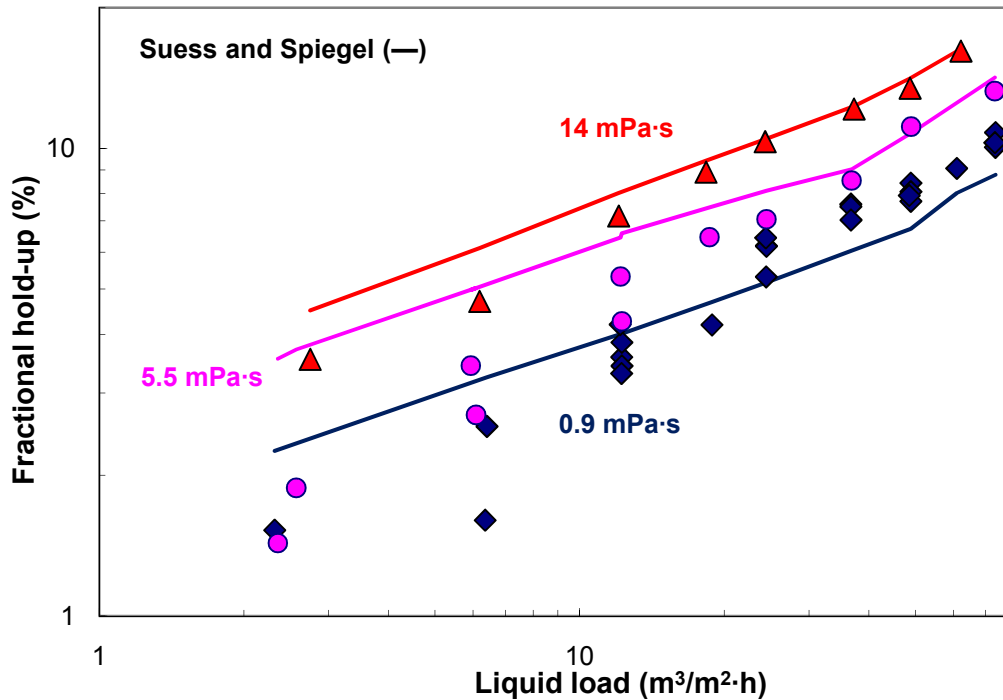
Figure 7.24. Hold-up of M250Y at a gas flow factor of 0.7 Pa$^{0.5}$, compared with model of Suess and Spiegel (1992) at baseline, intermediate viscosity, and high viscosity.

The predictions from Suess and Spiegel (1992) compare favorably with the data, but the model is not without questionable aspects. For example, it is strictly empirical and yet based on a fairly limited databank of packings (M250Y, M250X, and M500Y). As Brunazzi et al. (1995) also observed, the predictions are systematically high at low liquid loads and low at high loads. For these reasons, an attempt was made to develop an improved pre-loading hold-up model. This effort is discussed in the next section.

7.7.1.2 Present Work

As a first pass in the model formulation, the experimental hold-up data were plotted as a function of the Nusselt film thickness, since the two parameters should be

relatable in some respect. This approach was unsuccessful in collapsing the entire database. Next, a dimensionless approach was taken, akin to that applied in the development of the global mass transfer area correlation. Various dimensionless group combinations were examined but to no avail. Shetty and Cerro (1997) proposed an expression (equation 7.5) with a dependence on the Reynolds number and Galileo number (ratio of gravitational to viscous forces), but this was not found to be effective either.

$$h_{\mathrm{L}} = 6.096 N_{\mathrm{Re}}^{1/3} N_{\mathrm{Ga}}^{-1/3} \tag{7.5}$$

$$N_{\mathrm{Re}} = \frac{4\rho_{\mathrm{L}} q}{\mu_{\mathrm{L}}} \tag{7.6}$$

$$N_{\mathrm{Ga}} = \frac{\rho_{\mathrm{L}}^2 g p^3}{\mu_{\mathrm{L}}^2} \tag{7.7}$$

The incorporation of an additional geometric parameter was earlier demonstrated to offer an improved fit of the global effective area model (equation 6.10). A similar strategy was applied here, with the rationalization being that a geometric parameter basis might be better suited to capture phenomena like liquid accumulation within channel recesses. When the characteristic length of the Reynolds number was defined as before (i.e., by the Nusselt film thickness) and the characteristic length in the Galileo number was defined by the packing channel side dimension (S), the hold-up results fell into alignment.

$$Re_{\mathrm{L}} = \frac{\rho_{\mathrm{L}} u_{\mathrm{L}} \delta_{\mathrm{L}}}{\mu_{\mathrm{L}}} \tag{6.3}$$

228

$$Ga_p = \frac{\rho_L^2 g S^3}{\mu_L^2}$$
(7.8)

(This modified Galileo number will henceforth be denoted as Ga_p). A power law regression was subsequently performed to see if a better fit than the 1/3 and -1/3 exponents proposed by Shetty and Cerro could be obtained, with equation 7.9 being the result.

$$h_L = 21.84 \left[(Re_L)(Ga_p)^{-\frac{2}{3}} \right]^{0.718}$$
(7.9)

The $(Re_L)(Ga_p)^{-2/3}$ grouping is shown expanded in equation 7.10.

$$(Re_L)(Ga_p)^{-\frac{2}{3}} = \frac{1}{S^2 g^{\frac{2}{3}}} \left(\frac{\mu_L}{\rho_L} \right)^{\frac{1}{3}} \left(\frac{Q}{L_p} \right)$$
(7.10)

The pre-loading hold-up database is plotted alongside equation 7.9 in Figure 7.25. The significance of the correlation is not entirely clear, given its somewhat arbitrary derivation, but it is able to represent the majority of points within limits of ±25% and has less than half of the mean squared error of Suess and Spiegel (1992). The predicted dependence on viscosity is similar to that of Suess and Spiegel (1/3 x 0.718 = 0.24, compared with 0.25) and also somewhat close to the relation in the Nusselt film equation (1/3). The liquid load dependence is near that of Suess and Spiegel as well (0.718, compared with 0.59 for the high liquid-load regime). These exponents are about twice as large as the one in the Nusselt equation (1/3). The correlated dependence of the mass transfer area on liquid load in equation 6.10 (4/3 x 0.116 = 0.15) is notably weaker than in any of these relations, which indicates that there is both useful (i.e., related to the

wetting of the packing surface) and useless liquid hold-up (i.e., related to increasing film thickness) with respect to mass transfer.

Equation 7.9 is obviously not without flaws. For example, recall in Section 7.1 that the dependence of hold-up on liquid load was found to diminish with increasing load. Even though a constant exponent was used to fit the data, this observed relation would suggest that a more complex form might be required to truly capture the underlying phenomena. In addition, the M250X, MP252Y, and M250YS data are systematically lower than the others, implying that there is a geometric factor (and perhaps also texture-related factor) that is clearly still not being properly accounted for. To illustrate this deviation, the results for the three packings have been highlighted in Figure 7.25.
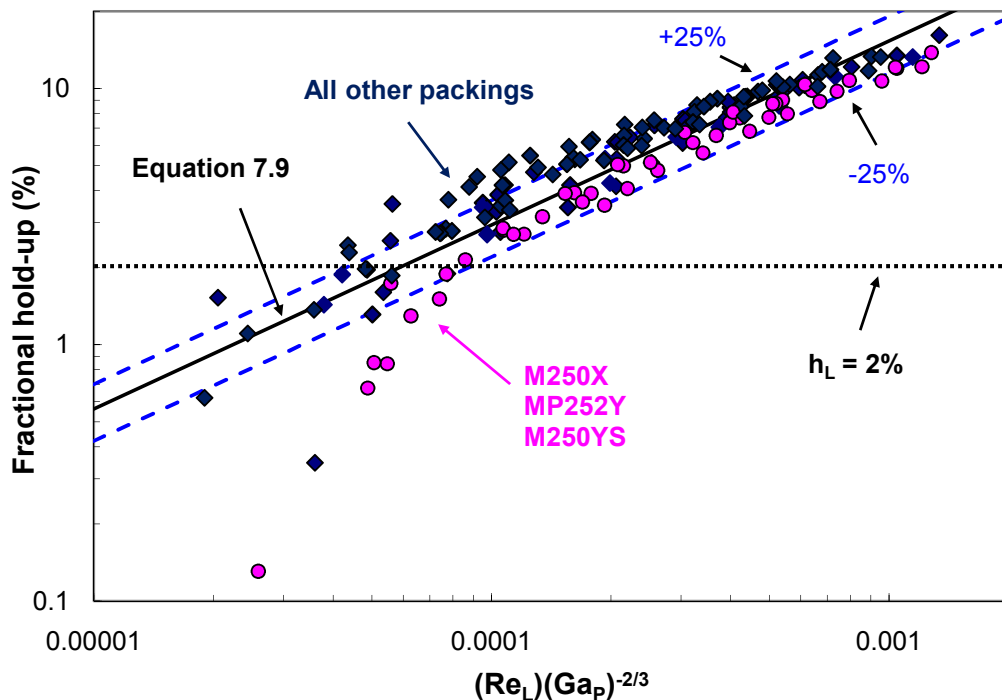

Figure 7.25. Hold-up database compared with global model (equation 7.9).

A very dramatic drop-off in hold-up is exhibited by several of the points at the lowest liquid loads. Considering that these data were difficult to measure on the volumetric basis and that they also lie outside of the practical range of most processes, it was thought justifiable to omit the points with a fractional hold-up of 2% or less. Equation 7.11 is the result of the regression of this reduced database and as can be seen, offers a more believable or representative fit of the results. The reduced database is displayed in Figure 7.26.

$$h_L = 6.94 \left[(Re_L)(Ga_P)^{-2/3} \right]^{0.573} \qquad (7.11)$$
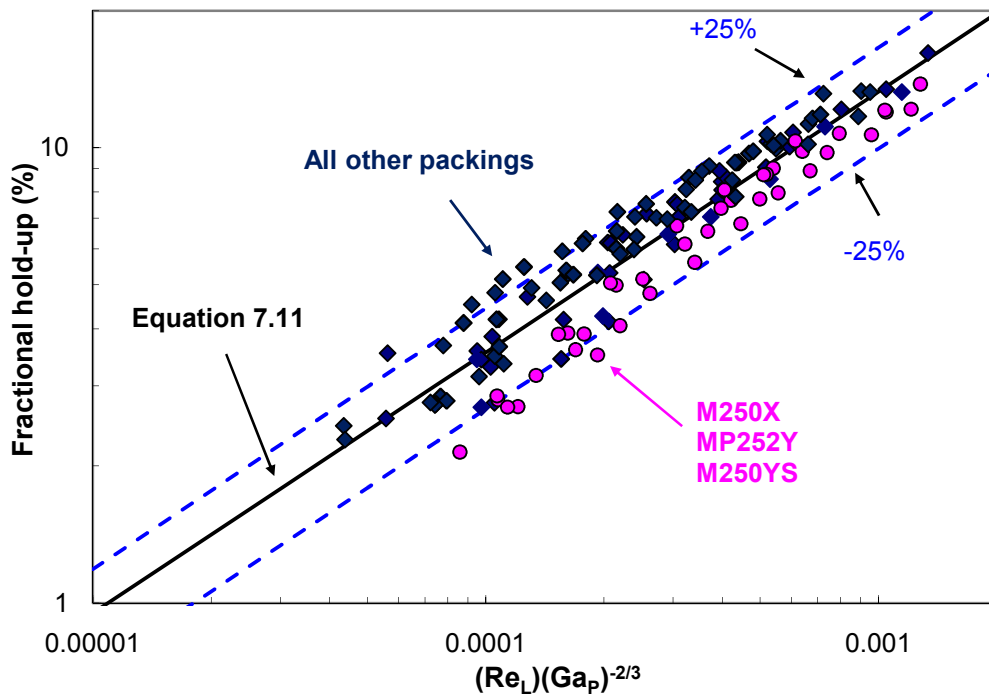
Figure 7.26. Reduced hold-up database compared with global model (equation 7.11).

231

7.7.2 Stichlmair et al.

The predictions for dry pressure drop from the Stichlmair et al. (1989) hydraulic model are plotted with the data for several packings in Figure 7.27. As a point of clarification, both the data and the model curves in the comparisons to be shown subsequently have been normalized by the experimental fit of the dry M250Y data (equation 7.2) – *not* by the predicted values from the models. The packing-specific constants for M250Y were established in Stichlmair et al.: $C_1 = 5$, $C_2 = 3$, and $C_3 = 0.45$. The constants for all of the other packings that were examined had to be regressed from the experimental databank on the basis of a minimum sum-of-squared-errors analysis. These values are summarized in Table 7.2, with the four packings specifically discussed highlighted in the table.

Table 7.2. Packing-specific constants in Stichlmair et al. model (equations 3.26 and 3.29).

Packing	C_1	C_2	C_3
M125Y	75	-19.67	2.06
M250Y	5	3	0.45
M500Y	12.14	-0.3	0.49
M250X	27.92	-3.72	0.39
MP252Y	4.65	0.54	0.4
M250YS	-22.75	5.58	0.28
M2Y	11.6	-2.81	0.93
F1Y	-16.69	5.86	0.24
P500	-7.6	3.81	0.39

The fit of the data as a function of both size and corrugation angle is good, which implies that the underlying particle-in-a-packed-bed theory and corresponding derived equations might be a valid means of interpreting pressure drop. The odd upturn exhibited by the

M125Y curve was likely caused by the limited amount of data at both low and high flow factors.
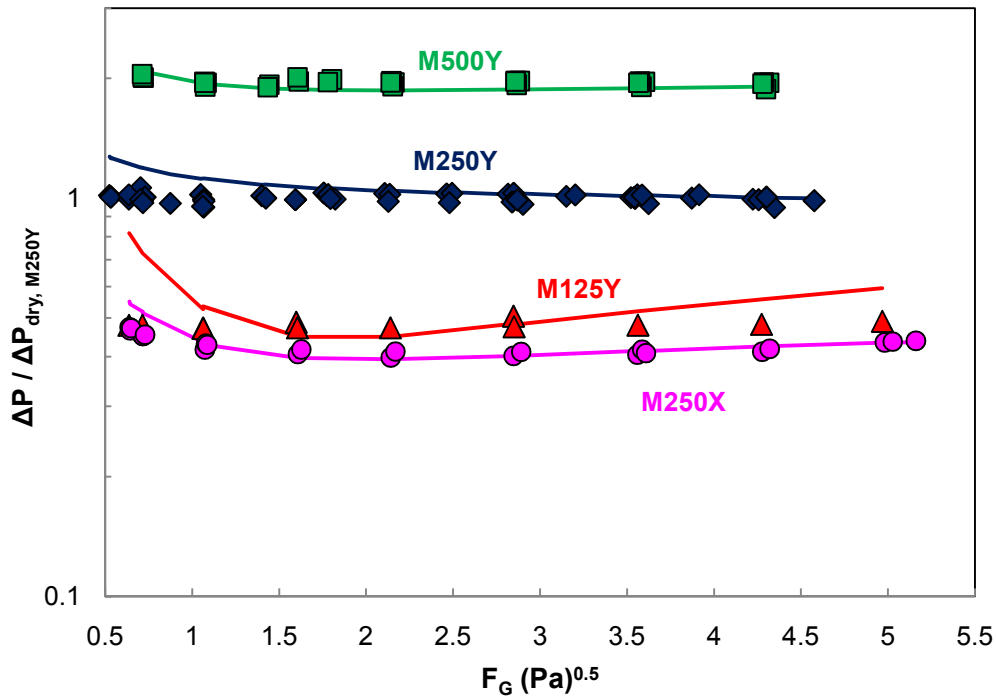
Figure 7.27. Normalized dry pressure drop of M125Y, M250Y, M500Y, and M250X compared with model of Stichlmair et al. (1989).

Figure 7.28 demonstrates how the Stichlmair et al. model measures up against the experimental (air-water) results for M250Y at liquid loads of 12.2, 24.4, and 48.8 $m^3/m^2 \cdot h$ (5, 10, and 20 gpm/ft^2). For the vast majority of F_G values, the pre-loading hold-up calculation (equation 3.30) and post-loading hold-up calculation (equation 3.32) yielded the same value, so for the sake of generality, the latter was used for the entire range of irrigated conditions.

$$h_0 = 0.555 \left(u_L^2 \frac{a_p}{g\varepsilon^{4.65}} \right)^{1/3} \tag{3.30}$$

233

$$h_{\mathrm{L}} = h_0 \left[1 + 20 \left(\frac{\Delta P}{Z \rho_{\mathrm{L}} g} \right)^2 \right] \qquad (3.32)$$
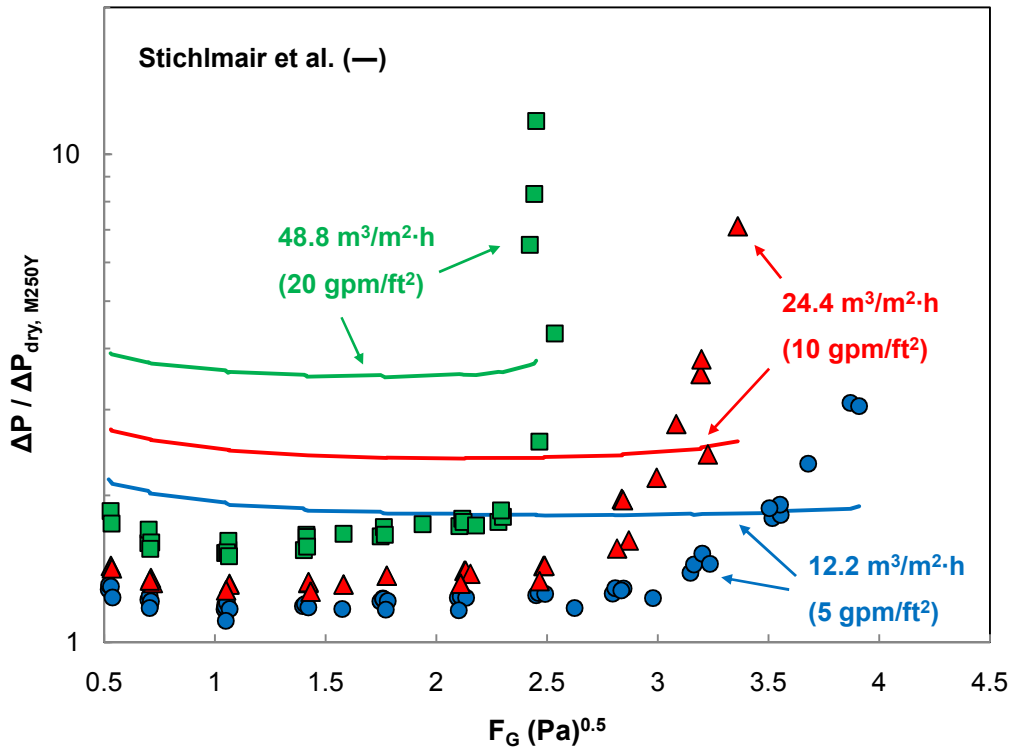
**Figure 7.28. Normalized pressure drop of M250Y at liquid loads of 12.2, 24.4, and 48.8 m³/m²·h (5, 10, and 20 gpm/ft²) compared with model of Stichlmair et al. (1989).**

The curves from two variations of the model are shown in Figure 7.29, where either the actual measured hold-up has been substituted in for equation 3.32 ("Expt. h_{L}") or the calculated value from equation 7.11 has been substituted in for the <u>pre-loading hold-up term</u> (h_0) in equation 3.32 ("Eqn. 7.11"). The original model overpredicts the irrigated points by over a factor of two and also appears to overly weight the effect of liquid load on pressure drop. Furthermore, it fails to match the loading behavior that was observed,

predicting a hold-up increase of only about 10% at these conditions. This latter issue is mitigated with the substitution of the experimental hold-up in place of equation 3.32, which suggests that the relation of the hold-up and pressure drop in the equation might not be quite correct. The predictive accuracy in the pre-loading region – most notably at 48.8 m^3/m^2·h (20 gpm/ft^2) – is also improved with this version of the model. The use of equation 7.11 results in the closest match of the pre-loading results, but again, because of the reliance on equation 3.32, the upturn in the data is missed.
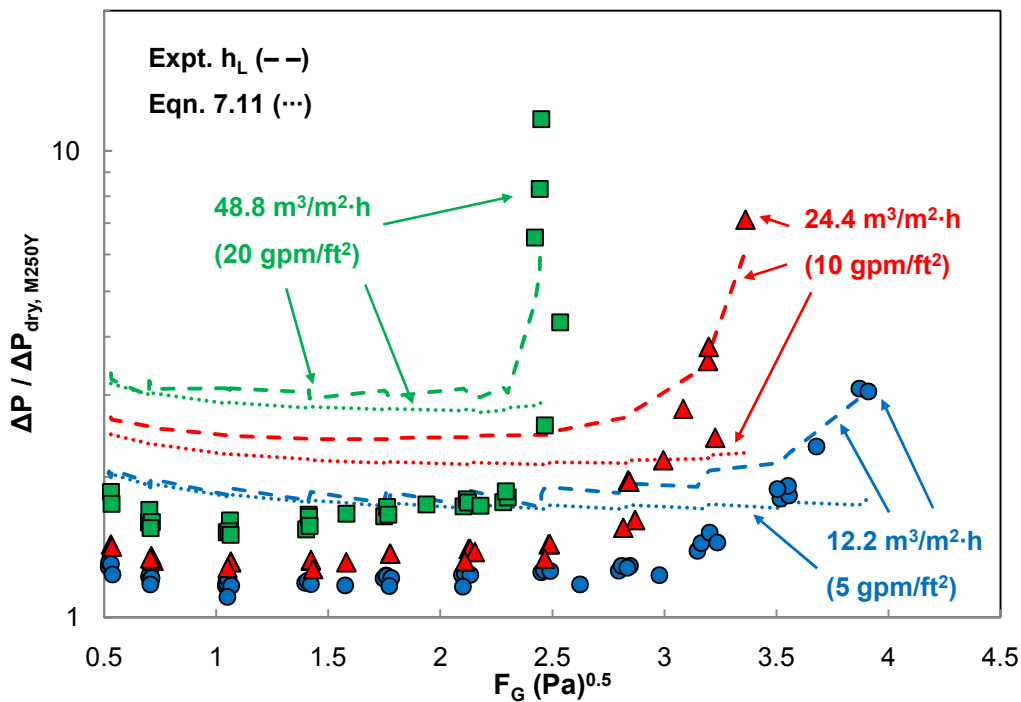
Figure 7.29. Normalized pressure drop of M250Y at liquid loads of 12.2, 24.4, and 48.8 m^3/m^2·h (5, 10, and 20 gpm/ft^2) compared with variations of model of Stichlmair et al. (1989).

As a final comment, the Stichlmair et al. correlation interestingly does not predict there to be any explicit effect of liquid viscosity or surface tension on hydraulic performance.

235

7.7.3 Rocha et al.

The predicted dry pressure drop from the Rocha et al. (1993) model is compared with the results for M125Y, M250Y, M500Y, and M250X in Figure 7.30. Rocha et al. does not contain adjustable constants like Stichlmair et al. and only requires knowledge of the packing channel side (S) and void fraction (ε). Hence, it is not too surprising that the data are not fit as well as in the previous case. The increase in pressure drop with packing size is overexaggerated, and the effect of the corrugation angle is underpredicted.
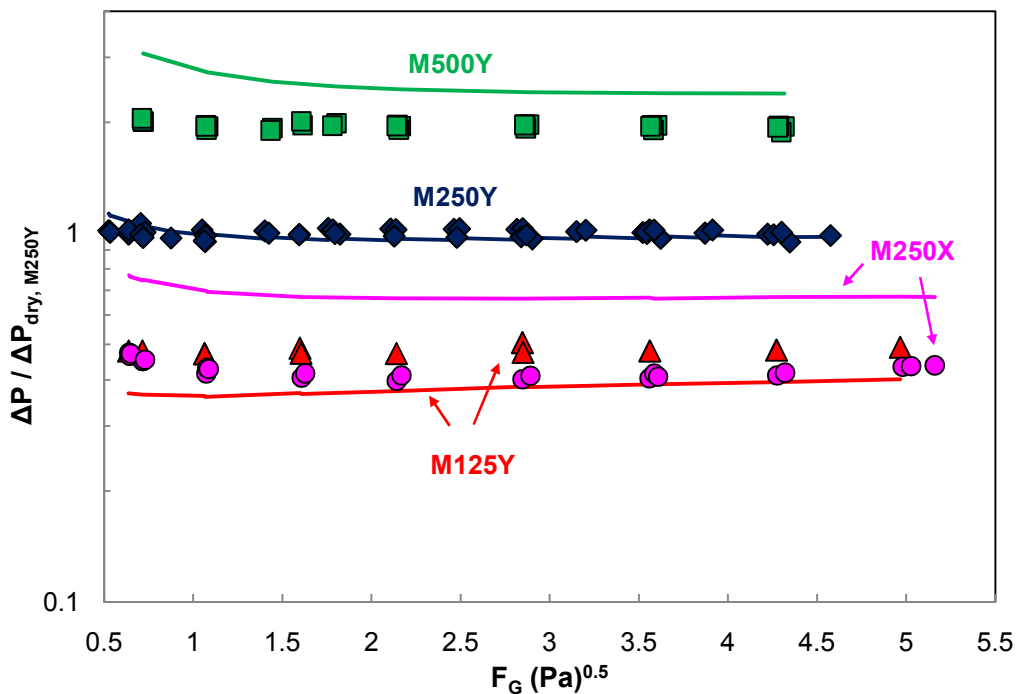
Figure 7.30. Normalized dry pressure drop of M125Y, M250Y, M500Y, and M250X compared with model of Rocha et al. (1993).

The data and model are compared under irrigated conditions in Figure 7.31. The model is successful in its match of the pre-loading points (within about 10%) but misses

the loading onset.   The pre-loading correspondence actually becomes worse when external hold-up values are utilized (Figure 7.32), although the use of the experimental hold-up does enable the pressure drop spike to be tracked.   Thus, the model is at least capable of capturing loading and flooding behavior.   The failure of the Eqn. 7.11 curves in the loading region is to be expected, since the hold-up correlation was intended exclusively for pre-loading conditions.
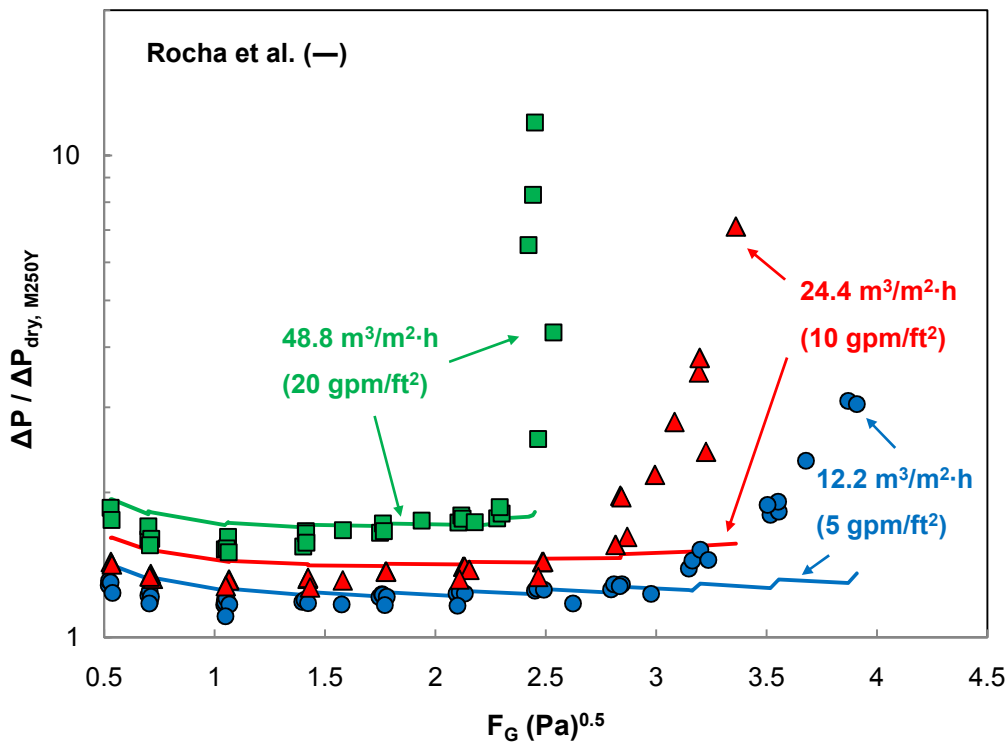

Figure 7.31. Normalized pressure drop of M250Y at liquid loads of 12.2, 24.4, and 48.8 m³/m²·h (5, 10, and 20 gpm/ft²) compared with model of Rocha et al. (1993).
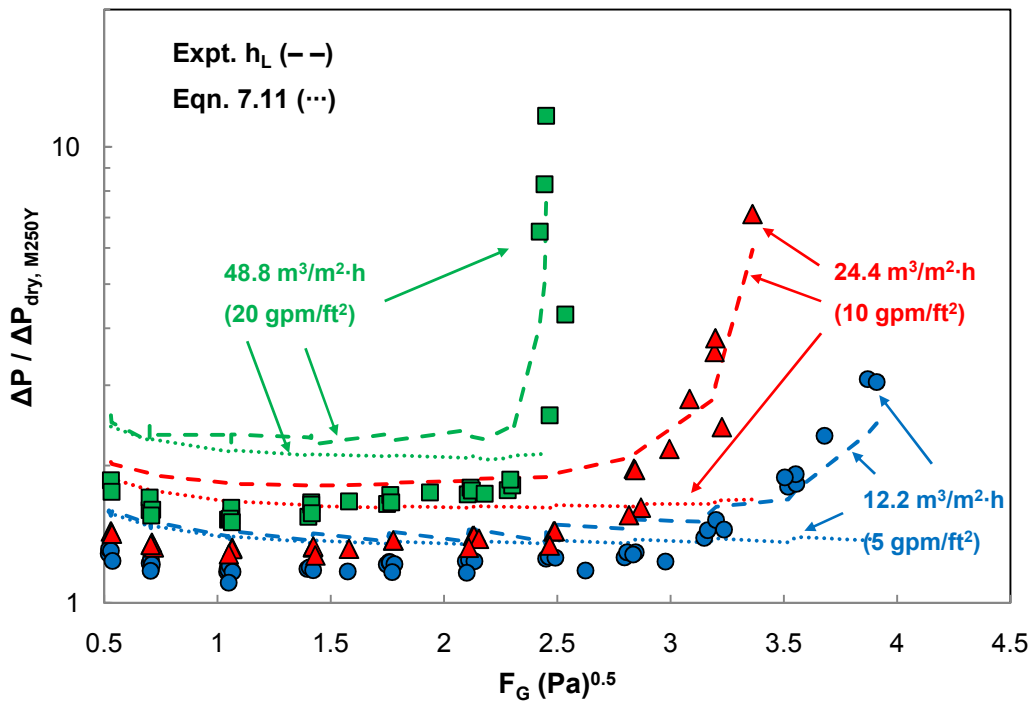
**Figure 7.32. Normalized pressure drop of M250Y at liquid loads of 12.2, 24.4, and 48.8 m³/m²·h (5, 10, and 20 gpm/ft²) compared with variations of model of Rocha et al. (1993).**

Rocha et al. was developed with air-water data but was also validated with results from distillation (i.e., low surface tension) studies. Figure 7.33, however, shows the experimental results and model to disagree over the effect of surface tension. This is due to Rocha et al. predicting there to be an increase in hold-up with a reduction in surface tension – about a factor of three for 30 mN/m versus 72 mN/m. The odd shape of the curves is related to a convergence failure of the model, which seems to be an issue when the internally-calculated hold-up becomes high.
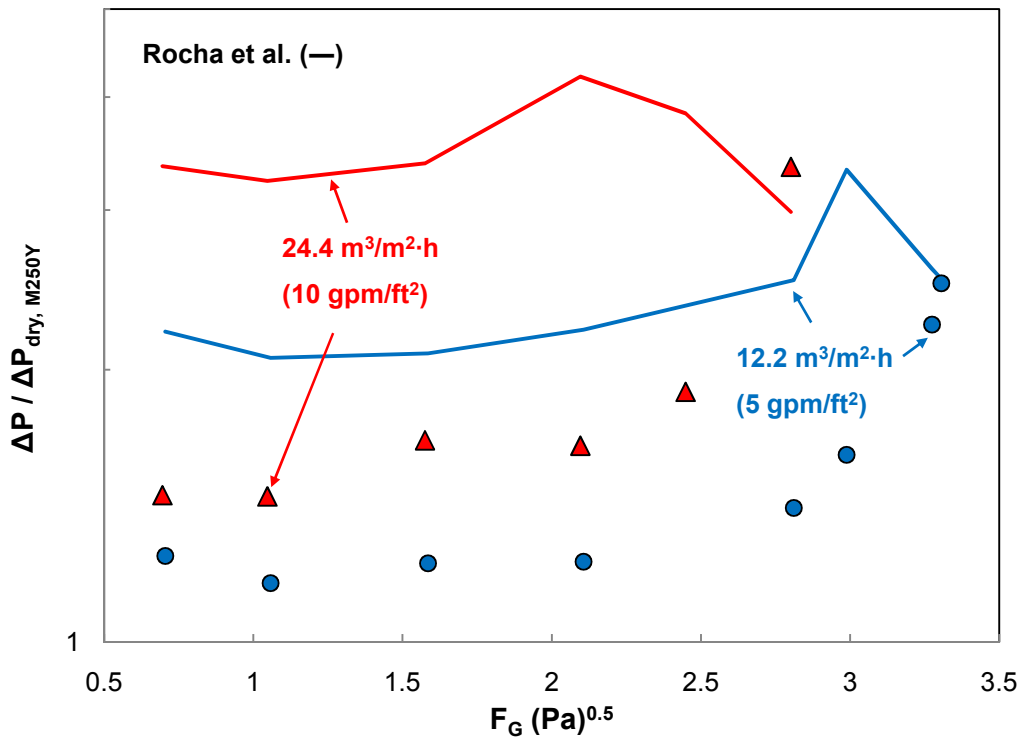
Figure 7.33. Normalized pressure drop of M250Y at liquid loads of 12.2 and 24.4 $m^3/m^2{\cdot}h$ (5 and 10 gpm/ft^2) compared with model of Rocha et al. (1993) at low surface tension.

When alternate (lower) hold-up values are applied, as in Figure 7.34, there is a more favorable coincidence with the data. During the validation of Rocha et al. with distillation systems, hold-up may have been influenced in some manner (other than surface tension) that enabled the model to predict the correct result, albeit not necessarily for the correct reason.

239
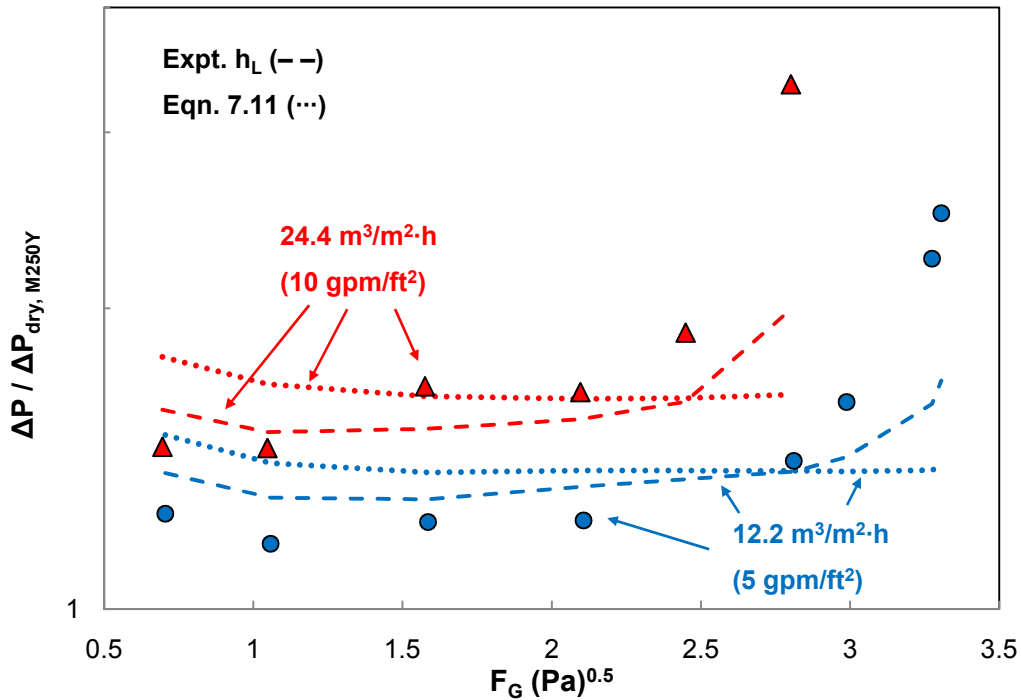
Figure 7.34. Normalized pressure drop of M250Y at liquid loads of 12.2 and 24.4 m³/m²·h (5 and 10 gpm/ft²) compared with variations of model of Rocha et al. (1993) at low surface tension.

As was just mentioned, Rocha et al. was observed to occasionally experience glitches with its implicit hold-up calculation. Problems were especially noticeable when the model was applied to viscous systems, since the internal correlation of hold-up with viscosity is rather strong. At a viscosity of approximately 14 mPa·s, for example, an enormous fractional hold-up of nearly 60% is predicted for respective liquid and gas loads of 48.8 m³/m²·h (20 gpm/ft²) and 0.7 Pa$^{0.5}$. Solution of the model equations was impossible in these situations, even when the flooding pressure drop (normally recommended to be specified as 1025 Pa/m) was extended to as high as 4000 Pa/m in hopes of facilitating the convergence. This problem could be mitigated with the substitution of an external hold-up, which indicates that there may be a fundamental flaw

with the association of pressure drop and hold-up within the model. The importance of having an accurate hold-up – particularly for the purpose of tracking loading/flooding – is also further emphasized by these results.

7.7.4 Delft

The predictions for dry pressure drop from the Delft model (Olujic et al., 2004) are displayed alongside the M125Y, M250Y, M500Y, and M250X data in Figure 7.35. The Delft model possesses no adjustable parameters, akin to Rocha et al., and its fit of these results can be classified as slightly better than Rocha et al. but not as good as Stichlmair et al., with the predominant weakness being the treatment of the packing corrugation angle.
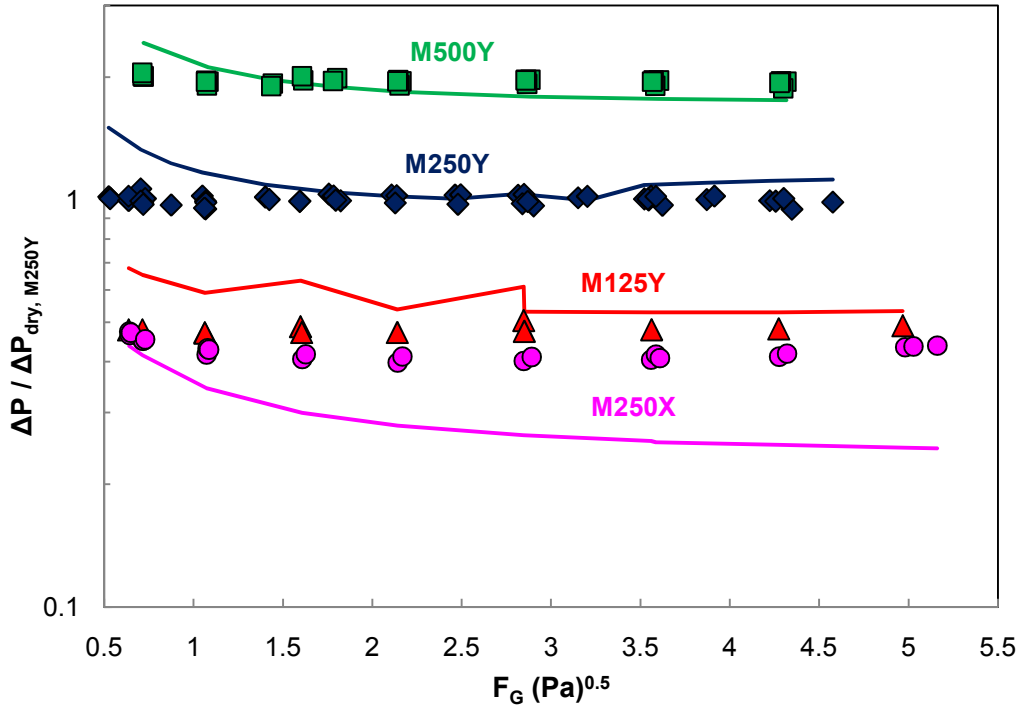
Figure 7.35. Normalized dry pressure drop of M125Y, M250Y, M500Y, and M250X compared with Delft model (2004).

Figure 7.36 presents a comparison on an irrigated basis. Unlike the models that have been evaluated thus far, the Delft model actually exhibits loading behavior within the range of experimental conditions. This onset, however, is predicted to occur at a much lower flow factor than the results would indicate. The slopes at this limit are flatter than what is typically observed, as well. The prediction in the pre-loading region is not entirely inaccurate but is not overly impressive either. A greater deviation between the data and model is apparent at 12.2 $m^3/m^2 \cdot h$ (5 gpm/ft^2) as compared with 48.8 $m^3/m^2 \cdot h$ (20 gpm/ft^2), suggesting that the impact of increasing liquid load on pressure drop is underestimated. The modified versions of the Delft model are displayed in Figure 7.37 and can be seen to be similar to the original. Even in the loading region, there is almost

242

no separation between the two curves in Figure 7.37, which implies that pressure drop and hold-up are essentially decoupled in the Delft model.
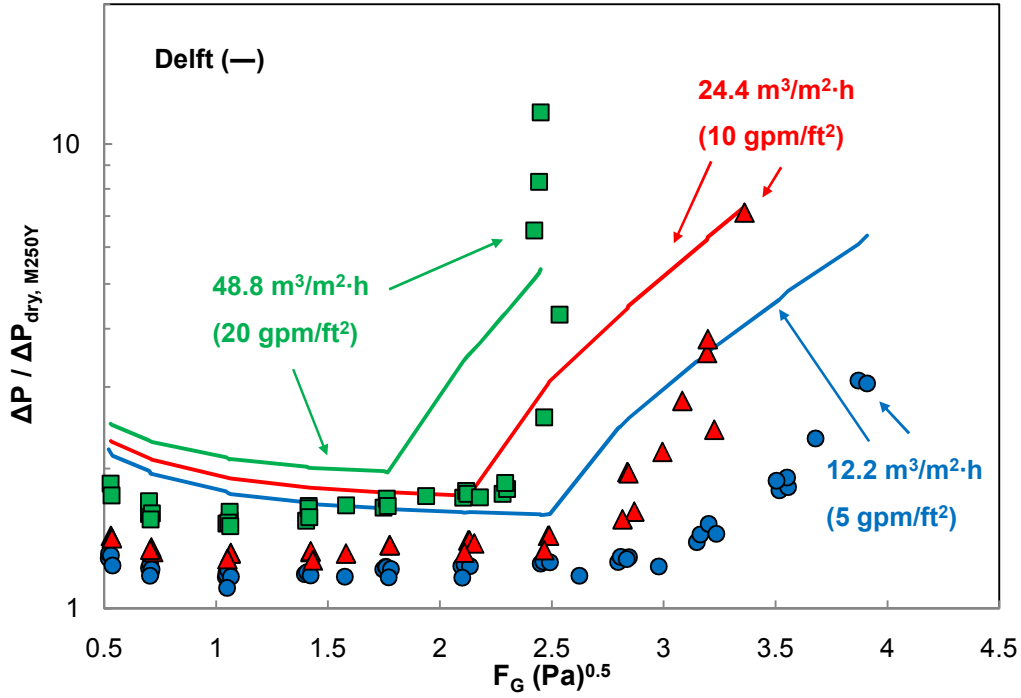

Figure 7.36. Normalized pressure drop of M250Y at liquid loads of 12.2, 24.4, and 48.8 m³/m²·h (5, 10, and 20 gpm/ft²) compared with Delft model (2004).
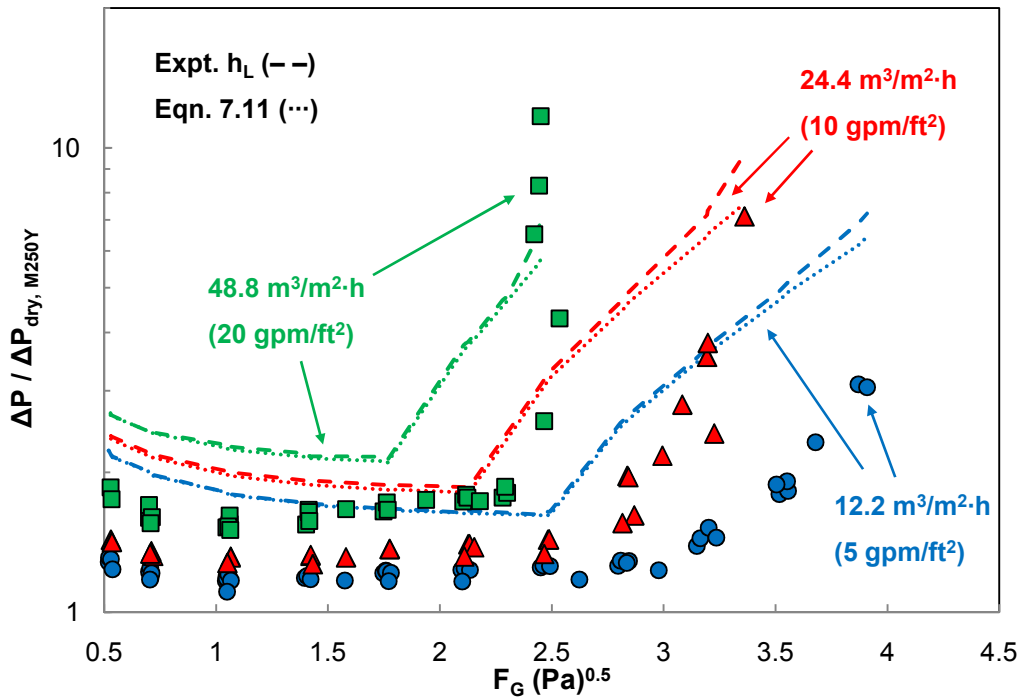
Figure 7.37. Normalized pressure drop of M250Y at liquid loads of 12.2, 24.4, and 48.8 m³/m²·h (5, 10, and 20 gpm/ft²) compared with variations of Delft model (2004).

7.7.5 GPDC (Generalized Pressure Drop Correlation)

A conversion of the graphical version of the generalized pressure drop correlation (GPDC) to a numerical one was desirable to allow for greater flexibility in its use. A representative equation was discovered to be coded implicitly in the GPDC85 prediction option in Aspen Plus® (software developed by AspenTech). This equation is replicated in equation 7.12 (with pressure drop in units of in H₂O/ft) and then shown in generic form in equation 7.13.

$$CP = \frac{7.8282\left(\dfrac{\Delta P}{Z}\right)^{1.087}}{\left[1+2.5292\left(\dfrac{\Delta P}{Z}\right)^{\left(1.087/1.7976\right)}F_{lv}^{0.34185}\right]^{1.7976}} \cdot \left[1-\exp\left(-1.0557F_{lv}^{-0.95216}\right)\right] \quad (7.12)$$

244

$$CP = \frac{C_1 \left(\frac{\Delta P}{Z}\right)^{C_2}}{\left[1 + C_3 \left(\frac{\Delta P}{Z}\right)^{\left(C_2/C_4\right)} F_{lv}^{C_5}\right]^{C_4}} \cdot \left[1 - \exp\left(C_6 F_{lv}^{C_7}\right)\right] \qquad (7.13)$$

The GPDC in Aspen Plus was an older version than the one presented by Kister et al. (2007), which specifically addressed structured packing and consequently had slightly modified curves of constant pressure drop (1.5 in H_2O/ft, 1 in H_2O/ft, etc.). For the purpose of this exercise, this same form was maintained, and the constants (C_1-C_7) in equation 7.13 were simply updated. Several points were estimated from the plot in Kister et al. (Table 7.3), and a sum-of-squared-errors analysis was performed to determine the new constants that should be used. The old and new parameters are presented in Table 7.4. The Kister et al. curves are almost perfectly replicated with the numerical form (Figure 7.38).

Table 7.3. Data points extracted from GPDC curves.

Pressure drop curve (in H$_2$O/ft)	CP	F_{lv}
	2.25	0.005
	2.1	0.01
	1.6	0.05
1.5	1.35	0.1
	0.82	0.5
	0.6	1
	0.4	2
	2.1	0.005
	1.95	0.01
	1.5	0.05
1	1.3	0.1
	0.8	0.5
	0.57	1
	0.38	2
	1.61	0.005
	1.55	0.01
	1.3	0.05
0.5	1.16	0.1
	0.7	0.5
	0.5	1
	0.3	2
	1.2	0.005
	1.17	0.01
	1.05	0.05
0.25	0.96	0.1
	0.6	0.5
	0.41	1
	0.24	2
	0.75	0.005
	0.75	0.01
	0.7	0.05
0.1	0.65	0.1
	0.46	0.5
	0.32	1
	0.2	2

Table 7.4. Constants in numerical version of GPDC.

|	C_1	C_2	C_3	C_4	C_5	C_6	C_7
GPDC-85 (Aspen)	7.8282	1.087	2.5292	1.7976	0.34185	-1.0557	-0.95216
GPDC (in H$_2$O/ft)	3.8617	0.6609	6.3763	0.7206	0.2898	-0.9093	-0.6819
GPDC (Pa/m)	1.3730	3.2369	0.9634	8.2370	0.0167	-0.8141	-0.6268
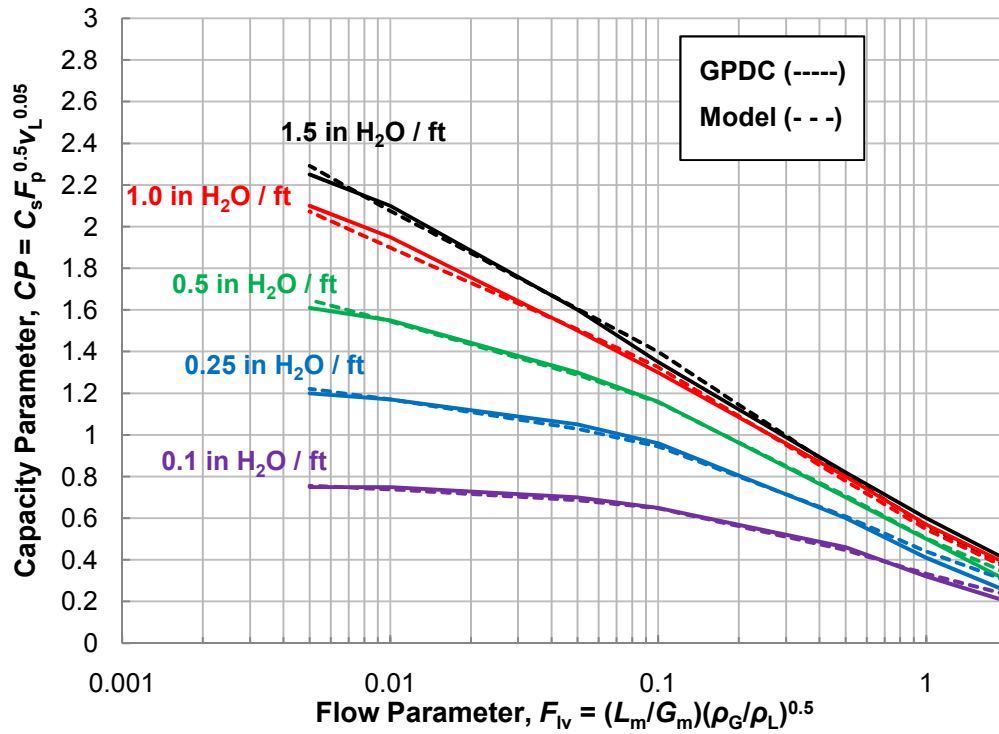
Figure 7.38. Comparison of actual GPDC and numerical version.

Calculation of the capacity parameter (CP) requires the use of a packing-specific parameter. For the packings that were studied, several (but not all) of these values were found in the literature. These are shown highlighted in Table 7.5.

Table 7.5. Packing factors associated with GPDC.

Packing	F_p (ft^{-1})	Source
M125Y	10	Kister and Gill (1992)
M250Y	20	Kister and Gill (1992)
M500Y	34	Kister and Gill (1992)
MP252Y	12	Kister et al. (2007)
M250X	10	Estimated
M250YS	18	Estimated
M2Y	16	Estimated
F1Y	30	Estimated
P500	34	Estimated

The factors for the other packings in the database could potentially be interpolated or extrapolated based on the four "known" values. Rough estimates for these numbers are presented in Table 7.5. For the following discussion, though, the analysis was restricted to the highlighted packings in order to make the evaluation of the GPDC as unbiased as possible. A comparison of the data and the GPDC predictions for dry pressure drop is presented in Figure 7.39. As a caveat, the GPDC is not explicitly equipped to deal with dry conditions. That is, zeroing out the flow parameter (F_{lv}), which is a direct function of liquid rate, causes the model to collapse. Hence, for these cases, a very low flow parameter of 0.0001 was assumed. The GPDC appears to be systematically underpredictive, although it does adequately capture the relative alignment of the packings.
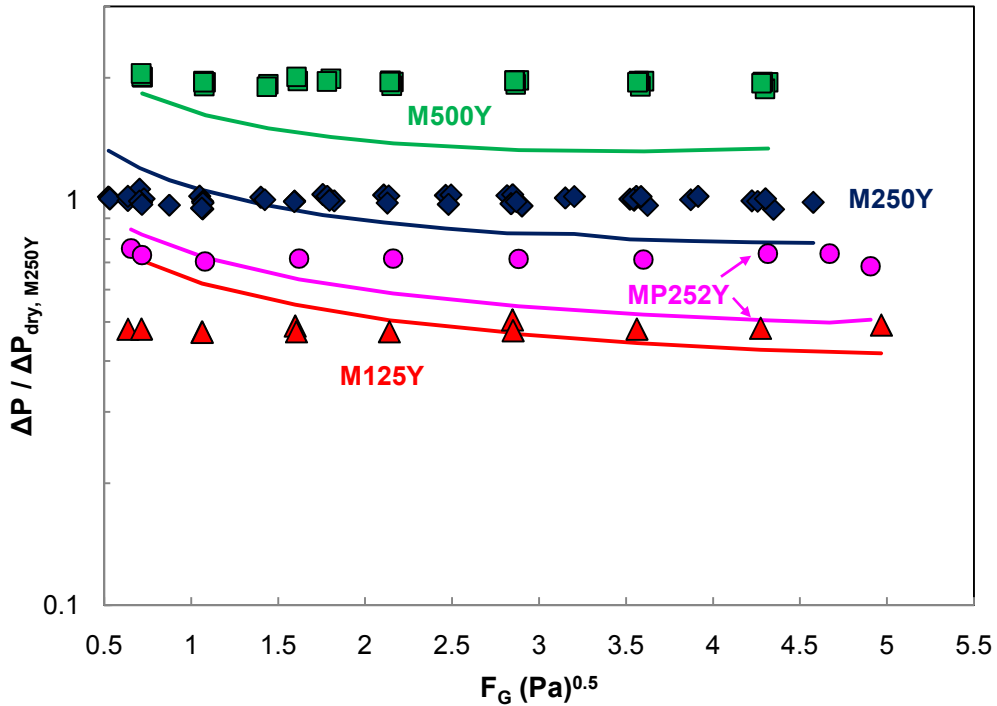
Figure 7.39. Normalized dry pressure drop of M125Y, M250Y, M500Y, and MP252Y compared with GPDC.

The results and GPDC predictions at 12.2, 24.4, and 48.8 $m^3/m^2 \cdot h$ (5, 10, and 20 gpm/ft^2) are shown in Figure 7.40. The fit is decent at 12.2 $m^3/m^2 \cdot h$ (5 gpm/ft^2) but gets progressively worse for the other liquid loads. Of the models that have been examined, the GPDC seems to do the best job at the higher flow factors in terms of predicting both the onset of loading and the shape of the curve.
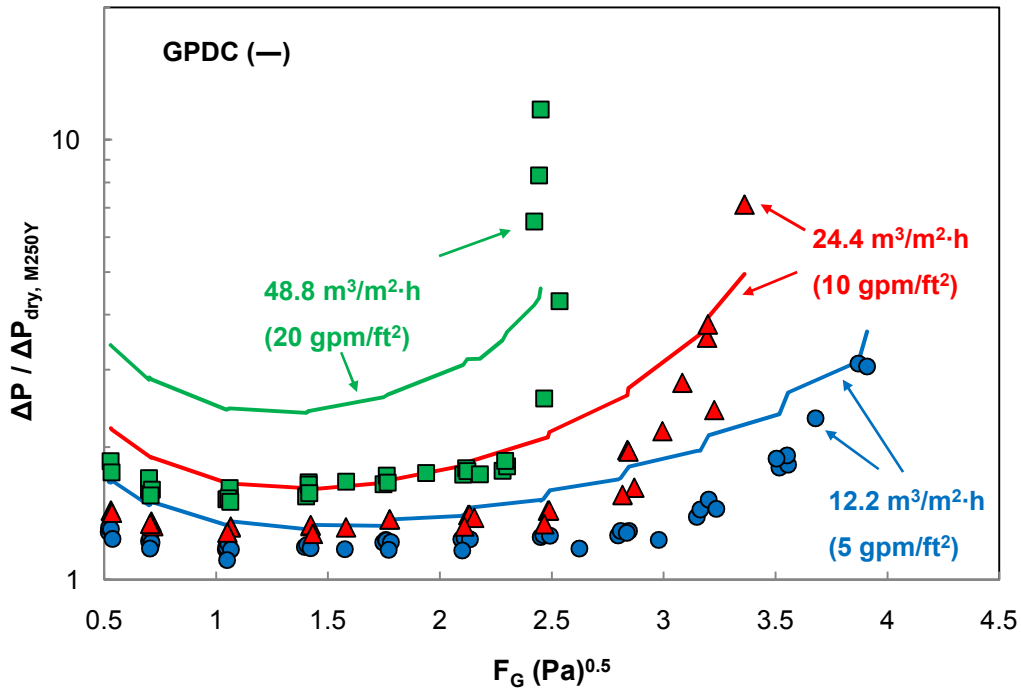
Figure 7.40. Normalized pressure drop of M250Y at liquid loads of 12.2, 24.4, and 48.8 m³/m²·h (5, 10, and 20 gpm/ft²) compared with GPDC.

As an aside, one might think that whereas adjusting some of the other literature models to match the data would be a tedious endeavor, the GPDC might be easier to "fix" via a simple tweaking of the packing factors. This is not true. As verification, the M250Y factor (20 ft^{-1}) was manipulated over values between that of M125Y (10 ft^{-1}) and M500Y (34 ft^{-1}). Not only did the literature-specified factor yield the best fit of the data, convergence issues were found to arise for the other values that were tested.

7.7.6 Conclusions

The intent of this section was to demonstrate the predictive capabilities of a few common hydraulic models and basically, illustrate some features that might go unnoticed

250

to, say, a casual user of a packed column simulation package, such as that found in Aspen Plus. The models are clearly far from perfect, and some may be better in a given situation than others. For instance, the GPDC offered a decent prediction of the M250Y loading region but was not so good at lower flow factors. Rocha et al. worked well in this limit, but it is not a guarantee that it would be as effective with other packings. Recall that it also was ill-equipped to handle viscous systems. Until a truly acceptable global model is developed, it is perhaps advisable to tailor certain models to specific scenarios. Using the two examples just given, Rocha et al. might be more suitable for "mild" operations guaranteed to be in the pre-loading region, whereas the GPDC might be a safer option if the approach to flooding were a concern. Table 7.6 is provided as a summary along these lines, where the mean squared error (MSE) of the various models relative to the pressure drop data (on a unit basis of Pa/m) is listed for each of the packings in the database. The full set of experiments (i.e., baseline, low surface tension, etc.) were included in this analysis, which could have exacerbated the MSE values for models such as Rocha et al., where an iterative solution for the pressure drop could not always be obtained (e.g., at high viscosity). In other cases, constants that were not necessarily optimized had to be used (e.g., packing factors in the GPDC). The models that actually exhibited loading behavior (e.g., Delft and GPDC) could furthermore be subject to favorable bias on a differential error basis, since particularly large residuals would be expected in the loading region. Hence, while the MSE analysis may not be a true representation of the accuracy of the different models, it is believed to at least be an indicator of their general quality.

251

Table 7.6. Mean squared error (MSE) associated with literature models relative to experimental data. MSE based on pressure drop in Pa/m. Modified model values denoted by parentheses (experimental hold-up) or brackets [equation 7.11].

Packing	MODEL			
	Stichlmair et al. (MSE x 10^4)	Rocha et al. (MSE x 10^4)	Delft (MSE x 10^4)	GPDC (MSE x 10^4)
M250Y	3.71	6.08	9.72	3.21
	(1.65)	(1.53)	(11.4)	
	[4.38]	[5.61]	[10.1]	
M500Y	6.30	6.26	13.6	4.11
	(1.56)	(2.11)	(16.7)	
	[6.02]	[4.37]	[12.6]	
M250X	3.13	6.09	2.26	2.57
	(1.36)	(7.03)	(2.21)	
	[2.68]	[2.11]	[2.22]	
MP252Y	1.71	6.53	236	2.32
	(1.10)	(1.23)	(276)	
	[1.67]	[1.74]	[245]	
M250YS	1.16	1.74	42.4	3.06
	(0.54)	(0.63)	(49.0)	
	[1.33]	[1.60]	[44.7]	
M125Y	18.5	5.77	1.58	2.09
	(9.70)	(1.28)	(1.23)	
	[2.30]	[4.72]	[1.68]	
M2Y	21.9	3.72	5.17	0.89
	(22.3)	(0.59)	(6.76)	
	[9.34]	[3.05]	[5.49]	
F1Y	0.009	1.36	0.14	
P500	1.99	4.39	7.49	4.59
	(0.80)	(2.64)	(8.54)	
	[1.93]	[3.98]	[7.33]	

For both the Stichlmair et al. and Rocha et al. models, the use of an alternate hold-up in place of the internal model hold-up virtually always improved the predictive accuracy, either significantly (experimental value) or slightly (equation 7.11). The implicit association of pressure drop and hold-up within the models does not seem to be quite correct, but the models can, nevertheless, be used with some confidence given reliable hold-up values. Of the "original" models, the GPDC was found to be the overall most reliable and consistent. Had more suitable packing factors been used, it probably would have exhibited even better performance.

Chapter 8: Absorber Economic Analysis

This chapter presents an economic analysis of an amine scrubber (absorber) in a CO_2 capture process. The intent of this exercise was to serve as a practical outlet for the work done on structured packing in the current research, and for this reason, the other non-packing-related equipment in the system, such as heat exchangers and the stripper (where trays are more likely to be installed), were neglected. The primary absorber cost components that were considered and the model framework (i.e., limitations/assumptions) are discussed. The results of the analysis, calculated from a Microsoft Excel program in which gas velocity was manipulated, are presented. M250X was determined to be the most economically favorable packing, but the minimum calculated cost investment did not vary too drastically from packing to packing. It was always around \$5-7/tonne CO_2 removed for absorber capacities in the 100-800 MW range. Lastly, suggestions for future analyses are provided.

8.1 COST COMPONENTS

Five major cost components were identified in relation to the absorber: the column body (including the shell and auxiliaries like manholes and ladders), packing, pressure drop, blower, and pump. These are outlined in the following sections.

8.1.1 Column Body

The purchased cost for packed towers can be divided into three categories (Peters and Timmerhaus, 1991):

- Shell (including heads, skirts, manholes, and nozzles);

- Internals (including supports and distributors);

- Auxiliaries (including platforms, ladders, handrails, and insulation).

8.1.1.1. Shell

The cost for column shells is often estimated on the basis of weight. Purchased costs for both 304 stainless steel (SS) (Table 8.1) and carbon steel (Table 8.2) shells (including two heads and a skirt) as a function of weight were approximated from Figure 16-24 in Peters and Timmerhaus (1991). The data were regressed in power law form (equations 8.1 and 8.2), and the resulting line fits were applied in the analysis.

Table 8.1. Shell fabrication cost (304 SS).

Weight (10^3 lb)	Purchased cost (10^3 \$, 1990)	Purchased cost (10^3 \$, current)	Current \$/lb
0.2	\$9	\$15	\$75
1	\$20	\$33	\$33
2	\$30	\$50	\$25
5	\$50	\$83	\$17
10	\$80	\$133	\$13
30	\$170	\$283	\$9
40	\$200	\$333	\$8
100	\$380	\$633	\$6

$$\text{SS purchased cost (\$)} = 518.8 \cdot [\text{Shell weight (lb)}]^{0.609} \qquad (8.1)$$

Table 8.2. Shell fabrication cost (carbon steel).

Weight (10^3 lb)	Purchased cost (10^3 \$, 1990)	Purchased cost (10^3 \$, current)	Current \$/lb
1	\$10	\$17	\$17
3	\$18	\$30	\$10
7	\$30	\$50	\$7
20	\$55	\$92	\$5
50	\$100	\$167	\$3
70	\$130	\$217	\$3

$$\text{Carbon steel purchased cost (\$)} = 249.1 \cdot [\text{Shell weight (lb)}]^{0.602} \qquad (8.2)$$

Stainless steel was considered to be imperative due to concerns over corrosion, but the construction of a shell entirely out of this material would presumably be cost prohibitive. Hence, it was assumed that the main body of the shell (3/8 in) would be made of carbon steel and that the inner and outer walls would be clad with stainless steel (1/8 in each). (The 5/8 in total thickness was presumed to be sufficient, but it is possible that for especially large columns, thicker walls could be necessary for structural support.) To relate the shell weights to the required column volumes output from the simulation, a steel density of 7.85 g/cm^3 (490 lb/ft^3) was assumed. The calculated shell weight was multiplied by a factor of 1.12 to account for the weight of the heads and skirt.

Manholes were considered for tower entry purposes. Prices for 18-in ID manholes with a 300-lb rating (Table 8.3) as a function of wall thickness were estimated from Figure 16-25 in Peters and Timmerhaus (1991). A cost of \$3,480 per manhole was calculated for a 5/8-in thick column. To determine the total number of required manholes, a ratio of one manhole per meter of tower height was assumed.

Table 8.3. Cost of manholes (18-in ID with 300-lb rating).

Wall thickness (in)	Installed cost ($, 1990) / connection / ID connection	Installed cost (10^3 $, current) / connection
0.5	$110	$3.30
0.625	$116	$3.48
0.75	$123	$3.69
1	$138	$4.14
1.25	$155	$4.65
1.5	$167	$5.01
2	$192	$5.76

8.1.1.2 Internals

The liquid distributor cost (equation 8.3) was correlated using informally obtained pricing information from Sulzer (Pilling, 2009) for a 304 SS Sulzer baffle distributor (Table 8.4).

Table 8.4. Liquid distributor cost (304 SS Sulzer baffle distributor).

Column diameter (m)	Purchased cost (10^3 $, current)	10^3 $/m (diameter)
5	$30	$6
10	$90	$9
15	$175	$12

$$\text{Distributor purchased cost (\$)} = 13{,}350 \cdot [\text{Column diameter (m)}]^{0.176} \quad (8.3)$$

For larger columns, the need for mechanical structures such as lattice truss beams to support the distributor as well as the packing becomes increasingly important. The cost of distributor supports for a 10 m diameter column was provided as $75,000, or about 5/6 of the distributor cost (Pilling, 2009). The same cost ratio was suggested to be roughly applicable for any column diameter (equation 8.4).

$$\text{Distributor supports purchased cost (\$)} = 5/6 \cdot \text{Distributor purchased cost} \quad (8.4)$$

For this analysis, supports were assumed to be necessary regardless of column size.

Packing would logically be included in this section as well, but because it can be considered as somewhat of a unique entity (due to its interchangeability) and because it was of particular interest in the context of this research, it was treated separately (see Section 8.1.2) for the purpose of this economic analysis.

8.1.1.3 Auxiliaries

The cost of ladders was listed in Peters and Timmerhaus (1991) as $0.68/lb. A ratio of 30 lb/ft was specified as typical. After converting to current dollars and changing to a $/height basis, this cost was designated as $111.55/m ($34/ft).

Platforms and handrails were also priced at $0.68/lb. The approximate weights of these auxiliaries ranged from 1,700 to 3,300 lbs for column diameters varying from 4 to 10 ft. Equation 8.5 was developed from this information.

Table 8.5. Cost of platforms/handrails.

Column diameter (ft) / (m)	Platform/handrail wt. (lb)	Installed cost (10^3 $, current)
4 / 1.22	1,700	$1.93
6 / 1.83	2,300	$2.61
8 / 2.44	2,800	$3.17
10 / 3.05	3,300	$3.74

$$\text{Platforms/handrails purchased cost } (\$) = 985.33 \cdot [\text{Column diameter } (m)] + 759.33 \qquad (8.5)$$

Insulation was deemed to be unneeded for the absorber.

8.1.2 Packing

Informal quotes for three stainless steel (300-series) packings were obtained from Sulzer (Pilling, 2008): M250Y ($50/ft^3), M500Y ($95/ft^3), and M750Y ($140/ft^3). These values were specified for a 4-6 m diameter column, but the cost per volume was presumed to not change as a function of column size. The quoted prices were also based on metal prices at the time of communication (October 2008). Fluctuations here could affect the analysis quantitatively, but probably not qualitatively. Equation 8.6 is a representation of the data as a function of specific area, a_p.

$$\text{Packing cost per volume}\left(\$/m^3\right) = 6.36a_p + 176.6 \qquad (8.6)$$

The required volume of packing for a given scenario was logically obtained by dividing the required mass transfer area (m^2) by the effective area of the packing (m^2/m^3), with the latter estimated from the model developed in the present work (equation 6.10). Thus, the packing cost was given by:

$$\text{Packing purchased cost}\left(\$\right) = \left\{ \frac{\text{Required mass transfer area}}{1.34\left[\left(\dfrac{\rho_L}{\sigma}\right)g^{\frac{1}{3}}\left(\dfrac{Q}{L_p}\right)^{\frac{4}{3}}\right]^{0.116} \cdot a_p} \right\} \cdot \left(6.36a_p + 176.6\right) \qquad (8.7)$$

8.1.3 Pressure Drop

The cost associated with pressure drop (i.e., blower work) was calculated from equation 8.8.

$$\text{Pressure drop cost }(\$/\text{yr}) = \frac{G\Delta P \cdot (\$/\text{MWh})}{\eta_{\text{blower}}} \qquad (8.8)$$

The electrical operation cost was specified as \$50/MWh, and an operating year was assumed to consist of 8,760 hours. The blower efficiency was assumed to be 75%, based on an estimate in a collaborative report between the Rochelle group and Trimeric Corporation (Rochelle et al., 2005).

8.1.4 Blower

The blower cost (equation 8.9) was scaled from an estimate in the aforementioned Trimeric report (Rochelle et al., 2005), where a price of \$510,000 per 620,000 kg/hr at pressure drops ranging from 10.3 to 17.2 kPa was provided (forced draft blower). An efficiency of 75% was implicitly included in this price. For the current work, a single blower was assumed, whereas a train of four blowers was specified in the report. The scale factors for gas flow (0.6) and pressure drop (0.5) were recommended by Peters and Timmerhaus (1991).

$$\text{Blower purchased cost }(\$) = (510,000)\left(\frac{G_{\text{m}}}{620,000\,\text{kg/hr}}\right)^{0.6}\left(\frac{\Delta P}{10.3\,\text{kPa}}\right)^{0.5} \qquad (8.9)$$

The pressure drop was estimated using the pre-loading version of the Stichlmair et al. (1989) model, which was partly chosen because its set of equations was the easiest to implement of the available literature correlations. The model was also demonstrated to adequately capture the relative pressure drop difference between the four packings of interest (M125Y, M250Y, M500Y, and M250X) in the previous chapter (see Figure

7.27), which was obviously important for a fair economic comparison. A potential disadvantage of using this model was its reliance on packing-specific constants. As was explained in Section 7.2.2, the parameters for M250Y were available in Stichlmair et al., but the values for the other packings had to be regressed (see Table 7.2).

8.1.5 Pump

The pump cost (equation 8.10) was also scaled from a Trimeric report value (Rochelle et al., 2005): \$68,000 per 732 L/s (0.732 m^3/s) at a head of 76 m (SS centrifugal pump). An efficiency of 65% was implicitly included in this estimate. As with the blower, a single pump was assumed to be sufficient here, but four pumps were actually utilized in the Trimeric analysis. The liquid flow scale factor of 0.33 was obtained from Peters and Timmerhaus (1991).

$$\text{Pump purchased cost } (\$) = (68{,}000)\left(\frac{Q}{0.732\,\text{m}^3/\text{s}}\right)^{0.33} \qquad (8.10)$$

8.2 FRAMEWORK OF ANALYSIS

Prior to developing the Excel model, several limitations and assumptions, in addition to the ones previously outlined, had to be established. These have been summarized in the bulleted points below.

- For the conversion of equipment cost to total fixed plant cost, a multiplication factor of 4 was applied. This factor was based on the Chilton method, which incorporates process piping, instrumentation, buildings and site development,

261

auxiliaries, outside lines, engineering and construction, contingencies, and a plant size factor into its estimate. The values used for these parameters are shown in Table 8.6.

- For the conversion of the installed cost to an annualized basis, a multiplication factor of 0.4 was applied. This factor was based on a cash flow analysis that assumed a 5-year MACRS depreciation schedule, a 10-year project life, a 2-year construction period (with the capital investment divided evenly between these years), and a 1-year start-up period. The percentages used for parameters such as rate of return (IRR) are listed in Table 8.7.

- 1990 dollars (the basis of Peters and Timmerhaus (1991)) were converted to current (2009) dollars by dividing by a factor 0.6. This factor was based on values from the U.S. Urban Consumer Price Index (CPI-U) compiled online by the Bureau of Labor Statistics (http://www.bls.gov/cpi/#tables). For reference, the index values in 2009 and in 1990 are listed as 214.5 and 130.7, respectively (130.7/214.5 = 0.6).

- Pressure drop was not allowed to exceed 656 Pa/m. This criterion was based on an 80% approach to flooding in terms of velocity, which translated to a 64% approach in terms of pressure drop based on the theoretical squared relation (i.e., Bernoulli equation), and was calculated from a flooding pressure drop of 1025 Pa/m, which is generally recommended as an approximate value (Rocha et al., 1993).

- The column was assumed to be square, and the column side length was assumed to be interchangeable with diameter in the context of the diameter-based cost correlations.

- Several sections of the column in addition to the packed bed were incorporated into the total height (and volume). These included the inlet ductwork for the gas (9.15 m or 30 ft), sump (6.1 m or 20 ft), water wash (9.15 m or 30 ft), and space for the liquid distributor (3.05 m or 10 ft), for a total of 27.5 m (90 ft).

- No constraints were placed on the column size, and liquid re-distribution was not taken into account.

- 7 m MEA (unloaded) at 40°C, with an assumed capacity of 1 mol CO_2/kg solvent, was used as the capture solvent. Its physical properties were: $\rho_L = 1.003$ g/cm^3, $\mu_L = 1.635$ mPa·s, and $\sigma = 57.94$ mN/m (Weiland et al., 1998; Vázquez et al., 1997a). The column was at atmospheric pressure.

- 90% removal of CO_2 from the flue gas (12 mol% CO_2) was specified.

- A gas throughput of 3 MMCFM was assumed to correspond to a 1000 MW plant.

- An order of magnitude estimate of 0.1 m^2/mol CO_2·hr was used for the required area, based on Aspen Plus simulation scenarios with 7 m MEA and no intercooling.

Table 8.6. Factors used in Chilton method for estimation of total fixed plant cost.

Item	Factor
Delivered equipment cost	1
Installed equipment cost	1.43
Process piping	0.42
Instrumentation	0.2
Buildings and site development	0.2
Auxiliaries	0.025
Outside lines	0.02
Engineering and construction	0.39
Contingencies	0.1
Size factor	0.01

Table 8.7. Parameters used in cash flow analysis.

Parameter	Percentage (%)
IRR	18
Income tax	40
Start-up	10 (based on total investment)
Maintenance	5 (based on total investment)

8.3 ECONOMIC ANALYSIS RESULTS

All of the above information was incorporated into an Excel program, which was set up to analyze the interaction of gas rate and column configuration. Basically, the SOLVER function was utilized to minimize the objective function (summed total of the five cost components) by varying the superficial gas velocity for a given throughput (0.15-3 MMCFM or roughly 50-1000 MW).

Table 8.8 summarizes the results from a few cases run with M250Y. The minimum cost was calculated to be around $5-7/tonne CO_2 removed. The total cost of capture and compression has been estimated to be around $50/tonne CO_2 for a 450 MW plant operating with 30 wt % MEA (Ramezan et al., 2007). Given that steam (for the

stripper reboiler) and compression work are expected to comprise the majority of this cost (Rochelle, 2009), the estimated values in the present analysis seemed reasonable. The packing and column costs were dominant (90%) in every instance. The column benefitted from economies of scale whereas the packing, which always accounted for slightly over \$3/tonne CO_2, did not. The minimum cost, which could roughly be interpreted as a capital cost due to the overwhelming contribution of the packing and column, decreased with greater throughput but only with an exponential dependence of around 0.2. This relation was weaker than might be anticipated and was a function of so much packing (again, with no scaling benefit) being required. The contribution of the pressure drop cost was lower than expected but did become somewhat significant as the gas load increased (2.6% at 100 MW vs. 7.5% at 800 MW). The Stichlmair et al. model (1989) was shown to be overpredictive, though, so the pressure drop contribution in reality could very well be smaller than estimated here. Over the entire MW range, the gas velocity and packing height remained relatively constant. The only parameter that changed much was the column side, increasing from 10 to 25 m.

Table 8.8. Results of economic analysis for M250Y.

Gas rate (MW)	Min. cost ($/tonne CO_2)	Cost breakdown ($/tonne CO_2)	Gas velocity (m/s)	Column side (m)	Packing height (m)	Pressure drop (Pa/m)
100	$6.80	Packing: 48% ($3.29) Column: 41% ($2.82) ΔP: 2.6% ($0.18)	1.51	9.7	10.2	173
250	$5.43	Packing: 60% ($3.27) Column: 30% ($1.60) ΔP: 3.7% ($0.20)	1.56	15.1	10.6	188
500	$4.94	Packing: 65% ($3.22) Column: 23% ($1.15) ΔP: 5.4% ($0.27)	1.72	20.3	11.5	234
800	$4.83	Packing: 66% ($3.18) Column: 21% ($1.01) ΔP: 7.5% ($0.36)	1.90	24.4	12.5	291

Figure 8.1 shows the variance of cost with gas velocity for throughputs ranging from 100 to 800 MW. While a distinct minimum was always evident, the sensitivity to velocity near this point did not appear to be especially high. The optimum velocity was always less than the 80% approach to flood, which is typically designated as a rule-of-thumb operating condition. An increasing discrepancy at superficial velocities below 1 m/s is noticeable, with large spikes arising in the 500 and 800 MW curves. This behavior was a result of the column becoming prohibitively wide (e.g., 38 m, to maintain a velocity of 0.5 m/s at 500 MW) under these circumstances.
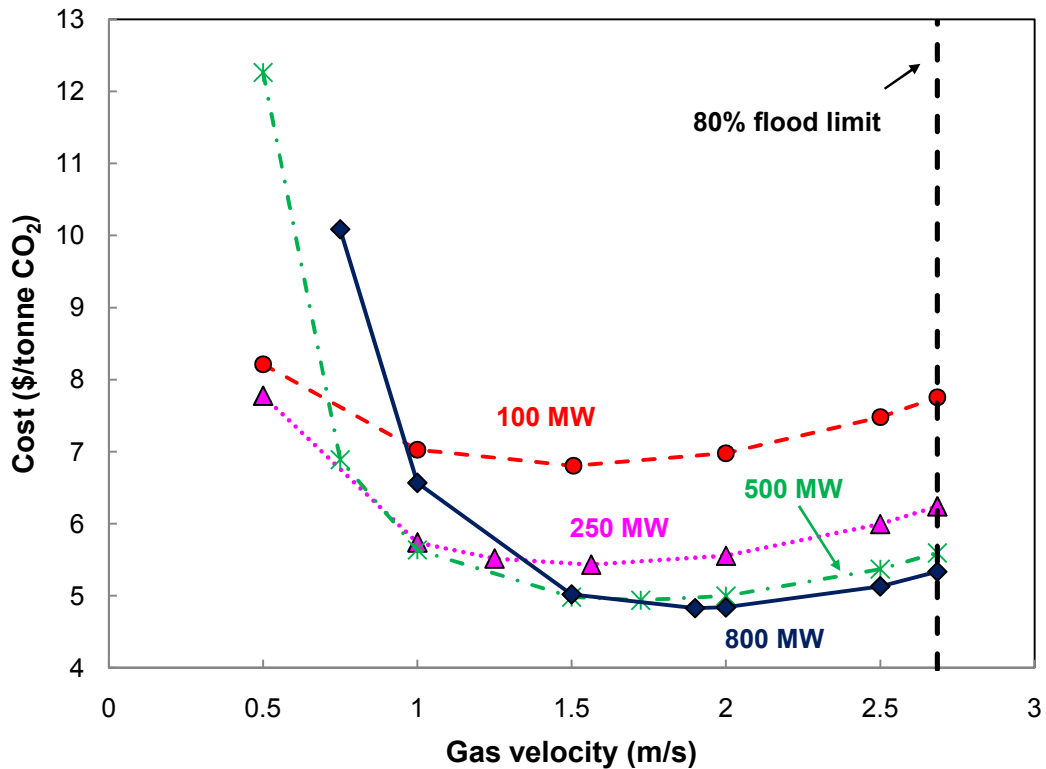
Figure 8.1. Absorber cost as a function of superficial gas velocity for M250Y.

The Excel analysis was run with M125Y, M500Y, and M250X, in addition to M250Y. Figure 8.2 compares the minimum calculated costs at 100, 250, 500, and 800 MW for the four packings. The trend with gas throughput is similar in every scenario. The use of M250X yielded the best results, which was not surprising given its excellent hydraulic characteristics. The reason for the crossover of the M125Y and M500Y curves is unknown but may have been attributable to inconsistencies in the pressure drop modeling (i.e., the regressed constants). The fact that M250Y seemed to be better than either M125Y or M500Y was also interesting and could possibly represent a tradeoff between fractional area efficiency (highest = M125Y, lowest = M500Y) and column size (highest = M125Y, lowest = M500Y/M250X).
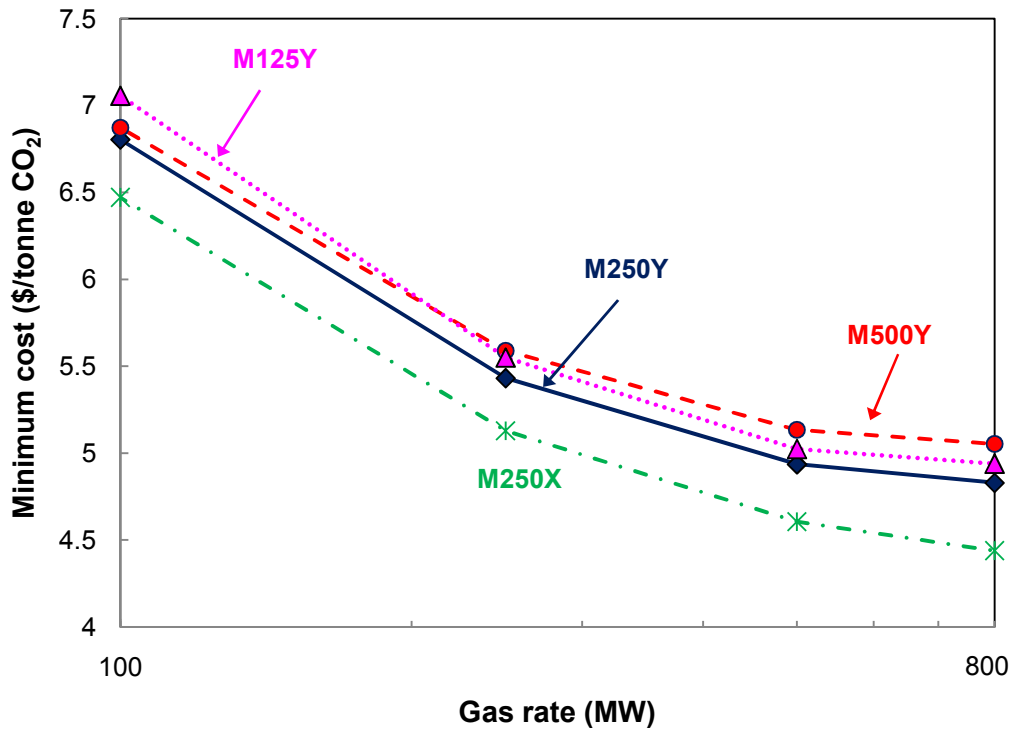
Figure 8.2. Minimum calculated absorber costs for M125Y, M250Y, M500Y, and M250X.

8.4 ADDITIONAL CONSIDERATIONS

The analysis performed here was obviously simplistic, but a foundation for future work was at the very least established. A few critical areas that should be addressed or considered in more rigorous analyses are:

- Use of more representative factors, in regard to the installed costs and/or annualized costs;

- Imposition of limits on the absorber size, which could necessitate the use of multiple towers, akin to the blower and pump trains;

- Incorporation of liquid re-distribution sections in the absorber;

- Incorporation of a better pressure drop model to allow for the accurate analysis of all packings, which at the moment cannot be compared on an entirely fair basis;

- Increasing the flexibility of the analysis to allow for variance in other factors, such as packing and solvent characteristics (i.e., capacity and loading). In other words, a model that could determine what a "perfect" system would be for a given operation would be desirable. This is clearly easier said than done. For example, giving the model free range in determining an optimal packing could result in physically implausible configurations, and so, constraints would perhaps need to be specified based on vendor capabilities.

Chapter 9: Conclusions and Recommendations

This chapter highlights the findings from the present research. The three major phases of the work (wetted-wall column (WWC) studies, packing experiments, and model development) are summarized, and the primary conclusions are stated. Last, recommendations for future work are provided.

9.1 SUMMARY OF WORK COMPLETED

The progression of the current work through its main stages is illustrated in the flow chart below (Figure 9.1).
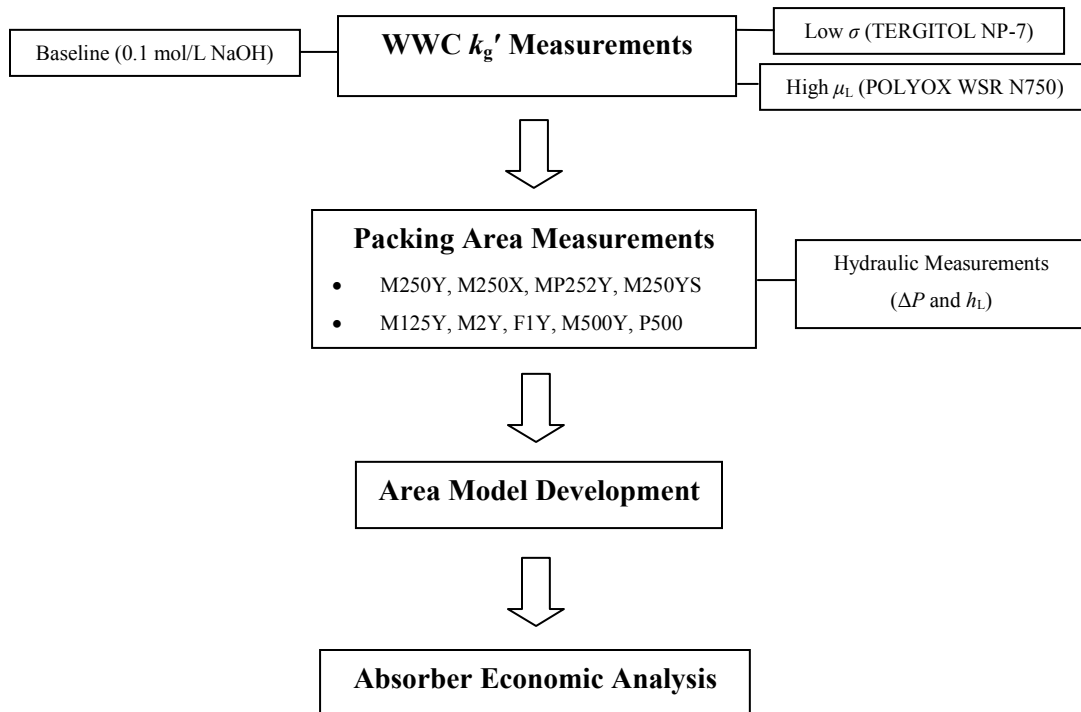
Figure 9.1. Flow diagram of objectives completed in the present research.

Rates of CO_2 absorption into 0.1 mol/L NaOH were measured using a wetted-wall column (WWC). The absorption rates of "doped" caustic solutions, modified to either have a low surface tension (125 ppm$_v$ TERGITOL NP-7 + 50 mg/L Dow Corning Q2-3183A antifoam) or high viscosity (1.25 wt % POLYOX WSR N750), were evaluated as well.

The mass transfer area of nine structured packings (M250Y, M500Y, M250X, MP252Y, M250YS, M125Y, M2Y, F1Y, and P500) was measured via absorption of CO_2 from air into 0.1 mol/L NaOH. Conditions of low surface tension and high viscosity were simulated using the same chemical systems as tested in the WWC. The experimental database included packing sizes from 125 to 500 m^2/m^3, liquid loads from 2.5 to 75 $m^3/m^2 \cdot h$ (1 to 30 gpm/ft^2), surface tension values from 30 to 72 mN/m, and viscosity values from 1 to 15 mPa·s. The hydraulic characteristics (pressure drop and hold-up) of the packings were also investigated in an effort to better understand the mass transfer results.

A global model for the mass transfer area was developed as a function of the liquid Weber and Froude numbers, with an idealized film-flow parameter (Nusselt film thickness) utilized as the dimensional basis of the analysis. The model satisfactorily represented the entire database (±13%). The incorporation of end and wall effects was demonstrated to potentially yield a more realistic version of the model.

Costs involved in the design and operation of an absorption column were obtained from a variety of sources, including texts, reports, and communications with vendors. This information was incorporated into an economic analysis that was configured to

calculate the geometric parameters (column width, packing height, etc.) and ultimately, total cost, as a function of the gas load for a CO_2-amine absorption process.

9.2 CONCLUSIONS

9.2.1 Wetted-Wall Column (WWC)

The average normalized k_g' (experimental k_g' / model k_g') values for the base case (0.1 mol/L NaOH), TERGITOL NP-7 system, and POLYOX system were respectively 1.10 ± 0.09, 1.09 ± 0.07, and 0.94 ± 0.05, with either the Pohorecki and Moniuk model (1988) or a diffusion-corrected version of this model being used as the normalizing factor. For the base case, the discrepancy between the data and model was of the same magnitude as the experimental error (10%). The model was accepted as valid. The surfactant system showed no appreciable difference from the base case, which was logical considering that the three mechanisms that could have had an effect (film barrier, rippling, or charge gradient) were ruled out based on past conclusions in the literature, the relatively short column length, and the nonionic nature of the additives, respectively. The normalized k_g' for the POLYOX system was also near unity, thereby affirming the validity of the applied model. Under normal circumstances, the diffusion coefficient of CO_2 in solution would be anticipated to vary inversely with viscosity, and consequently, a noticeable decrease in k_g' would be expected with a large (i.e., ten-fold) viscosity increase. Literature studies, however, suggested there to be a rather unique phenomena associated with high molecular-weight polymer solutions, wherein the long polymer chains would be anticipated to enhance the bulk solution viscosity but not necessarily the

272

local viscosity, as experienced by small molecules like CO_2. In light of this theory, the POLYOX WSR N750 was not expected to appreciably impact the diffusion of CO_2 or k_g', and the data corroborated this hypothesis.

9.2.2 Packing Studies

The mass transfer area model that was regressed as a function of $(We_L)(Fr_L)^{-1/3}$ or equivalently, as a function of liquid density (ρ_L, in kg/m^3), surface tension (σ, in N/m or kg/s^2), the gravitational constant (9.81 m/s^2), and the flow rate per wetted perimeter (Q/L_p, in $m^3/m \cdot s$), was capable of representing the entire database within acceptable limits ($\pm 13\%$).

$$a_f = 1.34 \left[(We_L)(Fr_L)^{-1/3} \right]^{0.116} = 1.34 \left[\left(\frac{\rho_L}{\sigma} \right) g^{1/3} \left(\frac{Q}{L_p} \right)^{4/3} \right]^{0.116} \tag{6.10}$$

This correlation was believed to have better predictive accuracy than other models in the literature and was shown to be flexible in its treatment of aqueous or hydrocarbon systems.

Packing specific area (125-500 m^2/m^3) and liquid load (2.5-75 $m^3/m^2 \cdot h$ or 1-30 gpm/ft^2) had the largest influence on the mass transfer area. Upward of a two-fold change in area was incurred over the range of operational liquid loads for a given packing. A greater area was generally associated with a higher liquid load, and fractional area (a_e/a_p) efficiency tended to increase with decreasing specific area.

Reducing the surface tension from 72 to 30 mN/m enhanced the mass transfer area by 10% for most packings. The effect was even greater for fine (high specific area) packings (15-20%).

Liquid viscosity did not have a statistically appreciable impact on the mass transfer area. This conclusion could be a function of the somewhat limited viscosity range that was tested (1-15 mPa·s) or the manner in which the k_g' data from the WWC was interpreted.

No significant dependence on gas velocity (0.6-2.3 m/s) or flow channel configuration was observed. The effect of surface texture (embossing) on the mass transfer area was debatable but at best yielded a weak enhancement (10%).

End and wall effects were demonstrated to have been potentially responsible for 5 to 15% of the measured mass transfer area, based on analyses from spray mass transfer studies. Adjustment of the raw data in this regard was justifiable, since doing so reduced bias in the residuals and also brought the higher, arguably illogical fractional-area values (approaching 1.3 in some situations) down closer to unity, but was not entirely endorsable without more data and a better understanding of the phenomena. The modified global correlation is shown below:

$$a_f = 1.2\left[(We_L)(Fr_L)^{-\frac{1}{3}}\right]^{0.109}$$

(6.23)

Pressure drop and liquid hold-up increased with packing size and liquid load. The dry pressure drop, in particular, scaled perfectly with the packing specific area. The pre-loading pressure drop increased by several factors over the minimum-to-maximum liquid

loads (e.g., 2.5 to 75 $m^3/m^2 \cdot h$ or 1 to 30 gpm/ft^2 for M250Y) for a given gas flow factor. Liquid load also strongly affected the pre-loading hold-up, driving it over the range of 1 to 10% in some cases.

The geometric channel configuration affected pressure drop by as much as a factor of two. The pressure drop of M250X and MP252Y was respectively 40% and 70% that of M250Y, even though all three packings had the same geometric area ($a_p = 250$ m^2/m^3). M250X and MP252Y had a 20% greater capacity under irrigated conditions as well.

Surface embossing yielded as much as a 20% increase in pressure drop and hold-up, but this difference could have been a function of the dimples simply creating additional surface area, rather than having a complex mechanistic effect.

Surface tension (30-72 mN/m) did not have a consistent, appreciable effect on the pre-loading pressure drop of M250Y and M500Y and had a relatively small effect on the liquid hold-up (15-30% lower at 30 mN/m).

The viscous systems (1-15 mPa·s) only exhibited a slight increase in pre-loading pressure drop (5-10%) compared to the base case but had hold-up values that were upwards of two times greater. Both the decrease in surface tension and increase in viscosity reduced the capacity of packings by 20%, but it was not completely clear if foaming played a role in this apparent decrease.

The mass transfer area, pressure drop, and liquid hold-up were not found to be relatable in any consistent fashion across the various scenarios that were investigated.

9.2.3 Absorber Economics

The costs associated with the absorber were lowest for M250X, compared with M125Y, M250Y, and M500Y. This assessment was logical given the favorable hydraulic and mass transfer area characteristics of M250X and the somewhat limited framework of the analysis. For every packing, the minimum cost for a 7 m MEA system was consistently in the range of $5-7/tonne CO_2 removed for gas throughputs from 100 to 800 MW, with the packing and column being by far the dominant costs (90%). The results seem reasonable and thus, at least serve as a common sense check on the analysis. The optimum gas velocity was always relatively far from the 80%-approach-to-flood limit that is often specified as a rule of thumb, and so, packing capacity may not be quite as relevant as pressure drop characteristics in these scenarios.

9.3 RECOMMENDATIONS FOR FUTURE WORK

9.3.1 Wetted-Wall Column (WWC)

The use of the literature k_g' models in the interpretation of the packing area results has been repeatedly defended. While this treatment was mostly attributable to confidence in the models, it was admittedly also due in part to a reluctance to utilize the WWC data as is. Given the great importance of k_g' in the analysis, a more thorough characterization of this parameter would be beneficial to perform, particularly with respect to the performance of the POLYOX system, where only a few experiments were conducted. With additional data, a k_g' correlation more tailored (in terms of solution concentration

276

and temperature) to the anticipated packed column experimental conditions than the model of Pohorecki and Moniuk (1988) could perhaps be developed.

9.3.2 Packing Studies

The present investigation examined a wide range of parameters and conditions and contributed significantly to not only our experimental database but also our understanding of packings. Still, much work can and should be done. In addition to testing more packings in general and expanding the database in this manner, a few particular venues warrant exploration. These include:

- Entrance/end/wall effects. The analysis performed in Section 6.10.2 indicated that the contributions of end and wall effects in particular may not be trivial, even with a 3 m (10 ft) packed bed. This result was a huge revelation and must absolutely be verified. The preliminary test that was referenced (Perry et al., 2010) should be elaborated on to thoroughly characterize both the magnitude of the sump effect and its dependence on parameters like liquid load or gas velocity. The findings from these studies should ultimately be used to correct the raw data obtained in the current work (if necessary). The wall effect could be more difficult to discern, since it is unclear how this contribution might be decoupled from the other sources of mass transfer. Regardless of what kind of quantitative effects are ultimately discerned, installation of a permanent sampling point below the packing bed, as well as construction of a chimney tray structure in this void space to minimize the mass transfer in the sump, would be wise. If further

improvements in the mass transfer area measurement accuracy are desired, the construction of a new, larger column (to reduce wall effects) indoors (to eliminate the subjection of the experiments to ambient conditions) could even be considered.

- Steeper corrugation angles. The results showed there to be no difference between the mass transfer area of M250Y (45°) and M250X (60°). A drop-off would seemingly have to exist at some point (i.e., 90°), but what about 70° or 75°? Characterization of these limits and the tradeoff between hydraulics and mass transfer, in terms of both mass transfer coefficients and effective area, would be an interesting endeavor.

- Expanded surface tension and viscosity limits. The conditions in the present work were intended to be representative of amine systems. The effects of surface tension and of viscosity in particular may not have been strong enough to be fully appreciated under these circumstances, in either the hydraulic or mass transfer tests. An expanded set of experiments would be especially useful in validating or exposing a weakness in the $(We_L)(Fr_L)^{-1/3}$ form.

- Density modifications. Density was not expected to vary nearly as much as surface tension or viscosity in the context of amine solutions, so it was not given any consideration. Nevertheless, it was correlated to be of equal importance as the surface tension in the global area model. As such, experiments that investigate the effect of density are worth pursuing. Confirmation of this relevance would be hugely supportive of the model form and its underlying basis

278

involving the Nusselt film thickness. Unfortunately, no recommendation can be given regarding what type of additive might be used to appreciably alter the density of caustic solutions.

As a final thought with respect to future work, one idea that deserves consideration is the use of solvents other than dilute caustic for the mass transfer area experiments. While the "doped" solutions that were utilized were assumed to be proxies for the systems of industrial relevance, such as amines or hydrocarbons, it would be ideal if the experiments actually involved these solvents. Direct testing of amines in the packed column apparatus was not possible due to their incompatibility with PVC but could be done in a different apparatus, such as the absorber/stripper system utilized by the Separations Research Program for CO_2-capture pilot-plant campaigns (Chen, 2007). The same basic methodology as with the caustic tests is applicable in theory, provided that:

- The kinetics (k_g') of the CO_2-amine system are sufficiently understood.

- The gas-film resistance is not a limiting factor, which might be a problem for the faster solvents.

- The CO_2 removal is not a statistical issue (on account of the faster kinetics relative to caustic).

- The physical properties (i.e., loading) of the solvent do not change much, and the system is close to irreversible.

This concept is unlikely to work with hydrocarbons, but a system such as methanol with a small amount of salt (e.g., KOH) dissolved might serve as a closer approximation than an aqueous solution containing surfactant.

9.3.3 Absorber Economics

The design and operation of CO_2 capture systems will be driven by cost. Even so, experience with the economic side of the process seems to be far lacking relative to the technical side, particularly within the Rochelle group. Hence, the analytical framework presented in Chapter 8 should continued to be built upon. This statement is in reference to not only the absorber but to the entire capture system. Regarding the absorber, several specific issues that should be addressed in the future were already discussed (see Section 8.4), but in general, the analysis must be more accurate in its handling of factors such as cost annualization and do a better job of adhering to realistic constraints such as column size limits.

Appendix A: Detailed Experimental Protocol

This appendix contains detailed operational instructions for the packed column, goniometer, and rheometer. Pictures of the packed column are included to show the layout and clearly label the experimental system.

A.1 PACKED COLUMN

A.1.1 Photographs and Labels

Process water valve
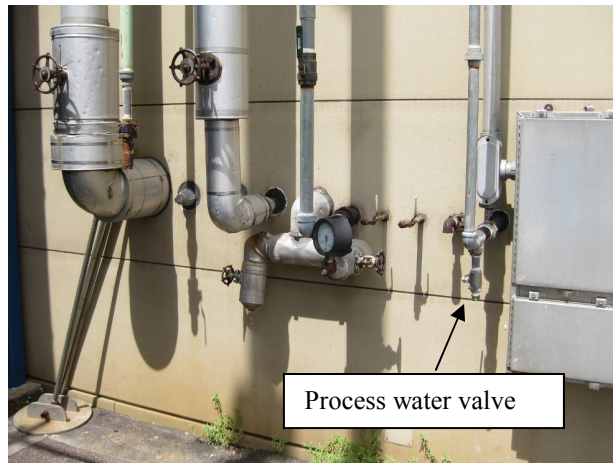
Figure A.1. Process water source.
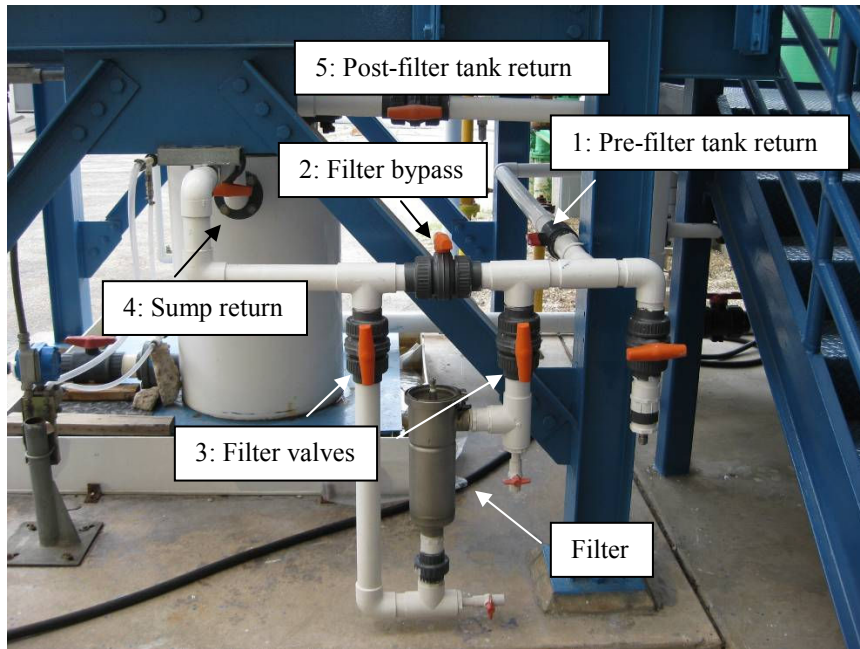
Figure A.2. Liquid line valves (north).
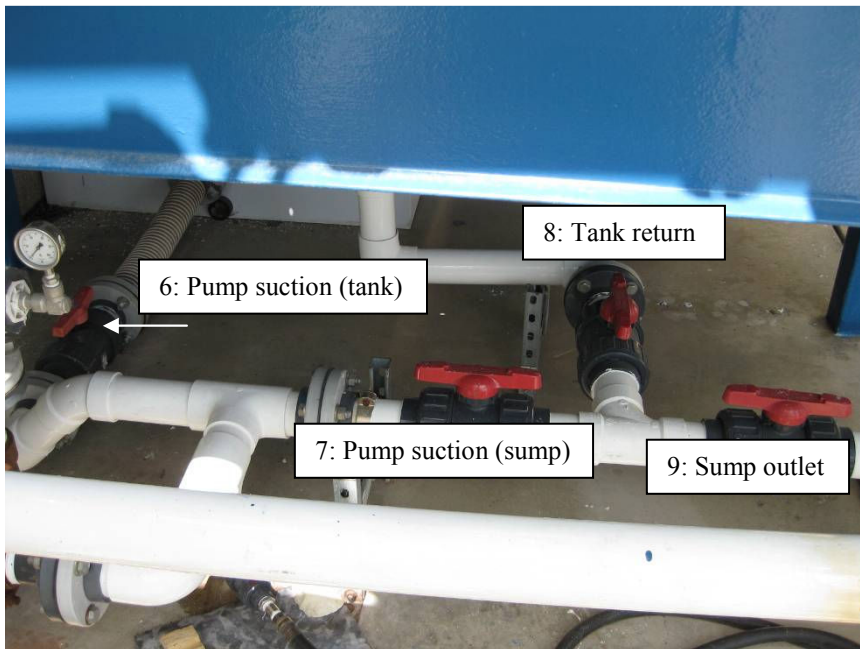
Figure A.3. Liquid line valves (south).
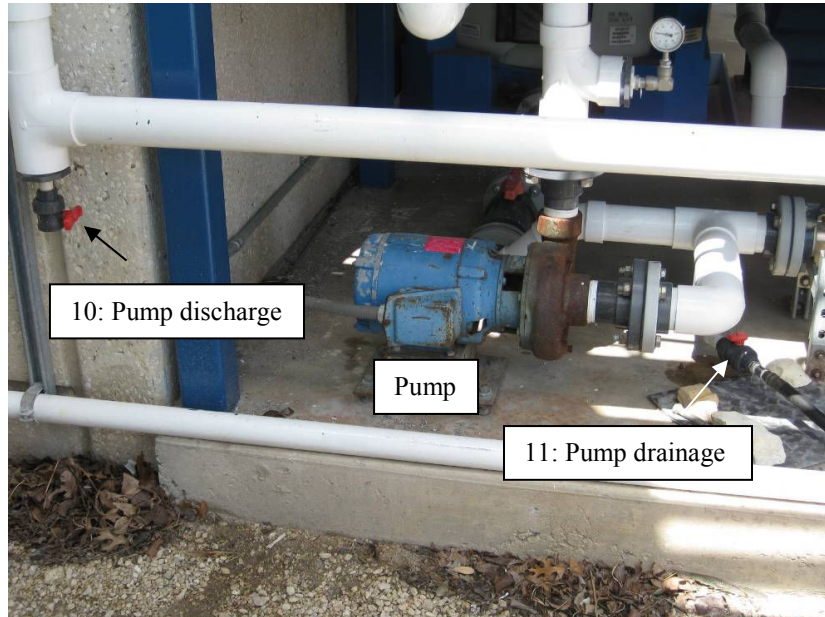
Figure A.4. Pump and associated valves.
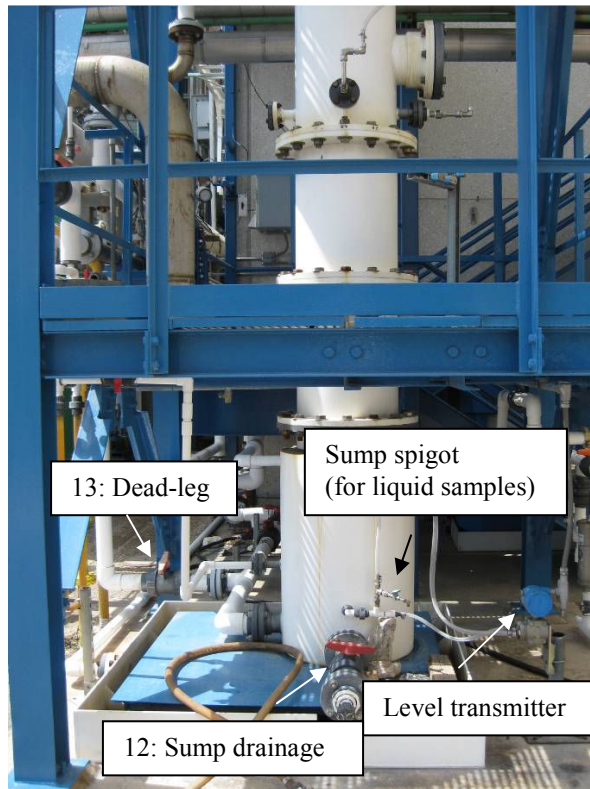
Figure A.5. Column sump.
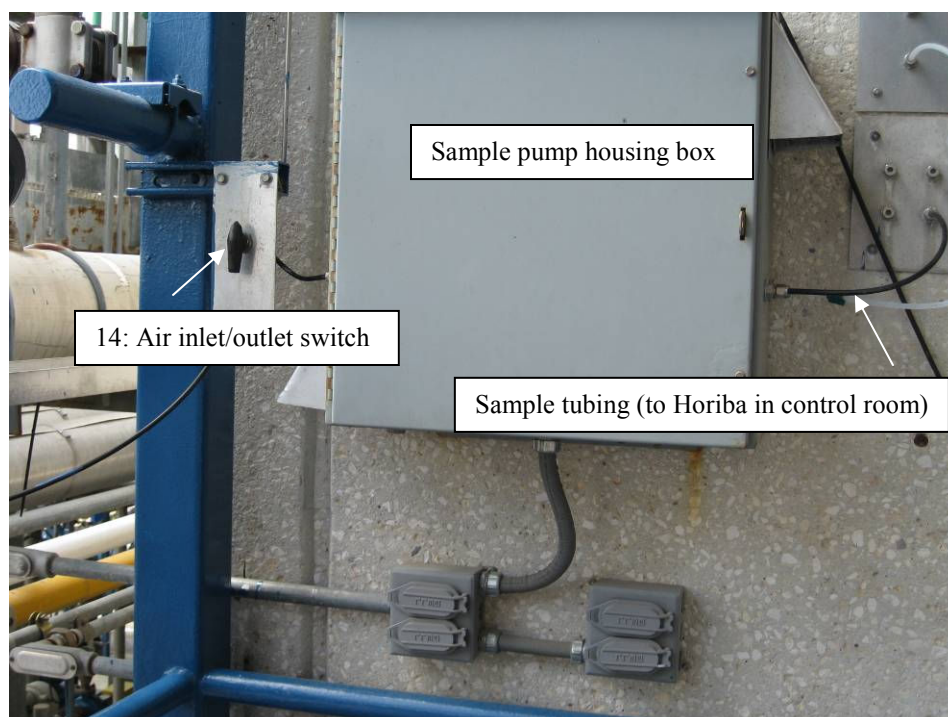
Figure A.6. Air sampling system.
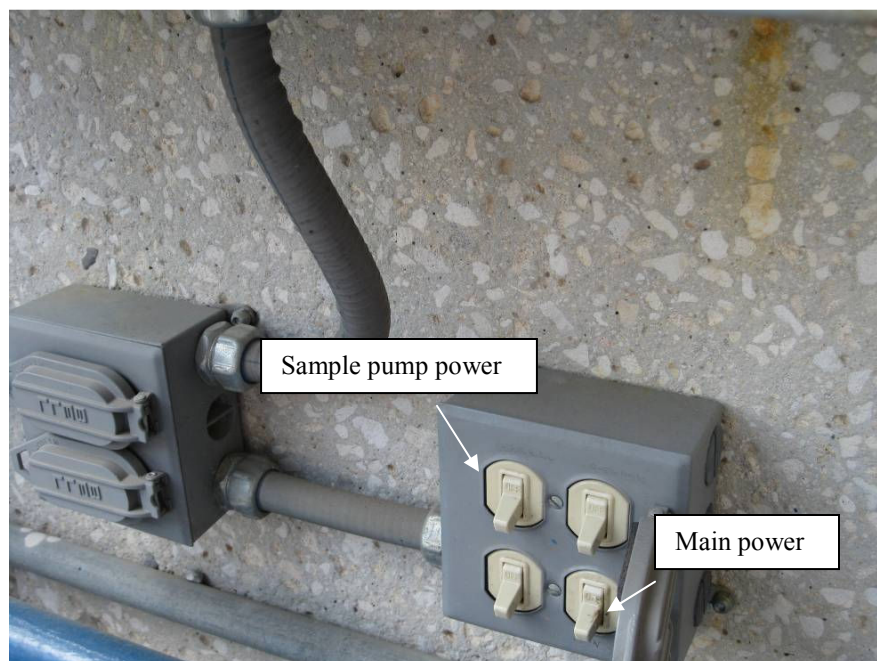
Figure A.7. Power for air sampling system.
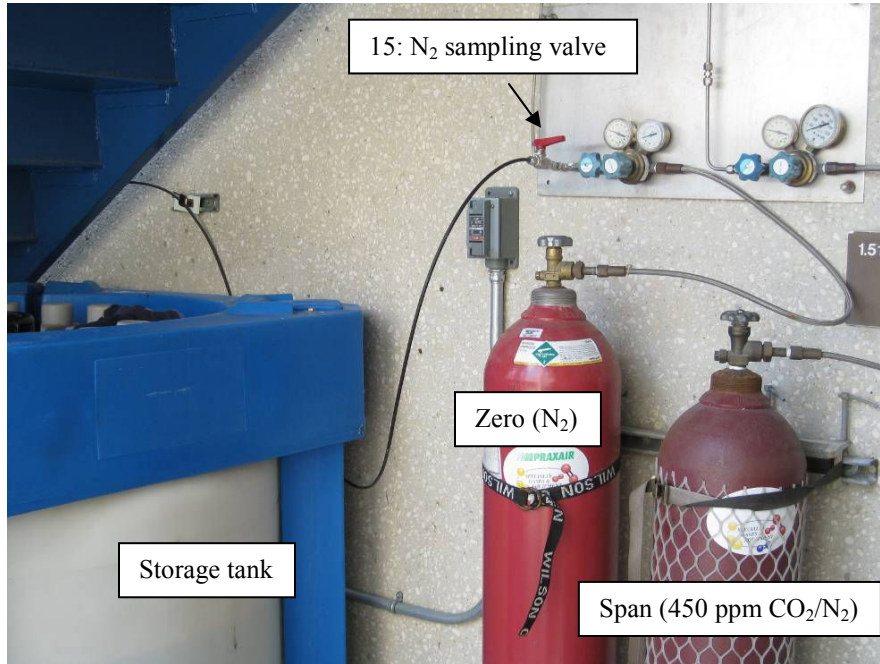
Figure A.8. Storage tank and gas cylinders.
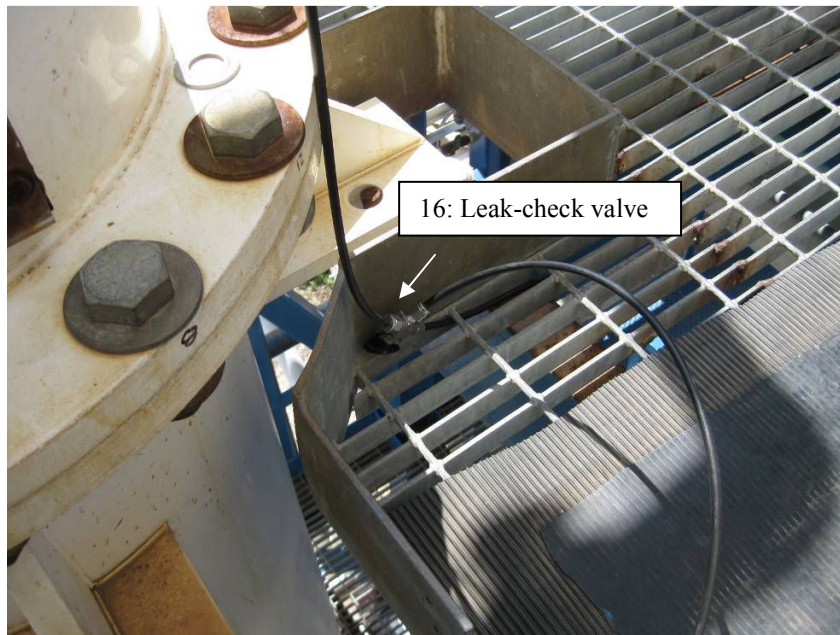
Figure A.9. Leak-check valve.
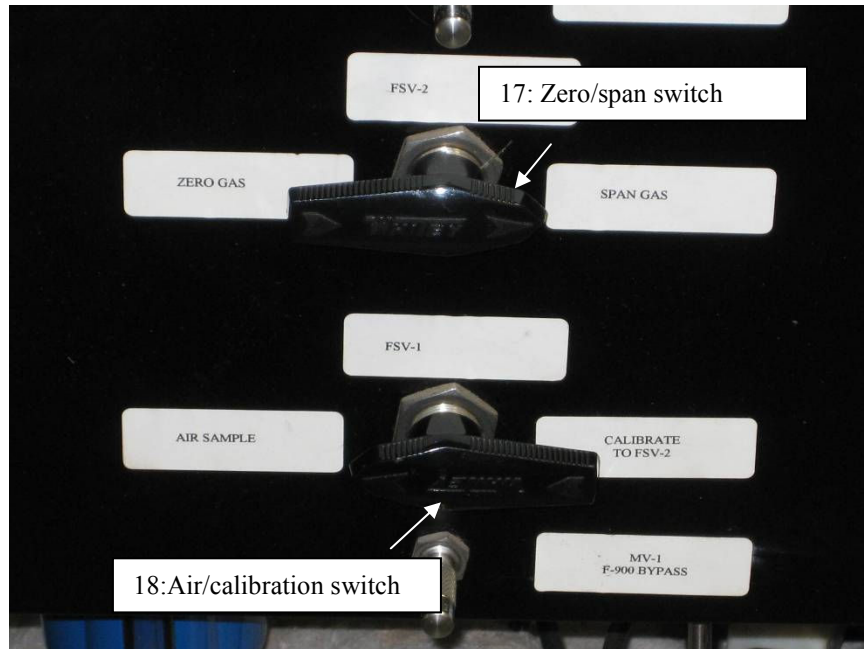
Figure A.10. Horiba valves.

Figure A.11. Column mid-section.
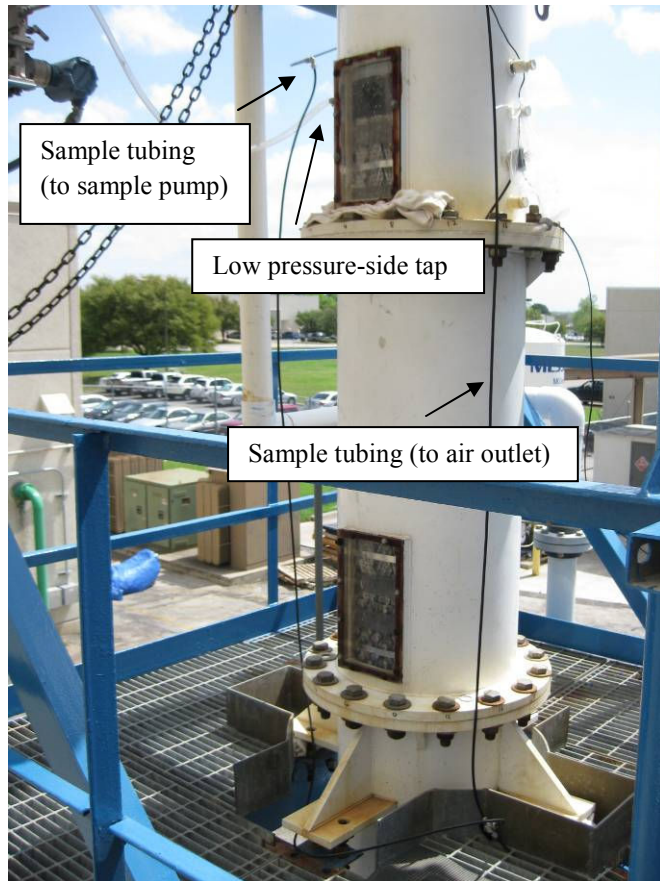
Figure A.12. Column top.

Table A.1. Valves associated with packed column (shown in Figures A.2-A.10).

Valve	Description	Liquid (L) / Gas (G)	Comments
1	Pre-filter tank return	L	
2	Filter bypass	L	
3a/3b	Filter valves	L	
4	Sump return	L	
5	Post-filter tank return	L	
6	Pump suction (tank)	L	
7	Pump suction (sump)	L	
8	Tank return	L	
9	Sump outlet	L	
10	Pump discharge	L	Used for waste discharge into drums
11	Pump drainage	L	Only open during filling/drainage
12	Sump drainage	L	Only open during drainage
13	Dead-leg	L	Only open during drainage
14	Air inlet/outlet switch	G	
15	N_2 sampling valve	G	Only open during leak check
16	Leak-check valve	G	
17	Zero/span switch (Horiba)	G	
18	Air/calibration switch (Horiba)	G	
AV401	Pneumatic valve	L	

A.1.2 Hydraulics Protocol

Start-up

1.   Connect hose to system (valve 11) and fill storage tank with process water.

    a.   Open valves: 1, 3a/3b, 5, 6, 8, 9, pneumatic valve (AV401).

    b.   Closed valves: 2, 4, 7.

2.   Arrange valves so that liquid can be pumped from storage tank to sump but is prevented from returning to tank.

    a.   Open valves: 1, 3a/3b, 4, 6.

b.　　Closed valves: 2, 5, 7-9, AV401.

3.　　Pump water into sump (recommended pump setting: 60% VSD) until it nearly overflows into level transmitter tubing and then stop pump. (If overflow occurs then bleed screw on transmitter can be removed to purge tubing.)

4.　　Arrange valves so that liquid circulation loop (through packing) bypasses storage tank entirely and only involves column sump.

a.　　Open valves: 3a/3b, 5, 7, 9, AV401.

b.　　Closed valves: 1, 2, 4, 6, 8.

5.　　Run pump at 60% VSD. Close AV401 shortly afterward but leave pump on to keep liquid lines primed. Under these conditions, there should still be at least 50 to 58 cm (20 to 23 in) of water in column sump to ensure that sump is not emptied during operation.

a.　　If < 50 cm (20 in), return to step #2. Add more water to sump.

b.　　If sump overflows, briefly open valve 1 to pump some water back to storage tank and then purge level transmitter tubing.

6.　　Establish liquid level under "baseline" conditions. Input this value to DeltaV.

a.　　Be consistent with baseline specification.

i.　　Blower: 0.65 m/s (200 ACFM); Pump: 60% VSD.

b.　　Allow 5-10 minutes for level to stabilize.

7.　　Open AV401, and begin hydraulic experiment. Set liquid load at fixed rate and ramp air rate up to the flood point, recording hold-up and pressure drop for each condition.

a. Data can be recorded via macro in Microsoft Excel logsheet on control room computer.

b. Evaporation (i.e., decrease in baseline level over time) is accounted for via an internal calculation in DeltaV. "Calculated" and "actual" levels should ideally be as close as possible. There are two options for this:

   i. Baseline level can be established every few points.

   ii. Outlet humidity (usually set at 100%) can be manually adjusted to track apparent rate of liquid loss.

c. The pressure taps should be purged often, especially after flooding or near-flooding conditions.

Shut-down

1. Arrange valves so that circulation loop includes storage tank before shutting down equipment to prevent sump from overflowing.

2. Drain system completely into sanitary sewer (via valves 11 and 12).

Note: Uncontaminated water is permissible for sanitary sewer disposal, but waste water (i.e., containing surfactants, etc.) must be contained in drums. These drums can be requested from the Environmental Health and Safety (EHS) department at the University of Texas at Austin.

A.1.3 Mass Transfer Protocol

Start-up

1.   Connect hose to system (valve 11) and fill storage tank with 0.75 m^3 (200 gallons) of process water.

   a.   Arrange valves so that all water flows once-through Micromotion device.

      i.   Open valves: 1, 5, 8, 9, AV401.

      ii.   Closed valves: 2-4, 6, 7.

   b.   Track inventory in DeltaV Control Studio (EXTRACTION → EX_FLOW → FT_420).   Flow should be stopped when counter reaches 185-190 gallons, to account for dead space in system (i.e., lag before Micromotion counter actually begins incrementing).

2.   Start liquid circulation (recommended pump setting: 65% VSD).

   a.   Open valves 2 and 6.

   b.   Close AV401.

3.   Add 3.65 kg (8.05 lbs) of solid NaOH pellets to storage tank. Allow pellets to dissolve for at least 1 hour.

4.   Calibrate Horiba VIA-510 analyzer using zero and span gases from cylinders.

   a.   Keep valve 18 on "calibrate" and alternate valve 17 between "span" and "zero" several times.

5.   Leak-check sample line tubing and sample pump.

   a.   Arrange valves so that Horiba draws from N_2 cylinder.

      i.   Open valve 15.

ii.　　　Flip valve 14 up, and switch valve 16 to proper flow path.

　　　　iii.　　Set valve 18 to "air sample."

　　b.　　Turn sample pump on and adjust regulator on N_2 cylinder so that gas is sampled under minimal pressure (< 1 psig). Horiba reading should approach zero. (Note: Horiba typically asymptotes around 5-7 ppm CO_2, as minor leakage is unavoidable.)

　　c.　　Shut down sample pump afterward. Close valve 15 and orient valve 16 to draw from air outlet.

6.　　Allow liquid to circulate through packing. Ensure at least 5 or 6 liquid inventory turnovers for sufficient mixing.

　　a.　　Open valves 3a/3b and AV401.

　　b.　　Close valve 2.

　　c.　　Recommendation: 36.6 $m^3/m^2{\cdot}h$ (15 gpm/ft^2) for 1 to 1.5 hours.

7.　　Take sample from spigot on column sump and verify NaOH concentration.

　　a.　　Titrate 10 cm^3 of solution with 0.1 mol/L HCl and phenolphthalein indicator. NaOH concentration should be within approximately 5% of 0.1 mol/L.

8.　　Pre-wet packing at 61 $m^3/m^2{\cdot}h$ (25 gpm/ft^2) for 10 minutes.

9.　　Begin mass transfer experiment. Set blower at a fixed rate (0.6, 1, or 1.5 m/s or equivalently, 180, 300, or 450 ACFM) and measure CO_2 removal at various liquid loads.

　　a.　　Data can be recorded via macro in Microsoft Excel logsheet.

b. Allow minimum of 10 minutes to reach steady state for each data point. Allow 20 minutes if transitioning from a high liquid load, such as pre-wetting conditions, to a lower one, such as 12.2 $m^3/m^2{\cdot}h$ (5 gpm/ft^2) or less, to minimize contributions from stagnant liquid (see discussion of film saturation in Section 6.1.2).

c. Collect sample from spigot on column sump for CO_2 content analysis (TIC) at end of each condition.

d. CO_2 inlet and outlet concentrations cannot be measured simultaneously, so inlet concentration needs to be input as a constant value in DeltaV. Verify this concentration often (every few data points at least) by flipping valve 14 down.

e. Do not exceed pressure drop of 815 Pa/m (1 in H_2O/ft).

Shut-down

1. Shut down blower and CO_2 sample pump.

2. Calibrate portable pH probe with buffer solutions (pH 7.0 and 10.0).

3. Circulate liquid at relatively high rate (at least 36.6 $m^3/m^2{\cdot}h$ or 15 gpm/ft^2) and add concentrated (38%) HCl to storage tank to neutralize caustic solution. Approximately 1.5 to 1.75 bottles (10 lb each) should be sufficient. Ensure proper protective gear is worn.

4. Test pH of solution. A pH between 6 and 11 is acceptable for disposal.

   a. Samples should be taken at 2 locations (sump spigot and pump discharge) and checked for consistency.

5. Drain system completely into sanitary sewer (via valves 11 and 12).

6. Flush system with water (to clean out residual salt) and drain.

Note: Only pure caustic solution (i.e., no surfactants, etc.) that has been neutralized is permissible for sanitary sewer disposal. If this is the case, ensure the proper discharge form (online) has been submitted to and accepted by EHS beforehand:

http://www.utexas.edu/safety/ehs/index.php   (link on right-hand side)

Otherwise, waste must be contained in drums.

A.2 GONIOMETER

A.2.1 Surface Tension

1. Prime the screw-type syringe by in-taking/expelling sample. Fill the syringe afterward.

2. Insert the syringe into its respective holder (above the goniometer stage), and properly secure it.

3. Turn the goniometer lamp on to its maximum setting.

4. Open the DROPimage program on the goniometer computer, and check the "Live Display" box. A small segment of the syringe tip should be visible, and dispensed droplets should be centered in the frame. The syringe holder can be adjusted as necessary.

5.   Slowly dispense a drop from the syringe. The "camera" icon can be clicked to take an up-to-date snapshot, which can subsequently be saved ("disk" icon). Ideally, images should be saved at the near-breaking point of the droplet (i.e., where any additional compression on the syringe will cause the drop to fall).

6.   Analyze the saved images using FTA32 Video 2.0 software.

   a.   Open the program and select the image file to import (automatically saved as .bmp files from DROPimage).

   b.   Check the "Calibrate by Needle Diameters" box in the Interfacial Tension tab and enter the appropriate needle size (e.g., 0.7112 mm for 22-gauge).

   c.   Input the densities of the light (air, 0.0012 g/cm^3) and heavy (liquid sample, 0.997 g/cm^3) phases in the Calibration tab.

   d.   Click the "IF Tension" button in the Images tab to have the program calculate the surface tension, based on the droplet geometry and the entered parameters.

7.   Shut down the equipment, and clean the syringe assembly (water and acetone).

A.2.2 Contact Angle

1.   Place the (clean) sample surface on the goniometer stage. The edge of the surface should be aligned with the edge of the stage on the side closer to the camera.

2.   Turn the goniometer lamp on to its maximum setting.

3.   Open the DROPimage program on the goniometer computer. Check the "Live Display" box, and select the "Contact Angle Tool" feature.

295

4. Dispense a 5 mm^3 (5 µL) sample drop near the surface edge using an appropriately sized syringe (e.g., 25 µL). The stage can be moved laterally and vertically if necessary until the drop comes into view of the camera.

5. Use the mouse buttons to bracket the drop with green (left click) and yellow (right click) lines.

6. Adjust the tilt of the stage using the screws underneath until a baseline value of 0 is attained. Affirm that the surface is level by clicking the "Snap" button.

7. Choose to "Start" the measurement from the "Contact Angle Tool" menu. Click the center of the drop to position a green line over it and then "Measure" to obtain contact angle values (left, right, and mean), evaluated by the fit of a circle over the drop. "End" the measurement afterward.

8. Shut down the equipment, and clean the surface before its next use.

A.3 RHEOMETER

1. Turn on the Julabo F25 bath, and allow it to equilibrate for a few minutes at its set-point of 25˚C. (The MCR 300 rheometer should be on and always remain on.)

2. Rinse and dry the stainless steel plate (type: CP 50-1) that will be used to shear samples, and attach it securely to the rheometer.

3. Start the "US200" program on the computer associated with the apparatus, and open a new file. Choose the "Flow Curve/CSR" option.

4. Click on the "gearbox" button to access initialization options.

    a.   Change the equipment system if necessary (should be CP 50-1 by default).

b.   Start the flow of cooling water by selecting "Send."

c.   Select "Zero Gap" to calibrate the device and then click on "Lift Position" to return the plate to its original position.

5.   Using an automatic pipet, dispense 700 mm^3 (700 μL) of sample at the center of the circular rheometer base.

6.   Choose "Meas. Position" on the computer to lower the plate on to the sample. Ideally, the solution should be squeezed such that liquid is barely visible along the outer rim of the plate.

7.   Define a procedure for the rheometer to follow and start the experiment. A warm-up period can be specified to get the system to the desired temperature before starting. (Rates lower than 100 s^{-1} are not recommended, as the rheometer tends to be unreliable in this range.)

8.   Copy the raw data into an analytical program such as Microsoft Excel.

9.   Once data collection has been completed, shut down the equipment.

a.   Lift the plate from its measuring position ("Lift Position") and stop the flow of cooling water ("Switch Off").

b.   Disconnect and clean the plate and rheometer base. Return the plate to its protective canister.

c.   Turn off the Julabo F25 bath.

Appendix B: Tabulated Data

This appendix contains data from the density measurements that were performed. The results from the WWC and packed column experiments have also been tabulated, although given the space limitations, only the most critical values have been chosen for representation. The complete data sets from these tests can be found in the electronic archives submitted together with this dissertation.

B.1 Density Data

Table B.1. Measured and reference density values for distilled deionized water.

T (°C)	$\rho_{L,meas}$ (g/cm^3)	$\rho_{L,ref}$[a] (g/cm^3)
20	0.9981	0.99823
	0.9982	0.99823
40	0.9921	0.99221

a: Reference values for pure water obtained from Haar et al. (1984)

Table B.2. Measured and predicted density values for 0.1 mol/L NaOH.

T (°C)	$\rho_{L,meas}$ (g/cm^3)	$\rho_{L,pred}$[a] (g/cm^3)
20	1.0026	1.0023
	1.0027	1.0023
40	0.9964	0.9995

a: Predicted values from correlation of Moniuk and Pohorecki (1991)

Table B.3. Measured density values for 0.1 mol/L NaOH + 125 ppm$_v$ TERGITOL NP-7 + 50 mg/L Q2-3183A antifoam, compared with predicted values for pure 0.1 mol/L NaOH.

T (°C)	$\rho_{L,meas}$ (g/cm^3)	Relative Difference (vs. Prediction[a] for 0.1 mol/L NaOH) (%)
20	1.0027	0.04
	1.0027	0.04
40	0.9965	-0.30

a: Predicted values from correlation of Moniuk and Pohorecki (1991)

Table B.4. Measured density values for 0.1 mol/L NaOH + 0.5 wt % POLYOX WSR N750, compared with predicted values for pure 0.1 mol/L NaOH.

T (°C)	$\rho_{L,meas}$ (g/cm^3)	Relative Difference (vs. Prediction[a] for 0.1 mol/L NaOH) (%)
20	1.0035	0.12
	1.0036	0.13
40	0.9973	-0.22

a: Predicted values from correlation of Moniuk and Pohorecki (1991)

Table B.5. Measured density values for 0.1 mol/L NaOH + 1.25 wt % POLYOX WSR N750, compared with predicted values for pure 0.1 mol/L NaOH.

T (°C)	$\rho_{L,meas}$ (g/cm^3)	Relative Difference (vs. Prediction[a] for 0.1 mol/L NaOH) (%)
20	1.0048	0.25
	1.0049	0.26
40	0.9978	-0.17

a: Predicted values from correlation of Moniuk and Pohorecki (1991)

Table B.6. Measured density values for 0.1 mol/L NaOH + 1.5 wt % POLYOX WSR N750, compared with predicted values for pure 0.1 mol/L NaOH.

T (°C)	$\rho_{L,meas}$ (g/cm^3)	Relative Difference (vs. Prediction[a] for 0.1 mol/L NaOH) (%)
20	1.0052	0.29
	1.0053	0.30
40	0.9982	-0.13

a: Predicted values from correlation of Moniuk and Pohorecki (1991)

B.2 Wetted-Wall Column (WWC) Data

The WWC data are presented in Table B.7, in order of date.

Table B.7. WWC experimental data.

T (°C)	P (kPa)	$P_{CO2,LM}$ (Pa)	Q (cm^3/s)	u_G (m/s)	k_g' x 10^{10} (kmol/m^2·Pa·s)	Normalized k_g'	K_G/k_G (%)	CO$_2$ Removal (%)
0.1 mol/L NaOH				**4/20/2006**				
27.4	584	297	1.74	0.112	5.98	1.36	26.3	25.3
27.4	584	446	1.74	0.119	5.31	1.21	23.1	22.4
27.4	584	246	1.74	0.109	5.93	1.35	26.5	25.5
27.4	584	353	1.74	0.114	4.94	1.13	22.5	22.0
27.4	584	302	1.74	0.112	5.00	1.15	23.0	22.5
0.1 mol/L NaOH				**5/2/2006**				
31.0	446	274	1.74	0.151	5.43	1.15	19.6	19.4
31.0	446	194	1.74	0.145	5.48	1.16	20.3	20.2
31.0	446	349	1.74	0.158	5.17	1.11	18.3	18.2
31.0	446	236	1.74	0.148	5.22	1.12	19.2	19.2
0.1 mol/L NaOH				**7/17/2006**				
28.0	205	205	1.51	0.314	4.68	1.05	9.1	9.6
28.0	205	148	1.51	0.293	4.57	1.02	9.4	10.0
28.1	205	187	1.51	0.307	4.63	1.04	9.1	9.7
28.1	205	222	1.51	0.321	4.76	1.08	9.0	9.5
28.1	205	168	1.51	0.300	4.81	1.09	9.6	10.2
0.1 mol/L NaOH				**7/18/2006**				
28.2	205	164	1.74	0.261	5.36	1.18	11.8	12.6
27.9	205	206	1.74	0.274	5.34	1.19	11.3	12.0
27.8	205	142	1.74	0.253	5.06	1.13	11.4	12.3
27.8	205	185	1.74	0.267	5.62	1.27	12.0	12.8
27.8	205	226	1.74	0.281	5.05	1.14	10.5	11.2
0.1 mol/L NaOH				**7/21/2006**				
28.8	205	167	1.74	0.301	5.04	1.11	10.0	10.6
28.7	205	221	1.74	0.322	4.81	1.06	9.1	9.6
28.7	205	148	1.74	0.294	4.72	1.04	9.6	10.2
28.6	205	205	1.74	0.315	4.55	1.01	8.8	9.3
28.6	205	187	1.74	0.308	4.70	1.05	9.2	9.8

T (°C)	P (kPa)	$P_{CO2,LM}$ (Pa)	Q (cm³/s)	u_G (m/s)	$k_g' \times 10^{10}$ (kmol/m²·Pa·s)	Normalized k_g'	K_G/k_G (%)	CO_2 Removal (%)
0.1 mol/L NaOH				**7/24/2006**				
28.1	239	148	1.74	0.194	5.03	1.12	14.1	15.2
28.1	239	257	1.74	0.218	5.12	1.15	13.2	14.0
28.0	239	205	1.74	0.206	5.17	1.16	13.9	14.8
28.1	239	177	1.74	0.200	4.95	1.11	13.6	14.7
28.0	239	231	1.74	0.212	5.35	1.22	14.0	14.9
28.0	239	147	1.74	0.194	5.43	1.23	15.1	16.2
0.1 mol/L NaOH				**7/25/2006**				
27.9	205	204	1.96	0.314	5.13	1.15	9.8	10.4
27.9	205	168	1.96	0.300	4.94	1.10	9.8	10.4
27.9	205	148	1.96	0.293	4.65	1.04	9.5	10.1
27.9	205	187	1.96	0.307	4.78	1.07	9.4	9.9
27.9	205	222	1.96	0.321	4.52	1.02	8.6	9.1
27.8	205	205	1.96	0.314	4.63	1.05	9.0	9.5
27.8	205	167	1.96	0.300	5.27	1.19	10.4	11.0
0.1 mol/L NaOH + 125 ppm$_v$ TERGITOL NP-7 + 50 mg/L Q2-3183A antifoam							**9/22/2006**	
31.8	239	275	4.22	0.278	4.77	1.00	10.4	10.9
31.7	239	234	4.22	0.266	5.09	1.07	11.4	11.9
31.8	239	256	4.22	0.272	4.54	0.95	10.1	10.6
31.8	239	296	4.22	0.284	4.32	0.91	9.4	9.8
0.1 mol/L NaOH				**9/25/2006**				
31.3	239	235	2.41	0.266	4.57	0.96	10.4	10.9
31.3	239	277	2.41	0.278	4.25	0.89	9.4	9.9
31.7	239	295	2.41	0.284	4.52	0.95	9.7	10.2
31.8	239	255	2.41	0.272	4.93	1.04	10.9	11.4
31.8	239	233	2.41	0.266	5.28	1.11	11.8	12.3
31.8	239	275	2.41	0.278	4.84	1.02	10.5	11.0
0.1 mol/L NaOH				**9/26/2006**				
32.1	239	255	4.22	0.273	4.99	1.03	11.0	11.5
32.2	239	294	4.22	0.285	4.81	1.00	10.3	10.8
32.3	239	233	4.22	0.267	5.35	1.11	11.9	12.5
32.3	239	275	4.22	0.261	4.80	1.00	10.5	11.0

T (°C)	P (kPa)	$P_{CO2,LM}$ (Pa)	Q (cm³/s)	u_G (m/s)	$k_g' \times 10^{10}$ (kmol/m²·Pa·s)	Normalized k_g'	K_G/k_G (%)	CO_2 Removal (%)
0.1 mol/L NaOH + 125 ppm$_v$ TERGITOL NP-7 + 50 mg/L Q2-3183A antifoam							9/26/2006	
31.7	239	274	4.22	0.278	5.04	1.05	10.9	11.4
31.7	239	254	4.22	0.272	5.19	1.09	11.4	11.9
31.8	239	293	4.22	0.284	5.04	1.05	10.7	11.2
31.8	239	233	4.22	0.266	5.41	1.13	12.0	12.6
0.1 mol/L NaOH				10/2/2006				
33.8	239	188	4.22	0.256	6.10	1.23	13.8	14.4
33.7	239	253	4.22	0.274	5.70	1.15	12.4	12.9
33.9	239	310	4.22	0.293	5.57	1.13	11.6	12.0
34.1	239	142	4.22	0.244	5.44	1.10	13.0	13.7
34.1	239	341	4.22	0.305	6.40	1.32	12.7	13.0
0.1 mol/L NaOH + 125 ppm$_v$ TERGITOL NP-7 + 50 mg/L Q2-3183A antifoam							10/2/2006	
33.9	239	311	4.22	0.293	5.22	1.05	10.9	11.3
33.9	239	142	4.22	0.244	5.70	1.14	13.5	14.2
34.0	239	253	4.22	0.274	5.59	1.13	12.2	12.7
34.1	239	189	4.22	0.256	5.60	1.13	12.8	13.4
34.1	239	344	4.22	0.305	5.71	1.16	11.5	11.8
0.1 mol/L NaOH				10/3/2006				
33.6	239	292	4.22	0.286	5.51	1.12	11.6	12.1
33.7	239	273	4.22	0.280	5.43	1.11	11.7	12.1
33.7	239	253	4.22	0.274	5.81	1.18	12.6	13.1
0.1 mol/L NaOH				10/4/2006				
33.8	239	142	4.22	0.244	5.43	1.09	12.9	13.6
34.1	239	188	4.22	0.256	6.33	1.26	14.2	14.8
34.0	239	251	4.22	0.274	6.45	1.30	13.8	14.2
34.1	239	309	4.22	0.293	5.94	1.19	12.2	12.6
34.1	239	342	4.22	0.305	6.13	1.24	12.2	12.5
0.1 mol/L NaOH + 125 ppm$_v$ TERGITOL NP-7 + 50 mg/L Q2-3183A antifoam							10/4/2006	
34.1	239	143	4.22	0.244	4.72	0.94	11.4	12.2
34.2	239	189	4.22	0.256	5.50	1.10	12.6	13.2
34.4	239	253	4.22	0.275	5.70	1.14	12.4	12.9
34.4	239	311	4.22	0.293	5.23	1.05	10.9	11.4
34.4	239	345	4.22	0.305	5.21	1.05	10.6	10.9

T (°C)	P (kPa)	$P_{CO2,LM}$ (Pa)	Q (cm^3/s)	u_G (m/s)	k_g' x 10^{10} (kmol/m^2·Pa·s)	Normalized k_g'	K_G/k_G (%)	CO$_2$ Removal (%)
0.1 mol/L NaOH				**10/5/2006**				
34.0	239	142	4.22	0.244	5.40	1.08	12.9	13.6
34.1	239	188	4.22	0.256	5.97	1.20	13.6	14.1
34.2	239	253	4.22	0.274	5.74	1.15	12.4	12.9
34.2	239	311	4.22	0.293	5.23	1.06	10.9	11.4
34.2	239	345	4.22	0.305	5.42	1.10	10.9	11.3
0.1 mol/L NaOH + 125 ppm$_v$ TERGITOL NP-7 + 50 mg/L Q2-3183A antifoam							**10/5/2006**	
34.0	239	143	4.22	0.244	5.05	1.01	12.1	12.9
34.1	239	189	4.22	0.256	5.70	1.14	13.0	13.6
34.1	239	253	4.22	0.274	5.49	1.10	12.0	12.5
34.1	239	310	4.22	0.293	5.58	1.12	11.6	12.0
34.1	239	344	4.22	0.305	5.52	1.11	11.1	11.5
0.1 mol/L NaOH				**10/31/2006**				
30.2	239	159	2.86	0.271	4.65	0.99	10.3	10.9
30.2	239	329	2.86	0.271	4.83	1.05	10.7	11.2
30.1	239	243	2.86	0.271	4.92	1.07	10.9	11.4
30.1	239	195	2.86	0.271	4.91	1.07	10.9	11.4
30.1	239	285	2.86	0.271	5.12	1.12	11.3	11.8
0.1 mol/L NaOH				**11/1/2006**				
29.9	239	241	4.22	0.271	5.54	1.19	12.1	12.5
29.9	239	158	4.22	0.271	5.49	1.18	12.0	12.5
29.9	239	284	4.22	0.271	5.41	1.17	11.8	12.3
29.9	239	329	4.22	0.271	5.02	1.08	11.1	11.6
29.9	239	194	4.22	0.271	5.30	1.14	11.6	12.1
0.1 mol/L NaOH + 125 ppm$_v$ TERGITOL NP-7 + 50 mg/L Q2-3183A antifoam							**11/1/2006**	
29.9	239	284	4.22	0.271	5.23	1.13	11.5	12.0
29.8	239	194	4.22	0.271	5.28	1.14	11.6	12.1
29.9	239	242	4.22	0.271	5.19	1.12	11.4	11.9
30.1	239	328	4.22	0.271	5.19	1.12	11.4	11.9

T (°C)	P (kPa)	$P_{CO2,LM}$ (Pa)	Q (cm^3/s)	u_G (m/s)	$k_g' \times 10^{10}$ (kmol/m^2·Pa·s)	Normalized k_g'	K_G/k_G (%)	CO$_2$ Removal (%)
0.1 mol/L NaOH				**11/2/2006**				
29.8	239	328	4.21	0.271	5.06	1.10	11.1	11.6
29.8	239	194	4.21	0.271	5.39	1.17	11.8	12.3
29.8	239	243	4.21	0.271	4.88	1.06	10.8	11.3
29.8	239	285	4.21	0.271	4.89	1.07	10.8	11.3
0.1 mol/L NaOH + 125 ppm$_v$ TERGITOL NP-7 + 50 mg/L Q2-3183A antifoam							**11/2/2006**	
29.8	239	194	4.21	0.271	5.22	1.14	11.5	12.0
29.8	239	284	4.21	0.271	5.33	1.18	11.7	12.2
29.8	239	328	4.21	0.271	5.11	1.15	11.2	11.7
29.8	239	242	4.21	0.271	5.00	1.13	11.0	11.5
29.9	239	159	4.21	0.271	4.67	1.06	10.4	10.9
0.1 mol/L NaOH				**12/1/2006**				
27.7	239	330	2.64	0.269	4.67	1.06	10.4	10.9
27.7	239	195	2.64	0.269	4.90	1.11	10.8	11.3
27.7	239	286	2.64	0.269	4.70	1.08	10.4	11.0
27.7	239	158	2.64	0.269	5.44	1.25	11.9	12.4
27.7	239	242	2.64	0.269	5.10	1.18	11.2	11.7
0.1 mol/L NaOH				**12/4/2006**				
27.8	377	371	1.96	0.171	4.99	1.12	16.3	16.6
27.8	377	296	1.96	0.171	5.37	1.21	17.4	17.5
27.8	377	577	1.96	0.171	4.75	1.09	15.7	16.0
27.7	377	504	1.96	0.171	4.89	1.12	16.0	16.3
27.7	377	437	1.96	0.171	5.00	1.14	16.3	16.6
0.1 mol/L NaOH				**2/28/2007**	**(1st expt.)**			
31.3	377	436	2.64	0.173	4.74	1.01	15.6	15.9
31.3	377	502	2.64	0.173	4.79	1.03	15.7	16.1
31.3	377	298	2.64	0.173	4.57	0.98	15.1	15.5
31.3	377	370	2.64	0.173	4.79	1.03	15.8	16.1

T (°C)	P (kPa)	$P_{CO2,LM}$ (Pa)	Q (cm^3/s)	u_G (m/s)	$k_g' \times 10^{10}$ (kmol/m^2·Pa·s)	Normalized k_g'	K_G/k_G (%)	CO$_2$ Removal (%)
0.1 mol/L NaOH				**2/28/2007**	**(2nd expt.)**			
31.2	377	434	2.64	0.173	5.03	1.07	16.4	16.7
31.2	377	501	2.64	0.173	4.96	1.06	16.2	16.5
31.2	377	296	2.64	0.173	4.98	1.06	16.3	16.6
31.2	377	370	2.64	0.173	4.80	1.02	15.8	16.1
31.2	377	233	2.64	0.173	4.57	0.97	15.1	15.5
0.1 mol/L NaOH				**3/27/2007**				
32.2	446	272	2.41	0.147	4.70	0.97	17.8	18.0
32.0	446	348	2.41	0.146	4.67	0.97	17.7	17.9
32.0	446	181	2.41	0.146	4.79	0.99	18.1	18.2
32.0	446	226	2.41	0.146	4.75	0.99	18.0	18.1
31.9	446	391	2.41	0.146	4.90	1.03	18.5	18.6
0.1 mol/L NaOH + 1.25 wt % POLYOX WSR N750						**3/27/2007**		
32.9	446	272	1.96	0.147	4.67	1.00	17.7	17.9
32.9	446	396	1.96	0.147	4.17	0.90	16.1	16.4
32.9	446	350	1.96	0.147	4.32	0.94	16.6	16.9
32.9	446	229	1.96	0.147	4.04	0.87	15.7	16.0
32.9	446	183	1.96	0.147	4.11	0.89	15.9	16.3
0.1 mol/L NaOH				**3/30/2007**				
31.9	446	182	1.51	0.146	4.51	0.94	17.2	17.4
32.0	446	393	1.51	0.146	4.62	0.97	17.6	17.8
32.0	446	273	1.51	0.146	4.46	0.94	17.1	17.3
32.0	446	348	1.51	0.146	4.62	0.98	17.6	17.8
32.0	446	226	1.51	0.146	4.74	1.00	17.9	18.1
0.1 mol/L NaOH + 1.25 wt % POLYOX WSR N750						**3/30/2007**		
32.4	446	349	2.19	0.147	4.47	0.97	17.1	17.3
32.5	446	273	2.19	0.147	4.33	0.94	16.6	16.9
32.5	446	228	2.19	0.147	4.42	0.96	16.9	17.2
32.5	446	182	2.19	0.147	4.44	0.96	17.0	17.2
32.5	446	393	2.19	0.147	4.63	1.02	17.6	17.8

T (°C)	P (kPa)	$P_{CO_2,LM}$ (Pa)	Q (cm^3/s)	u_G (m/s)	k_g' x 10^{10} (kmol/m^2·Pa·s)	Normalized k_g'	K_G/k_G (%)	CO$_2$ Removal (%)
0.1 mol/L NaOH			**6/13/2008**					
27.9	377	210	1.96	0.182	5.22	1.16	16.2	16.3
27.8	377	172	1.96	0.182	5.05	1.13	15.7	15.9
27.8	377	264	1.96	0.182	4.78	1.08	15.0	15.2

B.3 Packed Column Data

The packed column mass transfer area data (Table B.8) and hydraulic data (Table B.9) are grouped by packing and are further differentiated by Separations Research Program (SRP) run numbers (XXYY, with XX denoting the last two digits of the year and YY representing the run number from that year). In the cases where a packing was run multiple times and the system was unpacked and re-packed sometime in between, configuration numbers have been provided to distinguish the particular bed being tested. The bed heights have been included as well.

Table B.8. Packed column experimental data (mass transfer).

L (m³/m²·h)	u_G (m/s)	T_{corr} (°C)	$\Delta P/Z$ (Pa/m)	k_{OH^-} x 10^{-3} (m³/kmol·s)	D_{CO2} x 10^9 (m²/s)	H_{CO2} x 10^{-5} (m³·Pa/kmol)	[OH^-] (kmol/m³)	CO_2 In (ppm)	CO_2 Out (ppm)	a_f	Re_L	We_L x 10^4	Fr_L
M250Y	**SRP 0803**		**Baseline**		**Packing Config. 2**		**3.1 m**						
2.45	1.47	13.5	87	4.07	1.49	21.8	0.1055	411	302	0.67	2.70	10	0.64
5.98	1.47	13.1	91	3.98	1.47	21.6	0.1020	410	286	0.80	6.40	45	1.51
12.25	1.47	12.1	98	3.70	1.42	20.8	0.1009	410	282	0.84	12.54	146	2.96
18.30	1.47	11.7	108	3.60	1.40	20.6	0.1007	409	279	0.88	18.46	284	4.35
24.46	1.47	11.3	124	3.52	1.39	20.3	0.0997	409	276	0.91	24.34	457	5.74
36.63	1.47	11.0	324	3.44	1.37	20.1	0.0974	408	268	0.99	35.79	891	8.44
2.70	0.98	10.2	39	3.27	1.33	19.6	0.0951	408	273	0.66	2.60	11	0.61
6.15	0.98	10.0	41	3.21	1.32	19.4	0.0928	408	250	0.81	5.88	45	1.38
12.23	0.98	9.6	44	3.13	1.30	19.2	0.0928	407	242	0.87	11.53	141	2.72
18.38	0.98	9.4	50	3.09	1.29	19.1	0.0927	407	239	0.89	17.24	278	4.06
24.46	0.98	9.2	59	3.06	1.29	19.0	0.0922	407	234	0.93	22.81	447	5.38
36.66	0.98	9.1	131	3.03	1.28	18.9	0.0917	406	228	0.97	34.01	875	8.02
48.89	0.98	9.0	334	3.01	1.27	18.8	0.0908	406	222	1.03	45.15	1412	10.64
60.96	0.98	8.8	400	2.97	1.26	18.7	0.0895	406	216	1.08	56.00	2036	13.20
2.65	0.59	8.3	16	2.87	1.24	18.4	0.0884	406	207	0.71	2.42	11	0.57
12.22	0.59	8.2	18	2.86	1.24	18.4	0.0873	405	185	0.84	11.13	139	2.62
24.45	0.59	7.9	23	2.80	1.23	18.2	0.0871	405	172	0.92	22.10	442	5.21
36.68	0.58	7.8	43	2.77	1.22	18.1	0.0864	405	171	0.92	33.02	867	7.78
48.87	0.60	7.7	181	2.75	1.21	18.0	0.0854	405	166	0.99	43.81	1397	10.33
61.07	0.60	7.7	292	2.75	1.21	18.0	0.0836	405	162	1.02	54.54	2023	12.85
M250Y	**SRP 0822**		**Baseline**		**Packing Config. 3**		**3.1 m**						
3.18	0.98	31.9	36	12.86	2.46	36.6	0.1011	415	227	0.61	4.80	18	1.13
6.21	0.99	31.8	38	12.82	2.44	36.6	0.0981	417	201	0.75	9.21	55	2.17
12.24	0.98	31.5	40	12.61	2.41	36.3	0.0952	419	192	0.81	17.86	169	4.21
24.49	0.98	31.6	49	12.69	2.41	36.4	0.0941	421	177	0.91	35.50	537	8.37
36.79	0.99	31.8	87	12.83	2.41	36.6	0.0923	422	170	0.97	53.09	1056	12.51
48.84	0.98	31.8	252	12.86	2.41	36.6	0.0913	424	160	1.04	70.46	1694	16.61
61.00	0.98	31.9	316	12.89	2.40	36.6	0.0899	426	157	1.08	87.87	2454	20.71
73.22	0.98	32.0	392	13.01	2.41	36.8	0.0890	428	152	1.12	105.67	3331	24.91
61.15	0.59	32.8	234	13.63	2.44	37.5	0.0853	428	100	0.95	88.79	2477	20.93
48.90	0.59	33.0	173	13.77	2.44	37.6	0.0838	423	104	0.93	70.99	1707	16.73
36.70	0.59	33.0	52	13.78	2.43	37.7	0.0821	418	109	0.90	53.25	1059	12.55

L (m³/m²·h)	u_G (m/s)	T_{corr} (°C)	$\Delta P/Z$ (Pa/m)	k_{OH^-} x 10^{-3} (m³/kmol·s)	D_{CO2} x 10^9 (m²/s)	H_{CO2} x 10^{-5} (m³·Pa/kmol)	[OH⁻] (kmol/m³)	CO_2 In (ppm)	CO_2 Out (ppm)	a_f	Re_L	We_L x 10^4	Fr_L
24.45	0.59	33.0	22	13.84	2.43	37.7	0.0805	413	110	0.89	35.43	538	8.35
12.26	0.58	33.2	16	14.01	2.43	37.9	0.0776	407	122	0.81	17.71	170	4.17
6.20	0.59	33.3	15	14.10	2.42	38.0	0.0759	402	135	0.75	8.94	55	2.11
2.86	0.59	33.4	14	14.19	2.42	38.1	0.0745	397	158	0.64	4.13	15	0.97
2.89	1.48	33.7	76	14.36	2.43	38.3	0.0731	397	278	0.63	4.18	15	0.99
6.19	1.47	33.6	80	14.29	2.42	38.2	0.0717	399	263	0.74	8.82	54	2.08
12.21	1.47	33.2	87	14.02	2.40	37.9	0.0716	401	254	0.81	17.04	167	4.02
24.42	1.47	32.9	105	13.76	2.37	37.6	0.0711	404	246	0.89	33.67	528	7.94
36.69	1.47	32.8	296	13.69	2.36	37.5	0.0690	406	232	1.02	50.13	1037	11.82
48.91	1.47	32.7	362	13.57	2.35	37.3	0.0682	408	230	1.06	66.68	1674	15.72
61.13	1.47	32.5	433	13.48	2.33	37.2	0.0663	410	228	1.11	83.02	2425	19.57
M250Y SRP 0825 Low σ Packing Config. 3 3.1 m													
2.73	0.98	30.6	36	11.93	2.38	35.5	0.1003	414	206	0.73	3.99	32	0.94
6.14	0.98	30.6	39	11.95	2.36	35.5	0.0960	414	183	0.87	8.87	122	2.09
12.19	0.98	30.5	48	11.87	2.34	35.4	0.0947	414	170	0.95	17.30	380	4.08
24.45	0.98	30.5	54	11.85	2.34	35.3	0.0936	410	166	0.98	34.56	1210	8.15
36.69	0.97	30.6	143	11.99	2.34	35.5	0.0913	410	163	1.00	51.65	2378	12.17
48.87	0.98	31.0	395	12.26	2.35	35.8	0.0896	411	154	1.08	68.81	3836	16.22
61.12	0.98	31.3	555	12.44	2.35	36.1	0.0876	411	149	1.13	86.20	5575	20.32
3.01	1.47	31.6	73	12.71	2.36	36.4	0.0854	401	260	0.73	4.28	37	1.01
6.14	1.47	31.8	76	12.88	2.37	36.6	0.0832	401	245	0.83	8.65	121	2.04
12.28	1.47	31.7	83	12.79	2.35	36.5	0.0810	402	235	0.92	17.01	383	4.01
24.50	1.47	31.5	119	12.68	2.33	36.3	0.0795	402	228	0.99	33.64	1206	7.93
36.69	1.47	31.3	302	12.53	2.31	36.1	0.0778	402	217	1.08	50.21	2363	11.84
48.86	1.47	31.3	506	12.52	2.31	36.1	0.0765	402	213	1.14	66.59	3807	15.70
2.40	0.59	32.5	15	13.47	2.36	37.2	0.0724	432	156	0.73	3.30	25	0.78
6.12	0.59	32.7	16	13.62	2.36	37.4	0.0709	430	139	0.82	8.42	120	1.98
12.20	0.59	32.9	17	13.78	2.37	37.6	0.0696	435	132	0.87	16.80	379	3.96
24.47	0.59	33.3	24	14.05	2.38	37.9	0.0693	435	123	0.91	33.79	1210	7.97
M250Y SRP 0824 Intermediate μ_L Packing Config. 3 3.1 m													
2.63	0.98	30.5	36	11.82	2.26	35.4	0.1014	403	212	0.68	0.74	9	0.18
5.80	0.98	30.8	39	12.04	2.27	35.6	0.0983	403	187	0.82	1.64	35	0.39
12.30	0.98	30.6	42	11.90	2.25	35.4	0.0975	403	180	0.87	3.37	121	0.80
18.34	0.98	30.6	43	11.91	2.24	35.4	0.0965	404	175	0.91	4.97	234	1.17
24.53	0.98	30.8	47	12.10	2.25	35.7	0.0953	404	172	0.93	6.62	379	1.56

L (m³/m²·h)	u_G (m/s)	T_{corr} (°C)	ΔP/Z (Pa/m)	k_{OH^-} x 10^{-3} (m³/kmol·s)	D_{CO2} x 10^9 (m²/s)	H_{CO2} x 10^{-5} (m³·Pa/kmol)	[OH⁻] (kmol/m³)	CO_2 In (ppm)	CO_2 Out (ppm)	a_f	Re_L	We_L x 10^4	Fr_L
36.61	0.98	31.1	61	12.27	2.26	35.9	0.0937	404	167	0.96	9.87	740	2.33
48.86	0.98	31.3	68	12.45	2.27	36.1	0.0925	404	164	0.99	13.22	1198	3.12
61.11	0.98	31.6	406	12.67	2.27	36.4	0.0903	402	156	1.04	16.63	1742	3.92
36.60	1.47	31.5	351	12.64	2.26	36.3	0.0871	403	218	1.04	9.92	740	2.34
24.36	1.47	31.6	112	12.68	2.25	36.4	0.0852	403	229	0.97	6.61	378	1.56
18.33	1.47	31.7	100	12.79	2.25	36.5	0.0831	403	233	0.95	4.93	233	1.16
12.24	1.47	31.9	91	12.95	2.25	36.7	0.0812	400	241	0.89	3.29	119	0.77
6.14	1.47	32.1	84	13.07	2.26	36.8	0.0802	400	254	0.80	1.65	38	0.39
2.78	1.47	32.2	80	13.21	2.26	37.0	0.0791	400	275	0.66	0.75	10	0.18
2.84	0.59	32.5	15	13.40	2.27	37.2	0.0781	410	158	0.68	0.77	10	0.18
6.09	0.59	32.5	16	13.44	2.27	37.2	0.0771	410	135	0.80	1.64	37	0.39
12.22	0.59	32.7	17	13.54	2.27	37.3	0.0760	410	128	0.83	3.29	119	0.78
18.26	0.59	32.9	18	13.75	2.28	37.6	0.0752	408	122	0.87	4.97	233	1.17
24.50	0.59	33.1	20	13.89	2.29	37.7	0.0742	409	118	0.90	6.73	381	1.59
36.78	0.59	33.2	25	14.02	2.29	37.9	0.0732	410	113	0.93	10.22	753	2.41
48.88	0.59	33.5	84	14.28	2.31	38.2	0.0722	409	111	0.94	13.72	1213	3.23
61.04	0.59	33.6	365	14.37	2.30	38.3	0.0703	409	109	0.96	17.31	1763	4.08

M250Y — SRP 0805 — High μ_L — Packing Config. 2 — 3.1 m

L (m³/m²·h)	u_G (m/s)	T_{corr} (°C)	ΔP/Z (Pa/m)	k_{OH^-} x 10^{-3} (m³/kmol·s)	D_{CO2} x 10^9 (m²/s)	H_{CO2} x 10^{-5} (m³·Pa/kmol)	[OH⁻] (kmol/m³)	CO_2 In (ppm)	CO_2 Out (ppm)	a_f	Re_L	We_L x 10^4	Fr_L
2.44	0.98	14.7	40	4.38	1.44	22.5	0.0896	391	258	0.65	0.21	7	0.05
6.11	0.98	14.8	42	4.41	1.44	22.6	0.0887	391	240	0.76	0.54	34	0.13
13.06	0.98	14.7	47	4.39	1.44	22.5	0.0885	391	231	0.83	1.12	119	0.26
18.40	0.98	14.8	52	4.43	1.45	22.6	0.0884	391	226	0.86	1.57	210	0.37
24.53	0.98	15.1	50	4.49	1.45	22.8	0.0868	391	217	0.93	2.10	340	0.49
36.48	0.98	15.1	62	4.49	1.45	22.8	0.0859	391	218	0.92	3.12	658	0.74
48.98	0.97	14.7	436	4.40	1.43	22.6	0.0834	391	208	1.02	4.20	1077	0.99
2.50	1.47	14.8	87	4.42	1.42	22.6	0.0801	391	298	0.67	0.22	8	0.05
6.30	1.47	14.9	95	4.45	1.42	22.7	0.0787	391	285	0.79	0.54	35	0.13
12.28	1.47	14.7	104	4.38	1.41	22.5	0.0784	391	278	0.86	1.03	107	0.24
18.44	1.47	14.5	120	4.33	1.40	22.4	0.0781	391	277	0.88	1.54	210	0.36
24.43	1.47	14.6	475	4.37	1.41	22.5	0.0772	391	268	0.96	2.04	335	0.48
2.42	0.59	13.9	16	4.17	1.37	22.0	0.0753	391	192	0.74	0.20	7	0.05
6.12	0.59	13.6	17	4.09	1.35	21.8	0.0734	390	183	0.81	0.51	34	0.12
12.38	0.59	13.5	19	4.05	1.35	21.7	0.0736	390	175	0.86	1.03	108	0.24
24.67	0.59	13.5	26	4.05	1.35	21.7	0.0737	389	163	0.93	2.06	341	0.48
36.79	0.58	13.5	557	4.07	1.35	21.7	0.0733	389	163	0.93	3.07	665	0.72
48.81	0.59	13.8	726	4.15	1.36	21.9	0.0720	388	160	0.96	4.10	1067	0.97

311

L (m³/m²·h)	u_G (m/s)	T_corr (°C)	ΔP/Z (Pa/m)	k_OH- x 10⁻³ (m³/kmol·s)	D_CO2 x 10⁹ (m²/s)	H_CO2 x 10⁻⁵ (m³·Pa/kmol)	[OH⁻] (kmol/m³)	CO2 In (ppm)	CO2 Out (ppm)	a_f	Re_L	We_L x 10⁴	Fr_L
M500Y	**SRP 0807**		**Baseline**		**Packing Config. 2**		**2.8 m**						
2.46	0.98	23.3	82	7.66	1.97	29.2	0.0991	388	180	0.51	1.42	3	0.33
6.05	0.98	23.4	104	7.70	1.96	29.3	0.0951	388	150	0.65	3.45	13	0.81
12.20	0.98	23.3	146	7.64	1.95	29.2	0.0944	388	145	0.67	6.88	43	1.62
18.38	0.97	23.2	343	7.62	1.95	29.1	0.0937	388	146	0.66	10.32	85	2.43
24.47	0.98	23.4	493	7.70	1.94	29.2	0.0898	388	137	0.72	13.62	136	3.21
3.56	0.98	23.3	87	7.68	1.93	29.2	0.0878	386	173	0.57	1.95	5	0.46
2.51	0.98	23.6	210	7.79	1.93	29.4	0.0858	386	250	0.47	1.38	3	0.33
6.07	1.47	23.5	258	7.76	1.92	29.3	0.0838	386	214	0.65	3.31	13	0.78
3.62	1.47	23.3	224	7.69	1.91	29.2	0.0818	386	227	0.59	1.97	6	0.46
12.24	1.47	22.9	338	7.48	1.87	28.8	0.0798	386	207	0.71	6.57	42	1.55
2.45	0.59	22.3	35	7.23	1.84	28.4	0.0782	388	112	0.58	1.30	3	0.31
3.64	0.59	22.3	36	7.20	1.83	28.3	0.0770	388	106	0.61	1.94	6	0.46
6.14	0.59	22.1	41	7.13	1.82	28.2	0.0759	388	94	0.68	3.27	13	0.77
M500Y	**SRP 0808**		**Baseline**		**Packing Config. 2**		**2.8 m**						
2.49	0.98	20.1	83	6.25	1.81	26.6	0.1061	391	204	0.45	1.38	3	0.33
4.32	0.98	20.2	88	6.32	1.81	26.8	0.1042	391	187	0.51	2.39	7	0.56
6.15	0.98	20.4	92	6.37	1.81	26.9	0.1022	391	177	0.55	3.32	13	0.78
12.23	0.98	20.5	101	6.41	1.80	26.9	0.0978	391	159	0.64	6.45	42	1.52
18.32	0.98	20.4	114	6.38	1.79	26.9	0.0964	391	155	0.66	9.56	82	2.25
24.45	0.98	20.6	200	6.47	1.80	27.0	0.0941	391	149	0.69	12.66	132	2.98
30.50	0.97	20.6	414	6.50	1.78	27.1	0.0884	391	155	0.68	15.60	190	3.68
2.42	1.47	20.9	205	6.61	1.79	27.3	0.0875	391	258	0.47	1.24	3	0.29
4.27	1.47	20.9	222	6.61	1.79	27.3	0.0865	390	247	0.51	2.19	7	0.52
6.17	1.47	20.8	241	6.56	1.78	27.2	0.0856	390	239	0.56	3.15	13	0.74
12.16	1.47	20.3	303	6.39	1.75	26.8	0.0845	389	223	0.64	6.06	41	1.43
18.34	1.47	20.3	410	6.37	1.75	26.8	0.0836	388	219	0.67	9.09	80	2.14
2.39	0.59	19.0	34	5.86	1.67	25.8	0.0805	388	142	0.49	1.18	3	0.28
4.36	0.59	18.8	36	5.80	1.66	25.7	0.0786	388	131	0.54	2.15	7	0.51
6.12	0.59	18.7	37	5.75	1.65	25.6	0.0767	388	125	0.57	3.00	13	0.71
12.18	0.58	18.4	41	5.66	1.64	25.4	0.0763	388	110	0.64	5.95	41	1.40
18.36	0.59	18.3	47	5.63	1.62	25.3	0.0733	388	106	0.68	8.92	80	2.10
24.46	0.59	18.2	51	5.57	1.61	25.2	0.0704	388	101	0.72	11.78	129	2.78
30.58	0.58	18.0	218	5.53	1.59	25.1	0.0681	390	114	0.67	14.68	187	3.46

L (m³/m²·h)	uG (m/s)	Tcorr (°C)	ΔP/Z (Pa/m)	kOH- x 10⁻³ (m³/kmol·s)	DCO2 x 10⁹ (m²/s)	HCO2 x 10⁻⁵ (m³·Pa/kmol)	[OH⁻] (kmol/m³)	CO2 In (ppm)	CO2 Out (ppm)	af	ReL	WeL x 10⁴	FrL
M500Y	**SRP 0812**		**Baseline**		**Packing Config. 3**		**2.8 m**						
24.41	0.59	25.0	58	8.50	2.04	30.6	0.0935	393	67	0.70	14.47	138	3.41
18.32	0.59	25.3	47	8.65	2.05	30.8	0.0922	392	72	0.67	10.89	86	2.57
12.26	0.59	25.6	41	8.79	2.06	31.0	0.0897	392	74	0.67	7.30	44	1.72
6.24	0.59	25.7	37	8.89	2.06	31.2	0.0886	392	84	0.62	3.73	14	0.88
2.73	0.59	25.6	33	8.85	2.05	31.1	0.0876	392	107	0.53	1.64	4	0.39
2.42	0.98	30.7	81	12.00	2.39	35.6	0.1028	388	174	0.45	1.54	3	0.36
5.75	0.98	30.6	88	11.90	2.37	35.4	0.1000	388	147	0.55	3.64	13	0.86
12.17	0.98	30.2	102	11.64	2.33	35.1	0.0973	388	136	0.61	7.60	44	1.79
18.37	0.98	30.2	113	11.70	2.31	35.1	0.0926	388	125	0.68	11.45	88	2.70
24.45	0.98	30.4	123	11.79	2.32	35.3	0.0915	388	126	0.68	15.22	142	3.59
30.53	0.98	30.4	158	11.84	2.31	35.3	0.0896	386	125	0.68	19.02	206	4.48
36.64	0.98	30.5	195	11.93	2.31	35.4	0.0881	386	123	0.70	22.85	279	5.39
24.49	0.98	30.8	151	12.15	2.30	35.7	0.0824	386	125	0.71	15.34	143	3.62
12.19	0.98	30.9	96	12.20	2.30	35.7	0.0807	386	137	0.66	7.65	45	1.80
2.59	0.98	31.2	77	12.40	2.31	36.0	0.0794	384	185	0.47	1.64	3	0.39
M500Y	**SRP 0813**		**Low σ**		**Packing Config. 3**		**2.8 m**						
2.37	0.98	25.4	73	8.68	2.08	30.9	0.0983	390	164	0.55	1.41	7	0.33
6.02	0.98	25.7	79	8.87	2.08	31.2	0.0940	390	130	0.72	3.59	31	0.85
12.06	0.98	25.8	89	8.93	2.08	31.2	0.0921	390	120	0.77	7.19	100	1.69
18.32	0.98	26.5	100	9.32	2.10	31.8	0.0885	389	113	0.82	11.06	201	2.61
24.89	0.98	26.5	156	9.35	2.09	31.9	0.0851	389	118	0.81	15.13	336	3.57
30.53	0.98	26.7	129	9.46	2.09	32.0	0.0837	389	109	0.87	18.62	474	4.39
36.68	0.99	26.9	273	9.55	2.09	32.1	0.0825	389	108	0.88	22.43	644	5.29
12.22	0.98	27.0	85	9.63	2.08	32.3	0.0780	389	124	0.80	7.52	103	1.77
2.45	0.98	27.4	71	9.87	2.10	32.6	0.0771	389	167	0.59	1.52	7	0.36
M500Y	**SRP 0818**		**Intermediate μL**		**Packing Config. 3**		**2.8 m**						
2.67	0.98	31.0	77	12.21	2.28	35.8	0.1017	390	150	0.55	0.35	3	0.08
4.37	0.98	31.0	82	12.23	2.26	35.9	0.0963	390	132	0.65	0.58	8	0.14
6.09	0.98	30.7	85	12.06	2.24	35.6	0.0939	390	121	0.71	0.80	13	0.19
9.11	0.98	30.6	91	11.94	2.22	35.5	0.0931	390	117	0.74	1.19	26	0.28
12.16	0.98	30.4	95	11.83	2.21	35.3	0.0929	390	117	0.74	1.58	42	0.37
18.32	0.98	30.5	102	11.88	2.21	35.4	0.0912	390	113	0.77	2.38	83	0.56
24.51	0.98	30.5	135	11.89	2.20	35.4	0.0895	390	112	0.78	3.18	136	0.75
2.51	1.47	31.2	171	12.47	2.22	36.1	0.0821	387	216	0.56	0.33	3	0.08

313

L (m³/m²·h)	u_G (m/s)	T_{corr} (°C)	ΔP/Z (Pa/m)	k_{OH^-} x 10⁻³ (m³/kmol·s)	D_{CO2} x 10⁹ (m²/s)	H_{CO2} x 10⁻⁵ (m³·Pa/kmol)	[OH⁻] (kmol/m³)	CO_2 In (ppm)	CO_2 Out (ppm)	a_f	Re_L	We_L x 10⁴	Fr_L
4.09	1.47	31.3	178	12.55	2.21	36.2	0.0788	387	209	0.61	0.54	7	0.13
5.97	1.47	31.3	188	12.51	2.19	36.1	0.0755	387	198	0.68	0.78	13	0.18
9.05	1.47	31.0	200	12.31	2.16	35.9	0.0722	387	195	0.71	1.17	26	0.27
12.23	1.47	30.4	216	11.87	2.12	35.3	0.0715	387	196	0.72	1.56	43	0.37
18.34	1.47	30.1	308	11.70	2.10	35.1	0.0696	388	193	0.76	2.33	83	0.55
2.70	0.59	29.9	32	11.54	2.09	34.9	0.0683	388	88	0.65	0.35	3	0.08
6.09	0.59	30.2	34	11.75	2.10	35.1	0.0671	388	77	0.71	0.78	13	0.18
12.23	0.58	30.3	37	11.84	2.10	35.2	0.0658	388	74	0.73	1.57	43	0.37
18.38	0.59	30.2	45	11.76	2.08	35.1	0.0634	388	72	0.77	2.36	84	0.56
2.48	0.59	29.9	32	11.60	2.06	34.9	0.0616	385	106	0.60	0.32	3	0.08
M500Y **SRP 0816** **High μ_L**					**Packing Config. 3**		**2.8 m**						
2.50	0.98	28.5	82	10.50	2.11	33.6	0.1015	390	154	0.57	0.15	2	0.04
4.32	0.98	28.6	87	10.57	2.10	33.7	0.0980	390	144	0.62	0.26	6	0.06
6.28	0.98	28.3	92	10.39	2.07	33.4	0.0946	390	137	0.67	0.37	11	0.09
9.11	0.98	27.9	97	10.18	2.04	33.1	0.0929	390	137	0.68	0.52	21	0.12
12.33	0.98	27.9	102	10.18	2.04	33.1	0.0920	390	137	0.68	0.69	35	0.16
18.34	0.99	28.0	117	10.23	2.04	33.2	0.0903	390	133	0.71	1.02	67	0.24
24.34	0.97	28.1	247	10.28	2.03	33.2	0.0886	390	134	0.70	1.35	108	0.32
30.53	0.98	28.5	438	10.57	2.05	33.6	0.0865	390	139	0.69	1.69	157	0.40
36.66	0.98	28.8	680	10.78	2.06	33.9	0.0839	387	126	0.75	2.04	214	0.48
2.63	1.47	29.1	176	10.98	2.06	34.2	0.0809	387	230	0.53	0.15	3	0.03
4.23	1.47	29.3	186	11.07	2.05	34.3	0.0780	387	226	0.56	0.24	6	0.06
6.11	1.47	28.9	196	10.87	2.03	34.0	0.0751	387	218	0.61	0.34	11	0.08
9.10	1.47	28.5	210	10.61	1.99	33.6	0.0722	387	214	0.65	0.48	21	0.11
12.18	1.47	28.3	225	10.50	1.98	33.5	0.0714	388	215	0.65	0.64	34	0.15
2.41	0.59	28.3	31	10.46	1.98	33.4	0.0704	388	101	0.60	0.13	2	0.03
6.10	0.59	28.2	35	10.38	1.97	33.3	0.0695	388	90	0.66	0.33	11	0.08
12.33	0.59	28.0	39	10.26	1.94	33.1	0.0665	388	88	0.69	0.66	34	0.15
18.44	0.59	27.2	57	9.81	1.90	32.5	0.0647	387	89	0.71	1.00	68	0.23
M250X **SRP 0905** **Baseline**							**3.1 m**						
3.21	0.98	19.1	17	5.86	1.76	25.9	0.0998	437	263	0.67	3.92	18	1.13
6.10	0.98	18.4	17	5.61	1.71	25.3	0.0966	413	234	0.77	7.35	52	2.12
12.15	0.98	18.2	18	5.55	1.69	25.2	0.0935	413	231	0.81	14.34	164	4.14
18.33	0.98	17.9	20	5.44	1.68	25.0	0.0930	410	223	0.86	21.41	323	6.18
24.45	0.98	17.6	22	5.34	1.66	24.7	0.0923	406	215	0.90	28.31	521	8.17

L (m³/m²·h)	u_G (m/s)	T_{corr} (°C)	$\Delta P/Z$ (Pa/m)	k_{OH^-} x 10^{-3} (m³/kmol·s)	D_{CO2} x 10^9 (m²/s)	H_{CO2} x 10^{-5} (m³·Pa/kmol)	$[OH^-]$ (kmol/m³)	CO_2 In (ppm)	CO_2 Out (ppm)	a_f	Re_L	We_L x 10^4	Fr_L
36.63	0.98	17.3	29	5.22	1.64	24.5	0.0909	399	205	0.96	42.00	1018	12.13
48.83	0.99	17.1	50	5.17	1.63	24.4	0.0898	400	200	1.02	55.61	1641	16.05
67.30	0.98	17.5	150	5.29	1.63	24.6	0.0837	401	198	1.06	76.06	2798	21.96
2.42	2.29	20.0	74	6.22	1.74	26.5	0.0820	402	327	0.70	2.72	11	0.79
4.30	2.29	20.7	72	6.52	1.77	27.1	0.0803	398	323	0.68	4.81	28	1.39
6.08	2.29	21.3	71	6.79	1.80	27.6	0.0785	394	312	0.75	6.75	51	1.95
9.19	2.28	22.1	74	7.11	1.83	28.2	0.0778	396	310	0.78	10.22	101	2.95
12.24	2.29	22.7	77	7.41	1.86	28.7	0.0775	393	309	0.76	13.68	163	3.95
24.36	2.30	23.2	91	7.62	1.88	29.1	0.0761	394	303	0.85	27.29	514	7.88
36.74	2.29	23.5	110	7.79	1.89	29.3	0.0744	394	297	0.91	41.26	1022	11.91
48.79	2.29	23.8	160	7.92	1.90	29.5	0.0738	392	288	0.99	55.10	1643	15.91
61.03	1.47	23.6	166	7.85	1.89	29.4	0.0724	392	239	1.03	69.55	2397	20.08
36.66	1.47	23.8	56	7.94	1.89	29.6	0.0708	393	251	0.94	41.88	1027	12.09
24.44	1.47	23.7	41	7.89	1.88	29.5	0.0690	392	259	0.90	27.88	522	8.05
18.34	1.47	23.7	37	7.92	1.87	29.5	0.0671	391	264	0.86	20.87	324	6.02
12.25	1.47	23.8	35	7.94	1.87	29.6	0.0656	391	272	0.80	13.92	165	4.02
6.08	1.47	23.8	35	7.97	1.87	29.6	0.0652	391	283	0.73	6.91	51	2.00
3.02	1.47	24.0	32	8.02	1.87	29.7	0.0647	390	296	0.63	3.44	16	0.99
2.33	0.98	23.8	16	7.95	1.86	29.6	0.0643	390	262	0.61	2.66	10	0.77
M250X SRP 0906 Low σ						**3.1 m**							
2.73	0.98	22.6	17	7.29	1.93	28.6	0.0985	397	228	0.68	3.44	33	0.99
4.14	0.98	22.4	17	7.21	1.91	28.4	0.0956	396	217	0.75	5.14	67	1.48
6.06	0.98	22.2	17	7.15	1.90	28.3	0.0926	396	212	0.79	7.35	125	2.12
9.16	0.98	21.9	18	7.00	1.87	28.0	0.0897	395	208	0.83	10.86	247	3.14
12.22	0.98	21.8	19	6.97	1.86	28.0	0.0890	396	206	0.86	14.39	399	4.16
18.32	0.98	21.7	41	6.91	1.85	27.8	0.0883	396	200	0.90	21.44	781	6.19
24.42	0.98	21.9	25	7.01	1.85	28.0	0.0843	396	192	0.95	28.31	1259	8.17
36.61	0.99	21.7	219	6.95	1.83	27.9	0.0818	395	194	0.97	42.31	2472	12.21
48.67	0.98	21.7	347	6.95	1.82	27.9	0.0802	394	191	0.99	56.16	3972	16.21
60.88	0.98	22.0	463	7.09	1.83	28.1	0.0777	395	192	1.01	70.36	5775	20.31
12.23	0.98	22.1	18	7.12	1.83	28.2	0.0761	395	206	0.91	14.11	398	4.07
2.90	1.47	22.5	31	7.29	1.84	28.5	0.0746	397	288	0.67	3.36	36	0.97
6.07	1.47	22.2	33	7.18	1.82	28.3	0.0730	397	275	0.80	6.95	124	2.01
9.15	1.47	22.0	34	7.07	1.81	28.1	0.0714	396	271	0.83	10.25	243	2.96
12.22	1.47	21.7	35	6.97	1.79	27.9	0.0705	396	269	0.85	13.48	392	3.89
18.44	1.47	21.5	45	6.88	1.78	27.7	0.0700	396	263	0.91	20.19	776	5.83

315

L (m³/m²·h)	u_G (m/s)	T_{corr} (°C)	ΔP/Z (Pa/m)	k_{OH^-} x 10^{-3} (m³/kmol·s)	D_{CO2} x 10^9 (m²/s)	H_{CO2} x 10^{-5} (m³·Pa/kmol)	[OH⁻] (kmol/m³)	CO_2 In (ppm)	CO_2 Out (ppm)	a_f	Re_L	We_L x 10^4	Fr_L
24.41	1.47	21.4	104	6.83	1.77	27.6	0.0689	396	261	0.97	26.57	1237	7.67
36.59	1.47	21.5	291	6.87	1.77	27.7	0.0675	397	258	1.01	39.61	2426	11.44
48.69	1.47	21.6	401	6.92	1.77	27.8	0.0670	396	252	1.05	52.69	3905	15.21
24.51	1.47	21.7	135	6.94	1.77	27.8	0.0664	397	268	0.92	26.49	1244	7.65
M250X	**SRP 0908**		**High μ_L**			**3.1 m**							
2.80	1.47	23.0	34	7.50	1.83	28.9	0.1024	392	273	0.68	0.33	11	0.09
4.23	1.47	23.5	36	7.74	1.84	29.4	0.0998	390	266	0.72	0.49	22	0.14
6.12	1.47	23.4	36	7.69	1.83	29.2	0.0972	390	262	0.76	0.70	41	0.20
9.46	1.47	22.8	39	7.43	1.79	28.8	0.0946	390	259	0.81	1.05	84	0.30
13.06	1.47	22.6	40	7.32	1.77	28.6	0.0920	390	257	0.84	1.43	144	0.41
18.42	1.47	22.3	43	7.18	1.75	28.3	0.0909	390	253	0.88	2.01	255	0.58
24.70	1.47	22.2	50	7.14	1.74	28.3	0.0893	390	249	0.92	2.69	415	0.78
36.54	1.47	22.1	99	7.11	1.73	28.2	0.0876	391	245	0.98	3.97	797	1.15
48.95	1.47	22.3	437	7.20	1.74	28.3	0.0860	390	236	1.06	5.34	1300	1.54
3.20	0.99	22.6	17	7.37	1.75	28.6	0.0838	390	233	0.73	0.35	14	0.10
6.11	0.99	22.6	18	7.35	1.74	28.6	0.0815	388	226	0.78	0.67	41	0.19
8.72	0.99	22.5	19	7.33	1.73	28.6	0.0793	388	223	0.82	0.95	73	0.28
12.15	0.98	22.5	20	7.31	1.72	28.5	0.0770	388	220	0.84	1.33	128	0.38
18.32	0.98	22.5	21	7.31	1.71	28.5	0.0761	388	213	0.89	2.01	254	0.58
24.60	0.98	22.4	24	7.29	1.71	28.5	0.0747	388	209	0.94	2.71	415	0.78
36.58	0.98	22.4	29	7.26	1.70	28.4	0.0734	388	206	0.96	4.04	806	1.17
48.97	0.99	22.5	151	7.33	1.70	28.5	0.0722	387	198	1.04	5.45	1314	1.57
60.88	0.98	22.7	363	7.44	1.71	28.7	0.0717	388	194	1.06	6.83	1894	1.97
2.86	0.59	22.9	7	7.51	1.70	28.8	0.0674	389	180	0.73	0.32	12	0.09
12.78	0.59	22.7	9	7.44	1.69	28.7	0.0654	388	160	0.86	1.44	141	0.42
24.24	0.59	22.5	10	7.35	1.68	28.6	0.0651	389	151	0.93	2.73	409	0.79
36.82	0.59	22.6	12	7.37	1.67	28.6	0.0630	390	147	0.97	4.16	823	1.20
MP252Y	**SRP 0913**		**Baseline**			**3.0 m**							
2.71	1.47	26.0	57	8.99	2.12	31.4	0.0974	391	276	0.64	4.04	14	0.95
4.38	1.47	26.2	58	9.11	2.12	31.6	0.0951	390	267	0.71	6.47	31	1.52
6.22	1.48	26.1	59	9.07	2.11	31.5	0.0927	392	262	0.76	9.06	55	2.13
9.18	1.47	25.8	61	8.90	2.08	31.2	0.0904	394	259	0.81	13.12	104	3.09
12.23	1.47	25.5	64	8.77	2.06	31.0	0.0880	392	257	0.83	17.26	167	4.07
18.32	1.47	25.6	69	8.80	2.05	31.0	0.0868	392	253	0.87	25.70	327	6.06
24.45	1.47	25.8	74	8.91	2.06	31.2	0.0856	391	250	0.89	34.25	528	8.07

L (m³/m²·h)	u_G (m/s)	T_{corr} (°C)	$\Delta P/Z$ (Pa/m)	$k_{OH^-} \times 10^{-3}$ (m³/kmol·s)	$D_{CO2} \times 10^9$ (m²/s)	$H_{CO2} \times 10^{-5}$ (m³·Pa/kmol)	[OH⁻] (kmol/m³)	CO_2 In (ppm)	CO_2 Out (ppm)	a_f	Re_L	$We_L \times 10^4$	Fr_L
36.67	1.47	25.9	94	8.96	2.06	31.3	0.0842	392	242	0.96	51.38	1039	12.11
48.88	1.47	26.1	142	9.12	2.07	31.5	0.0825	391	237	1.01	68.57	1679	16.16
61.09	1.47	26.3	203	9.19	2.07	31.6	0.0812	390	230	1.08	85.94	2440	20.26
61.20	0.98	26.9	150	9.56	2.08	32.2	0.0754	388	182	1.06	87.21	2467	20.56
48.91	0.98	27.0	90	9.63	2.08	32.3	0.0743	389	185	1.04	69.61	1698	16.41
36.67	0.98	27.0	52	9.64	2.07	32.3	0.0728	387	191	1.00	52.02	1050	12.26
24.48	0.98	27.0	36	9.65	2.06	32.3	0.0708	387	200	0.95	34.57	535	8.15
18.31	0.98	27.1	32	9.70	2.05	32.3	0.0662	389	207	0.94	25.63	329	6.04
12.22	0.98	27.2	30	9.74	2.05	32.4	0.0655	391	216	0.89	17.04	167	4.02
9.17	0.98	27.2	28	9.76	2.04	32.4	0.0645	389	222	0.85	12.76	104	3.01
5.85	0.98	27.3	28	9.82	2.05	32.5	0.0635	386	229	0.80	8.14	49	1.92
2.53	0.98	27.1	27	9.73	2.03	32.4	0.0625	387	250	0.67	3.52	12	0.83
4.50	0.59	27.4	11	9.87	2.04	32.6	0.0615	388	173	0.75	6.25	32	1.47
12.23	0.59	26.9	13	9.62	2.02	32.2	0.0613	388	162	0.83	16.82	167	3.97
24.42	0.59	26.9	15	9.62	2.01	32.2	0.0605	386	149	0.90	33.63	529	7.93
48.88	0.59	27.1	49	9.73	2.02	32.4	0.0603	385	137	0.97	67.61	1685	15.94
MP252Y			**SRP 0914**	**Low σ**	**3.0 m**								
2.74	0.98	27.9	27	10.14	2.23	33.1	0.0959	388	211	0.72	4.20	34	0.99
6.11	0.98	28.2	29	10.31	2.23	33.3	0.0928	386	193	0.83	9.23	130	2.18
9.71	0.98	27.7	33	9.98	2.19	32.8	0.0897	385	187	0.89	14.33	278	3.38
12.22	0.98	27.4	49	9.85	2.17	32.6	0.0888	386	181	0.95	17.79	407	4.19
18.34	0.98	27.4	34	9.85	2.16	32.6	0.0872	386	179	0.97	26.53	799	6.25
24.46	0.98	27.4	39	9.82	2.15	32.6	0.0856	385	177	1.00	35.32	1290	8.33
36.64	0.99	27.4	257	9.81	2.14	32.6	0.0844	385	177	1.01	52.54	2528	12.38
48.87	0.98	27.6	396	9.93	2.15	32.7	0.0836	386	170	1.07	70.13	4089	16.53
2.35	1.47	27.5	57	9.93	2.14	32.7	0.0801	388	274	0.70	3.41	26	0.80
4.38	1.47	27.9	57	10.17	2.14	33.0	0.0766	383	266	0.74	6.33	74	1.49
6.11	1.47	27.9	58	10.16	2.12	33.0	0.0732	387	258	0.84	8.72	128	2.06
9.18	1.47	27.5	62	9.95	2.10	32.7	0.0724	385	254	0.88	12.86	251	3.03
12.29	1.48	27.1	65	9.67	2.07	32.3	0.0716	385	252	0.91	16.95	405	3.99
18.33	1.48	26.8	79	9.53	2.05	32.1	0.0708	386	247	0.97	25.11	788	5.92
24.45	1.47	26.8	175	9.50	2.05	32.0	0.0702	385	242	1.01	33.37	1272	7.87
36.62	1.47	26.8	336	9.49	2.04	32.0	0.0688	384	233	1.11	49.90	2492	11.76
48.86	1.47	26.9	447	9.59	2.04	32.2	0.0667	385	227	1.18	66.62	4032	15.70
4.18	0.59	27.5	11	9.92	2.06	32.6	0.0647	387	161	0.79	5.80	67	1.37

L (m³/m²·h)	u_G (m/s)	T_{corr} (°C)	$\Delta P/Z$ (Pa/m)	k_{OH^-} x 10⁻³ (m³/kmol·s)	D_{CO2} x 10⁹ (m²/s)	H_{CO2} x 10⁻⁵ (m³·Pa/kmol)	[OH⁻] (kmol/m³)	CO_2 In (ppm)	CO_2 Out (ppm)	a_f	Re_L	We_L x 10⁴	Fr_L
12.20	0.59	27.3	13	9.80	2.05	32.5	0.0641	384	147	0.88	16.77	401	3.95
MP252Y	**SRP 0916**	**High μL**				**3.0 m**							
3.26	0.98	31.3	28	12.42	2.27	36.1	0.1005	392	215	0.68	0.52	15	0.12
4.28	0.99	31.6	28	12.68	2.28	36.4	0.0975	389	208	0.71	0.67	24	0.16
9.22	0.98	31.1	31	12.26	2.23	35.9	0.0944	391	193	0.83	1.38	84	0.32
12.16	0.98	30.3	32	11.70	2.17	35.2	0.0914	391	193	0.86	1.76	132	0.42
18.37	0.98	29.9	34	11.46	2.15	34.8	0.0902	390	191	0.88	2.63	261	0.62
24.49	0.99	29.7	36	11.35	2.14	34.7	0.0901	391	188	0.91	3.48	421	0.82
36.74	0.98	29.7	44	11.32	2.13	34.6	0.0884	389	180	0.97	5.20	827	1.23
48.69	0.98	29.7	93	11.34	2.12	34.7	0.0865	389	176	1.00	6.91	1324	1.63
61.18	0.98	29.9	212	11.45	2.12	34.8	0.0851	390	171	1.05	8.77	1944	2.07
2.93	1.47	29.9	59	11.47	2.12	34.8	0.0837	392	279	0.66	0.43	12	0.10
4.25	1.47	29.9	60	11.46	2.11	34.8	0.0823	392	273	0.71	0.62	23	0.15
6.25	1.47	29.8	62	11.41	2.10	34.7	0.0809	391	267	0.75	0.89	43	0.21
12.43	1.47	29.2	68	10.99	2.06	34.2	0.0795	391	258	0.84	1.68	134	0.40
18.36	1.47	28.4	73	10.52	2.02	33.5	0.0781	391	257	0.86	2.44	255	0.57
24.51	1.47	28.4	81	10.48	2.01	33.5	0.0775	390	254	0.90	3.23	412	0.76
36.70	1.47	28.3	154	10.48	2.00	33.4	0.0759	391	246	0.98	4.82	808	1.14
48.80	1.47	28.4	401	10.49	2.00	33.5	0.0748	391	240	1.04	6.43	1300	1.52
6.12	0.59	28.9	12	10.86	2.02	34.0	0.0725	393	162	0.76	0.83	41	0.20
9.23	0.59	28.8	13	10.80	2.01	33.9	0.0702	390	159	0.78	1.25	82	0.29
24.56	0.59	28.8	16	10.75	2.00	33.8	0.0699	390	145	0.87	3.31	418	0.78
61.01	0.59	29.0	42	10.91	2.01	34.0	0.0679	390	130	0.97	8.37	1915	1.97
M250YS	**SRP 0902**			**Baseline**		**3.1 m**							
3.15	0.98	18.8	33	5.76	1.75	25.7	0.1015	393	250	0.59	3.89	16	0.92
6.15	0.98	18.7	34	5.73	1.73	25.6	0.0984	393	234	0.69	7.45	50	1.76
9.08	0.98	18.5	35	5.64	1.71	25.4	0.0954	393	230	0.72	10.58	94	2.49
12.23	0.98	18.7	36	5.71	1.72	25.5	0.0946	392	228	0.74	14.08	153	3.32
18.27	0.98	18.8	38	5.74	1.72	25.6	0.0941	392	219	0.79	20.82	298	4.91
24.44	0.98	18.8	40	5.75	1.72	25.6	0.0934	391	213	0.82	27.66	483	6.52
36.63	0.98	18.9	51	5.80	1.72	25.7	0.0922	391	203	0.90	41.25	946	9.72
48.87	0.98	19.2	81	5.90	1.73	25.9	0.0906	392	197	0.94	54.99	1530	12.96
61.05	0.98	19.3	132	5.97	1.73	26.0	0.0881	392	190	1.00	68.60	2219	16.17
48.83	1.47	19.4	141	6.01	1.73	26.1	0.0869	392	247	0.96	54.25	1524	12.79
36.71	1.47	19.5	103	6.02	1.73	26.1	0.0852	392	253	0.92	39.90	940	9.41

318

L	u_G	T_{corr}	$\Delta P/Z$	k_{OH^-} x 10^{-3}	D_{CO2} x 10^9	H_{CO2} x 10^{-5}	$[OH^-]$	CO_2 In	CO_2 Out	a_f	Re_L	We_L x 10^4	Fr_L
($m^3/m^2 \cdot h$)	(m/s)	(°C)	(Pa/m)	($m^3/kmol \cdot s$)	(m^2/s)	($m^3 \cdot Pa/kmol$)	($kmol/m^3$)	(ppm)	(ppm)				
24.47	1.47	19.3	83	5.97	1.71	26.0	0.0829	393	261	0.87	25.82	472	6.09
18.32	1.48	19.2	78	5.93	1.70	25.9	0.0804	393	267	0.84	19.15	290	4.51
12.22	1.47	19.2	74	5.92	1.69	25.9	0.0782	393	274	0.80	12.67	147	2.99
9.16	1.47	18.9	72	5.81	1.67	25.7	0.0771	392	280	0.76	9.43	91	2.22
6.16	1.47	18.7	71	5.74	1.66	25.5	0.0759	392	287	0.72	6.30	47	1.49
4.18	1.47	18.5	69	5.68	1.65	25.4	0.0747	392	294	0.66	4.27	25	1.01
3.19	1.47	18.2	69	5.58	1.63	25.2	0.0736	392	302	0.61	3.27	16	0.77
3.09	0.59	18.0	13	5.48	1.62	25.0	0.0724	393	203	0.63	3.13	15	0.74
6.10	0.59	18.0	14	5.50	1.62	25.0	0.0716	393	188	0.70	6.17	46	1.45
12.27	0.58	18.1	14	5.53	1.62	25.1	0.0710	391	179	0.74	12.44	148	2.93
24.44	0.59	18.2	17	5.59	1.62	25.2	0.0694	391	163	0.84	24.79	465	5.84
48.71	0.58	18.1	51	5.55	1.61	25.1	0.0689	391	151	0.91	49.23	1468	11.60
4.37	0.58	17.8	13	5.41	1.59	24.8	0.0681	394	199	0.67	4.43	26	1.04
M250YS	**SRP 0903**		**Low σ**		**3.1 m**								
3.55	0.99	26.3	31	9.17	2.13	31.7	0.1017	395	221	0.66	4.73	49	1.12
6.11	0.98	26.0	33	9.01	2.11	31.4	0.0992	395	199	0.78	7.96	120	1.88
12.22	0.99	25.3	35	8.68	2.06	30.9	0.0966	394	194	0.83	15.39	377	3.63
18.39	0.98	25.2	37	8.64	2.05	30.8	0.0941	394	188	0.87	22.95	743	5.41
24.42	0.98	25.1	45	8.59	2.04	30.7	0.0932	393	182	0.91	30.23	1188	7.13
36.67	0.99	24.9	186	8.45	2.02	30.5	0.0913	393	180	0.96	45.10	2336	10.63
9.15	0.98	24.9	34	8.47	2.00	30.5	0.0869	394	201	0.83	11.19	231	2.64
4.49	0.98	24.7	33	8.39	1.98	30.4	0.0846	392	218	0.75	5.46	70	1.29
3.18	1.47	24.9	67	8.46	1.98	30.5	0.0822	392	275	0.68	3.85	40	0.91
4.40	1.47	24.5	68	8.29	1.96	30.2	0.0799	393	271	0.74	5.28	68	1.24
6.12	1.47	24.1	71	8.07	1.92	29.8	0.0776	393	264	0.81	7.18	117	1.69
9.20	1.47	23.8	75	7.92	1.91	29.6	0.0773	394	261	0.84	10.50	228	2.48
12.20	1.47	23.4	79	7.73	1.88	29.2	0.0757	394	259	0.88	13.75	364	3.24
18.33	1.47	22.9	91	7.52	1.86	28.9	0.0746	393	258	0.90	20.47	715	4.82
24.46	1.48	22.6	109	7.36	1.84	28.6	0.0735	393	253	0.95	27.16	1155	6.40
36.64	1.47	22.2	202	7.16	1.81	28.2	0.0731	393	247	1.01	40.46	2261	9.54
24.59	0.59	21.6	29	6.92	1.78	27.8	0.0721	394	144	0.90	27.42	1168	6.46
12.21	0.59	21.4	16	6.83	1.76	27.6	0.0687	394	156	0.85	13.61	364	3.21
6.07	0.59	21.2	15	6.77	1.75	27.5	0.0678	395	168	0.79	6.76	113	1.59
3.96	0.59	21.1	14	6.73	1.74	27.4	0.0669	395	180	0.74	4.41	56	1.04
M125Y	**SRP 0910**		**Baseline**		**3.2 m**								
3.00	0.98	25.8	18	8.91	2.11	31.2	0.1002	394	291	0.69	8.78	57	2.07

319

L (m³/m²·h)	u_G (m/s)	T_{corr} (°C)	$\Delta P/Z$ (Pa/m)	k_{OH^-} x 10^{-3} (m³/kmol·s)	D_{CO2} x 10^9 (m²/s)	H_{CO2} x 10^{-5} (m³·Pa/kmol)	$[OH^-]$ (kmol/m³)	CO_2 In (ppm)	CO_2 Out (ppm)	a_f	Re_L	We_L x 10^4	Fr_L
SRP 0911													
6.14	0.98	25.9	19	8.97	2.11	31.3	0.0984	394	278	0.81	17.76	189	4.19
9.19	0.98	25.6	19	8.80	2.08	31.0	0.0965	394	274	0.84	26.19	368	6.17
12.23	0.98	25.4	20	8.71	2.07	30.9	0.0947	392	270	0.88	34.60	591	8.15
18.35	0.98	25.5	21	8.74	2.07	30.9	0.0945	392	263	0.95	51.78	1161	12.20
24.46	0.98	25.5	22	8.77	2.07	31.0	0.0937	392	259	0.99	68.99	1875	16.26
36.65	0.98	25.6	29	8.82	2.07	31.1	0.0928	391	251	1.06	103.45	3681	24.38
48.83	0.98	25.5	44	8.77	2.06	31.0	0.0920	390	246	1.11	138.07	5946	32.54
61.08	0.98	25.5	67	8.77	2.06	31.0	0.0910	390	242	1.16	173.10	8646	40.80
72.49	0.98	25.6	90	8.81	2.06	31.0	0.0898	389	235	1.23	206.31	11528	48.63
3.05	1.47	25.2	37	8.63	2.03	30.8	0.0882	389	320	0.73	8.69	59	2.05
4.26	1.47	25.2	38	8.63	2.02	30.8	0.0866	387	315	0.77	12.01	102	2.83
6.14	1.47	25.1	38	8.58	2.01	30.7	0.0849	387	312	0.82	17.11	187	4.03
9.14	1.48	24.8	39	8.41	1.99	30.4	0.0833	386	309	0.86	25.12	361	5.92
12.26	1.47	24.6	41	8.30	1.98	30.2	0.0830	387	307	0.91	33.46	588	7.89
18.36	1.47	24.5	43	8.24	1.97	30.1	0.0825	386	301	0.98	49.90	1150	11.76
24.45	1.47	24.7	46	8.35	1.98	30.3	0.0817	385	299	1.00	66.38	1853	15.65
36.66	1.47	24.6	57	8.31	1.97	30.2	0.0809	386	294	1.08	99.57	3642	23.47
48.91	1.48	24.7	75	8.35	1.97	30.3	0.0800	387	289	1.16	132.93	5892	31.33
60.99	1.47	24.8	99	8.44	1.97	30.4	0.0789	389	287	1.22	166.14	8524	39.16
3.19	0.58	25.3	7	8.71	1.99	30.8	0.0775	389	246	0.72	8.75	62	2.06
12.19	0.59	25.2	8	8.62	1.98	30.7	0.0762	388	225	0.88	33.35	584	7.86
24.50	0.59	25.1	9	8.59	1.97	30.7	0.0757	388	210	1.01	67.10	1871	15.82
72.12	0.59	25.2	60	8.66	1.98	30.8	0.0749	387	186	1.20	199.12	11355	46.93
M125Y					**3.2 m**								
					Low σ								
2.83	0.98	30.1	17	11.56	2.35	35.0	0.0996	391	276	0.73	9.27	128	2.19
6.09	0.99	30.5	18	11.86	2.36	35.4	0.0967	390	261	0.86	19.71	457	4.65
9.21	0.98	30.2	19	11.61	2.34	35.1	0.0962	391	255	0.91	29.39	907	6.93
12.25	0.98	29.9	20	11.42	2.32	34.8	0.0959	389	252	0.93	38.82	1457	9.15
18.37	0.98	29.9	22	11.44	2.32	34.8	0.0954	391	245	1.01	57.93	2858	13.66
24.41	0.99	29.8	29	11.35	2.31	34.7	0.0947	391	242	1.05	76.80	4589	18.10
36.63	0.98	29.6	50	11.25	2.30	34.6	0.0934	390	235	1.12	114.93	9018	27.09
48.74	0.98	29.7	75	11.28	2.29	34.6	0.0924	389	230	1.17	152.93	14522	36.05
61.02	0.98	29.8	106	11.39	2.30	34.8	0.0908	389	223	1.23	192.13	21153	45.29
2.84	1.47	30.1	37	11.57	2.30	35.0	0.0884	388	308	0.78	8.96	127	2.11
4.39	1.47	30.1	39	11.62	2.29	35.0	0.0859	386	305	0.81	13.78	263	3.25
6.15	1.47	30.1	41	11.58	2.28	35.0	0.0834	387	300	0.88	19.03	460	4.49

L (m³/m²·h)	u_G (m/s)	T_{corr} (°C)	$\Delta P/Z$ (Pa/m)	$k_{OH^-} \times 10^{-3}$ (m³/kmol·s)	$D_{CO2} \times 10^9$ (m²/s)	$H_{CO2} \times 10^{-5}$ (m³·Pa/kmol)	$[OH^-]$ (kmol/m³)	CO_2 In (ppm)	CO_2 Out (ppm)	a_r	Re_L	$We_L \times 10^4$	Fr_L
9.15	1.47	30.0	44	11.53	2.27	34.9	0.0832	386	294	0.96	28.12	890	6.63
12.22	1.47	29.8	47	11.41	2.26	34.7	0.0829	387	291	1.00	37.27	1438	8.78
18.31	1.48	29.5	55	11.22	2.24	34.5	0.0821	387	289	1.05	55.61	2818	13.11
24.45	1.47	29.5	63	11.19	2.23	34.4	0.0810	387	286	1.08	74.01	4559	17.45
36.69	1.47	29.5	91	11.21	2.23	34.5	0.0799	385	281	1.14	110.86	8964	26.13
48.72	1.47	29.7	135	11.34	2.24	34.6	0.0799	386	276	1.21	147.67	14395	34.81
61.03	0.58	29.9	56	11.47	2.24	34.8	0.0784	387	171	1.18	186.62	21018	43.99
24.45	0.59	30.0	12	11.56	2.25	34.9	0.0778	386	190	1.04	75.18	4586	17.72
12.23	0.59	30.0	9	11.52	2.24	34.9	0.0773	387	202	0.95	37.62	1445	8.87
3.17	0.59	30.2	7	11.71	2.25	35.1	0.0768	385	225	0.79	9.79	153	2.31
M2Y — **SRP 0830** — **Baseline 3.1 m**													
3.40	0.98	28.9	28	10.77	2.28	34.0	0.1009	436	263	0.66	6.04	29	1.42
6.10	0.98	28.8	28	10.72	2.26	33.9	0.0972	436	247	0.75	10.59	76	2.50
12.26	0.98	28.5	30	10.52	2.22	33.6	0.0936	436	239	0.82	20.66	240	4.87
24.41	0.98	28.5	33	10.52	2.22	33.6	0.0927	436	228	0.89	40.76	754	9.61
36.67	0.98	28.2	37	10.37	2.20	33.4	0.0914	435	222	0.94	60.90	1484	14.35
48.92	0.98	28.2	47	10.34	2.19	33.3	0.0904	435	216	0.98	80.77	2395	19.04
61.04	0.98	28.2	68	10.36	2.18	33.3	0.0885	436	211	1.02	100.35	3460	23.65
73.29	0.98	28.1	69	10.27	2.17	33.2	0.0872	436	211	1.04	120.22	4694	28.34
2.55	1.47	28.2	57	10.39	2.17	33.4	0.0844	422	313	0.65	4.16	17	0.98
6.12	1.47	27.7	60	10.07	2.13	32.9	0.0816	422	298	0.78	9.84	74	2.32
12.29	1.47	27.1	64	9.69	2.08	32.3	0.0787	420	293	0.84	19.35	236	4.56
18.41	1.47	26.7	67	9.47	2.06	32.0	0.0776	420	290	0.88	28.71	461	6.77
24.38	1.47	26.2	71	9.22	2.03	31.6	0.0767	424	288	0.93	37.70	735	8.89
36.64	1.47	25.8	81	9.00	2.00	31.3	0.0755	424	282	0.99	56.29	1446	13.27
48.86	1.47	25.5	96	8.83	1.98	31.0	0.0748	424	278	1.05	74.66	2333	17.60
61.10	1.47	25.3	146	8.72	1.96	30.8	0.0728	421	274	1.09	93.19	3384	21.97
73.34	0.59	25.3	24	8.69	1.96	30.8	0.0710	471	167	1.07	112.09	4595	26.42
48.89	0.59	25.2	19	8.64	1.94	30.7	0.0688	471	180	1.01	74.74	2339	17.62
24.42	0.59	25.1	14	8.61	1.94	30.7	0.0682	471	189	0.97	37.24	735	8.78
12.28	0.59	25.0	13	8.58	1.92	30.6	0.0661	470	205	0.89	18.66	234	4.40
2.52	0.59	24.8	11	8.49	1.90	30.5	0.0623	470	235	0.78	3.83	17	0.90
F1Y — **SRP 0708** — **Baseline 3.0 m**													
6.09	1.47	34.0	133	14.52	2.56	38.5	0.0913	380	201	0.62	5.02	19	1.18
12.20	1.47	33.3	144	13.99	2.52	37.9	0.0913	380	189	0.68	9.75	60	2.30
18.35	1.47	32.9	159	13.64	2.49	37.5	0.0906	380	188	0.70	14.42	118	3.40

L (m³/m²·h)	u_G (m/s)	T_{corr} (°C)	$\Delta P/Z$ (Pa/m)	k_{OH^-} x 10^{-3} (m³/kmol·s)	D_{CO2} x 10^9 (m²/s)	H_{CO2} x 10^{-5} (m³·Pa/kmol)	$[OH^-]$ (kmol/m³)	CO_2 In (ppm)	CO_2 Out (ppm)	a_f	Re_L	We_L x 10^4	Fr_L
24.46	1.47	32.5	180	13.31	2.46	37.1	0.0892	380	185	0.73	19.02	189	4.48
30.56	1.47	32.0	214	12.95	2.42	36.7	0.0874	380	183	0.76	23.56	273	5.55
36.67	1.47	31.8	290	12.77	2.39	36.5	0.0848	380	180	0.80	28.00	369	6.60
6.16	0.98	29.4	80	11.11	2.30	34.4	0.0958	391	151	0.67	4.81	19	1.13
12.23	0.98	29.5	68	11.17	2.31	34.5	0.0956	391	142	0.71	9.49	59	2.24
18.30	0.98	29.6	84	11.26	2.31	34.6	0.0943	391	138	0.73	14.11	116	3.33
24.45	0.98	29.8	89	11.36	2.31	34.7	0.0924	391	135	0.75	18.75	188	4.42
36.68	0.98	30.1	128	11.59	2.32	35.0	0.0906	391	130	0.78	28.06	369	6.61
48.89	0.98	30.2	261	11.66	2.31	35.1	0.0881	388	127	0.81	37.35	596	8.80
6.05	0.59	33.4	12	14.03	2.53	38.0	0.0955	390	76	0.64	4.96	19	1.17
12.17	0.59	33.4	19	14.03	2.52	38.0	0.0955	390	68	0.68	9.93	60	2.34
18.33	0.59	33.5	55	14.14	2.53	38.1	0.0949	390	66	0.69	14.90	119	3.51
24.52	0.59	33.4	34	14.08	2.52	38.0	0.0932	390	63	0.72	19.85	193	4.68
36.69	0.59	33.4	39	14.10	2.51	38.1	0.0919	390	59	0.75	29.66	378	6.99
F1Y	**SRP 0711**					**Intermediate μ_L**		**3.0 m**					
2.44	0.98	33.5	75	14.13	2.40	38.1	0.0885	411	191	0.53	0.28	2	0.07
6.15	0.98	33.8	92	14.39	2.41	38.4	0.0865	411	160	0.65	0.69	11	0.16
12.24	0.98	32.8	162	13.58	2.34	37.4	0.0850	408	151	0.71	1.34	35	0.32
24.43	0.98	34.1	103	14.64	2.39	38.6	0.0807	398	132	0.79	2.72	111	0.64
30.55	0.97	34.3	231	14.80	2.40	38.8	0.0796	398	134	0.78	3.37	161	0.80
18.47	0.97	34.3	225	14.85	2.39	38.8	0.0781	401	146	0.73	2.03	69	0.48
2.45	1.47	34.7	155	15.21	2.40	39.2	0.0751	388	243	0.52	0.28	2	0.07
6.05	1.47	34.9	168	15.39	2.39	39.4	0.0710	388	224	0.63	0.69	11	0.16
12.23	1.47	34.6	249	15.14	2.35	39.1	0.0670	383	208	0.72	1.32	35	0.31
P500	**SRP 0827**					**Baseline**		**3.1 m**					
3.23	1.47	29.8	213	11.39	2.33	34.8	0.0980	392	187	0.61	2.10	5	0.50
6.01	1.47	29.7	240	11.31	2.29	34.6	0.0928	392	173	0.69	3.83	14	0.90
9.11	1.47	29.4	274	11.13	2.25	34.4	0.0876	386	169	0.72	5.60	27	1.32
12.13	1.47	29.3	299	11.06	2.24	34.3	0.0860	386	170	0.73	7.35	44	1.73
18.31	1.47	29.2	410	10.97	2.23	34.2	0.0846	384	170	0.73	11.00	87	2.59
3.43	0.98	29.3	99	11.07	2.22	34.3	0.0823	384	136	0.63	2.06	5	0.48
6.03	0.98	29.4	104	11.17	2.22	34.4	0.0799	384	129	0.67	3.61	14	0.85
12.22	0.98	29.3	116	11.09	2.20	34.3	0.0776	384	123	0.71	7.23	44	1.70
18.35	0.98	30.0	128	11.61	2.22	34.9	0.0724	385	121	0.74	10.94	87	2.58
24.42	0.98	30.3	146	11.75	2.23	35.1	0.0712	385	120	0.75	14.53	140	3.43
36.70	0.97	30.1	250	11.67	2.21	35.0	0.0693	385	119	0.77	21.82	277	5.14

L (m³/m²·h)	u_G (m/s)	T_{corr} (°C)	$\Delta P/Z$ (Pa/m)	k_{OH^-} x 10^{-3} (m³/kmol·s)	D_{CO2} x 10^9 (m²/s)	H_{CO2} x 10^{-5} (m³·Pa/kmol)	$[OH^-]$ (kmol/m³)	CO_2 In (ppm)	CO_2 Out (ppm)	a_f	Re_L	We_L x 10^4	Fr_L
42.77	0.98	29.9	346	11.52	2.19	34.8	0.0676	385	119	0.79	25.37	357	5.98
3.82	0.59	30.8	39	12.16	2.23	35.6	0.0655	382	80	0.63	2.29	6	0.54
6.09	0.59	31.2	41	12.47	2.25	36.0	0.0634	382	73	0.67	3.63	14	0.86
12.24	0.59	30.6	46	12.06	2.20	35.5	0.0613	383	72	0.69	7.27	45	1.71
24.42	0.59	30.8	63	12.15	2.21	35.6	0.0606	383	68	0.72	14.48	141	3.41
30.55	0.59	31.3	92	12.54	2.23	36.1	0.0593	383	65	0.74	18.15	205	4.28
P500 SRP 0828			Low σ		**3.1 m**								
3.16	0.98	26.8	90	9.48	2.15	32.1	0.1015	396	108	0.74	1.97	11	0.46
6.10	0.98	26.6	96	9.38	2.12	32.0	0.0969	396	102	0.80	3.76	32	0.89
9.13	0.98	26.6	104	9.42	2.11	32.0	0.0924	393	105	0.80	5.51	63	1.30
12.21	0.98	27.1	102	9.71	2.13	32.4	0.0900	393	103	0.81	7.33	102	1.73
18.36	0.98	27.2	113	9.74	2.13	32.5	0.0897	393	102	0.82	10.98	201	2.59
24.56	0.98	27.3	124	9.84	2.13	32.6	0.0874	391	103	0.82	14.64	327	3.45
30.57	0.97	27.5	168	9.95	2.13	32.7	0.0860	391	104	0.81	18.15	471	4.28
24.40	0.98	27.8	130	10.17	2.12	33.0	0.0795	392	108	0.83	14.35	323	3.38
12.22	0.98	28.1	100	10.31	2.12	33.2	0.0759	392	112	0.82	7.19	102	1.69
30.56	0.98	28.1	154	10.33	2.11	33.2	0.0741	392	110	0.84	17.89	470	4.22
3.48	1.47	28.4	185	10.52	2.11	33.5	0.0701	389	196	0.70	2.05	13	0.48
6.07	1.47	28.4	196	10.58	2.10	33.6	0.0662	389	187	0.77	3.55	32	0.84
9.19	1.47	28.2	206	10.46	2.07	33.4	0.0622	388	188	0.79	5.26	63	1.24
12.24	1.47	28.4	218	10.60	2.08	33.6	0.0607	389	189	0.79	6.95	101	1.64
18.29	1.47	28.5	260	10.61	2.07	33.6	0.0594	389	185	0.82	10.36	198	2.44
12.22	0.59	28.5	41	10.65	2.07	33.6	0.0582	389	67	0.79	6.92	101	1.63
18.33	0.59	28.7	46	10.80	2.07	33.8	0.0555	386	67	0.80	10.38	199	2.45
9.18	0.59	28.9	38	10.92	2.08	34.0	0.0543	386	71	0.78	5.20	63	1.23
36.73	0.98	29.5	811	11.31	2.10	34.5	0.0532	388	118	0.92	21.05	636	4.96

The hydraulic data are shown in Table B.9. For a few of the higher capacity packings, at very low liquid loads, hold-up values very close to zero (sometimes even negative) were measured. These are denoted by an "N" in the table, to indicate that a measurement was made but that it was essentially negligible.

Table B.9. Packed column experimental data (hydraulics).

L	F_G	$T_{air,in}$	$T_{liq,in}$	$T_{air,out}$	$\Delta P/Z$	h_L	Re_L	We_L x 10^4	Fr_L
$(m^3/m^2{\cdot}h)$	$(Pa)^{0.5}$	(°C)	(°C)	(°C)	(Pa/m)	(%)			
M250Y	SRP 0617		Baseline		Packing Config. 1			3.1 m	
0	0.525	44.2	38.9	35.8	9.5	0	0	0	0
0	0.532	24.5	25.2	25.1	9.7	0	0	0	0
0	0.533	25.3	26.3	26.1	9.7	0	0	0	0
0	0.704	44.8	37.0	35.0	17.1	0	0	0	0
0	0.713	25.5	26.5	26.2	16.3	0	0	0	0
0	0.715	24.4	24.5	25.1	16.4	0	0	0	0
0	0.875	44.7	39.4	34.7	23.4	0	0	0	0
0	1.049	43.8	37.5	35.0	34.5	0	0	0	0
0	1.067	24.5	24.6	25.0	34.6	0	0	0	0
0	1.068	25.8	26.6	26.2	34.4	0	0	0	0
0	1.401	42.8	37.7	34.4	58.7	0	0	0	0
0	1.424	24.7	24.8	24.9	59.6	0	0	0	0
0	1.757	42.1	38.3	33.8	90.8	0	0	0	0
0	1.776	26.7	26.7	26.2	91.2	0	0	0	0
0	1.783	25.2	25.0	24.9	92.4	0	0	0	0
0	2.108	41.5	38.5	33.5	126.7	0	0	0	0
0	2.137	27.1	24.8	25.3	129.4	0	0	0	0
0	2.463	41.4	37.9	32.8	168.9	0	0	0	0
0	2.494	27.5	25.0	25.3	173.4	0	0	0	0
0	2.816	41.7	37.5	32.3	216.3	0	0	0	0
0	2.849	28.0	25.1	25.3	222.2	0	0	0	0
0	3.151	42.2	37.7	32.3	263.0	0	0	0	0
0	3.203	29.3	25.0	25.5	273.2	0	0	0	0
0	3.523	43.7	38.4	31.9	321.1	0	0	0	0
0	3.560	30.6	25.0	25.5	332.7	0	0	0	0
0	3.872	44.9	38.2	31.9	381.5	0	0	0	0
0	3.914	32.4	24.9	25.7	396.9	0	0	0	0
0	4.223	47.1	37.9	32.2	445.4	0	0	0	0
0	4.576	49.4	37.5	32.3	512.4	0	0	0	0
12.22	0.520	41.5	36.3	37.5	11.8	3.50	20.32	178	4.79
12.24	0.522	40.4	35.9	36.4	12.1	3.58	20.20	178	4.76
12.22	0.530	35.7	33.5	31.6	12.4	3.42	19.24	174	4.53
12.25	0.537	28.6	25.3	25.6	12.1	3.81	16.20	162	3.82
12.22	0.700	40.0	38.1	36.3	19.5	3.58	21.05	180	4.96
12.24	0.706	35.5	34.5	31.8	20.2	3.43	19.63	175	4.63
12.24	0.707	28.0	25.5	25.8	19.3	3.85	16.23	162	3.83
12.21	1.043	41.0	36.4	37.5	39.1	3.54	20.36	178	4.80
12.22	1.046	38.8	39.4	36.9	40.1	3.52	21.57	182	5.08
12.21	1.048	38.4	37.1	36.1	39.9	3.54	20.61	179	4.86
12.22	1.054	35.4	35.2	32.0	41.1	3.45	19.88	176	4.69

L	F_G	$T_{air,in}$	$T_{liq,in}$	$T_{air,out}$	$\Delta P/Z$	h_L	Re_L	We_L x 10^4	Fr_L
$(m^3/m^2 \cdot h)$	$(Pa)^{0.5}$	(°C)	(°C)	(°C)	(Pa/m)	(%)			
12.21	1.067	27.6	25.5	25.9	40.8	3.91	16.19	161	3.82
12.22	1.397	38.5	37.4	36.9	68.3	3.56	20.76	179	4.89
12.21	1.407	35.3	35.4	32.2	69.8	3.46	19.96	176	4.70
12.22	1.423	27.2	25.4	25.9	70.2	3.99	16.18	161	3.81
12.21	1.746	38.5	38.6	36.9	105.7	3.58	21.24	181	5.01
12.26	1.759	36.4	35.2	33.0	108.5	4.07	19.96	177	4.70
12.20	1.761	35.4	35.5	32.3	108.4	3.49	19.99	176	4.71
12.23	1.781	26.9	25.3	26.0	109.7	4.11	16.13	161	3.80
12.22	2.096	38.8	38.8	36.5	150.8	3.59	21.31	181	5.02
12.24	2.110	36.5	35.1	33.3	153.6	4.25	19.88	176	4.68
12.21	2.134	27.0	25.1	26.0	155.9	4.25	16.07	161	3.79
12.21	2.450	39.5	37.2	36.2	204.0	3.57	20.65	179	4.87
12.22	2.451	40.9	36.7	36.0	204.1	4.13	20.47	178	4.82
12.23	2.461	37.4	36.3	33.3	207.7	4.38	20.33	178	4.79
12.22	2.491	27.6	25.0	26.0	211.6	4.44	16.04	161	3.78
12.22	2.796	41.7	36.8	36.5	262.6	4.23	20.54	179	4.84
12.23	2.809	38.4	36.0	33.2	271.3	4.55	20.21	178	4.76
12.23	2.845	28.2	25.1	25.8	277.9	4.65	16.09	161	3.79
12.22	3.148	42.8	36.4	36.3	360.8	4.51	20.38	178	4.80
12.24	3.164	40.8	36.2	32.9	378.6	4.94	20.30	178	4.79
12.21	3.201	29.7	25.2	25.7	407.5	5.24	16.09	161	3.79
12.22	3.518	43.2	36.9	32.7	573.8	5.65	20.56	179	4.85
12.22	3.555	31.2	25.4	25.7	594.4	6.01	16.18	161	3.81
12.22	3.870	47.5	36.8	32.0	1180.1	8.70	20.51	178	4.83
12.23	3.909	35.3	25.9	25.8	1184.0	9.06	16.36	162	3.86
24.45	0.530	27.0	27.2	27.0	13.7	6.17	33.69	521	7.94
24.45	0.534	28.5	25.2	26.2	13.7	6.13	32.20	512	7.59
24.44	0.711	27.1	27.5	27.2	22.2	6.19	33.88	522	7.99
24.47	0.711	27.6	25.4	26.2	22.0	6.17	32.41	514	7.64
24.44	1.065	27.4	27.7	27.2	45.9	6.25	34.04	523	8.02
24.45	1.065	27.0	25.5	26.2	45.7	6.26	32.43	513	7.64
24.45	1.421	26.8	25.6	26.2	78.6	6.38	32.50	514	7.66
24.44	1.423	27.9	27.9	27.4	79.1	6.35	34.18	524	8.06
24.44	1.775	29.0	28.2	27.5	122.9	6.50	34.40	526	8.11
24.47	1.777	26.8	25.6	26.3	123.0	6.54	32.56	515	7.67
24.43	2.126	29.7	28.1	27.5	175.9	6.68	34.32	525	8.09
24.45	2.132	27.0	25.6	26.3	176.8	6.73	32.48	513	7.66
24.46	2.483	31.0	28.6	27.4	239.9	6.85	34.75	529	8.19
24.44	2.488	27.5	25.5	26.3	241.1	6.95	32.43	513	7.64
24.43	2.838	32.3	28.5	27.5	421.7	7.74	34.66	527	8.17
24.45	2.843	28.4	25.4	26.2	420.3	7.85	32.37	513	7.63
24.44	3.194	34.7	28.5	27.4	946.8	10.31	34.66	527	8.17
24.46	3.197	31.0	24.6	26.0	1016.8	10.83	31.80	509	7.50
24.49	3.361	38.4	28.3	27.4	2089.2	16.35	34.58	528	8.15
36.67	0.526	31.3	29.5	28.7	14.7	7.57	53.13	1046	12.52
36.59	0.531	28.5	27.2	27.1	15.1	7.50	50.44	1021	11.89
36.67	0.705	30.8	29.0	28.8	23.8	7.60	52.55	1042	12.39
36.67	0.711	28.6	27.3	27.3	24.2	7.51	50.60	1025	11.93
36.67	1.066	29.7	29.1	28.7	49.8	7.72	52.66	1042	12.41
36.67	1.070	28.4	27.9	27.3	50.0	7.59	51.26	1031	12.08
36.67	1.418	29.7	28.7	28.7	85.6	7.88	52.16	1038	12.29
36.67	1.421	28.5	27.9	27.5	85.7	7.72	51.30	1031	12.09
36.67	1.774	30.0	28.8	28.3	134.9	8.14	52.32	1040	12.33
36.67	1.776	29.5	29.2	27.6	134.7	7.89	52.74	1043	12.43

325

L	F_G	$T_{air,in}$	$T_{liq,in}$	$T_{air,out}$	$\Delta P/Z$	h_L	Re_L	$We_L \times 10^4$	Fr_L
($m^3/m^2 \cdot h$)	$(Pa)^{0.5}$	(°C)	(°C)	(°C)	(Pa/m)	(%)			
36.67	2.127	31.0	29.1	28.2	193.5	8.32	52.65	1043	12.41
36.68	2.128	30.5	28.7	27.8	193.8	8.02	52.19	1039	12.30
36.66	2.482	30.8	27.1	28.1	267.3	8.58	50.37	1023	11.87
36.67	2.484	31.3	29.0	27.8	268.8	8.24	52.52	1042	12.38
36.90	2.785	32.4	28.6	27.8	1078.9	12.69	52.46	1049	12.36
36.84	2.805	33.6	26.6	27.7	2089.4	19.55	50.15	1027	11.82
48.90	0.529	30.8	31.4	30.2	17.7	8.36	73.63	1718	17.36
48.90	0.533	31.1	30.1	29.0	16.9	8.08	71.75	1699	16.91
48.90	0.700	38.5	34.1	33.8	25.5	7.70	77.82	1759	18.34
48.89	0.701	30.9	30.9	30.5	27.2	8.42	72.98	1711	17.20
48.90	0.713	31.4	30.6	29.2	26.4	8.08	72.44	1706	17.07
48.90	1.047	38.1	36.1	37.6	51.3	8.47	80.99	1789	19.09
48.90	1.061	31.5	30.1	29.5	53.4	8.16	71.75	1700	16.91
48.91	1.061	31.1	31.5	30.5	55.8	8.57	73.83	1721	17.40
48.89	1.402	37.4	34.4	36.3	89.5	8.58	78.29	1763	18.45
49.05	1.413	31.7	32.0	30.6	97.7	8.60	74.90	1737	17.65
48.89	1.414	31.3	31.8	30.4	96.7	8.73	74.25	1724	17.50
48.89	1.416	31.5	30.0	29.4	92.8	8.34	71.60	1698	16.88
48.90	1.749	36.9	34.1	36.2	143.9	8.80	77.89	1760	18.36
48.90	1.763	32.1	31.7	30.6	152.7	8.74	74.21	1724	17.49
48.90	1.767	31.8	29.9	29.3	147.9	8.58	71.40	1696	16.83
48.88	2.104	37.4	34.6	34.4	212.9	9.04	78.69	1766	18.55
48.90	2.118	33.0	32.0	30.2	222.9	8.91	74.56	1727	17.57
48.90	2.123	32.3	30.4	29.2	220.7	8.77	72.20	1704	17.02
48.87	2.179	40.2	34.8	33.7	227.7	8.69	78.98	1769	18.62
48.89	2.280	38.0	34.9	34.1	252.3	9.13	79.07	1771	18.64
48.90	2.300	32.9	30.2	29.2	262.5	8.90	71.93	1701	16.96
48.94	2.422	39.1	34.4	33.7	1040.8	13.50	78.35	1766	18.47
48.94	2.443	40.3	34.4	33.7	1344.9	15.15	78.40	1766	18.48
49.00	2.451	37.2	33.7	29.9	1910.9	18.26	77.33	1759	18.23
73.34	0.528	33.0	30.5	30.2	20.5	9.97	108.52	3352	25.58
73.34	0.532	28.7	28.7	27.6	26.0	10.69	104.50	3299	24.63
73.37	0.533	33.8	31.5	30.8	23.2	9.88	110.77	3383	26.11
73.35	0.708	29.0	29.0	27.9	43.9	10.80	105.16	3308	24.79
73.34	0.711	32.8	32.0	30.2	33.9	10.05	111.97	3397	26.39
73.35	1.056	32.7	31.4	30.3	72.8	10.32	110.58	3379	26.06
73.36	1.058	29.1	29.1	28.0	100.1	11.19	105.34	3311	24.83
73.35	1.411	32.5	31.2	30.4	150.5	10.79	110.01	3371	25.93
73.33	1.416	29.5	29.3	28.2	179.3	11.54	105.69	3314	24.91
73.35	1.766	32.6	30.8	30.0	365.3	11.69	109.24	3362	25.75
73.36	1.768	30.1	29.5	28.4	417.1	12.53	106.26	3323	25.04
73.35	2.111	34.6	31.0	29.9	1233.5	16.28	109.68	3367	25.85
73.38	2.112	32.6	30.2	28.7	1277.1	17.09	107.77	3344	25.40
73.40	2.160	36.0	32.1	29.8	1993.4	21.16	112.26	3404	26.46

M250Y	SRP 0712		Baseline		Packing Config. 2			3.1 m	
2.32	0.705	29.6	20.0	28.6	17.3	1.53	2.71	10	0.64
2.38	2.124	29.6	20.0	28.5	132.0	2.05	2.77	10	0.65
2.50	3.551	32.8	20.9	26.7	382.8	2.51	2.98	11	0.70
2.42	4.448	38.0	19.9	25.4	643.6	2.62	2.82	10	0.67
6.41	0.703	28.1	22.4	30.8	19.1	2.54	7.92	53	1.87
6.08	1.760	28.6	21.7	30.8	98.1	2.57	7.39	49	1.74
6.09	2.827	29.9	21.5	30.0	249.1	2.87	7.36	49	1.74
6.10	3.544	32.6	20.9	28.2	430.7	3.28	7.29	49	1.72

326

L	F_G	$T_{air,in}$	$T_{liq,in}$	$T_{air,out}$	$\Delta P/Z$	h_L	Re_L	$We_L \times 10^4$	Fr_L
$(m^3/m^2 \cdot h)$	$(Pa)^{0.5}$	(°C)	(°C)	(°C)	(Pa/m)	(%)			
6.12	4.256	37.6	19.8	26.9	826.9	4.52	7.11	48	1.68
12.14	0.711	30.7	19.3	28.1	20.0	4.20	13.94	150	3.29
12.23	1.772	29.9	19.6	28.1	104.4	4.37	14.14	153	3.33
12.18	2.835	30.4	19.1	27.5	273.3	4.74	13.93	151	3.28
12.24	3.552	32.4	18.6	26.4	622.1	6.15	13.80	151	3.25
18.37	1.078	18.6	17.2	18.2	44.0	5.87	20.01	294	4.72
18.53	1.445	18.9	16.8	18.5	73.6	6.02	19.97	297	4.71
18.94	2.159	19.6	16.2	18.7	165.5	6.35	20.12	306	4.74
18.68	2.879	21.5	15.5	18.9	296.0	6.26	19.50	297	4.60
18.61	3.241	23.7	15.1	18.7	491.9	7.15	19.20	293	4.53
18.32	3.509	29.0	15.3	18.5	742.8	8.63	19.04	287	4.49
24.39	0.720	25.9	16.0	20.8	22.2	6.43	25.79	465	6.08
24.08	1.432	25.0	16.1	20.9	76.5	6.49	25.52	456	6.01
24.37	2.154	24.6	16.1	20.8	177.4	6.60	25.81	465	6.08
24.49	2.869	25.7	16.0	21.0	353.6	7.05	25.88	468	6.10
24.22	3.226	27.7	16.0	20.6	660.0	8.33	25.63	460	6.04
M250Y	**SRP 0715**	12.9	**Baseline (Dry)**		**Packing Config. 2**			**3.1 m**	
0	0.729	12.9			17.3	0	0	0	0
0	1.823	13.3			93.6	0	0	0	0
0	2.902	21.1			215.6	0	0	0	0
0	3.623	23.1			326.6	0	0	0	0
0	4.348	27.4			447.9	0	0	0	0
M250Y	**SRP 0821**		**Baseline**		**Packing Config. 3**			**3.1 m**	
0	0.637	28.2	25.6	27.8	13.3	0	0	0	0
0	0.706	28.2	25.5	27.9	16.0	0	0	0	0
0	1.067	28.3	25.6	27.7	33.1	0	0	0	0
0	1.595	28.9	25.7	27.7	73.0	0	0	0	0
0	2.128	29.6	25.8	27.5	123.3	0	0	0	0
0	2.839	31.3	25.9	27.3	209.7	0	0	0	0
0	3.546	33.7	25.9	27.3	323.3	0	0	0	0
0	4.257	37.2	25.9	27.5	450.6	0	0	0	0
6.36	0.698	39.6	26.6	37.5	17.1	1.60	8.63	55	2.04
6.35	1.046	38.7	26.7	37.5	35.0	1.61	8.65	55	2.04
6.46	1.575	38.3	26.7	37.4	77.6	1.63	8.81	56	2.08
6.32	2.448	39.2	26.6	37.1	178.1	1.88	8.59	54	2.02
6.42	3.144	40.8	26.1	36.7	299.7	2.10	8.64	56	2.04
6.45	3.672	42.6	25.9	36.7	484.0	2.80	8.63	56	2.03
6.41	4.206	46.9	25.8	35.0	764.7	3.63	8.56	55	2.02
12.22	0.705	36.9	26.6	34.3	19.0	3.30	16.61	163	3.92
12.23	1.050	36.7	26.7	35.2	37.5	3.37	16.65	163	3.93
12.21	1.575	36.9	26.8	35.8	84.2	3.54	16.66	163	3.93
12.18	2.101	37.4	26.4	35.8	142.8	3.85	16.48	162	3.88
12.21	2.624	38.3	26.0	35.8	218.0	4.17	16.38	162	3.86
12.21	2.978	39.3	25.8	35.5	288.6	4.33	16.30	162	3.84
12.26	3.236	41.1	25.6	35.3	396.1	4.74	16.29	162	3.84
12.20	3.504	43.3	25.5	35.0	597.1	5.39	16.20	161	3.82
12.22	3.679	45.8	26.0	34.7	806.5	7.18	16.40	162	3.87
18.84	0.697	37.4	27.4	35.6	20.4	4.19	26.05	338	6.14
24.44	0.705	34.7	25.9	31.7	21.7	5.31	32.74	515	7.72
24.47	1.050	34.3	26.6	32.1	43.3	5.29	33.24	519	7.83
24.45	1.581	34.4	26.4	32.2	95.0	5.35	33.08	517	7.80
24.53	2.110	35.4	26.1	32.1	163.1	5.42	32.98	519	7.77

L	F_G	$T_{air,in}$	$T_{liq,in}$	$T_{air,out}$	$\Delta P/Z$	h_L	Re_L	$We_L \times 10^4$	Fr_L
$(m^3/m^2 \cdot h)$	$(Pa)^{0.5}$	(°C)	(°C)	(°C)	(Pa/m)	(%)			
24.44	2.466	36.2	26.0	32.1	220.5	5.43	32.77	515	7.72
24.45	2.816	37.3	25.8	32.0	328.8	5.63	32.69	515	7.71
24.47	2.995	38.7	25.6	31.9	514.9	6.36	32.57	515	7.68
24.46	3.083	40.2	25.7	31.6	699.9	7.01	32.58	514	7.68
36.71	0.709	31.2	26.4	30.2	23.9	7.02	49.71	1019	11.72
36.73	1.060	31.1	26.2	30.2	47.1	7.07	49.52	1018	11.67
36.64	1.590	31.4	25.9	30.0	105.5	7.16	49.08	1011	11.57
36.64	2.118	32.2	25.6	29.8	183.8	7.31	48.75	1008	11.49
36.83	2.652	33.9	25.4	29.6	341.4	7.79	48.75	1015	11.49
36.84	2.745	35.6	25.4	29.5	508.0	8.38	48.74	1015	11.49
35.57	2.826	36.1	25.2	29.4	766.7	9.67	46.93	956	11.06
48.53	0.707	37.8	25.8	32.9	25.3	7.93	64.83	1613	15.28
48.92	1.055	37.1	26.3	32.9	52.3	7.93	66.03	1642	15.56
48.85	1.064	27.9	25.7	27.8	52.2	0.00	65.17	1630	15.36
48.94	1.581	36.5	26.3	32.9	120.7	8.09	66.05	1643	15.57
48.92	1.938	36.3	26.1	32.2	184.5	8.07	65.82	1640	15.51
48.94	2.292	36.9	26.0	32.1	268.6	8.09	65.69	1639	15.48
48.89	2.466	38.1	25.9	31.7	425.8	8.59	65.39	1634	15.41
48.88	2.535	39.1	25.8	31.6	745.6	10.15	65.31	1633	15.39
60.94	0.713	32.8	25.4	29.7	28.3	9.06	80.74	2350	19.03
61.07	1.062	32.8	25.6	29.7	57.6	9.10	81.25	2363	19.15
61.13	1.418	33.4	25.6	29.9	108.2	9.24	81.35	2367	19.18
61.14	1.596	33.7	25.7	29.9	152.1	9.29	81.44	2368	19.19
61.11	1.768	34.0	25.7	30.0	191.9	9.34	81.39	2366	19.18
61.14	2.032	34.8	25.7	30.1	268.0	9.40	81.44	2368	19.19
61.14	2.207	35.2	25.7	30.2	424.4	9.99	81.48	2368	19.20
61.14	2.387	37.1	25.7	30.2	813.2	11.58	81.54	2369	19.22
73.14	0.698	35.8	27.1	34.8	31.9	10.28	100.62	3236	23.72
73.27	1.046	39.0	26.7	37.1	86.9	9.98	99.93	3234	23.55
73.34	1.054	36.0	27.2	34.3	88.6	10.37	101.06	3253	23.82
73.35	1.405	36.0	27.1	34.2	202.0	10.71	100.91	3251	23.78
73.35	1.576	38.7	26.8	35.9	267.1	10.27	100.18	3241	23.61
73.31	1.667	36.1	26.9	33.5	298.0	10.88	100.44	3243	23.67
73.36	1.750	38.9	26.8	35.9	326.3	10.72	100.18	3242	23.61
73.33	1.938	37.0	26.7	33.0	463.3	11.33	100.03	3238	23.58
73.33	2.109	38.6	26.5	33.0	680.9	11.99	99.60	3232	23.48
73.35	2.163	38.8	26.4	32.8	808.3	12.41	99.38	3231	23.42

M250Y	SRP 0823		Low σ		Packing Config. 3			3.1 m	
0	0.636	28.5	25.9	28.3	13.6	0	0	0	0
0	0.704	28.6	26.0	28.3	16.0	0	0	0	0
0	1.061	28.8	26.0	28.4	32.9	0	0	0	0
0	1.594	29.3	26.1	28.3	72.7	0	0	0	0
0	2.479	30.9	26.1	28.3	162.5	0	0	0	0
0	3.542	34.5	26.1	28.3	324.6	0	0	0	0
4.29	0.698	38.7	27.1	35.2	16.8	0.35	5.90	66	1.39
4.38	1.050	38.3	26.8	35.2	34.2	0.85	5.98	68	1.41
4.17	1.579	38.4	26.7	35.2	75.9	0.96	5.68	62	1.34
4.63	2.454	39.5	26.3	35.1	172.7	1.58	6.26	74	1.47
4.55	3.505	42.6	25.9	34.5	427.7	2.64	6.08	72	1.43
4.13	4.040	47.3	25.5	33.0	709.5	4.13	5.48	61	1.29
6.10	0.704	38.8	29.9	35.4	18.0	1.31	8.90	120	2.10
6.13	1.049	38.8	26.8	35.6	36.2	1.40	8.38	119	1.97
6.19	1.574	39.1	26.6	35.9	79.1	1.68	8.42	121	1.98

328

L	F_G	$T_{air,in}$	$T_{liq,in}$	$T_{air,out}$	$\Delta P/Z$	h_L	Re_L	We_L x 10^4	Fr_L
$(m^3/m^2 \cdot h)$	$(Pa)^{0.5}$	(°C)	(°C)	(°C)	(Pa/m)	(%)			
6.30	2.095	39.4	26.9	36.0	132.3	1.93	8.62	124	2.03
6.29	2.798	40.5	26.6	35.8	231.9	2.35	8.55	124	2.02
6.35	3.155	42.7	26.0	35.3	334.0	2.95	8.52	126	2.01
6.40	3.506	44.4	25.6	35.0	511.5	3.89	8.51	127	2.01
5.77	3.864	48.4	25.4	34.3	745.5	4.95	7.63	106	1.80
9.20	0.701	39.4	26.7	37.5	18.9	1.90	12.55	234	2.96
9.23	1.046	39.2	26.8	37.5	37.2	1.90	12.60	235	2.97
9.27	1.569	39.4	27.0	37.7	82.1	1.98	12.73	237	3.00
9.32	2.093	40.0	26.7	37.8	138.4	2.11	12.72	239	3.00
9.26	2.970	41.9	26.2	37.5	304.5	2.81	12.50	236	2.95
9.06	3.406	44.3	25.7	37.1	578.3	4.07	12.09	226	2.85
9.43	3.492	46.2	25.3	36.7	658.4	4.52	12.46	241	2.94
12.45	0.705	37.5	26.0	33.1	20.1	2.75	16.73	386	3.94
12.14	1.058	37.3	26.7	33.3	39.9	2.78	16.53	371	3.90
12.44	1.585	37.1	26.4	33.5	88.9	3.02	16.84	386	3.97
12.92	2.107	37.5	26.2	33.4	151.3	3.36	17.43	411	4.11
12.52	2.811	39.4	25.8	33.4	296.2	3.65	16.73	388	3.94
12.30	2.988	40.7	25.7	33.4	379.9	3.98	16.38	376	3.86
12.22	3.275	43.3	25.5	33.1	626.8	5.16	16.22	372	3.82
12.77	3.305	44.0	25.5	33.1	708.1	5.69	16.95	400	4.00
18.33	0.694	42.9	25.5	38.6	21.3	3.43	24.32	731	5.73
18.30	1.043	41.9	26.2	38.7	43.2	3.50	24.67	733	5.82
18.38	1.563	41.2	26.0	39.1	101.4	3.74	24.68	738	5.82
18.31	2.437	41.8	26.0	38.9	227.0	4.17	24.57	733	5.79
18.26	2.785	42.7	25.6	38.5	372.4	4.79	24.30	727	5.73
18.41	2.965	44.0	25.5	37.9	540.0	5.73	24.43	737	5.76
18.33	3.057	45.1	25.3	37.1	679.8	6.60	24.21	730	5.71
24.41	0.695	41.3	26.6	37.3	22.9	4.15	33.16	1188	7.82
24.42	1.047	40.8	26.7	37.3	48.8	4.26	33.25	1190	7.84
24.45	1.575	40.8	26.5	37.1	120.1	4.62	33.20	1191	7.83
24.42	2.096	41.4	26.2	36.6	201.3	4.90	32.91	1186	7.76
24.47	2.449	42.3	25.9	35.8	308.0	5.31	32.76	1187	7.72
24.42	2.802	44.3	25.6	35.2	701.0	7.30	32.47	1180	7.65
30.57	0.694	39.5	29.1	41.3	30.1	5.13	43.93	1760	10.35
30.57	1.042	39.6	28.9	41.2	82.7	5.51	43.73	1757	10.31
30.55	1.565	40.0	28.3	40.2	183.0	5.92	43.14	1748	10.17
30.64	2.093	40.8	27.8	38.7	295.8	6.51	42.73	1749	10.07
30.54	2.444	42.1	27.0	37.3	479.2	7.44	41.92	1731	9.88
30.55	2.621	43.5	26.5	36.4	728.6	8.61	41.46	1726	9.77
36.64	0.698	37.8	29.3	35.2	41.5	6.13	52.85	2383	12.46
36.73	1.047	37.7	29.1	35.3	107.3	6.47	52.72	2389	12.43
36.66	1.577	38.0	28.5	35.3	218.0	7.00	52.01	2372	12.26
36.68	2.106	38.8	27.9	34.5	453.4	8.25	51.33	2364	12.10
36.68	2.281	39.8	27.4	34.2	599.7	9.06	50.80	2356	11.97
36.64	2.370	41.0	27.0	33.9	769.8	9.96	50.28	2345	11.85
48.90	0.696	38.0	28.0	36.3	306.6	8.63	68.49	3819	16.14
48.92	1.049	38.2	27.9	36.5	400.6	8.99	68.42	3820	16.13
48.88	1.401	38.8	27.7	36.0	517.2	9.44	68.05	3808	16.04
48.87	1.577	39.4	27.5	35.5	584.2	9.70	67.79	3803	15.98
48.91	1.750	39.9	27.3	35.5	675.2	10.00	67.55	3803	15.92
48.91	1.928	40.8	27.1	35.5	822.4	10.65	67.30	3798	15.86

M250Y	SRP 0713		Intermediate μ_L		Packing Config. 2			3.1 m	
2.35	0.715	27.5	17.7	21.6	17.9	1.43	0.46	7	0.11

L (m³/m²·h)	F_G (Pa)$^{0.5}$	$T_{air,in}$ (°C)	$T_{liq,in}$ (°C)	$T_{air,out}$ (°C)	ΔP/Z (Pa/m)	h_L (%)	Re_L	We_L x 10^4	Fr_L
2.57	0.720	25.6	16.0	20.4	18.1	1.88	0.48	7	0.11
2.39	2.152	26.8	17.6	21.5	139.1	1.71	0.46	7	0.11
2.39	2.155	24.6	16.3	20.6	127.8	1.98	0.45	7	0.11
2.58	3.589	26.5	16.6	20.4	355.7	2.04	0.49	8	0.11
1.67	4.400	32.9	16.5	20.4	821.0	2.57	0.31	4	0.07
6.09	0.714	28.2	18.2	23.7	18.5	2.69	1.20	32	0.28
5.93	0.718	27.7	18.2	22.3	19.2	3.43	1.17	31	0.28
6.05	2.146	27.2	18.0	22.1	146.8	3.79	1.19	32	0.28
6.09	3.224	28.1	18.1	22.1	351.1	4.25	1.20	32	0.28
6.16	3.583	30.0	17.9	21.6	485.6	4.63	1.21	32	0.28
6.13	3.705	33.5	17.6	22.8	1158.8	6.01	1.19	32	0.28
12.17	0.714	28.7	19.1	23.4	20.6	5.32	2.47	102	0.58
12.23	0.723	21.6	16.7	19.6	20.8	4.27	2.32	101	0.55
12.22	1.786	28.0	18.9	23.4	110.1	5.54	2.47	103	0.58
12.24	1.801	21.2	16.9	19.6	106.9	4.55	2.33	101	0.55
12.17	2.859	28.2	18.7	23.0	292.8	5.94	2.44	102	0.58
12.19	2.876	21.9	16.6	19.6	272.2	4.86	2.30	100	0.54
12.29	3.222	29.7	18.1	22.5	495.2	6.78	2.43	103	0.57
18.62	0.715	28.3	20.3	25.6	21.8	6.46	3.93	210	0.93
18.32	1.779	28.0	19.8	25.0	118.8	6.60	3.80	204	0.90
18.33	2.848	28.8	19.7	25.0	371.5	7.31	3.79	204	0.89
18.39	3.222	26.1	17.2	21.4	605.8	9.44	3.53	200	0.83
24.48	0.701	31.8	22.8	34.0	22.7	7.05	5.56	340	1.31
24.48	1.754	32.1	22.6	34.4	131.3	7.32	5.54	339	1.31
24.44	2.457	32.9	21.9	33.6	283.2	7.67	5.40	336	1.27
24.50	2.819	34.0	20.9	31.5	583.5	9.08	5.27	334	1.24
36.79	0.707	27.9	28.7	29.1	28.0	8.54	9.99	710	2.36
36.68	1.060	28.0	28.5	29.1	68.3	8.66	9.91	706	2.33
36.77	2.210	29.8	26.9	28.8	477.3	10.46	9.31	694	2.19
36.72	2.288	30.0	26.8	28.9	536.9	10.69	9.27	691	2.19
36.61	2.354	31.6	26.2	28.6	829.4	12.40	9.02	683	2.13
48.95	0.702	29.2	25.8	28.2	161.0	11.13	11.88	1102	2.80
48.88	1.064	29.1	25.9	28.1	329.5	11.78	11.88	1100	2.80
49.01	1.415	29.2	25.8	28.1	405.1	11.99	11.87	1103	2.80
48.91	1.771	29.7	25.6	28.0	533.3	12.20	11.77	1098	2.77
48.88	1.916	30.3	25.5	27.9	641.4	12.63	11.70	1095	2.76
48.99	1.968	30.9	25.4	27.8	720.0	12.97	11.67	1097	2.75
73.12	0.725	30.2	20.2	27.6	355.4	13.26	15.35	2053	3.62
73.33	1.065	29.9	20.2	26.9	522.0	13.38	15.43	2064	3.64

M250Y	SRP 0804		High μ_L		Packing Config. 2			3.1 m	
0	0.718	20.4	19.0	21.0	16.3	0	0	0	0
0	1.795	21.1	19.0	20.8	91.3	0	0	0	0
0	2.869	23.7	19.0	20.7	216.4	0	0	0	0
0	3.586	28.8	19.0	21.0	336.8	0	0	0	0
0	4.302	33.4	19.0	21.3	466.3	0	0	0	0
2.75	0.717	21.9	19.6	21.7	18.2	3.54	0.26	9	0.06
2.52	1.792	22.5	21.2	21.8	101.0	3.49	0.25	8	0.06
2.61	2.865	25.0	20.3	21.6	255.6	4.15	0.25	8	0.06
2.17	3.585	28.3	19.7	21.3	442.7	4.61	0.21	6	0.05
2.27	3.764	31.0	19.3	21.1	499.1	4.72	0.21	7	0.05
6.19	0.717	25.3	19.0	21.9	19.5	4.71	0.57	35	0.13
6.11	1.790	24.5	18.0	22.0	109.9	5.02	0.55	34	0.13
6.12	2.863	26.0	17.7	21.8	284.2	5.71	0.54	34	0.13

330

L (m³/m²·h)	F_G (Pa)$^{0.5}$	$T_{air,in}$ (°C)	$T_{liq,in}$ (°C)	$T_{air,out}$ (°C)	$\Delta P/Z$ (Pa/m)	h_L (%)	Re_L	We_L x 10^4	Fr_L
6.06	3.582	29.8	16.9	21.6	559.1	6.68	0.52	33	0.12
12.05	0.717	25.3	15.9	22.4	21.6	7.16	1.01	102	0.24
12.23	1.786	25.0	15.5	22.7	120.2	7.60	1.01	104	0.24
12.16	2.862	26.5	16.3	22.5	342.6	8.30	1.03	104	0.24
12.13	3.221	30.6	14.8	22.2	615.4	9.15	0.98	102	0.23
18.32	0.710	26.1	15.3	23.6	23.3	8.90	1.50	204	0.35
18.43	1.786	25.8	15.8	23.6	129.7	9.29	1.53	208	0.36
18.38	2.326	27.9	15.2	22.6	230.9	8.95	1.50	205	0.35
18.29	2.859	27.8	14.9	23.0	526.7	10.28	1.48	203	0.35
24.31	0.718	24.7	15.3	24.4	24.4	10.33	1.99	327	0.47
24.44	1.431	24.3	15.6	24.3	86.8	10.43	2.02	332	0.48
24.43	2.142	24.6	15.1	23.2	247.4	10.96	1.99	329	0.47
24.42	2.324	25.3	14.8	22.5	324.6	11.20	1.97	328	0.46
37.23	0.713	23.6	14.7	22.8	29.1	12.14	2.99	662	0.71
36.58	1.072	23.9	14.9	23.6	60.3	12.04	2.96	644	0.70
36.53	1.247	23.8	15.0	25.6	94.7	11.90	2.97	644	0.70
36.76	1.420	24.2	15.1	25.8	248.0	12.85	2.99	651	0.71
48.68	0.710	23.2	15.2	25.7	36.9	13.45	3.98	1041	0.94
49.21	0.804	21.9	15.0	22.8	47.2	14.28	4.00	1058	0.94
49.03	0.888	23.3	15.3	25.9	60.9	13.46	4.02	1055	0.95
48.81	0.893	21.3	14.6	22.0	63.5	14.18	3.91	1039	0.92
48.89	1.068	23.6	15.2	25.2	313.5	14.53	3.99	1048	0.94
48.92	1.079	20.8	14.2	20.7	333.6	15.39	3.87	1038	0.91
62.11	0.697	22.9	15.0	24.2	156.5	16.15	5.05	1559	1.19
61.82	0.799	22.8	15.0	24.0	294.1	16.50	5.02	1547	1.18

M500Y	SRP 0625	Baseline			Packing Config. 1			3.0 m	
12.42	0.536	23.2	23.0	23.9	25.6		7.15	44	1.69
12.13	0.713	23.0	23.1	23.7	43.3		6.98	43	1.65
12.20	0.893	22.8	23.0	23.6	66.1		7.01	43	1.65
12.29	1.072	22.9	23.0	23.5	92.0		7.07	43	1.67
12.25	1.249	23.5	23.2	23.3	121.9		7.07	43	1.67
12.22	1.430	23.7	23.3	23.3	160.8		7.08	43	1.67
12.24	1.608	24.2	23.5	23.3	219.6		7.11	43	1.68
12.23	1.786	24.8	23.5	23.4	282.9		7.10	43	1.67
12.22	1.964	25.4	23.6	23.4	364.4		7.12	43	1.68
12.22	2.323	28.1	23.9	23.1	955.4		7.17	43	1.69
24.45	0.532	28.2	27.5	29.3	34.5		15.56	143	3.67
24.44	0.709	28.2	27.4	29.0	56.0		15.52	142	3.66
24.48	0.884	28.2	27.5	28.8	83.9		15.57	143	3.67
24.42	1.061	28.4	27.5	28.8	124.2		15.55	142	3.67
24.45	1.415	29.2	27.6	28.8	254.8		15.59	143	3.67
24.44	1.591	29.7	27.7	28.9	349.9		15.63	143	3.68
24.42	1.769	30.8	27.8	29.0	726.4		15.63	143	3.68
24.41	1.936	33.6	27.9	28.2	1581.4		15.67	143	3.69
36.66	0.535	25.1	24.0	24.0	43.1		21.59	271	5.09
36.70	0.713	24.6	23.9	24.0	70.8		21.52	271	5.07
36.68	0.892	24.2	24.3	24.0	109.2		21.72	272	5.12
36.66	1.071	23.2	23.7	23.8	162.1		21.42	270	5.05
36.69	1.249	23.5	23.8	23.8	225.6		21.48	271	5.06
36.67	1.428	24.0	24.0	23.9	327.4		21.58	271	5.09
36.66	1.606	26.4	24.1	24.1	1018.0		21.64	272	5.10
48.89	0.535	26.9	26.1	26.0	61.4		30.16	447	7.11
48.89	0.711	27.6	26.7	26.2	98.1		30.54	449	7.20

L	F_G	$T_{air,in}$	$T_{liq,in}$	$T_{air,out}$	$\Delta P/Z$	h_L	Re_L	$We_L \times 10^4$	Fr_L
(m³/m²·h)	(Pa)$^{0.5}$	(°C)	(°C)	(°C)	(Pa/m)	(%)			
48.86	0.888	26.9	26.9	26.4	144.2		30.70	450	7.24
48.92	1.065	27.2	27.1	26.8	202.9		30.84	451	7.27
48.89	1.241	28.1	27.6	27.4	295.4		31.18	453	7.35
48.91	1.421	29.5	26.5	26.7	1192.8		30.43	449	7.17
61.11	0.535	25.8	25.9	25.8	79.6		37.55	647	8.85
61.11	0.712	25.7	25.9	25.8	118.0		37.55	647	8.85
61.12	0.889	25.8	26.0	25.8	169.0		37.66	648	8.88
61.12	1.066	26.0	26.0	25.8	246.3		37.62	648	8.87
61.12	1.241	27.1	26.1	25.9	664.9		37.70	648	8.89
61.08	1.321	27.6	26.2	25.9	1306.6		37.78	648	8.90

M500Y	**SRP 0806**		**Baseline**		**Packing Config. 2**			**2.8 m**	
0	0.719	18.8	16.2	17.9	33.7	0	0	0	0
0	1.082	19.5	16.1	17.8	69.8	0	0	0	0
0	1.444	19.6	16.1	17.8	117.8	0	0	0	0
0	1.803	19.4	16.2	17.9	183.6	0	0	0	0
0	2.164	19.9	16.2	18.0	252.9	0	0	0	0
0	2.884	22.2	16.3	18.2	434.9	0	0	0	0
0	3.603	25.4	16.3	18.4	654.5	0	0	0	0
0	4.317	30.1	16.3	19.1	909.2	0	0	0	0
2.40	0.714	22.0	18.2	20.4	39.4	2.45	1.23	3	0.29
2.54	1.436	22.8	18.3	20.5	139.4	2.54	1.31	3	0.31
2.60	2.153	26.0	18.5	20.6	374.2	2.49	1.34	3	0.32
2.62	2.869	25.7	18.8	20.4	665.0	3.59	1.36	3	0.32
2.69	3.230	27.9	18.6	20.4	838.7	3.51	1.39	3	0.33
2.40	3.586	30.9	18.6	20.6	1433.5	6.46	1.24	3	0.29
6.09	0.717	20.7	18.2	20.0	43.0	5.15	3.12	13	0.74
6.11	1.077	21.0	18.0	20.1	89.3	5.24	3.12	13	0.73
6.09	1.438	22.3	17.7	20.2	162.9	5.39	3.09	13	0.73
6.08	2.158	23.1	17.7	20.3	432.6	5.97	3.08	13	0.73
6.10	2.516	24.8	17.7	20.3	652.6	6.51	3.09	13	0.73
6.09	2.692	25.8	17.8	20.4	816.0	7.07	3.09	13	0.73
6.18	2.865	27.1	18.0	20.2	1201.7	9.15	3.15	13	0.74
11.98	0.723	19.8	18.8	19.2	48.3	7.23	6.23	40	1.47
12.23	1.081	20.3	18.3	19.5	97.6	7.44	6.29	41	1.48
12.24	1.440	20.8	18.3	19.7	196.6	7.74	6.30	41	1.48
12.24	1.796	21.5	18.1	19.9	348.7	8.14	6.26	41	1.48
12.19	2.163	23.0	17.9	20.0	683.4	9.39	6.20	41	1.46
12.25	2.244	23.4	17.8	19.9	1099.6	11.76	6.22	41	1.47
18.21	0.718	23.0	18.8	21.8	53.7	8.61	9.48	80	2.24
18.31	1.075	23.3	18.8	21.8	122.2	8.88	9.53	81	2.25
18.31	1.431	23.5	18.8	21.8	258.9	9.29	9.52	81	2.24
18.32	1.611	23.7	18.7	21.7	382.8	9.64	9.51	81	2.24
18.38	1.789	24.3	18.7	21.7	706.9	11.37	9.53	81	2.25
24.39	0.720	22.4	19.0	21.9	58.2	9.29	12.77	131	3.01
24.45	1.074	22.9	19.2	21.9	131.5	9.63	12.84	132	3.03
24.45	1.433	23.3	19.0	21.8	301.6	10.09	12.78	132	3.01
24.39	1.622	24.4	18.8	21.7	721.1	12.07	12.70	131	2.99
30.54	0.712	26.2	19.6	25.4	70.4	9.95	16.21	192	3.82
30.57	0.724	20.5	16.5	18.7	68.2	10.36	15.02	186	3.54
30.56	1.065	26.4	19.7	25.7	174.5	10.37	16.24	192	3.83
30.55	1.085	18.6	16.4	18.2	165.1	11.11	14.97	186	3.53
30.56	1.425	26.7	19.7	25.4	361.6	11.02	16.26	192	3.83
30.62	1.440	19.5	16.4	18.5	343.4	11.76	15.00	186	3.54

L (m³/m²·h)	F_G (Pa)$^{0.5}$	$T_{air,in}$ (°C)	$T_{liq,in}$ (°C)	$T_{air,out}$ (°C)	$\Delta P/Z$ (Pa/m)	h_L (%)	Re_L	$We_L \times 10^4$	Fr_L
30.60	1.583	27.1	19.7	25.3	1080.6	15.28	16.28	193	3.84
36.89	0.712	26.4	19.4	24.9	78.5	11.28	19.49	262	4.59
36.74	0.725	18.7	16.2	17.6	74.1	11.60	17.89	252	4.22
36.67	0.892	24.6	19.0	23.1	126.2	11.38	19.18	258	4.52
36.61	0.904	16.8	16.7	17.2	123.6	12.05	18.07	252	4.26
36.69	1.072	25.0	19.1	23.1	189.1	11.56	19.22	259	4.53
36.69	1.083	17.0	16.6	17.3	172.1	12.22	18.06	252	4.26
36.63	1.248	25.4	19.1	23.1	279.3	11.70	19.21	258	4.53
36.65	1.263	17.3	16.4	17.4	244.5	12.49	17.97	251	4.24
36.67	1.429	25.6	19.2	23.7	507.6	12.87	19.26	259	4.54
36.70	1.442	18.1	16.3	17.4	492.0	13.82	17.93	252	4.23
36.74	1.458	26.3	19.3	23.8	888.1	15.29	19.33	260	4.56
48.91	0.718	18.0	16.2	17.9	111.6	13.32	23.84	406	5.62
48.89	0.899	18.1	16.2	17.9	166.4	13.40	23.86	406	5.62
48.86	1.081	18.2	16.2	17.9	239.3	13.69	23.84	405	5.62
48.98	1.258	19.0	16.3	18.0	594.3	15.66	23.92	407	5.64

M500Y	SRP 0819		Baseline		Packing Config. 3			2.8 m	
0	0.720	21.4	18.1	21.1	33.8	0	0	0	0
0	1.075	21.8	18.3	21.3	67.5	0	0	0	0
0	1.614	22.6	18.6	21.6	147.6	0	0	0	0
0	2.153	23.5	18.7	21.7	245.1	0	0	0	0
0	2.866	25.4	18.8	21.7	420.2	0	0	0	0
0	3.582	28.9	19.0	21.8	628.8	0	0	0	0
0	4.299	33.0	19.1	21.8	869.4	0	0	0	0
4.35	0.704	27.3	21.7	26.7	40.8	2.84	2.43	8	0.57
4.25	0.710	29.0	22.2	28.2	40.1	2.74	2.40	7	0.57
4.37	1.060	28.8	22.7	28.0	83.0	2.87	2.50	8	0.59
4.43	1.602	28.9	22.7	27.8	199.2	3.27	2.53	8	0.60
4.50	2.130	29.7	22.2	27.5	371.5	3.65	2.54	8	0.60
4.19	2.661	31.0	21.8	27.1	599.1	3.97	2.34	7	0.55
4.49	2.842	32.2	21.5	26.8	774.8	4.81	2.49	8	0.59
6.06	0.704	29.8	23.3	31.2	41.4	4.80	3.51	13	0.83
6.01	0.718	26.8	21.2	26.6	42.8	4.20	3.31	13	0.78
6.09	1.060	29.9	22.0	30.8	85.1	4.97	3.42	13	0.81
6.00	1.592	30.3	22.1	30.7	209.3	5.22	3.37	13	0.80
6.06	2.117	31.2	22.3	30.2	390.6	5.63	3.43	13	0.81
6.08	2.479	32.4	22.0	29.7	581.7	6.09	3.42	13	0.81
6.26	2.657	34.8	21.7	28.3	839.8	7.27	3.49	14	0.82
9.10	0.713	29.0	20.6	26.0	45.4	5.28	4.95	26	1.17
9.09	0.714	29.8	21.7	28.4	45.1	5.38	5.07	26	1.20
9.07	1.069	29.3	20.6	26.0	92.7	5.25	4.92	26	1.16
9.17	1.601	29.4	21.1	26.4	232.6	5.58	5.04	26	1.19
9.12	2.132	30.5	21.0	26.5	453.4	6.16	5.00	26	1.18
9.00	2.314	31.1	20.8	26.5	595.9	6.60	4.91	25	1.16
9.26	2.489	32.4	20.7	26.6	785.6	7.32	5.04	26	1.19
9.16	2.540	33.0	20.8	26.7	1048.4	8.96	5.00	26	1.18
12.23	0.715	26.8	22.0	24.3	47.9	6.56	6.87	43	1.62
12.20	1.070	26.3	21.8	24.7	96.8	6.68	6.82	42	1.61
12.23	1.602	26.6	21.8	24.8	244.1	7.05	6.84	43	1.61
12.22	1.957	27.5	21.2	24.9	397.9	7.37	6.73	42	1.59
12.21	2.312	31.0	20.3	26.0	712.8	7.86	6.58	42	1.55
12.21	2.399	32.5	20.2	25.8	1089.0	9.73	6.58	42	1.55
18.30	0.715	30.4	21.3	27.6	51.2	8.10	10.12	83	2.38

333

L	F_G	$T_{air,in}$	$T_{liq,in}$	$T_{air,out}$	$\Delta P/Z$	h_L	Re_L	$We_L \times 10^4$	Fr_L
$(m^3/m^2 \cdot h)$	$(Pa)^{0.5}$	(°C)	(°C)	(°C)	(Pa/m)	(%)			
18.32	1.067	30.1	21.9	27.6	104.5	8.17	10.28	84	2.42
18.29	1.593	30.1	21.9	27.8	310.6	8.63	10.24	83	2.41
18.38	1.866	30.8	21.3	27.3	616.2	9.43	10.17	84	2.40
18.34	1.898	30.8	21.2	27.1	793.2	10.22	10.10	83	2.38
24.51	0.712	29.5	21.0	27.5	56.1	9.27	13.46	135	3.17
24.46	1.062	29.9	21.5	28.1	126.9	9.30	13.59	135	3.20
24.47	1.420	30.2	21.7	28.7	274.6	9.55	13.66	135	3.22
24.44	1.589	31.6	21.8	29.4	571.5	10.44	13.65	135	3.22
24.53	1.625	32.4	21.9	29.7	1180.0	13.21	13.75	136	3.24

M500Y	**SRP 0820**		**Low σ**		**Packing Config. 3**			**2.8 m**	
2.80	0.707	30.7	24.0	30.0	36.4	1.96	1.65	9	0.39
2.79	0.714	23.6	23.5	24.0	37.9	1.97	1.62	9	0.38
2.66	1.064	30.6	23.9	29.9	72.4	1.78	1.56	8	0.37
2.81	1.595	30.7	23.9	29.7	158.3	1.93	1.65	9	0.39
2.66	2.123	31.9	23.9	29.5	285.9	2.22	1.56	8	0.37
2.98	2.480	34.0	23.8	29.2	426.3	2.10	1.74	10	0.41
3.71	3.078	35.6	23.8	28.9	1200.9	4.71	2.18	14	0.51
4.63	0.709	29.6	25.3	28.4	37.2	2.78	2.81	21	0.66
4.25	0.713	23.6	23.0	24.1	38.8	2.72	2.44	18	0.58
4.51	1.060	29.4	24.0	28.4	74.9	2.76	2.65	20	0.63
4.36	1.595	29.7	23.9	28.3	166.8	2.91	2.56	19	0.60
4.42	2.123	30.4	23.8	28.2	313.4	3.39	2.59	19	0.61
4.34	2.308	30.9	23.8	27.9	376.3	3.37	2.54	18	0.60
4.24	2.662	32.1	23.6	27.8	640.0	3.93	2.47	18	0.58
4.16	2.712	33.1	23.5	27.7	829.0	4.85	2.42	17	0.57
6.07	0.707	29.7	23.8	28.4	39.2	3.49	3.55	32	0.84
6.17	0.715	23.6	22.4	24.2	39.4	3.66	3.50	33	0.82
6.05	1.066	29.4	23.5	28.6	78.6	3.47	3.52	32	0.83
6.20	1.591	29.6	23.5	28.6	172.8	3.69	3.61	33	0.85
6.13	2.121	30.4	23.6	28.6	350.0	4.16	3.58	33	0.84
6.20	2.458	31.8	23.4	28.4	844.3	6.20	3.59	33	0.85
8.94	0.702	30.0	24.2	30.6	39.7	5.06	5.28	62	1.24
9.09	1.064	30.0	24.1	30.6	80.7	5.23	5.36	64	1.26
8.94	1.592	30.5	24.0	30.5	179.3	5.32	5.26	62	1.24
9.11	1.767	30.8	23.8	30.4	217.9	5.34	5.34	64	1.26
9.28	2.115	32.4	23.5	30.6	572.3	5.89	5.39	65	1.27
9.06	2.174	32.8	23.3	30.2	730.6	6.24	5.25	63	1.24
9.10	0.712	23.6	21.9	24.2	44.2	5.18	5.10	63	1.20
12.32	0.709	28.7	23.3	27.4	44.9	6.01	7.13	105	1.68
12.18	1.067	28.7	23.1	27.5	86.5	6.05	7.02	103	1.66
12.23	1.421	29.2	23.6	27.6	146.4	6.24	7.14	104	1.68
12.24	1.769	29.9	23.4	27.8	238.2	6.48	7.10	104	1.67
12.20	0.707	23.8	22.0	24.1	101.5	6.67	6.85	102	1.61
18.53	0.707	29.8	24.1	29.4	47.9	7.39	10.92	208	2.57
18.40	1.061	30.5	23.8	30.1	105.3	7.51	10.79	205	2.54
18.35	1.414	30.7	23.8	30.5	178.1	7.52	10.75	204	2.53
18.35	1.587	31.0	24.0	30.6	231.1	7.63	10.79	205	2.54
18.55	1.599	31.3	23.8	30.3	1166.5	10.91	10.86	208	2.56
18.41	0.716	24.4	21.7	24.3	352.9	8.99	10.27	202	2.42
24.45	0.715	29.9	24.0	30.2	58.5	8.50	14.37	330	3.39
24.44	1.056	30.2	23.9	30.5	131.4	8.80	14.34	330	3.38
24.48	1.412	30.3	23.8	30.7	209.2	8.91	14.35	330	3.38
24.86	1.501	31.4	23.8	30.5	1024.3	12.59	14.57	339	3.43

L	F$_G$	T$_{air,in}$	T$_{liq,in}$	T$_{air,out}$	ΔP/Z	h$_L$	Re$_L$	We$_L$ x 10^4	Fr$_L$
(m^3/m^2·h)	(Pa)$^{0.5}$	(°C)	(°C)	(°C)	(Pa/m)	(%)			
24.47	0.719	24.4	21.7	24.2	466.9	10.99	13.64	325	3.21
30.63	0.713	28.6	23.7	27.7	160.8	10.20	17.90	480	4.22
30.59	1.071	28.4	23.7	27.5	231.6	9.89	17.88	479	4.22
30.78	1.247	28.6	23.7	27.5	903.9	12.78	18.01	484	4.24
30.57	0.714	24.4	21.7	24.2	605.0	12.74	17.03	471	4.01

M500Y	SRP 0817		Intermediate µ$_L$		Packing Config. 3			2.8 m	
0	0.715	21.9	20.9	22.7	33.5	0	0	0	0
0	1.071	22.0	20.9	22.8	68.9	0	0	0	0
0	1.606	22.5	20.9	22.8	149.9	0	0	0	0
0	2.146	23.8	21.0	22.9	250.6	0	0	0	0
0	2.860	26.0	21.0	22.9	428.2	0	0	0	0
0	3.574	29.2	21.0	23.1	645.0	0	0	0	0
0	4.286	33.1	21.0	23.5	899.4	0	0	0	0
2.62	0.710	29.4	24.4	28.2	40.1	3.68	0.30	3	0.07
2.54	1.064	29.5	23.9	28.2	80.9	3.88	0.29	3	0.07
2.56	1.594	30.0	23.8	28.4	181.2	4.08	0.29	3	0.07
2.59	2.124	30.9	23.8	28.5	346.4	4.26	0.30	3	0.07
2.57	2.655	32.5	23.7	28.5	556.8	4.55	0.29	3	0.07
2.76	2.833	33.9	23.7	28.5	662.0	4.71	0.31	3	0.07
2.66	3.014	34.5	23.7	28.6	780.0	4.87	0.30	3	0.07
2.10	3.270	37.3	23.7	28.5	1110.5	5.61	0.24	2	0.06
4.28	0.705	32.7	26.5	30.2	41.9	5.47	0.52	7	0.12
4.25	1.060	32.4	24.7	30.4	84.3	5.52	0.50	7	0.12
4.37	1.590	32.5	24.3	30.2	189.2	5.77	0.51	7	0.12
4.29	2.122	32.8	24.3	30.2	370.2	6.24	0.50	7	0.12
4.48	2.471	33.6	24.2	30.0	531.0	6.56	0.52	7	0.12
4.18	2.829	35.6	24.0	29.5	899.4	7.71	0.48	6	0.11
5.98	0.711	26.2	23.5	25.4	44.0	6.31	0.68	11	0.16
6.02	1.070	26.2	22.5	25.4	89.1	6.41	0.67	12	0.16
6.04	1.600	26.8	22.3	25.5	210.2	6.69	0.66	12	0.16
6.09	2.132	27.8	22.3	25.8	403.1	7.12	0.67	12	0.16
6.07	2.309	28.7	22.3	25.9	492.1	7.33	0.67	12	0.16
6.08	2.400	29.7	22.3	26.0	596.6	7.72	0.67	12	0.16
6.06	2.575	32.4	22.7	26.3	828.3	8.32	0.67	12	0.16
9.03	0.714	24.2	23.2	24.8	44.7	7.02	1.02	23	0.24
8.90	1.072	24.7	23.2	24.8	89.8	6.99	1.00	22	0.24
9.20	1.601	25.3	23.0	24.9	202.4	7.40	1.03	23	0.24
8.94	2.139	26.7	22.7	25.0	476.0	8.38	1.00	22	0.23
9.18	2.318	28.3	22.6	25.1	693.8	9.50	1.02	23	0.24
9.11	2.336	29.2	22.6	25.2	864.9	10.18	1.01	23	0.24
12.18	0.710	23.9	22.0	24.0	49.1	9.12	1.33	37	0.31
12.26	1.072	24.1	21.8	24.2	100.1	9.25	1.33	37	0.31
12.25	1.608	24.8	22.1	24.3	246.2	9.63	1.34	37	0.32
12.19	1.871	25.5	21.8	24.3	370.6	9.95	1.33	37	0.31
12.21	1.962	26.5	21.9	24.4	488.7	10.45	1.33	37	0.31
12.31	2.031	27.8	22.0	24.6	847.7	12.16	1.35	38	0.32
18.22	0.705	30.6	24.8	30.6	50.4	10.12	2.14	74	0.50
18.37	1.057	30.8	25.0	30.5	102.2	10.27	2.17	75	0.51
18.30	1.588	31.5	24.7	30.8	280.9	10.70	2.15	75	0.51
18.37	1.766	32.1	24.5	31.2	417.9	11.19	2.14	75	0.50
18.37	1.853	32.5	24.4	31.0	529.0	11.67	2.14	75	0.50
18.48	1.925	33.3	24.2	30.6	891.4	13.14	2.14	76	0.50
24.44	0.722	30.1	25.0	30.2	247.6	13.14	2.89	122	0.68

L	F_G	$T_{air,in}$	$T_{liq,in}$	$T_{air,out}$	$\Delta P/Z$	h_L	Re_L	We_L x 10^4	Fr_L
$(m^3/m^2 \cdot h)$	$(Pa)^{0.5}$	(°C)	(°C)	(°C)	(Pa/m)	(%)			
24.46	1.061	30.1	24.9	30.0	303.9	12.50	2.88	122	0.68
24.44	1.416	30.5	24.7	29.7	325.2	11.97	2.86	121	0.67
24.60	1.740	31.3	24.6	29.7	907.9	14.67	2.87	122	0.68
M500Y	**SRP 0815**		**High μ_L**		**Packing Config. 3**			**2.8 m**	
0	0.712	22.7	20.8	23.4	33.8	0	0	0	0
0	1.070	23.6	21.0	23.5	68.4	0	0	0	0
0	1.434	24.1	21.5	23.8	114.7	0	0	0	0
0	1.781	30.9	22.0	24.7	176.6	0	0	0	0
0	2.141	25.7	21.8	23.9	248.1	0	0	0	0
0	2.858	27.5	21.9	24.0	426.5	0	0	0	0
0	3.566	30.4	21.9	24.2	638.1	0	0	0	0
0	4.278	34.4	21.9	24.5	889.2	0	0	0	0
2.37	0.706	33.6	25.0	30.9	39.6	4.53	0.13	2	0.03
2.58	1.058	33.4	26.5	31.2	81.7	4.87	0.14	2	0.03
2.36	1.590	32.9	25.2	31.3	176.7	4.95	0.13	2	0.03
2.52	2.116	33.3	24.2	31.1	332.7	5.39	0.13	2	0.03
2.62	2.470	34.1	24.0	30.8	493.5	5.71	0.13	2	0.03
2.37	2.739	35.6	23.9	30.5	782.1	6.50	0.12	2	0.03
4.01	0.709	30.9	24.3	28.3	43.4	5.93	0.21	5	0.05
4.27	1.064	30.7	23.7	28.6	85.6	6.00	0.22	5	0.05
4.16	1.596	30.7	23.2	28.6	193.4	6.35	0.21	5	0.05
4.26	2.125	31.6	23.1	28.8	380.9	6.82	0.21	5	0.05
4.17	2.303	32.4	23.1	28.9	475.9	6.87	0.21	5	0.05
4.10	2.477	33.8	23.1	28.8	704.1	7.64	0.20	5	0.05
6.21	0.706	32.2	24.2	33.7	42.0	6.38	0.32	10	0.08
6.10	0.710	32.7	23.4	29.9	45.2	7.05	0.31	10	0.07
6.24	1.054	32.5	24.4	33.4	85.8	6.45	0.32	10	0.08
6.20	1.059	32.7	23.2	30.1	89.8	7.06	0.31	10	0.07
6.04	1.585	32.8	24.1	33.3	192.1	6.48	0.31	10	0.07
6.04	1.593	33.0	23.4	30.2	204.3	7.31	0.30	10	0.07
6.09	1.934	33.4	23.7	33.3	321.8	6.83	0.31	10	0.07
6.16	2.117	32.9	23.8	30.3	455.0	8.01	0.31	10	0.07
6.09	2.295	33.7	23.5	30.0	691.3	9.06	0.31	10	0.07
9.02	0.717	25.2	23.3	25.4	47.7	8.88	0.45	19	0.11
9.06	1.066	25.2	22.7	25.5	96.2	9.03	0.45	19	0.11
9.20	1.605	26.1	22.6	25.5	235.3	9.56	0.45	19	0.11
9.09	1.779	26.6	22.3	25.5	316.4	9.72	0.45	19	0.10
9.05	1.868	27.2	22.1	25.4	398.7	10.05	0.44	19	0.10
9.09	1.955	27.9	22.0	25.5	530.3	10.70	0.44	19	0.10
12.18	0.702	31.8	25.9	31.9	47.8	9.72	0.66	32	0.16
12.16	0.704	33.7	23.1	31.7	49.6	9.83	0.61	31	0.14
12.19	1.054	31.9	25.5	32.1	96.4	9.85	0.65	32	0.15
12.04	1.062	33.6	23.3	31.8	103.6	10.00	0.61	30	0.14
12.21	1.582	32.1	24.9	33.6	225.7	10.55	0.64	31	0.15
12.22	1.586	33.2	24.6	32.1	245.1	10.23	0.64	31	0.15
12.22	1.849	33.6	23.5	31.9	516.1	11.37	0.62	31	0.15
12.45	1.911	34.5	23.6	31.7	844.6	13.30	0.63	32	0.15
18.35	0.704	32.4	25.0	34.3	52.5	11.84	0.97	62	0.23
18.38	1.053	32.6	25.6	34.7	106.9	11.93	0.99	63	0.23
18.35	1.404	32.9	24.9	34.8	185.6	12.00	0.96	62	0.23
18.33	1.758	33.7	24.6	34.0	549.6	13.61	0.95	62	0.23
18.47	1.788	34.5	24.2	33.0	806.1	15.41	0.95	62	0.22
24.41	0.692	32.6	24.3	31.9	100.5	13.25	1.26	99	0.30

336

L	F_G	$T_{air,in}$	$T_{liq,in}$	$T_{air,out}$	$\Delta P/Z$	h_L	Re_L	We_L x 10^4	Fr_L
$(m^3/m^2 \cdot h)$	$(Pa)^{0.5}$	(°C)	(°C)	(°C)	(Pa/m)	(%)			
24.52	0.887	32.5	24.3	31.7	126.7	12.80	1.27	100	0.30
24.50	1.060	32.6	24.3	31.5	162.8	12.71	1.27	100	0.30
24.42	1.238	32.8	24.1	31.4	200.0	12.54	1.26	99	0.30
24.46	1.499	33.2	23.9	31.3	435.2	13.53	1.25	99	0.29
24.47	1.532	33.6	23.7	31.2	516.4	13.88	1.25	99	0.29

M250X	SRP 0904		Baseline			3.1 m			
0	0.640	23.7	21.6	24.3	6.4	0	0	0	0
0	0.643	20.5	20.3	20.9	6.4	0	0	0	0
0	0.716	30.8	22.0	25.2	7.5	0	0	0	0
0	0.718	23.9	21.7	24.3	7.5	0	0	0	0
0	1.073	23.9	21.7	24.3	14.7	0	0	0	0
0	1.079	20.6	20.2	21.0	15.4	0	0	0	0
0	1.608	24.2	21.7	24.0	30.3	0	0	0	0
0	2.142	24.8	21.8	25.0	50.6	0	0	0	0
0	2.847	26.4	21.8	25.0	86.6	0	0	0	0
0	3.559	28.8	21.8	25.2	132.0	0	0	0	0
0	3.587	25.7	20.1	21.0	137.9	0	0	0	0
0	4.276	32.2	21.9	25.0	188.8	0	0	0	0
0	4.981	37.3	21.9	25.5	264.4	0	0	0	0
0	5.160	39.5	22.1	25.7	284.9	0	0	0	0
2.76	0.716	28.7	23.4	22.2	8.4	N	3.49	14	1.01
2.58	1.075	27.2	23.2	22.2	16.7	N	3.25	13	0.94
3.01	1.614	26.3	23.2	22.2	33.5	N	3.79	16	1.09
3.03	2.151	25.6	23.3	22.0	57.7	N	3.83	17	1.10
2.90	2.866	25.9	23.3	22.0	98.0	N	3.66	15	1.06
3.05	3.580	27.9	23.1	21.6	152.7	N	3.83	17	1.11
2.85	4.299	31.2	22.9	21.6	238.4	N	3.57	15	1.03
2.66	5.198	38.8	22.6	21.1	424.3	N	3.30	13	0.95
6.28	0.707	28.5	22.2	27.1	8.8	0.84	7.74	55	2.23
6.08	1.071	28.0	21.3	27.1	16.8	0.80	7.33	52	2.12
6.07	1.603	27.8	21.0	27.1	34.5	0.86	7.26	52	2.10
6.05	2.130	28.0	20.9	27.1	57.3	0.91	7.23	51	2.09
6.04	2.839	29.1	20.7	27.3	99.0	1.00	7.17	51	2.07
6.09	3.542	31.3	20.4	27.4	152.6	1.10	7.18	52	2.07
6.14	4.262	34.0	20.1	27.2	254.6	1.42	7.18	52	2.07
6.09	4.789	37.7	19.9	27.2	391.8	2.05	7.09	51	2.05
6.12	5.146	41.9	20.0	27.2	555.6	2.98	7.15	52	2.06
8.73	0.719	22.7	20.6	21.9	9.0	1.89	10.35	94	2.99
8.78	1.072	22.5	20.6	22.0	17.3	1.87	10.38	95	3.00
8.94	1.611	22.5	20.5	22.2	35.9	1.90	10.57	98	3.05
9.13	2.148	22.9	20.5	22.2	60.8	1.99	10.78	101	3.11
9.19	2.863	24.2	20.4	22.2	104.8	2.09	10.84	102	3.13
9.13	3.579	26.6	20.4	22.3	163.2	2.19	10.76	101	3.11
9.13	4.297	31.0	20.6	22.0	304.5	2.73	10.80	101	3.12
9.18	4.657	34.1	20.9	21.8	469.6	3.65	10.95	103	3.16
9.22	5.015	39.6	22.1	21.7	760.7	5.33	11.32	105	3.27
12.23	0.710	30.5	21.1	27.4	9.5	2.80	14.67	166	4.23
11.93	1.058	29.4	21.3	27.5	17.9	2.64	14.37	160	4.15
12.22	1.601	29.0	21.4	27.5	36.0	2.72	14.74	166	4.26
12.23	2.130	29.0	21.2	27.7	60.5	2.78	14.69	166	4.24
12.25	2.837	29.8	20.9	27.7	103.4	2.91	14.63	166	4.22
12.24	3.549	32.2	20.5	27.8	173.5	3.18	14.47	165	4.18
12.20	3.899	33.7	20.2	27.7	229.3	3.41	14.32	164	4.13

337

L	F_G	$T_{air,in}$	$T_{liq,in}$	$T_{air,out}$	$\Delta P/Z$	h_L	Re_L	$We_L \times 10^4$	Fr_L
($m^3/m^2 \cdot h$)	$(Pa)^{0.5}$	(°C)	(°C)	(°C)	(Pa/m)	(%)			
12.23	4.257	35.5	20.1	28.0	343.9	3.97	14.33	164	4.14
12.24	4.601	39.1	20.3	28.6	597.0	5.45	14.41	165	4.16
12.20	4.782	42.5	21.5	28.3	817.8	6.68	14.76	166	4.26
18.41	0.705	29.1	21.0	26.4	9.8	3.92	22.02	328	6.36
18.30	1.070	28.2	21.2	26.4	19.0	3.92	21.96	325	6.34
18.38	1.604	27.7	21.0	26.3	38.3	3.96	22.00	327	6.35
18.33	2.138	27.8	20.7	26.3	65.1	4.03	21.78	325	6.29
18.32	2.847	28.7	20.4	26.1	112.2	4.20	21.61	323	6.24
18.35	3.554	30.7	20.1	26.2	211.0	4.67	21.47	323	6.20
18.35	4.267	35.2	20.1	25.9	613.3	6.82	21.46	323	6.19
18.35	4.427	37.7	20.6	26.0	884.0	8.38	21.76	325	6.28
24.54	0.702	28.4	21.4	27.9	10.4	4.99	29.64	531	8.56
24.45	1.071	28.0	21.4	27.6	19.7	4.98	29.55	528	8.53
24.44	1.601	28.0	21.3	27.6	39.6	5.02	29.46	527	8.51
24.49	2.130	28.3	21.2	28.1	67.3	5.08	29.45	529	8.50
24.44	2.834	29.6	20.9	28.3	117.2	5.21	29.18	525	8.42
24.45	3.540	31.8	20.6	28.4	265.9	5.92	28.99	524	8.37
24.44	3.889	34.8	20.6	30.0	454.1	6.89	28.92	523	8.35
24.47	4.077	37.1	20.8	28.1	740.4	8.46	29.14	526	8.41
36.62	0.719	27.7	21.2	26.5	11.3	6.14	43.96	1033	12.69
36.63	1.063	27.5	21.3	27.9	21.3	6.24	44.08	1034	12.72
36.67	1.600	27.0	21.2	25.7	42.9	6.27	44.06	1035	12.72
36.59	2.130	27.4	21.0	27.2	72.8	6.34	43.77	1030	12.64
36.81	2.842	28.7	20.8	27.3	128.7	6.49	43.83	1038	12.65
36.68	3.550	31.6	20.6	27.6	428.0	8.24	43.50	1030	12.56
36.69	3.763	35.1	20.8	27.1	881.6	11.02	43.66	1032	12.60
48.38	0.710	31.2	22.1	27.1	13.1	7.67	59.44	1658	17.16
48.83	1.068	29.9	22.1	27.1	24.9	7.76	59.93	1683	17.30
48.90	1.602	29.2	22.0	27.2	50.9	7.80	59.84	1685	17.27
48.91	2.129	29.0	21.7	27.3	90.7	7.96	59.44	1681	17.16
48.91	2.838	30.0	21.3	27.3	226.2	8.67	58.95	1676	17.02
48.89	3.194	31.6	21.0	27.8	442.1	9.94	58.52	1669	16.89
48.91	3.369	33.7	20.8	27.4	872.4	12.55	58.26	1667	16.82
61.14	0.712	21.6	20.4	21.1	14.1	9.02	72.07	2408	20.80
61.14	1.074	21.5	20.5	21.1	26.6	9.07	72.16	2409	20.83
61.07	1.611	21.7	20.5	21.0	54.8	9.13	72.08	2405	20.81
61.10	2.150	22.4	20.4	21.1	98.4	9.31	72.07	2406	20.81
61.10	2.868	23.8	20.4	21.0	328.1	10.54	72.06	2406	20.80
61.07	3.044	25.4	20.5	21.4	692.6	12.65	72.14	2406	20.82
61.07	3.082	26.3	20.7	21.5	821.4	13.35	72.45	2410	20.91
73.05	0.714	27.9	21.3	26.2	16.9	9.82	87.98	3269	25.40
73.30	1.065	27.3	21.4	26.2	32.1	9.87	88.50	3290	25.55
73.33	1.597	27.2	21.4	27.1	79.0	10.02	88.61	3294	25.58
73.33	2.308	28.1	21.3	27.7	212.4	10.55	88.26	3289	25.48
73.45	2.488	28.9	21.2	27.0	275.7	10.77	88.26	3296	25.48
73.33	2.670	29.7	21.2	27.0	440.7	11.50	88.06	3286	25.42
73.44	2.752	31.7	21.2	27.4	1104.5	15.33	88.27	3295	25.48

M250X	SRP 0907		High μ_L			3.1 m			
0	0.649	18.0	16.0	16.6	6.5	0	0	0	0
0	0.729	18.3	16.0	16.5	7.8	0	0	0	0
0	1.086	18.7	16.1	16.4	15.5	0	0	0	0
0	1.627	19.1	16.1	16.5	31.8	0	0	0	0
0	2.168	19.9	16.1	16.5	53.6	0	0	0	0

L	F_G	$T_{air,in}$	$T_{liq,in}$	$T_{air,out}$	$\Delta P/Z$	h_L	Re_L	$We_L \times 10^4$	Fr_L
$(m^3/m^2 \cdot h)$	$(Pa)^{0.5}$	(°C)	(°C)	(°C)	(Pa/m)	(%)			
0	2.892	21.5	16.2	16.7	91.2	0	0	0	0
0	3.609	23.5	16.2	17.4	136.6	0	0	0	0
0	4.320	28.0	16.4	18.7	195.6	0	0	0	0
0	5.028	32.5	16.6	20.0	270.2	0	0	0	0
2.98	0.716	32.1	21.1	22.5	9.1	1.29	0.26	11	0.08
2.88	1.071	31.3	21.1	22.5	17.4	1.24	0.25	10	0.07
2.84	1.608	30.8	20.9	22.4	35.1	1.32	0.25	10	0.07
2.90	2.504	31.6	20.9	21.5	78.4	1.51	0.25	10	0.07
2.95	3.580	34.3	20.8	21.5	167.4	1.80	0.25	10	0.07
2.96	4.664	39.4	20.5	21.1	385.2	2.32	0.25	10	0.07
2.91	5.013	44.4	20.1	22.1	518.2	2.91	0.25	10	0.07
6.38	0.718	30.4	21.0	22.7	9.5	3.16	0.55	38	0.16
6.18	1.074	30.1	19.8	22.7	18.1	3.12	0.51	35	0.15
6.11	1.606	30.0	19.5	22.5	37.0	3.14	0.50	35	0.15
5.97	2.152	30.7	19.5	22.1	62.3	3.17	0.49	33	0.14
6.31	2.864	31.7	19.2	21.7	108.2	3.45	0.51	36	0.15
6.37	3.585	34.2	18.8	21.7	189.4	3.78	0.51	37	0.15
6.35	4.124	37.0	18.6	21.2	335.1	4.15	0.51	37	0.15
6.44	4.301	39.1	18.5	21.2	416.0	4.41	0.51	37	0.15
6.02	4.659	42.6	18.8	21.6	653.3	5.20	0.48	34	0.14
9.05	0.711	32.4	20.1	23.0	9.9	3.51	0.76	67	0.22
8.96	1.070	31.6	20.0	23.1	18.7	3.48	0.75	66	0.22
9.05	1.611	31.2	20.1	22.4	38.2	3.62	0.76	67	0.22
9.22	2.146	31.2	20.4	22.5	65.8	3.76	0.79	69	0.23
9.12	2.862	31.9	20.1	22.5	113.4	3.91	0.77	68	0.22
9.18	3.574	34.0	19.4	22.4	221.1	4.48	0.75	68	0.22
9.11	4.117	37.2	18.8	21.6	472.2	5.46	0.73	67	0.21
9.12	4.303	40.4	19.1	21.3	691.7	6.42	0.74	67	0.21
12.22	0.721	28.5	19.4	22.3	10.3	4.79	1.00	110	0.29
12.16	1.075	28.5	21.6	22.2	19.3	4.90	1.08	112	0.31
12.34	1.612	28.7	20.9	23.0	38.6	4.93	1.07	114	0.31
12.30	2.148	29.4	20.0	23.2	65.7	5.07	1.03	112	0.30
12.38	2.856	30.8	19.7	23.2	116.2	5.35	1.03	113	0.30
12.36	3.580	33.8	19.2	22.2	274.1	6.18	1.01	112	0.29
12.42	3.945	36.6	18.7	21.3	526.1	7.48	0.99	112	0.29
12.15	4.034	38.0	18.7	21.2	654.2	8.11	0.97	108	0.28
18.53	0.711	30.2	19.4	21.7	11.1	7.36	1.52	220	0.44
18.33	1.071	29.8	20.3	22.0	20.6	7.36	1.56	218	0.45
18.32	1.614	29.7	19.8	22.6	42.1	7.40	1.53	217	0.44
18.32	2.147	29.8	19.8	22.0	71.3	7.62	1.52	217	0.44
18.31	2.866	30.7	19.3	21.8	128.5	7.94	1.50	215	0.43
18.38	3.582	33.6	18.9	21.3	432.7	9.75	1.48	216	0.43
18.34	3.671	35.6	18.6	21.0	582.8	10.76	1.47	214	0.42
18.33	3.765	37.0	18.9	21.0	793.7	12.05	1.48	215	0.43
24.44	0.717	23.8	20.3	21.9	11.4	8.74	2.07	352	0.60
24.41	1.071	23.2	20.0	21.9	21.3	8.73	2.05	351	0.59
24.44	1.610	23.2	19.8	22.0	44.0	8.83	2.04	351	0.59
24.43	2.145	23.7	19.3	21.7	75.1	8.93	2.00	348	0.58
24.44	2.868	25.2	18.9	21.1	139.4	9.25	1.97	347	0.57
24.42	3.408	29.8	18.2	20.5	512.3	11.50	1.92	343	0.55
24.45	3.502	30.9	18.1	20.2	705.3	12.57	1.92	344	0.55
24.49	3.535	33.1	18.4	20.2	882.5	13.32	1.94	346	0.56
36.73	0.713	26.3	18.7	21.1	12.9	10.76	2.94	682	0.85
36.61	1.080	25.8	18.7	20.9	24.8	10.69	2.93	679	0.85

339

L	F_G	T_air,in	T_liq,in	T_air,out	ΔP/Z	h_L	Re_L	We_L x 10^4	Fr_L
(m³/m²·h)	(Pa)^0.5	(°C)	(°C)	(°C)	(Pa/m)	(%)			
36.71	1.618	26.0	18.7	20.9	51.7	10.75	2.94	681	0.85
36.60	2.152	26.5	18.6	20.7	107.5	10.93	2.92	678	0.84
36.66	2.870	28.8	18.4	20.6	478.6	13.00	2.90	677	0.84
36.69	2.963	29.9	18.4	20.4	602.8	13.66	2.90	678	0.84
36.64	2.984	33.0	18.5	20.5	1349.3	18.76	2.92	678	0.84
49.17	0.710	28.0	20.1	22.3	14.5	11.99	4.13	1127	1.19
48.39	0.718	28.9	19.3	21.2	14.9	12.10	3.97	1088	1.15
48.89	1.075	27.7	20.0	21.9	28.5	11.95	4.10	1115	1.18
48.78	1.075	28.6	19.3	21.4	28.6	12.14	3.99	1102	1.15
48.91	1.343	28.9	19.3	21.5	45.2	12.02	4.01	1108	1.16
48.72	1.612	27.5	19.8	21.9	125.6	12.25	4.06	1107	1.17
48.92	1.617	28.5	19.4	21.4	119.9	12.41	4.02	1109	1.16
48.96	1.618	31.3	19.5	21.6	120.2				
49.02	1.797	29.1	19.4	21.5	165.3	12.43	4.02	1112	1.16
48.91	1.970	29.0	19.3	21.4	215.8	12.91	4.00	1108	1.16
48.93	2.149	29.6	19.3	21.5	277.0	12.98	4.01	1108	1.16
48.86	2.151	32.4	19.4	21.5	312.4				
49.03	2.151	28.0	19.7	21.9	312.5	13.29	4.06	1117	1.17
48.83	2.414	28.6	19.4	21.5	483.0	14.23	4.02	1106	1.16
48.90	2.479	30.2	19.0	21.2	963.6	17.60	3.96	1103	1.14
60.55	0.713	28.5	20.7	22.8	16.6	13.80	5.21	1607	1.51
61.00	1.070	28.2	20.7	22.8	35.6	13.85	5.25	1627	1.52
61.11	1.968	28.8	20.4	22.5	395.8	15.39	5.20	1626	1.50
61.15	2.145	29.3	20.2	22.4	521.2	16.07	5.17	1624	1.49
60.85	2.253	30.3	19.9	22.0	729.4	17.36	5.09	1605	1.47

MP252Y	SRP 0912		Baseline			3.0 m			
0	0.623	32.9	31.1	34.9	9.8	0	0	0	0
0	0.635	28.7	30.3	28.5	9.5	0	0	0	0
0	0.706	28.7	30.4	28.6	11.5	0	0	0	0
0	1.054	35.1	30.9	36.3	23.5	0	0	0	0
0	1.062	28.4	30.4	28.5	23.4	0	0	0	0
0	1.591	28.7	30.5	28.8	48.9	0	0	0	0
0	2.126	29.4	30.6	28.9	83.7	0	0	0	0
0	2.789	37.5	30.8	38.2	139.8	0	0	0	0
0	2.830	30.8	30.6	29.6	142.4	0	0	0	0
0	3.528	33.0	30.6	30.8	213.7	0	0	0	0
0	4.211	38.6	30.6	34.2	309.8	0	0	0	0
0	4.906	41.6	30.6	35.2	405.7	0	0	0	0
2.51	0.721	28.7	27.4	21.8	13.3	N	3.48	12	0.82
2.46	1.073	28.0	28.0	21.9	26.1	N	3.45	11	0.81
2.60	1.612	27.6	27.5	20.9	55.4	N	3.61	13	0.85
2.56	2.868	29.0	27.3	20.8	165.3	N	3.53	12	0.83
2.43	3.595	31.1	27.2	19.9	260.8	N	3.35	11	0.79
2.47	4.665	36.9	27.1	20.7	458.1	N	3.39	11	0.80
6.06	0.714	32.1	27.5	21.3	14.1	0.85	8.40	51	1.98
6.31	1.072	30.8	27.2	21.6	27.7	0.84	8.69	55	2.05
6.13	1.612	29.9	26.9	21.6	58.3	0.85	8.39	52	1.98
6.58	2.867	30.3	26.8	21.3	173.2	1.21	8.98	58	2.12
6.22	3.589	31.9	26.6	20.5	276.3	1.29	8.46	53	2.00
6.25	4.665	36.4	26.4	20.5	507.2	1.80	8.47	53	2.00
8.83	0.714	29.5	27.2	21.4	14.4	1.51	12.17	96	2.87
9.20	1.075	28.4	26.4	21.9	28.7	1.64	12.46	102	2.94
9.29	1.611	27.5	26.8	21.3	61.2	1.74	12.68	104	2.99

L	F_G	$T_{air,in}$	$T_{liq,in}$	$T_{air,out}$	$\Delta P/Z$	h_L	Re_L	$We_L \times 10^4$	Fr_L
$(m^3/m^2 \cdot h)$	$(Pa)^{0.5}$	(°C)	(°C)	(°C)	(Pa/m)	(%)			
9.41	2.868	28.6	26.7	21.3	180.3	2.07	12.82	106	3.02
9.25	3.588	30.5	26.5	20.9	292.0	2.32	12.54	102	2.96
9.19	4.661	36.4	26.2	20.7	557.7	3.00	12.38	101	2.92
12.71	0.712	30.4	26.7	22.1	15.1	2.85	17.34	175	4.09
12.20	1.078	29.9	27.0	21.5	29.4	2.78	16.75	163	3.95
12.21	1.617	29.7	27.0	21.5	62.4	2.86	16.74	164	3.95
12.44	2.145	30.0	26.6	21.8	107.9	3.01	16.91	168	3.99
12.35	2.869	31.5	26.1	21.5	187.3	3.18	16.61	165	3.92
12.59	3.587	34.1	25.7	20.7	304.8	3.48	16.79	170	3.96
12.16	4.308	37.9	25.5	20.3	487.2	3.84	16.15	160	3.81
12.03	4.669	42.5	25.7	20.4	620.7	3.94	16.06	158	3.78
18.19	0.719	32.4	26.5	21.5	15.6	3.89	24.68	316	5.82
18.32	1.074	31.1	26.7	21.3	31.1	3.96	24.96	321	5.88
18.33	1.614	29.9	26.7	21.3	67.5	4.08	24.97	321	5.89
18.27	2.151	29.7	26.5	21.5	115.9	4.24	24.77	319	5.84
18.31	2.872	30.8	26.1	21.1	206.1	4.52	24.65	319	5.81
18.34	3.586	32.8	25.9	21.1	349.4	4.96	24.55	319	5.79
18.29	4.305	36.0	25.7	20.6	581.2	5.52	24.41	317	5.75
18.31	4.669	40.8	25.9	20.2	816.5	6.15	24.53	318	5.78
24.69	0.717	31.8	26.6	22.0	16.7	5.05	33.56	527	7.91
24.49	1.074	30.7	27.1	21.6	33.1	5.08	33.65	522	7.93
24.44	1.611	30.2	26.9	21.6	69.7	5.22	33.43	519	7.88
24.44	2.148	30.3	26.7	21.6	120.2	5.39	33.30	519	7.85
24.47	2.867	31.8	26.3	21.2	213.9	5.73	33.06	518	7.79
24.47	3.589	34.7	26.0	20.7	381.3	6.27	32.83	516	7.74
24.46	3.948	37.1	25.9	20.7	503.4	6.50	32.78	516	7.73
24.45	4.128	38.9	26.0	20.5	602.5	6.63	32.82	516	7.73
24.42	4.300	43.6	26.6	20.8	1214.5	10.02	33.19	517	7.82
36.61	0.717	30.8	27.4	22.3	18.1	6.74	50.63	1023	11.93
36.68	1.077	30.3	27.3	22.3	35.3	6.79	50.69	1026	11.95
36.66	1.614	30.5	27.3	22.0	74.4	6.92	50.68	1026	11.95
36.66	2.152	31.0	27.1	21.9	130.9	7.11	50.45	1024	11.89
36.71	2.866	32.2	26.9	21.8	236.4	7.48	50.23	1023	11.84
36.78	3.585	35.1	26.5	21.3	589.2	8.30	49.91	1023	11.76
36.71	3.841	39.2	26.4	20.9	1046.3	10.51	49.74	1019	11.72
48.69	0.722	28.6	28.1	22.8	19.1	8.08	68.44	1657	16.13
48.84	1.070	28.4	28.1	22.8	37.7	8.31	68.58	1665	16.16
48.92	1.610	28.6	27.9	22.8	80.1	8.61	68.47	1667	16.14
48.87	2.148	29.2	27.7	22.5	141.9	8.92	68.06	1661	16.04
48.89	2.862	31.3	27.3	21.9	387.1	9.77	67.46	1656	15.90
48.91	3.049	33.4	26.9	21.5	534.5	10.44	66.93	1651	15.78
48.89	3.225	34.6	26.7	21.5	702.3	11.22	66.68	1648	15.72
48.87	3.314	36.2	26.7	21.1	919.7	12.45	66.54	1645	15.68
60.89	0.718	34.0	27.3	21.4	22.0	8.72	83.99	2387	19.80
61.01	1.071	32.9	27.3	21.9	42.7	8.79	84.28	2396	19.87
61.13	1.613	31.5	27.3	22.0	98.0	9.00	84.47	2404	19.91
61.14	2.149	31.2	27.2	22.0	189.0	9.33	84.22	2401	19.85
61.14	2.868	33.4	26.8	21.6	816.4	11.65	83.46	2393	19.67
61.14	2.922	34.9	26.6	21.1	927.4	12.26	83.10	2388	19.59
73.37	0.717	31.3	27.3	20.4	24.4	10.36	101.32	3258	23.88
73.40	1.079	30.8	27.5	22.1	51.0	10.43	101.80	3266	23.99
73.35	1.612	30.6	27.5	22.2	141.2	10.80	101.82	3264	24.00
73.37	2.147	31.0	27.5	22.1	408.3	11.60	101.70	3263	23.97
73.45	2.507	32.3	27.3	22.1	758.2	13.15	101.51	3265	23.93

L	F_G	$T_{air,in}$	$T_{liq,in}$	$T_{air,out}$	$\Delta P/Z$	h_L	Re_L	We_L x 10^4	Fr_L
$(m^3/m^2 \cdot h)$	$(Pa)^{0.5}$	(°C)	(°C)	(°C)	(Pa/m)	(%)			
73.35	2.560	33.6	27.2	21.9	861.9	13.67	101.09	3254	23.83
73.36	2.591	34.9	27.2	21.8	1063.7	14.94	101.01	3253	23.81
MP252Y	**SRP 0915**		**High μ_L**			**3.0 m**			
0	0.655	20.0	26.6	18.3	10.7	0	0	0	0
0	0.717	20.0	26.6	18.3	12.2	0	0	0	0
0	1.079	20.0	26.6	18.3	25.1	0	0	0	0
0	1.621	20.3	26.5	18.0	54.3	0	0	0	0
0	2.161	21.0	26.5	18.1	92.6	0	0	0	0
0	2.882	22.6	26.5	18.1	157.6	0	0	0	0
0	3.599	25.3	26.5	18.4	237.2	0	0	0	0
0	4.316	29.6	26.5	19.2	343.5	0	0	0	0
0	4.670	33.4	26.5	20.2	397.9	0	0	0	0
2.44	0.721	36.1	28.2	21.8	14.3	0.68	0.25	7	0.06
2.67	1.068	35.4	28.0	21.9	28.1	0.86	0.27	9	0.06
2.48	1.614	34.7	28.0	21.1	59.8	0.91	0.25	8	0.06
2.37	2.151	34.3	28.0	21.1	101.7	0.79	0.24	7	0.06
2.66	3.235	36.0	27.9	19.8	223.8	1.55	0.27	9	0.06
2.46	4.312	40.6	27.6	19.7	435.8	1.50	0.24	8	0.06
2.75	4.664	45.7	27.2	21.0	546.8	1.95	0.27	9	0.06
6.04	0.714	32.7	28.4	23.9	15.1	2.70	0.61	34	0.14
6.08	1.073	32.2	28.0	23.5	29.7	2.77	0.61	34	0.14
6.21	1.605	31.6	27.9	23.5	61.4	2.96	0.62	36	0.15
5.92	2.139	31.5	27.9	23.5	106.7	3.04	0.59	33	0.14
6.42	2.862	33.0	27.9	22.5	188.6	3.45	0.64	38	0.15
6.26	3.583	36.7	27.5	21.8	314.9	3.55	0.62	36	0.15
6.25	4.298	39.2	27.3	21.9	505.0	3.68	0.61	36	0.14
6.14	4.655	42.9	27.2	22.0	624.8	3.55	0.60	35	0.14
6.12	4.745	44.6	27.3	22.3	678.3	3.76	0.60	34	0.14
8.77	0.715	32.9	26.8	22.4	15.4	3.90	0.85	63	0.20
8.92	1.078	32.5	26.7	22.4	30.7	4.08	0.86	64	0.20
9.23	1.610	32.7	27.1	22.0	65.0	4.35	0.90	68	0.21
9.32	2.145	33.3	27.0	22.0	114.0	4.59	0.91	69	0.21
8.78	2.864	34.9	26.2	21.9	200.8	4.70	0.84	62	0.20
8.97	3.587	37.2	25.8	20.9	352.3	5.27	0.85	64	0.20
9.18	4.306	40.8	25.5	20.9	628.5	5.66	0.86	67	0.20
8.96	4.662	46.5	25.4	20.1	863.1	6.06	0.84	64	0.20
12.62	0.715	24.1	29.0	24.9	16.3	5.15	1.30	117	0.31
12.08	1.080	24.2	29.0	23.6	31.7	5.15	1.24	109	0.29
12.23	1.611	24.5	28.8	23.4	66.7	5.40	1.25	111	0.29
12.23	2.145	25.3	28.0	23.0	114.5	5.70	1.22	110	0.29
12.20	2.857	26.5	27.5	23.0	197.4	6.13	1.20	109	0.28
12.15	3.224	28.8	26.9	22.0	272.6	6.43	1.18	108	0.28
12.23	3.586	31.1	26.4	21.2	364.4	6.81	1.17	108	0.28
12.21	3.946	33.2	26.2	21.2	490.5	7.08	1.17	108	0.27
12.24	4.306	37.0	26.4	20.8	677.7	7.43	1.17	109	0.28
12.21	4.486	40.2	26.8	20.8	893.8	8.57	1.18	108	0.28
18.30	0.713	33.2	28.0	23.6	17.1	6.55	1.83	215	0.43
18.28	1.076	32.7	28.8	22.8	33.8	6.63	1.87	216	0.44
18.32	1.607	32.6	28.1	23.4	71.5	6.82	1.84	216	0.43
18.39	2.149	32.8	28.0	22.8	123.9	7.11	1.84	217	0.43
18.28	2.856	34.5	27.3	22.8	232.7	7.62	1.80	214	0.42
18.33	3.579	38.0	26.7	22.2	549.2	8.46	1.77	213	0.42
18.36	3.885	41.7	26.5	21.3	882.8	10.04	1.77	214	0.42

342

L	F_G	$T_{air,in}$	$T_{liq,in}$	$T_{air,out}$	$\Delta P/Z$	h_L	Re_L	$We_L \times 10^4$	Fr_L
$(m^3/m^2 \cdot h)$	$(Pa)^{0.5}$	(°C)	(°C)	(°C)	(Pa/m)	(%)			
24.82	0.720	32.6	27.9	21.9	18.2	7.72	2.48	357	0.58
24.43	1.072	31.5	28.1	22.6	35.5	7.69	2.45	349	0.58
24.48	1.610	30.7	28.0	22.6	74.7	7.79	2.45	349	0.58
24.46	2.149	30.2	27.8	22.4	133.4	8.01	2.44	349	0.57
24.50	2.861	31.0	27.5	22.4	275.9	8.41	2.42	349	0.57
24.59	3.219	32.1	27.4	22.0	482.9	8.97	2.42	350	0.57
24.53	3.580	36.8	27.3	21.6	879.8	10.62	2.41	349	0.57
36.75	0.713	34.7	27.7	22.8	20.4	9.76	3.65	686	0.86
36.62	1.072	34.0	27.7	22.6	41.0	9.74	3.63	682	0.86
36.55	1.611	33.7	27.5	22.6	98.5	9.92	3.61	679	0.85
36.57	2.148	33.9	27.1	22.2	293.7	10.57	3.57	677	0.84
36.75	2.506	34.6	26.9	21.6	491.4	11.23	3.57	682	0.84
36.74	2.689	36.7	26.5	21.2	669.5	11.92	3.53	678	0.83
36.61	2.784	38.4	26.4	20.8	832.8	12.68	3.51	674	0.83
48.55	0.723	33.4	29.8	23.5	22.3	10.68	5.11	1112	1.20
48.88	1.071	32.9	29.3	24.0	49.4	10.75	5.07	1119	1.19
48.89	1.610	32.4	28.9	24.0	194.0	11.27	5.02	1116	1.18
48.88	2.145	33.2	28.6	23.3	473.7	12.07	4.98	1113	1.17
48.83	2.321	34.0	28.3	23.0	662.8	12.79	4.93	1108	1.16
48.89	2.413	34.8	28.0	22.5	907.6	13.99	4.89	1107	1.15
60.48	0.720	33.3	28.3	23.0	28.7	12.16	6.10	1582	1.44
61.01	1.077	32.7	28.6	23.1	148.7	12.48	6.21	1610	1.46
61.15	1.431	32.7	28.6	23.1	301.3	13.00	6.22	1616	1.47
61.19	1.612	32.9	28.4	22.9	386.2	13.13	6.20	1616	1.46
61.23	1.789	33.0	28.4	22.7	499.6	13.48	6.19	1616	1.46
61.14	1.965	34.0	28.2	22.5	691.4	14.12	6.15	1610	1.45
61.17	2.020	35.3	28.0	22.5	850.5	14.81	6.13	1609	1.44

M250YS	SRP 0832		Baseline (Dry)			3.1 m			
0	0.734	7.8	7.7	8.2	15.4	0	0	0	0
0	1.061	23.9	16.3	28.0	28.0	0	0	0	0
0	1.099	8.0	7.6	8.3	31.3	0	0	0	0
0	1.648	8.5	7.6	8.4	66.7	0	0	0	0
0	2.197	9.3	7.5	8.3	113.6	0	0	0	0
0	2.845	25.3	16.3	25.6	172.5	0	0	0	0
0	2.935	12.5	7.5	8.2	196.7	0	0	0	0
0	3.664	14.8	7.5	8.3	302.7	0	0	0	0
0	4.397	19.2	7.5	8.6	424.4	0	0	0	0
0	4.645	31.6	16.4	23.1	438.1	0	0	0	0
0	5.004	36.6	16.4	22.8	505.3	0	0	0	0

M250YS	SRP 0901		Baseline			3.1 m			
0	0.727	17.3	9.0	15.2	15.6	0	0	0	0
0	1.083	17.4	9.2	15.6	30.3	0	0	0	0
0	1.626	17.5	9.3	16.0	61.7	0	0	0	0
0	2.171	17.8	9.4	16.4	104.0	0	0	0	0
0	2.892	18.9	9.5	16.5	175.4	0	0	0	0
0	3.613	21.6	9.6	16.8	274.4	0	0	0	0
0	4.329	25.3	9.6	17.8	382.8	0	0	0	0
0	5.035	29.9	9.5	19.4	506.7	0	0	0	0
2.78	0.716	28.0	14.1	21.5	15.7	0.13	2.81	12	0.66
2.88	1.073	26.9	15.2	21.5	31.5	0.18	2.99	13	0.70
2.75	1.615	26.1	15.0	21.3	66.9	0.22	2.83	12	0.67
2.59	2.508	25.9	14.7	20.7	154.0	0.27	2.65	11	0.62

L (m³/m²·h)	F_G (Pa)^0.5	T_air,in (°C)	T_liq,in (°C)	T_air,out (°C)	ΔP/Z (Pa/m)	h_L (%)	Re_L	We_L x 10⁴	Fr_L
3.11	3.591	28.9	14.4	19.7	328.9	0.80	3.15	15	0.74
2.78	4.322	33.7	14.0	19.0	548.2	1.31	2.79	12	0.66
2.78	4.683	35.8	13.9	18.7	665.3	1.70	2.78	12	0.66
6.09	0.712	27.5	15.9	25.3	16.2	1.73	6.42	46	1.51
6.13	1.067	27.4	16.0	25.7	32.3	1.71	6.48	47	1.53
6.02	1.599	27.2	16.1	25.9	68.7	1.73	6.37	45	1.50
5.99	2.135	27.5	16.0	26.0	116.9	1.79	6.33	45	1.49
6.15	3.202	29.6	15.3	26.0	269.5	1.99	6.39	47	1.51
6.40	3.916	33.0	14.8	25.2	495.7	2.90	6.55	49	1.54
6.24	4.647	39.9	14.2	23.2	904.0	4.77	6.31	47	1.49
9.20	0.722	24.4	13.6	18.0	16.8	2.15	9.15	89	2.16
9.23	1.079	23.7	13.0	18.0	33.9	2.18	9.03	89	2.13
9.13	1.627	23.1	13.0	18.1	72.1	2.24	8.92	88	2.10
9.21	2.166	22.8	12.9	18.0	124.0	2.31	8.99	89	2.12
8.91	3.239	23.9	12.7	18.0	295.0	2.75	8.64	84	2.04
9.12	3.968	27.0	12.2	17.6	618.9	4.10	8.73	87	2.06
9.23	4.150	28.8	12.0	17.3	736.9	4.68	8.78	88	2.07
9.16	4.332	32.0	12.2	17.1	921.7	5.64	8.76	87	2.06
12.32	0.716	29.9	15.1	25.3	17.4	2.69	12.71	147	3.00
12.32	1.069	28.5	15.3	25.4	33.7	2.72	12.80	148	3.02
12.24	1.604	27.3	15.4	24.8	72.1	2.73	12.73	146	3.00
12.24	2.145	26.9	15.1	24.3	123.6	2.78	12.65	146	2.98
12.22	2.854	27.5	14.7	24.2	220.1	2.92	12.50	145	2.95
12.25	3.569	29.5	14.2	23.2	465.1	3.93	12.36	145	2.91
12.24	3.936	32.2	13.7	21.9	780.3	5.52	12.20	144	2.88
12.25	4.035	34.2	13.6	21.0	903.5	6.13	12.17	144	2.87
18.39	0.714	26.8	15.3	24.8	18.5	3.60	19.12	289	4.51
18.30	1.068	26.4	15.9	25.3	35.5	3.59	19.29	288	4.55
18.30	1.606	26.3	15.7	25.3	75.0	3.61	19.20	287	4.53
18.39	2.138	26.6	15.5	25.3	129.4	3.68	19.21	289	4.53
18.36	2.848	27.8	15.3	25.1	230.6	3.83	19.05	288	4.49
18.37	3.206	29.4	14.9	24.6	361.6	4.29	18.87	287	4.45
18.27	3.567	32.0	14.6	23.8	749.2	6.24	18.65	283	4.40
24.58	0.714	24.4	18.8	23.5	19.6	4.07	27.88	485	6.57
24.44	1.069	24.1	18.7	23.4	37.9	4.06	27.62	480	6.51
24.45	1.607	24.1	18.2	23.4	79.5	4.16	27.34	478	6.44
24.44	2.144	24.5	17.6	23.2	137.6	4.30	26.89	475	6.34
24.48	2.859	25.4	17.2	22.8	258.3	4.56	26.65	474	6.28
24.50	3.218	27.9	16.1	22.3	567.0	6.21	26.00	470	6.13
24.50	3.310	29.7	15.6	21.9	767.8	7.35	25.61	467	6.04
36.59	0.725	28.7	14.1	19.3	20.5	5.60	36.83	897	8.68
36.65	1.076	27.3	14.1	19.3	39.7	5.68	36.85	899	8.69
36.67	1.620	25.5	14.0	19.1	84.6	5.81	36.77	898	8.67
36.67	2.162	24.4	13.7	18.7	149.1	6.05	36.56	896	8.62
36.70	2.882	24.8	13.4	18.2	480.3	7.82	36.22	894	8.54
36.74	3.024	26.8	13.0	17.8	971.9	11.01	35.89	892	8.46
48.74	0.713	25.5	16.0	23.0	22.5	6.81	51.48	1474	12.13
48.86	1.071	25.4	16.0	23.3	43.4	6.91	51.72	1482	12.19
48.88	1.606	25.5	16.0	23.3	91.5	7.05	51.70	1483	12.19
48.87	2.146	26.1	15.8	23.2	164.9	7.28	51.46	1479	12.13
48.90	2.502	26.8	15.6	23.1	308.1	7.92	51.14	1476	12.05
48.92	2.684	28.7	15.2	22.7	639.6	9.99	50.69	1472	11.95
48.95	2.717	29.5	15.1	22.6	779.4	10.90	50.58	1472	11.92
61.03	0.717	26.9	16.7	26.5	24.5	7.96	65.60	2160	15.46

344

L	F_G	$T_{air,in}$	$T_{liq,in}$	$T_{air,out}$	$\Delta P/Z$	h_L	Re_L	We_L x 10^4	Fr_L
($m^3/m^2 \cdot h$)	$(Pa)^{0.5}$	(°C)	(°C)	(°C)	(Pa/m)	(%)			
61.09	1.066	26.5	16.8	26.6	47.0	8.03	65.88	2167	15.53
61.11	1.600	26.4	16.7	26.1	101.3	8.23	65.73	2165	15.49
61.07	2.134	26.9	16.4	26.0	215.9	8.80	65.28	2158	15.39
61.15	2.313	27.6	16.2	25.5	335.8	9.40	64.92	2156	15.30
61.17	2.495	29.8	15.7	24.3	766.4	11.79	64.17	2147	15.13
73.00	0.711	27.9	15.6	27.0	26.9	8.90	76.49	2881	18.03
73.23	1.066	27.6	16.0	27.0	51.8	8.99	77.35	2906	18.23
73.23	1.596	27.7	16.1	26.9	136.0	9.32	77.63	2911	18.30
73.33	1.871	27.8	16.2	26.5	237.7	9.78	77.90	2920	18.36
73.32	2.135	28.5	16.2	26.1	443.6	10.65	77.89	2919	18.36
73.34	2.224	29.1	16.2	25.7	563.9	11.13	77.84	2919	18.35
73.35	2.317	29.7	16.1	24.8	877.2	12.74	77.71	2918	18.32
M125Y	**SRP 0909**		**Baseline**			**3.1 m**			
0	0.637	31.4	26.7	26.7	6.4	0	0	0	0
0	0.715	31.3	26.7	26.1	8.0	0	0	0	0
0	1.064	31.5	26.8	25.5	16.4	0	0	0	0
0	1.064	38.9	27.3	29.8	16.3	0	0	0	0
0	1.599	29.6	23.1	25.7	36.1	0	0	0	0
0	1.605	31.6	26.9	25.5	35.2	0	0	0	0
0	2.140	31.9	26.8	25.0	59.9	0	0	0	0
0	2.847	31.7	23.2	25.1	109.0	0	0	0	0
0	2.850	32.8	26.8	24.8	102.7	0	0	0	0
0	3.562	35.2	26.8	24.8	156.8	0	0	0	0
0	4.273	39.3	26.8	25.4	220.8	0	0	0	0
0	4.967	43.2	26.9	27.6	297.1	0	0	0	0
3.00	0.705	36.9	26.0	28.0	8.4	N	8.80	58	2.07
2.78	1.062	35.6	26.9	28.0	16.9	N	8.30	51	1.96
2.97	1.600	34.7	26.6	27.4	36.1	N	8.82	57	2.08
3.08	2.131	34.5	26.4	27.4	62.7	N	9.11	60	2.15
3.01	2.842	35.2	26.5	26.9	110.9	N	8.92	58	2.10
3.19	3.554	37.1	26.4	26.7	175.0	N	9.43	64	2.22
2.99	4.968	46.1	26.0	27.3	442.6	N	8.77	57	2.07
6.27	0.707	36.5	26.6	27.3	8.7	1.11	18.64	198	4.39
6.22	1.066	35.4	26.4	28.0	17.7	1.09	18.37	194	4.33
6.22	1.600	34.5	26.3	28.4	37.5	1.09	18.34	194	4.32
6.22	2.122	34.2	26.1	28.5	65.3	1.11	18.29	194	4.31
6.16	2.836	35.0	25.9	27.8	114.5	1.17	18.04	191	4.25
6.03	3.547	37.2	25.6	27.3	185.0	1.23	17.51	183	4.13
6.40	4.260	39.7	25.3	27.3	329.0	1.71	18.46	202	4.35
6.43	4.965	47.5	25.3	28.0	626.2	2.97	18.55	203	4.37
9.11	0.708	33.5	25.2	27.1	9.0	1.37	26.23	363	6.18
9.17	1.064	32.6	25.2	27.5	18.1	1.36	26.42	367	6.23
9.19	1.599	32.0	25.3	27.2	38.3	1.34	26.49	369	6.24
9.14	2.128	31.9	25.2	27.2	66.4	1.34	26.29	365	6.20
9.15	2.842	32.6	24.8	26.9	119.4	1.41	26.12	364	6.16
9.21	3.554	34.7	24.5	26.6	199.0	1.56	26.09	368	6.15
9.16	4.262	37.6	24.3	26.6	383.8	2.21	25.86	364	6.09
9.13	4.621	41.2	24.2	26.4	550.4	2.87	25.72	361	6.06
9.09	4.976	44.8	24.5	26.6	833.6	4.28	25.77	360	6.07
12.27	0.718	33.3	25.1	27.8	9.5	1.98	35.24	596	8.31
12.25	1.070	32.5	25.3	27.2	18.7	1.92	35.33	596	8.33
12.20	1.595	32.1	25.3	27.2	39.4	1.86	35.19	592	8.29
12.21	2.125	32.1	25.0	27.3	68.8	1.85	35.01	591	8.25

345

| L | F_G | $T_{air,in}$ | $T_{liq,in}$ | $T_{air,out}$ | $\Delta P/Z$ | h_L | Re_L | $We_L \times 10^4$ | Fr_L |
$(m^3/m^2 \cdot h)$	$(Pa)^{0.5}$	$(°C)$	$(°C)$	$(°C)$	(Pa/m)	$(\%)$			
12.24	2.841	33.2	24.7	26.9	123.9	1.94	34.87	592	8.22
12.22	3.553	35.0	24.5	26.9	213.3	2.17	34.63	589	8.16
12.23	4.260	38.8	24.3	26.5	453.8	3.07	34.50	588	8.13
12.20	4.620	42.6	24.4	26.4	710.9	4.31	34.47	586	8.12
12.15	4.708	45.0	24.8	26.6	798.6	4.67	34.69	585	8.18
12.20	4.792	46.6	25.6	27.1	896.3	5.13	35.50	594	8.37
18.45	0.711	34.6	25.3	27.5	10.1	2.76	53.31	1180	12.57
18.33	1.068	33.7	25.7	27.5	20.0	2.74	53.34	1170	12.57
18.34	1.599	33.3	25.5	27.6	41.5	2.76	53.18	1169	12.53
18.34	2.128	33.4	25.5	27.5	72.5	2.80	53.13	1169	12.52
18.35	2.836	34.4	25.2	27.5	133.1	2.93	52.83	1167	12.45
18.32	3.550	36.8	25.0	27.3	259.8	3.24	52.49	1162	12.37
18.42	4.259	40.9	25.0	27.0	646.3	5.02	52.77	1172	12.44
18.32	4.530	44.9	25.4	27.0	967.1	6.68	52.94	1165	12.48
24.66	0.709	35.0	26.0	28.0	10.3	3.14	72.36	1925	17.06
24.48	1.066	33.7	26.2	28.1	20.4	3.15	72.09	1904	16.99
24.47	1.595	32.6	25.9	28.0	44.1	3.21	71.58	1898	16.87
24.45	2.129	32.5	25.6	27.7	76.5	3.30	71.12	1891	16.76
24.40	2.835	33.4	25.2	27.7	145.7	3.49	70.33	1878	16.58
24.46	3.550	35.5	24.8	27.2	329.9	4.10	69.79	1877	16.45
24.47	3.909	38.0	24.6	26.7	538.2	5.06	69.59	1876	16.40
24.45	4.176	42.0	24.9	26.5	871.6	6.84	69.94	1878	16.48
36.65	0.710	32.4	26.4	28.4	11.4	4.62	108.40	3739	25.55
36.69	1.060	32.3	26.4	28.5	22.2	4.66	108.54	3745	25.58
36.68	1.597	32.5	26.2	28.3	49.5	4.74	107.92	3736	25.44
36.63	2.128	32.9	25.9	28.1	89.0	4.84	107.17	3718	25.26
36.68	2.837	34.1	25.5	28.0	185.0	5.05	106.28	3711	25.05
36.58	3.547	37.1	25.1	27.5	521.9	6.22	105.05	3681	24.76
36.66	3.816	41.3	25.1	26.9	950.9	8.34	105.39	3697	24.84
49.02	0.713	32.8	25.5	27.5	13.2	5.24	142.15	6021	33.51
48.90	1.064	32.2	25.6	27.5	25.8	5.25	141.99	6000	33.47
48.88	1.599	31.9	25.5	27.5	57.7	5.34	141.69	5990	33.40
48.93	2.126	32.1	25.4	27.4	106.3	5.50	141.41	5994	33.33
48.92	2.840	33.4	25.1	27.2	261.4	5.97	140.67	5978	33.16
48.92	3.194	35.3	25.0	27.0	452.6	6.67	140.37	5973	33.09
48.92	3.462	38.0	25.1	26.9	770.0	8.25	140.49	5976	33.11
48.93	3.552	39.5	25.2	27.0	974.4	9.41	141.07	5988	33.25
60.91	0.706	34.1	25.5	27.2	16.0	5.98	176.52	8645	41.61
61.06	1.065	33.4	25.6	27.5	37.3	6.00	177.53	8691	41.84
61.11	1.598	32.8	25.6	27.5	80.2	6.06	177.42	8699	41.82
61.06	2.130	32.9	25.4	27.5	146.4	6.20	176.69	8674	41.65
61.17	2.840	34.2	25.2	27.3	416.7	6.98	176.04	8679	41.49
61.14	3.020	35.6	25.0	27.0	556.1	7.46	175.48	8664	41.36
61.14	3.197	37.1	25.0	26.9	812.5	8.71	175.23	8659	41.30
61.12	3.233	38.5	25.0	26.9	915.8	9.14	175.30	8657	41.32
73.26	0.708	31.6	24.1	25.8	17.1	6.97	205.66	11602	48.47
73.26	1.064	31.7	24.4	26.3	36.2	6.96	207.13	11639	48.82
73.38	1.597	31.7	24.6	26.6	87.4	7.06	208.57	11695	49.16
73.32	2.134	32.4	24.8	26.6	177.9	7.29	209.31	11701	49.34
73.27	2.488	33.1	24.9	26.8	320.6	7.62	209.63	11698	49.41
73.43	2.663	33.9	25.0	26.9	428.5	7.91	210.44	11750	49.60
73.35	2.840	34.8	25.1	27.0	566.7	8.39	210.56	11735	49.63
73.34	3.019	36.7	25.3	27.1	843.6	9.70	211.55	11757	49.86

L	F_G	$T_{air,in}$	$T_{liq,in}$	$T_{air,out}$	$\Delta P/Z$	h_L	Re_L	$We_L \times 10^4$	Fr_L
$(m^3/m^2 \cdot h)$	$(Pa)^{0.5}$	(°C)	(°C)	(°C)	(Pa/m)	(%)			
M2Y	SRP 0831		Baseline			3.1 m			
0	0.726	19.0	14.7	15.5	14.2	0	0	0	0
0	1.085	19.1	14.8	15.8	27.9	0	0	0	0
0	1.628	19.2	14.8	15.8	57.3	0	0	0	0
0	2.173	19.5	14.9	16.0	98.9	0	0	0	0
0	2.894	20.8	15.0	15.9	169.7	0	0	0	0
0	3.616	22.8	15.1	15.9	265.0	0	0	0	0
0	4.339	26.6	15.2	16.0	374.7	0	0	0	0
0	4.631	37.5	16.5	24.7	433.9	0	0	0	0
2.65	0.708	33.4	16.2	28.1	13.5	0.62	3.53	17	0.83
2.78	1.067	31.8	17.7	28.1	27.7	0.71	3.86	19	0.91
2.57	1.595	30.4	17.3	28.2	58.1	0.71	3.52	16	0.83
2.82	2.484	30.2	17.1	28.1	133.3	0.89	3.85	19	0.91
2.61	3.548	31.6	16.9	27.1	281.5	1.23	3.54	17	0.83
2.64	4.268	36.1	16.5	26.2	462.3	1.59	3.55	17	0.84
2.60	4.627	39.4	16.3	25.9	572.3	1.82	3.47	16	0.82
6.26	0.711	30.6	19.1	30.3	14.2	2.29	8.97	73	2.11
6.29	1.057	30.4	17.6	31.1	28.1	2.41	8.70	72	2.05
6.47	1.582	30.1	17.6	31.3	59.6	2.61	8.95	76	2.11
6.05	2.114	29.9	17.6	31.3	100.8	2.65	8.36	68	1.97
6.22	2.826	30.5	17.3	30.5	178.4	2.91	8.52	71	2.01
6.36	3.890	33.3	16.4	29.1	404.9	3.88	8.53	73	2.01
6.13	4.263	37.4	15.7	26.9	588.7	4.81	8.08	68	1.91
6.39	4.445	40.7	15.6	26.3	700.9	5.53	8.40	73	1.98
12.19	0.724	27.3	15.6	21.3	17.1	4.12	16.02	213	3.78
12.21	1.075	26.8	15.9	21.3	31.8	4.11	16.18	214	3.81
12.26	1.614	26.2	16.1	21.4	66.4	4.11	16.31	216	3.85
12.31	2.148	26.0	15.9	21.5	112.5	4.26	16.28	217	3.84
12.28	2.865	26.8	15.6	21.5	200.4	4.46	16.12	216	3.80
12.21	3.404	28.3	15.2	21.4	304.2	4.69	15.88	213	3.74
12.29	3.585	29.5	14.9	21.5	362.6	4.69	15.86	214	3.74
12.22	3.764	31.2	14.7	21.5	511.4	5.32	15.67	212	3.69
12.26	3.941	33.4	14.7	21.5	712.3	6.03	15.73	213	3.71
18.34	0.715	35.1	16.7	27.4	15.9	4.92	24.80	426	5.85
18.36	1.061	32.8	16.8	28.0	31.0	4.96	24.88	427	5.86
18.30	1.599	31.6	16.7	28.2	66.0	5.01	24.72	424	5.83
18.33	2.481	31.5	16.5	28.0	154.9	5.23	24.65	424	5.81
18.31	3.194	32.1	16.1	27.3	274.8	5.55	24.34	422	5.74
18.32	3.551	33.9	15.7	26.3	553.4	6.92	24.12	420	5.68
18.35	3.666	35.9	15.6	25.4	761.9	7.95	24.10	421	5.68
24.45	0.711	30.0	15.4	23.5	17.8	6.16	31.95	678	7.53
24.45	1.072	29.3	15.7	23.6	34.5	6.17	32.20	680	7.59
24.45	1.610	28.7	15.8	23.6	71.2	6.20	32.27	681	7.61
24.45	2.145	28.4	15.7	23.6	124.5	6.29	32.25	681	7.60
24.48	2.859	28.8	15.6	23.3	225.8	6.50	32.19	681	7.59
24.42	3.214	29.6	15.5	22.9	327.4	6.72	32.00	678	7.54
24.52	3.398	31.8	15.4	22.8	645.2	8.17	32.02	681	7.55
24.48	3.469	33.6	15.5	22.3	881.4	9.26	32.06	680	7.56
36.83	0.717	24.7	19.8	20.0	20.1	7.53	53.73	1405	12.66
36.70	1.076	24.3	19.6	20.6	37.8	7.56	53.25	1393	12.55
36.70	1.617	23.8	19.0	20.6	79.5	7.67	52.54	1386	12.38
36.66	2.152	23.8	18.3	21.0	139.1	7.84	51.58	1374	12.16
36.68	2.513	24.3	17.6	21.1	193.1	8.05	50.67	1364	11.94

L (m³/m²·h)	F_G (Pa)$^{0.5}$	$T_{air,in}$ (°C)	$T_{liq,in}$ (°C)	$T_{air,out}$ (°C)	$\Delta P/Z$ (Pa/m)	h_L (%)	Re_L	$We_L \times 10^4$	Fr_L
36.68	2.870	25.2	16.8	20.9	287.2	8.45	49.75	1354	11.73
36.67	3.049	27.3	15.9	20.6	594.9	9.64	48.55	1340	11.44
36.64	3.122	28.6	15.5	20.4	850.2	10.71	48.02	1333	11.32
48.74	0.708	29.8	18.8	25.4	20.2	8.49	69.31	2217	16.34
48.90	1.068	30.0	18.6	25.9	40.4	8.58	69.24	2225	16.32
48.90	1.603	30.0	18.5	25.9	89.4	8.81	69.16	2224	16.30
48.89	2.137	30.0	18.3	25.7	159.2	9.14	68.68	2218	16.19
48.92	2.671	31.2	17.9	25.2	395.1	10.04	68.12	2212	16.06
48.95	2.847	34.4	17.4	25.4	980.9	13.13	67.30	2203	15.86
61.08	0.714	30.9	18.1	27.8	22.8	9.28	85.41	3208	20.13
61.12	1.066	30.5	18.2	28.0	47.6	9.40	85.73	3215	20.21
61.09	1.596	30.5	18.1	27.6	110.2	9.69	85.58	3211	20.17
61.10	2.127	30.8	17.9	27.0	219.2	10.11	85.07	3203	20.05
61.15	2.488	31.5	17.6	26.9	509.1	11.20	84.59	3199	19.94
61.16	2.574	32.1	17.3	26.5	793.2	12.71	83.96	3190	19.79
72.96	0.714	30.5	16.8	24.3	25.8	10.68	98.75	4256	23.27
73.34	1.072	30.1	17.0	24.2	56.8	10.83	99.87	4304	23.54
73.34	1.609	29.5	17.2	23.7	150.3	11.18	100.29	4311	23.64
73.36	1.965	29.5	17.2	23.3	319.7	11.75	100.37	4314	23.66
73.36	2.146	29.9	17.2	23.2	454.2	12.18	100.26	4312	23.63
73.37	2.323	31.1	17.1	23.1	705.4	13.19	100.18	4311	23.61
73.34	2.355	31.8	17.1	23.2	885.5	14.19	100.14	4309	23.60

F1Y	SRP 0707		Baseline (Dry)			3.0 m			
0	0.347	39.5	29.7	39.8	9.8	0	0	0	0
0	0.529	32.3	26.6	27.8	17.7	0	0	0	0
0	0.696	39.6	29.5	39.3	26.6	0	0	0	0
0	0.705	32.6	26.8	28.4	29.0	0	0	0	0
0	1.043	38.8	29.6	39.3	57.2	0	0	0	0
0	1.060	35.6	27.4	30.3	47.9	0	0	0	0
0	1.398	37.6	29.9	36.7	99.0	0	0	0	0
0	1.410	38.7	27.9	31.3	105.6	0	0	0	0
0	1.744	38.1	30.1	37.3	149.2	0	0	0	0
0	1.759	37.8	28.2	32.0	168.1	0	0	0	0
0	2.093	38.7	30.2	37.4	208.5	0	0	0	0
0	2.109	38.1	28.6	32.8	201.2	0	0	0	0
0	2.447	39.5	30.3	36.7	283.2	0	0	0	0
0	2.458	40.0	29.0	33.4	297.4	0	0	0	0
0	2.799	40.8	30.4	36.3	353.7	0	0	0	0
0	2.811	41.2	29.2	33.5	361.0	0	0	0	0
0	3.143	43.2	30.5	37.1	425.8	0	0	0	0
0	3.154	43.2	29.5	34.5	429.1	0	0	0	0
0	3.489	46.7	30.5	37.7	516.3	0	0	0	0
0	3.501	44.7	29.6	35.3	512.5	0	0	0	0
0	3.838	49.6	30.6	36.8	617.1	0	0	0	0
0	3.845	47.5	29.7	36.1	609.8	0	0	0	0
0	4.185	50.6	29.8	37.8	717.4	0	0	0	0
0	4.208	53.6	30.7	34.5	742.8	0	0	0	0

P500	SRP 0829		Baseline			3.1 m			
0	0.715	26.2	19.4	21.3	39.1	0	0	0	0
0	1.076	25.8	19.4	21.2	78.2	0	0	0	0
0	1.615	25.6	19.4	21.2	164.5	0	0	0	0
0	2.154	25.8	19.4	21.0	286.2	0	0	0	0
0	2.873	27.0	19.4	20.4	486.1	0	0	0	0

L	F_G	$T_{air,in}$	$T_{liq,in}$	$T_{air,out}$	$\Delta P/Z$	h_L	Re_L	$We_L \times 10^4$	Fr_L
(m³/m²·h)	(Pa)⁰·⁵	(°C)	(°C)	(°C)	(Pa/m)	(%)			
0	3.591	29.6	19.4	20.2	729.5	0	0	0	0
0	4.311	33.7	19.4	20.1	1025.9	0	0	0	0
3.09	0.706	31.8	18.3	32.0	43.8	1.86	1.59	4	0.37
3.05	1.055	31.7	18.6	32.7	91.8	1.92	1.58	4	0.37
3.10	1.582	31.7	18.1	33.0	197.5	2.01	1.58	4	0.37
3.02	2.110	31.8	18.0	33.0	383.1	2.30	1.54	4	0.36
3.10	2.462	32.3	18.0	32.6	538.3	2.66	1.58	4	0.37
2.98	2.640	33.1	18.0	31.8	637.1	2.76	1.52	4	0.36
2.95	2.821	34.3	17.8	31.3	775.8	3.22	1.50	4	0.35
3.06	2.912	35.4	17.6	30.9	872.4	3.58	1.55	4	0.36
6.19	0.710	31.3	19.6	29.4	47.9	3.35	3.29	13	0.78
6.35	1.058	31.2	18.6	29.8	98.5	3.46	3.28	14	0.77
6.15	1.593	31.4	18.2	30.1	214.7	3.51	3.15	13	0.74
5.99	2.117	31.9	18.4	30.5	448.6	3.93	3.08	13	0.73
6.09	2.292	32.3	18.3	30.6	556.5	4.26	3.13	13	0.74
6.12	2.471	33.2	18.0	30.4	739.4	5.03	3.12	13	0.74
6.41	2.528	34.0	17.7	30.4	849.9	5.51	3.24	14	0.76
9.27	0.701	31.0	19.1	32.0	49.3	5.26	4.86	26	1.14
9.16	1.055	30.9	18.1	32.1	101.4	5.24	4.69	25	1.10
9.31	1.585	31.0	18.3	31.8	222.9	5.48	4.79	26	1.13
8.78	2.116	32.2	18.2	31.4	512.5	5.98	4.50	24	1.06
9.05	2.294	33.1	17.6	31.2	742.0	7.05	4.58	25	1.08
8.88	2.381	34.0	17.4	30.7	873.9	7.43	4.46	24	1.05
12.12	0.711	30.3	18.3	27.1	53.8	5.84	6.22	41	1.47
12.45	1.064	30.3	19.2	27.1	109.7	5.96	6.54	43	1.54
12.37	1.600	30.6	19.2	27.1	273.9	6.29	6.49	42	1.53
12.53	1.948	31.5	18.5	27.5	464.0	6.78	6.48	43	1.53
12.07	2.128	32.6	18.3	27.7	674.8	7.40	6.20	40	1.46
12.19	2.215	33.4	18.1	28.1	888.6	8.54	6.23	41	1.47
18.23	0.702	31.4	17.1	31.3	54.8	7.23	9.10	79	2.14
18.33	1.054	31.0	18.0	31.4	112.4	7.32	9.34	81	2.20
18.32	1.587	31.0	17.6	31.2	296.0	7.77	9.25	80	2.18
18.34	1.849	31.2	17.5	30.6	493.3	8.34	9.24	80	2.18
18.33	1.942	31.5	17.4	30.1	658.5	8.99	9.21	80	2.17
18.37	1.995	31.8	17.3	29.5	805.4	9.63	9.20	80	2.17
18.32	2.019	32.1	17.2	27.5	932.8	10.14	9.15	80	2.16
24.46	0.711	29.5	21.4	24.8	61.7	7.80	13.53	135	3.19
24.45	1.072	28.7	21.4	24.8	125.7	7.88	13.55	135	3.19
24.45	1.431	28.4	20.7	24.9	267.5	8.18	13.30	134	3.14
24.46	1.602	28.4	20.3	24.9	347.1	8.35	13.21	133	3.11
24.42	1.780	28.6	19.5	24.8	641.6	9.72	12.94	132	3.05
24.39	1.835	29.3	19.0	24.5	783.4	10.43	12.74	131	3.00
36.60	0.713	29.4	18.6	25.5	68.9	10.18	18.97	257	4.47
36.70	1.069	29.0	18.8	25.5	144.6	10.28	19.08	258	4.50
36.70	1.245	29.0	18.9	25.7	239.1	10.56	19.13	258	4.51
36.71	1.423	28.9	18.7	25.8	360.0	10.78	19.06	258	4.49
36.73	1.602	30.2	18.4	25.7	825.0	12.92	18.93	257	4.46
36.64	1.620	30.8	18.3	25.6	921.8	13.28	18.83	256	4.44
48.80	0.703	32.0	17.8	31.9	70.2	11.72	24.77	411	5.84
48.87	1.056	31.7	17.8	31.9	201.4	12.05	24.81	412	5.85
48.89	1.235	31.7	17.9	32.0	308.8	12.32	24.90	413	5.87
48.91	1.407	31.9	18.1	31.8	600.7	13.78	25.00	414	5.89
48.98	1.437	32.3	18.2	31.5	972.9	15.70	25.08	415	5.91

349

Appendix C: Interfacial Depletion Calculation

This appendix contains representative calculations intended to illustrate the significance (or lack thereof) of interfacial depletion of hydroxide ion in the WWC system (referenced in Section 4.1.4).

The pseudo-first-order assumption central to this work essentially requires there to be no appreciable difference between bulk and interfacial hydroxide concentrations. To properly interpret the results, it was imperative that this criterion be upheld. First, from the CO_2-OH^- reaction stoichiometry, we have:

$$N_{OH^-} = 2N_{CO_2} \tag{C.1}$$

The flux of hydroxide ion can be defined in terms of the bulk and interfacial concentrations (superscripts b and i, respectively).

$$N_{OH^-} = k_L^0 \left([OH^-]^b - [OH^-]^i\right) \tag{C.2}$$

The flux of CO_2 is given by equation 4.7.

$$N_{CO_2} = K_G P_{CO_2,LM} \tag{4.7}$$

Substituting into equation C.1:

$$k_L^0 \left([OH^-]^b - [OH^-]^i\right) = 2K_G P_{CO_2,LM} \tag{C.3}$$

The liquid-film mass transfer coefficient was calculated from the theories of Pigford (1941), Hobler (1966), and Bird et al. (2002). An estimate for the diffusion coefficient associated with the ions in solution was necessary. The effective diffusion coefficient for a Na^+-OH^- binary system was used for this purpose. (TIC analysis showed the bulk

depletion of hydroxide to be at most 5% in a given experiment, and so, CO_3^{2-} was ignored here.) Equations C.4-C.7 are from Geankoplis (2003).

$$D_{Na^+}\left(cm^2/s\right)@\,25^\circ C = \left(2.662\times10^{-7}\right)\frac{50.1}{n_{Na^+}} \tag{C.4}$$

$$D_{OH^-}\left(cm^2/s\right)@\,25^\circ C = \left(2.662\times10^{-7}\right)\frac{197.6}{n_{OH^-}} \tag{C.5}$$

n_{Na+} and n_{OH-} represent the ion valencies, which are both simply one in this case.

$$D_{eff}\,@\,25^\circ C = \frac{n_+ + n_-}{\dfrac{n_-}{D_{Na^+}} + \dfrac{n_+}{D_{OH^-}}} \tag{C.6}$$

$$D_{eff} = \left(D_{eff}\,@\,25^\circ C\right)\cdot\frac{T}{334\mu_w\left(mPa\cdot s\right)} \tag{C.7}$$

The values for the effective diffusion coefficient were actually quite similar to those calculated for CO_2 (equation 4.5). Thus, the range of k_L^0 values was roughly the same as that referenced in the Experimental Methods: 0.007 to 0.014 cm/s. Assuming a worst-case scenario, based on the conditions that were run – that is, $k_L^0 = 0.0096$ cm/s, $N_{CO2} = 2.31 \times 10^{-4}$ mol/m^2·s (from 12/4/06 experiment) – and a bulk hydroxide concentration of 0.1 mol/L, equation C.3 can be solved to yield a value of 0.0976 mol/L (about 2.5% depletion) for the interfacial hydroxide concentration – hardly significant.

The conditions of the packed column experiment (very low CO_2 partial pressures) were such that interfacial depletion would be even less of a concern, and so, an example calculation for this system is presumed to be unnecessary.

Appendix D: Error Propagation Analysis

This appendix outlines and summarizes the results from an analysis in which the propagation of various measurement errors in the packing mass transfer area experiment was evaluated.

The equation used to calculate the effective area (equation 4.13) is reproduced below:

$$a_e = \frac{u_G \ln\left(\dfrac{y_{CO_2,in}}{y_{CO_2,out}}\right)}{ZRT} \cdot \frac{H_{CO_2}}{\sqrt{k_{OH^-}[OH^-]D_{CO_2,L}}} \tag{4.13}$$

The anticipated uncertainty or deviation in the effective area was presumed to arise from uncertainties in the air flow rate, CO_2 concentration, and temperature measurements. The error associated with a given variable was first determined by differentiating it with respect to any or all measured parameters used inherently in its calculation. The equations associated with the reaction rate constant (k_{OH^-}) are displayed for example:

$$\log_{10}\left(\frac{k_{OH^-}}{k_{OH^-}^\infty}\right) = 0.221I - 0.016I^2 \tag{4.4}$$

$$\log_{10}k_{OH^-}^\infty = 11.895 - \frac{2382}{T} \tag{4.4a}$$

The rate constant only needed to be differentiated with respect to temperature (*T*) here, since the ionic strength (or NaOH concentration) was assumed constant. The differentiated result was then multiplied by the uncertainty in the measurement, and in cases involving multiple implicit variables, this process was repeated. The total error was

finally calculated by squaring each component, summing these values, and then taking the square root of this sum. This procedure is illustrated in equation D.1 for the effective area.

$$
a_{\mathrm{e,unc}} = \sqrt{ \begin{array}{l} \left(\dfrac{da_{\mathrm{e}}}{du_{\mathrm{G}}} \cdot u_{\mathrm{G,unc}} \right)^2 + \left(\dfrac{da_{\mathrm{e}}}{dy_{\mathrm{CO_2,in}}} \cdot y_{\mathrm{CO_2,in,unc}} \right)^2 + \left(\dfrac{da_{\mathrm{e}}}{dy_{\mathrm{CO_2,out}}} \cdot y_{\mathrm{CO_2,out,unc}} \right)^2 + \left(\dfrac{da_{\mathrm{e}}}{dT} \cdot T_{\mathrm{unc}} \right)^2 \\[3mm] + \left(\dfrac{da_{\mathrm{e}}}{dH_{\mathrm{CO_2}}} \cdot H_{\mathrm{CO_2,unc}} \right)^2 + \left(\dfrac{da_{\mathrm{e}}}{dk_{\mathrm{OH^-}}} \cdot k_{\mathrm{OH^-,unc}} \right)^2 + \left(\dfrac{da_{\mathrm{e}}}{dD_{\mathrm{CO_2,L}}} \cdot D_{\mathrm{CO_2,L,unc}} \right)^2 \end{array} }
$$

(D.1)

The completion of this exercise required the application or assumption of several numerical values. The uncertainties in the temperature (T_{unc}) and CO_2 analyzer measurements ($y_{\mathrm{CO2,unc}}$) were respectively ±1.8 K and ±5 ppm. The uncertainty in the air flow rate was influenced by the annubar pressure transmitter measurement (±0.017 in H_2O or 4.2 Pa) and the air density, which in turn was a function of the static pressure (±0.004 psi or 27.2 Pa) and air temperature (±1.8 K) measurements.

$$
u_{\mathrm{G}} = \frac{C_1 \sqrt{P_{\mathrm{annubar}} + C_2}}{\sqrt{\rho_{\mathrm{G}}}}
$$

(D.2)

$$
\rho_{\mathrm{G}} = \frac{P_{\mathrm{static}} M_{\mathrm{air}}}{R T_{\mathrm{air}}}
$$

(D.3)

The experimental conditions were specified as follows:

- Temperature: 25°C;

- Gas velocity: 1 m/s;

- Packing height: 3.048 m;

- Solution concentration: 0.1 mol/L NaOH;

- CO_2 concentrations: 400 ppm in, 250 ppm out.

The absolute error in the calculated mass transfer area was 13.8 m^2/m^3 for this set of parameters. The uncertainty associated with the temperature measurement dominated the calculation, whereas the uncertainties with the gas flow and CO_2 measurement were fairly insignificant. This result was logical, since temperature is implicit in most of the terms in equation 4.13. The error propagation calculations and analysis can be viewed in complete detail in Akintunji (2008).

Appendix E: SOLVER Macro Code

The Visual Basic code that was utilized to repeatedly implement the SOLVER function and thereby facilitate the solution of the literature hydraulic models is displayed below.

```
Sub Solver_Repeat()
'
' Solver_Repeat Macro
'


'

    For I = 1 To 100

        SolverReset

        SolverOk SetCell:=ActiveCell, MaxMinVal:=3, ValueOf:="0",
ByChange:=ActiveCell.Offset(0, 1)

        SolverSolve UserFinish:=True

        ActiveCell.Offset(1, 0).Select

    Next I

End Sub
```

References

Akintunji A. "Error Propagation Analysis." Fall Research Thesis. University of Texas at Austin. Austin, TX. 2008.

Alix P, Raynal L. Liquid distribution and liquid hold-up in modern high capacity packings. *Chem. Eng. Res. Des.* 2008;86:585-591.

Aroonwilas A. *Mass-Transfer with Chemical Reaction in Structured Packing for CO_2 Absorption Process*. University of Regina. Ph.D. Dissertation. 2001.

Aroonwilas A, Tontiwachwuthikul P. High-efficiency structured packing for CO_2 separation using 2-amino-2-methyl-1-propanol (AMP). *Sep. Purif. Technol.* 1997;12:67-79.

Aroonwilas A, Tontiwachwuthikul P, Chakma A. Effects of operating and design parameters on CO_2 absorption in columns with structured packings. *Sep. Purif. Technol.* 2001;24:403-411.

Ataki A, Bart H-J. Experimental and CFD Simulation Study for the Wetting of a Structured Packing Element with Liquids. *Chem. Eng. Technol.* 2006;29(3):336-347.

Barrett PVL. *Gas Absorption on a Sieve Plate*. University of Cambridge. Ph.D. Dissertation. 1966.

Billet R, Schultes M. Predicting Mass Transfer in Packed Columns. *Chem. Eng. Technol.* 1993;16(1):1-9.

Billet R, Schultes M. Prediction of Mass Transfer Columns with Dumped and Arranged Packings: Updated Summary of the Calculation Method of Billet and Schultes. *Chem. Eng. Res. Des.* 1999;77(A6):498-504.

Bird RB, Stewart WE, Lightfoot EN. *Transport Phenomena*. New York, John Wiley & Sons, Inc.: 2002.

Bishnoi S. *Carbon Dioxide Absorption and Solution Equilibrium in Piperazine Activated Methyldiethanolamine*. University of Texas at Austin. Ph.D. Dissertation. 2000.

Bishnoi S, Rochelle GT. Absorption of carbon dioxide into aqueous piperazine: reaction kinetics, mass transfer, and solubility. *Chem. Eng. Sci.* 2000;55(22):5531-5543.

Bravo JL, Fair JR. Generalized Correlation for Mass Transfer in Packed Distillation Columns. *Ind. Eng. Chem. Process Des. Dev.* 1982;21(1):162-170.

Bravo JL, Rocha JA, Fair JR. Mass transfer in gauze packings. *Hydrocarbon Process.* 1985;64(1):91-95.

Brunazzi E, Nardini G, Paglianti A, Petarca L. Interfacial Area of Mellapak Packing: Absorption of 1,1,1-Trichloroethane by Genosorb 300. *Chem. Eng. Technol.* 1995;18(4):248-255.

Burnett JC, Jr., Himmelblau DM. The Effect of Surface Active Agents on Interphase Mass Transfer. *AIChE J.* 1970;16(2):185-193.

Chen E. *Carbon Dioxide Absorption into Piperazine Promoted Potassium Carbonate using Structured Packing*. University of Texas at Austin. Ph.D. Dissertation. 2007.

Cullinane JT. *Thermodynamics and Kinetics of Aqueous Piperazine with Potassium Carbonate for Carbon Dioxide Absorption*. University of Texas at Austin. Ph.D. Dissertation. 2005.

Danckwerts PV. Significance of Liquid-Film Coefficients in Gas Absorption. *Ind. Eng. Chem.* 1951;43(6):1460-1467.

Danckwerts PV. *Gas-Liquid Reactions*. New York, McGraw-Hill: 1970.

Derks PW, Hogendoorn KJ, Versteeg GF. Solubility of N_2O in and Density, Viscosity, and Surface Tension of Aqueous Piperazine Solutions. *J. Chem. Eng. Data.* 2005;50(6):1947-1950.

357

Dragan M, Dragan S, Siminiceanu I. Characterisation of Mellapak 750Y Structured Packing Determining the Effective Mass Transfer Area. *Studia Universitatis Babes-Bolyai, Chemia*. 2000;45(1-2):11-22.

Dugas RE. *Carbon Dioxide Absorption, Desorption and Diffusion in Aqueous Piperazine and Monoethanolamine*. University of Texas at Austin. Ph.D. Dissertation. 2009.

Emmert RE, Pigford RL. A Study of Gas Absorption in Falling Liquid Films. *Chem. Eng. Prog.* 1954;50(2):87-93.

Fair JR, Bravo JL. Prediction of Mass Transfer Efficiencies and Pressure Drop for Structured Tower Packings in Vapor/Liquid Service. *ICHEME Symp. Ser.* 1987;104:A183-A201.

Fair JR, Bravo JL. Distillation Columns Containing Structured Packing. *Chem. Eng. Prog.* 1990;86(1):19-29.

Fair JR, Seibert AF, Behrens M, Saraber PP, Olujic Z. Structured Packing Performance - Experimental Evaluation of Two Predictive Models. *Ind. Eng. Chem. Res.* 2000;39(6):1788-1796.

Freeman SA, Dugas RE, Van Wagener D, Nguyen T, Rochelle GT. Carbon dioxide capture with concentrated, aqueous piperazine. *Int. J. Greenhouse Gas Control*. 2010;4(2):119-124.

Geankoplis CJ. *Transport Processes and Separation Process Principles*. Upper Saddle River, NJ, Pearson Education, Inc.: 2003.

Glasscock D. *Modeling and Experimental Study of Carbon Dioxide Absorption into Aqueous Alkanolamines*. University of Texas at Austin. Ph.D. Dissertation. 1990.

Goff GS. *Oxidative Degradation of Aqueous Monoethanolamine in CO_2 Capture Processes: Iron and Copper Catalysis, Inhibition, and O_2 Mass Transfer*. University of Texas at Austin. Ph.D. Dissertation. 2005.

Green CW. *Hydraulic Characterization of Structured Packing via X-Ray Computed Tomography*. University of Texas at Austin. Ph.D. Dissertation. 2006.

Green CW, Farone J, Briley JK, Eldridge RB, Ketcham RA, Nightingale B. Novel Application of X-ray Computed Tomography: Determination of Gas/Liquid Contact Area and Liquid Holdup in Structured Packing. *Ind. Eng. Chem. Res.* 2007;46(17):5734-5753.

Haar L, Gallagher JS, Kell GS. *NBS/NRC Steam Tables: Thermodynamic and Transport Properties and Computer Programs for Vapor and Liquid States of Water in SI Units*. Washington, D.C., Hemisphere Publishing Corporation: 1984.

Hardy R. (Koch-Glitsch, LP, Wichita, KS). Personal Communication to Robert E. Tsai. 2007.

Haubrock J, Hogendoorn JA, Versteeg GF. The Applicability of Activities in Kinetic Expressions: a More Fundamental Approach to Represent the Kinetics of the System CO_2-OH- in Terms of Activities. *Int. J. Chem. React. Eng.* 2005;3:1-17.

Henni A, Hromek JJ, Tontiwachwuthikul P, Chakma A. Volumetric Properties and Viscosities for Aqueous AMP Solutions from 25°C to 70°C. *J. Chem. Eng. Data.* 2003;48(3):551-556.

Henriques de Brito M, von Stockar U, Bangerter AM, Bomio P, Laso M. Effective Mass-Transfer Area in a Pilot Plant Column Equipped with Structured Packings and with Ceramic Rings. *Ind. Eng. Chem. Res.* 1994;33(3):647-656.

Higbie R. The Rate of Absorption of A Pure Gas into A Still Liquid During Short Periods of Exposure. *Trans. Am. Inst. Chem. Engrs.* 1935;31:365-389.

Hikita H, Asai S. Absorption of Carbon Dioxide by Sodium Hydroxide Solutions in a Liquid-jet Column and a Wetted-wall Column. *Kagaku Kogaku.* 1964;28(12):1017-1022.

Hilliard M. *A Predictive Thermodynamic Model for an Aqueous Blend of Potassium Carbonate, Piperazine, and Monoethanolamine for Carbon Dioxide Capture from Flue Gas*. University of Texas at Austin. Ph.D. Dissertation. 2008.

Hobler T. *Mass Transfer and Absorbers*. Oxford, Pergamon Press: 1966.

Hoffmann A, Maćkowiak JF, Górak A, Haas M, Löning J-M, Runowski T, Hallenberger K. Standardization of Mass Transfer Measurements: A Basis for the Description of Absorption Processes. *Chem. Eng. Res. Des.* 2007;85(1):40-49.

Jasper JJ. The Surface Tension of Pure Liquid Compounds. *J. Phys. Chem. Ref. Data.* 1972;1:841-1009.

Johnstone HF, Pigford RL. Distillation in a Wetted-Wall Column. *Trans. Am. Inst. Chem. Engrs.* 1942;38:25-51.

Kettner A. "Finding a new method to decrease the surface tension of a caustic absorption, to enhance the SRP database." Summer Research Thesis. University of Texas at Austin. Austin, TX. 2006.

King CJ. Turbulent Liquid Phase Mass Transfer at a Free Gas-Liquid Interface. *Ind. Eng. Chem. Fundam.* 1966;5(1):1-8.

Kister HZ, Gill DR. Flooding and Pressure Drop Prediction for Structured Packings. *ICHEME Symp. Ser.* 1992;128:A109-A123.

Kister HZ, Scherffius J, Afshar K, Abkar E. Realistically Predict Capacity and Pressure Drop for Packed Columns. *Chem. Eng. Prog.* 2007;103(7):28-38.

Komiyama J, Fuoss RM. Conductance in Water-Poly(vinyl alcohol) Mixtures. *Proc. Natl. Acad. Sci. U. S. A.* 1972;69(4):829-833.

Kucka L, Kenig EY, Gorak A. Kinetics of the Gas-Liquid Reaction Between Carbon Dioxide and Hydroxide Ions. *Ind. Eng. Chem. Res.* 2002;41(24):5952-5957.

Lewis WK, Whitman WG. Principles of Gas Absorption. *Ind. Eng. Chem.* 1924;16(12):1215-1220.

Lohse M, Alper E, Quicker G, Deckwer WD. Diffusivity and Solubility of Carbon Dioxide in Diluted Polymer Solutions. *AIChE J.* 1981;27(4):626-631.

Luo S, Li H, Fei W, Wang Y-d. Liquid Film Characteristics on Surface of Structured Packing. *Chin. J. Chem. Eng.* 2009;17(1):47-52.

McGlamery GG. *Liquid Film Transport Characteristics of Textured Metal Surfaces*. University of Texas at Austin. Ph.D. Dissertation. 1988.

Moniuk W, Pohorecki R. Viscosity and Density of Sodium and Potassium Alkaline Solutions. *Hung. J. Ind. Chem.* 1991;19(3):175-178.

Moser F, Kessler A. Increased Capacity Thanks to Improved Geometry. *Sulzer Tech. Rev.* 1999;81(3):24-26.

Mshewa MM. *Carbon Dioxide Desorption/Absorption with Aqueous Mixtures of Methyldiethanolamine and Diethanolamine at 40 to 120°C*. University of Texas at Austin. Ph.D. Dissertation. 1995.

Murrieta CR, Seibert AF, Fair JR, Rocha JA. Liquid-Side Mass-Transfer Resistance of Structured Packings. *Ind. Eng. Chem. Res.* 2004;43(22):7113-7120.

Nakajima ES, Maffia MC, Meirelles AJA. Influence of Liquid Viscosity and Gas Superficial Velocity on Effective Mass Transfer Area in Packed Columns. *J. Chem. Eng. Jpn.* 2000;33(3):561-566.

Nakov S. Study of the Influence of Liquid Phase Viscosity on the Effective Surface Area of Arranged Packings with Vertical Walls at Low Liquid Superficial Velocity. *Chem. Eng. Technol.* 2000;23(7):615-618.

Nawrocki PA, Xu ZP, Chuang KT. Mass Transfer in Structured Corrugated Packing. *Can. J. Chem. Eng.* 1991;69(6):1336-1343.

Nguyen Ly L-A, Carbonell RG, McCoy BJ. Diffusion of Gases Through Surfactant Films: Interfacial Resistance to Mass Transfer. *AIChE J.* 1979;25(6):1015-1024.

Nicolaiewsky EMA, Fair JR. Liquid Flow over Textured Surfaces. 1. Contact Angles. *Ind. Eng. Chem. Res.* 1999;38(1):284-291.

Nicolaiewsky EMA, Tavares FW, Rajagopal K, Fair JR. Liquid film flow and area generation in structured packed columns. *Powder Technol.* 1999;104(1):84-94.

Nijsing RATO, Hendriksz RH, Kramers H. Absorption of Carbon Dioxide in Jets and Falling Films of Electrolyte Solutions, with and without Chemical Reaction. *Chem. Eng. Sci.* 1959;10:88-104.

Olujic Z. Development of a Complete Simulation Model for Predicting the Hydraulic and Separation Performance of Distillation Columns Equipped with Structured Packings. *Chem. Biochem. Eng. Q.* 1997;11(1):31-46.

Olujic Z, Behrens M, Colli L, Paglianti A. Predicting the Efficiency of Corrugated Sheet Structured Packings with Large Specific Surface Area. *Chem. Biochem. Eng. Q.* 2004;18(2):89-96.

Olujic Z, Jansen H, Kaibel B, Rietfort T, Zich E. Stretching the Capacity of Structured Packings. *Ind. Eng. Chem. Res.* 2001;40(26):6172-6180.

Olujic Z, Kamerbeek AB, de Graauw J. A corrugation geometry based model for efficiency of structured distillation packing. *Chem. Eng. Process.* 1999;38(4-6):683-695.

Olujic Z, Seibert AF, Fair JR. Influence of corrugation geometry on the performance of structured packings: an experimental study. *Chem. Eng. Process.* 2000;39(4):335-342.

Onda K, Takeuchi H, Okumoto Y. Mass Transfer Coefficients Between Gas and Liquid Phases in Packed Columns. *J. Chem. Eng. Jpn.* 1968;1(1):56-62.

Osmers HR, Metzner AB. Diffusion in Dilute Polymeric Solutions. *Ind. Eng. Chem. Fundam.* 1972;11(2):161-169.

Pacheco MA. *Mass Transfer, Kinetics and Rate-based Modeling of Reactive Absorption*. University of Texas at Austin. Ph.D. Dissertation. 1998.

Paul S, Mandal B. Density and Viscosity of Aqueous Solutions of (2-Piperidineethanol + Piperazine) from (288 to 333) K and Surface Tension of Aqueous Solutions of (*N*-Methyldiethanolamine + Piperazine), (2-Amine-2-methyl-1-propanol + Piperazine), and (2-Piperidineethanol + Piperazine) from (293 to 323) K. *J. Chem. Eng. Data.* 2006;51(6):2242-2245.

Paul S, Mandal B. Density and Viscosity of Aqueous Solutions of (*N*-Methyldiethanolamine + Piperazine) and (2-Amino-2-methyl-1-propanol + Piperazine) from (288 to 333) K. *J. Chem. Eng. Data.* 2006;51(5):1808-1810.

Perry D, Nutter DE, Hale A. Liquid Distribution for Optimum Packing Performance. *Chem. Eng. Prog.* 1990;86(1):30-35.

Perry M, Wang C, Seibert AF. (Separations Research Program, Austin, TX). Personal Communication to Robert E. Tsai. 2010.

Peters MS, Timmerhaus KD. *Plant Design and Economics for Chemical Engineers*. New York, McGraw-Hill, Inc.: 1991.

Petre CF, Larachi F, Iliuta I, Grandjean BPA. Pressure drop through structured packings: Breakdown into the contributing mechanisms by CFD modeling. *Chem. Eng. Sci.* 2003;58(1):163-177.

Pigford RL. *Counter-Diffusion in a Wetted Wall Column*. University of Illinois at Urbana-Champaign. Ph.D. Dissertation. 1941.

Pilling M. (Sulzer Chemtech USA, Inc., Tulsa, OK). Personal Communication to Robert E. Tsai. 2008.

Pilling M. (Sulzer Chemtech USA, Inc., Tulsa, OK). Personal Communication to Robert E. Tsai. 2009.

Pinsent BRW, Pearson L, Roughton FJW. Kinetics of Combination of Carbon Dioxide with Hydroxide Ions. *Trans. Faraday Soc.* 1956;52:1512-1520.

Pohorecki R, Moniuk W. Kinetics of Reaction between Carbon Dioxide and Hydroxyl Ions in Aqueous Electrolyte Solutions. *Chem. Eng. Sci.* 1988;43(7):1677-1684.

Ramezan M, Skone TJ, ya Nsakala N, Liljedahl GN, Gearhart LN, Hestermann R, Rederstorff B. "Carbon Dioxide Capture from Existing Coal-Fired Power Plants." Final Report for U.S. Department of Energy-National Energy Technology Laboratory (DOE/NETL-401/110907). November, 2007.

Rao AB, Rubin ES. A Technical, Economic, and Environmental Assessment of Amine-Based CO_2 Capture Technology for Power Plant Greenhouse Gas Control. *Environ. Sci. Technol.* 2002;36(20):4467-4475.

Rejl JF, Linek V, Moucha T, Valenz L. Methods standardization in the measurement of mass-transfer characteristics in packed absorption columns. *Chem. Eng. Res. Des.* 2009;87:695-704.

Rischbieter E, Schumpe A, Wunder V. Gas Solubilities in Aqueous Solutions of Organic Substances. *J. Chem. Eng. Data.* 1996;41(4):809-812.

Rizzuti L, Augugliaro V, Lo Cascio G. The Influence of the Liquid Viscosity on the Effective Interfacial Area in Packed Columns. *Chem. Eng. Sci.* 1981;36(6):973-978.

Rizzuti L, Brucato A. Liquid viscosity and flow rate effects on interfacial area in packed columns. *Chem. Eng. J.* 1989;41(1):49-52.

Rocha JA, Bravo JL, Fair JR. Distillation Columns Containing Structured Packings: A Comprehensive Model for Their Performance. 1. Hydraulic Models. *Ind. Eng. Chem. Res.* 1993;32(4):641-651.

Rocha JA, Bravo JL, Fair JR. Distillation Columns Containing Structured Packings: A Comprehensive Model for Their Performance. 2. Mass-Transfer Model. *Ind. Eng. Chem. Res.* 1996;35(5):1660-1667.

Rochelle GT. Amine Scrubbing for CO_2 Capture. *Science*. 2009;325(5948):1652-1654.

Rochelle GT, Fisher KS, Beitler C, Rueter C, Searcy K, Jassim M. "Integrating MEA Regeneration with CO_2 Compression and Peaking to Reduce CO_2 Capture Costs." Final Report for Trimeric Corp. (Subcontract of DOE Contract DE-FG02-04ER84111). June, 2005.

Rochelle GT et al. "CO_2 Capture by Aqueous Absorption, Second Quarterly Progress Report 2009." Luminant Carbon Management Program. The University of Texas at Austin. 2009.

Schultes M, Chambers S. How to Surpass Conventional and High Capacity Structured Packings with Raschig Super-Pak. *Chem. Eng. Res. Des.* 2007;85(1):118-129.

Schultheiss P. "Reaction Kinetics and Effective Area of Carbon Dioxide Absorption into Aqueous Sodium Hydroxide Solution." Fall Research Thesis. University of Texas at Austin. Austin, TX. 2006.

Sedelies R, Steiff A, Weinspach P-M. Mass Transfer Area in Different Gas-Liquid Reactors as a Function of Liquid Properties. *Chem. Eng. Technol.* 1987;10(1):1-15.

Seeton CJ. Viscosity-temperature correlation for liquids. *Tribol. Lett.* 2006;22(1):67-78.

Sherwood TK, Pigford RL, Wilke CR. *Mass Transfer*. New York, McGraw-Hill: 1975.

Shetty S, Cerro RL. Spreading of Liquid Point Sources over Inclined Solid Surfaces. *Ind. Eng. Chem. Res.* 1995;34:4078-4086.

Shetty S, Cerro RL. Fundamental Liquid Flow Correlations for the Computation of Design Parameters for Ordered Packings. *Ind. Eng. Chem. Res.* 1997;36(3):771-783.

Shetty S, Cerro RL. Spreading of a Liquid Point Source over a Complex Surface. *Ind. Eng. Chem. Res.* 1998;37(2):626-635.

Shetty S, Kantak MV, Kelkar BG. Gas-Phase Backmixing in Bubble-Column Reactors. *AIChE J.* 1992;38(7):1013-1026.

Shi MG, Mersmann A. Effective Interfacial Area in Packed Columns. *Ger. Chem. Eng.* 1985;8:87-96.

Sidi-Boumedine R, Raynal L. Influence of the viscosity on the liquid hold-up in trickle-bed reactors with structured packings. *Catal. Today*. 2005;105:673-679.

Solomon S et al., eds. *Climate Change 2007: The Physical Science Basis*. Cambridge, Cambridge University Press: 2007.

Spiegel L, Meier W. Correlations of the performance characteristics of the various mellapak types. *ICHEME Symp. Ser.* 1988;104:A203-A215.

Stichlmair J, Bravo JL, Fair JR. General model for prediction of pressure drop and capacity of countercurrent gas/liquid packed columns. *Gas Sep. Purif.* 1989;3:19-28.

Suess P, Spiegel L. Hold-up of Mellapak structured packings. *Chem. Eng. Process.* 1992;31(2):119-124.

Vázquez G, Alvarez E, Navaza JM, Rendo R, Romero E. Surface Tension of Binary Mixtures of Water + Monoethanolamine and Water + 2-Amino-2-methyl-1-propanol and Tertiary Mixtures of These Amines with Water from 25°C to 50°C. *J. Chem. Eng. Data.* 1997;42(1):57-59.

Vázquez G, Antorrena G, Chenlo F, Paleo F. Effect of Viscosity on Interfacial Area in the Absorption of CO_2 by Carbonate/Bicarbonate Solutions. *Chem. Biochem. Eng. Q.* 1989;3(1-2):7-12.

Vázquez G, Chenlo F, Pereira G. Enhancement of the Absorption of CO_2 in Alkaline Buffers by Organic Solutes: Relation with Degree of Dissociation and Molecular OH Density. *Ind. Eng. Chem. Res.* 1997;36(6):2353-2358.

Wang GQ, Yuan XG, Yu KT. Review of Mass-Transfer Correlations for Packed Columns. *Ind. Eng. Chem. Res.* 2005;44(23):8715-8729.

Weiland RH, Dingman JC, Cronin DB, Browning GJ. Density and Viscosity of Some Partially Carbonated Aqueous Alkanolamine Solutions and Their Blends. *J. Chem. Eng. Data.* 1998;43(3):378-382.

Weimer T, Schaber K. Absorption of CO_2 from the Atmosphere as a Method for the Estimation of Effective Interfacial Areas in Packed Columns. *ICHEME Symp. Ser.* 1997;142:417-427.

Wilson I. *Gas-Liquid Contact Area of Random and Structured Packing.* University of Texas at Austin. M.S. Thesis. 2004.

Yeh NK. *Liquid Phase Mass Transfer in Spray Contactors.* University of Texas at Austin. Ph.D. Dissertation. 2002.

Young T. Essay on the Cohesion of Fluids. *Philos. Trans. R. Soc. London.* 1805;95:65.

Zhao L, Cerro RL. Experimental Characterization of Viscous Film Flows over Complex Surfaces. *Int. J. Multiphase Flow.* 1992;18(4):495-516.

Vita

Robert Edison Tsai was born on June 6, 1983 in Hinsdale, IL to Robert Wei-Gun Tsai and Shwu-Mei Chou Tsai. After graduating valedictorian from William Fremd High School in Palatine, IL in 2001, he enrolled at the University of Illinois at Urbana-Champaign. During his undergraduate tenure, he participated in summer internships with Ecolab in Joliet, IL in 2003 and with Kraft Foods in Glenview, IL in 2004. He received his Bachelor of Science degree in chemical engineering in May of 2005, graduating magna cum laude with Bronze Tablet honors, and began his graduate studies at the University of Texas at Austin in August of 2005. He has accepted a full-time employment offer with UOP in Des Plaines, IL.

Permanent address: 1059 W. Partridge Dr., Palatine, IL 60067

This dissertation was typed by the author.